Metallo – Porphyrin Compounds as Anti-Cancer Compounds and their Interaction with Different Conformations of DNA

Syntheses, Model and *in vitro* Studies of Metallo – Porphyrin Compounds

---

DISSERTATION

zur
Erlangung der naturwissenschaftlichen Doktorwürde
(Dr. sc. nat)

vorgelegt der

Mathematisch – naturwissenschaftlichen Fakultät

der

UNIVERSITÄT ZÜRICH

von
Philipp M. Antoni
aus Deutschland

Prüfungskomitee

Prof. Dr. Roger Alberto (Vorsitz)
Prof. Dr. Roland K. O. Sigel (Beisitz)
PD Dr. Bernhard Spingler (Leitung der Dissertation)

Zürich 2012

Metallo – Porphyrin Compounds as Anti-Cancer Compounds and their Interaction with Different Conformations of DNA

Syntheses, Model and *In Vitro* Studies of Metallo – Porphyrin Compounds

---

1. List of Synthesized Compounds

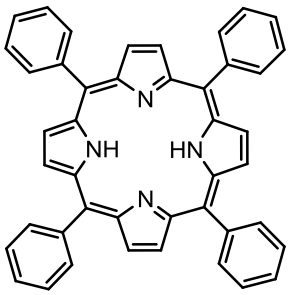

TPP, **1**

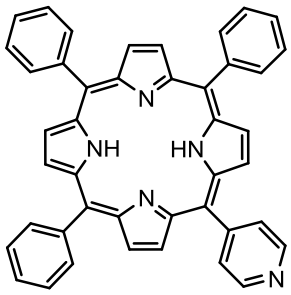

MPyTPP, **2**

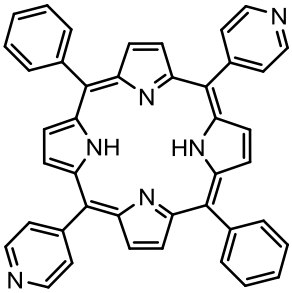

trans-DPyDPP, **3**

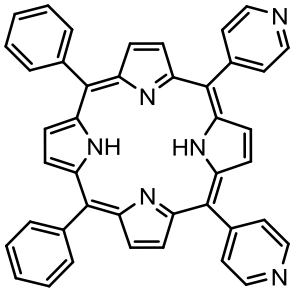

cis-DPyDPP, **4**

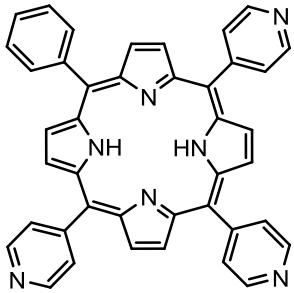

TriPyMPP, **5**

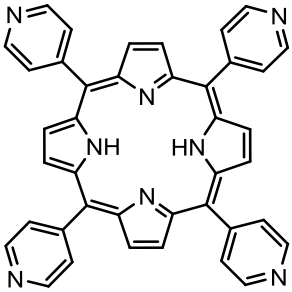

TPyP, **6**

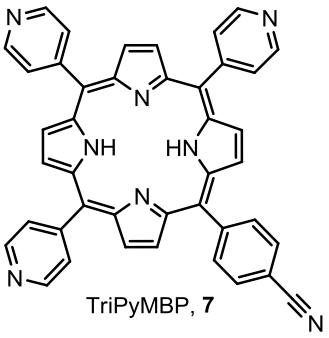

TriPyMBP, **7**

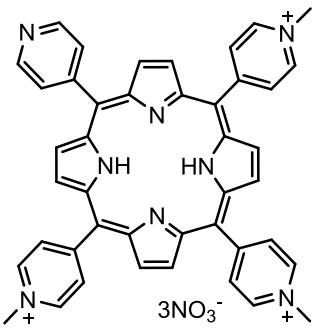

TriMePyMPP, **8**

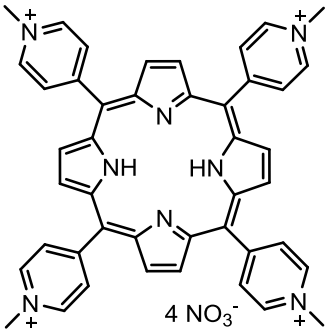

TMePyP, **10**

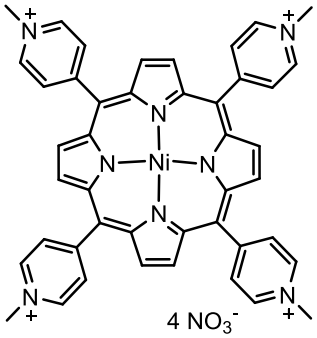

Ni-TMePyP, **11**

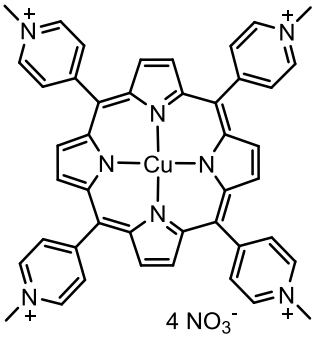

Cu-TMePyP, **12**

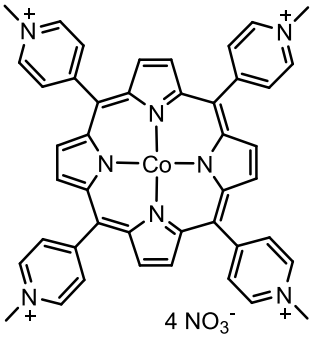

Co-TMePyP, **13**

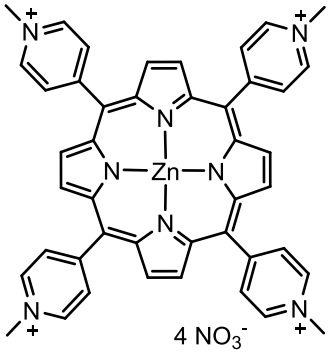

Zn-TMePyP, **14**

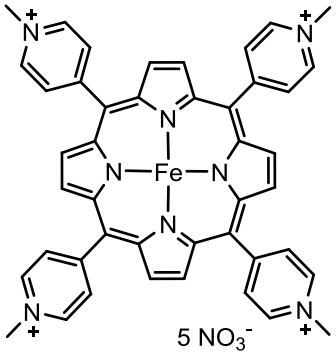

Fe^{3+}-TMePyP, **15**

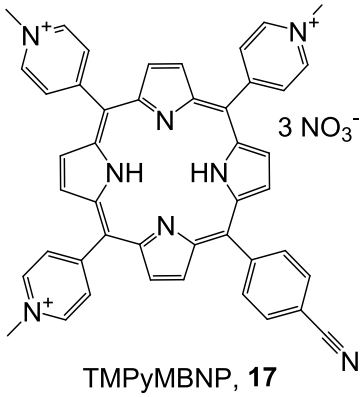

TMPyMBNP, **17**

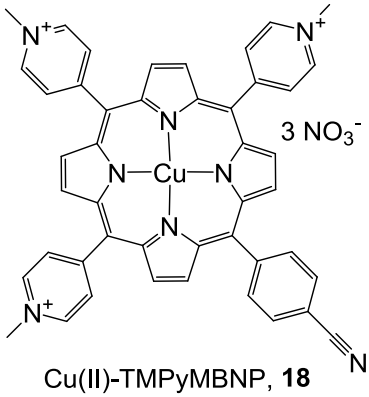

Cu(II)-TMPyMBNP, **18**

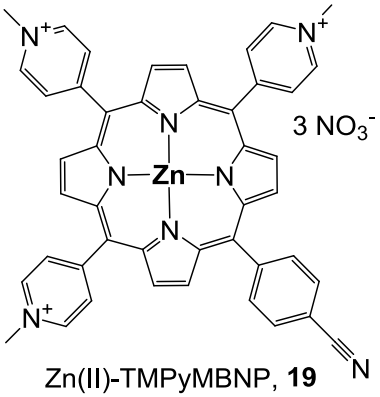

Zn(II)-TMPyMBNP, **19**

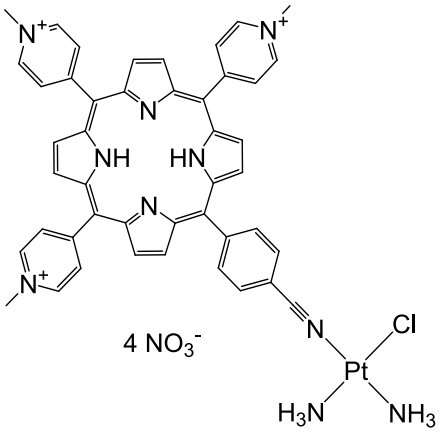

cis-$(NH_3)_2$ClPt-TMPyMBNP, **20**

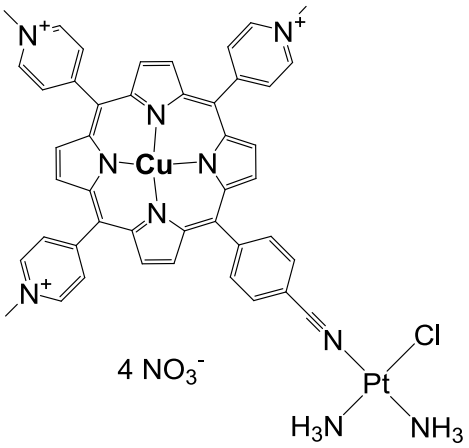

cis-$(NH_3)_2$ClPt-Cu(II)TMPyMBNP, **21**

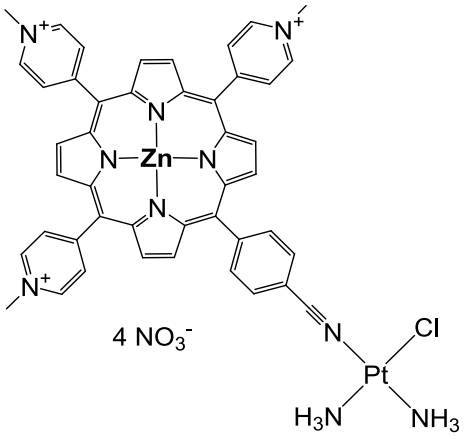

cis-$(NH_3)_2$ClPt-Zn(II)TMPyMBNP, **22**

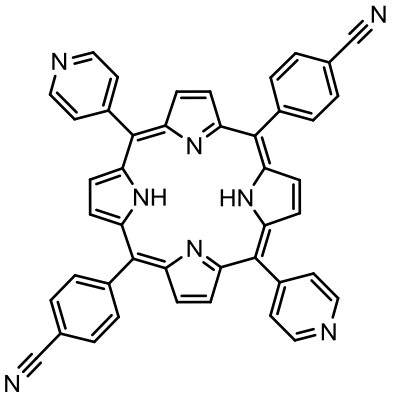

trans-DPyDBNP, **25**

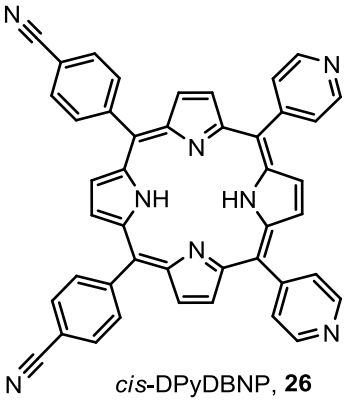

cis-DPyDBNP, **26**

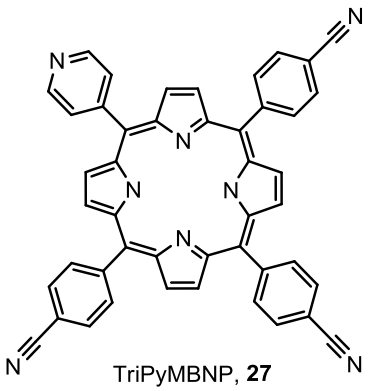

TriPyMBNP, **27**

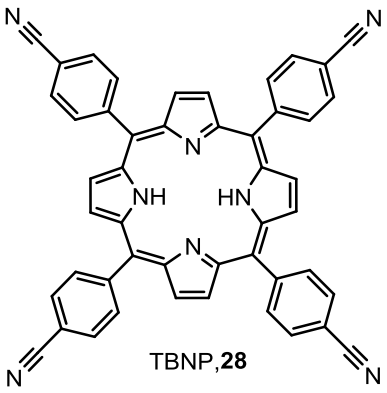

TBNP,**28**

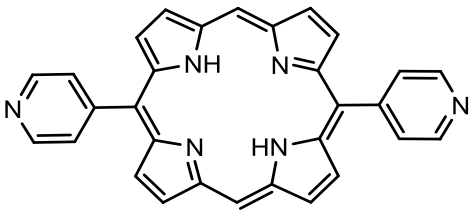

5,15-pyridyl-porphyrin, **29**

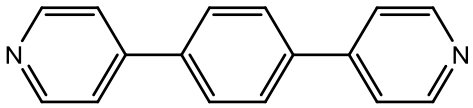

1,4-bis(4',4''-pyridyl)benzeneipyridine, **30**

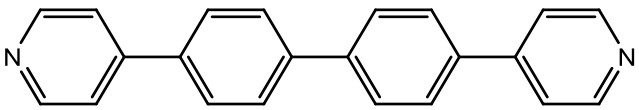

1,1'-bis(4'',4'''-pyridyl)-4,4'-biphenyl, **31**

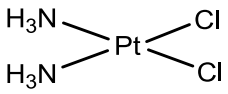

cisplatin, **32**

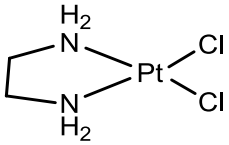

enPtCl$_2$, **33**

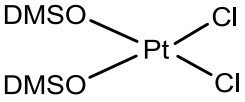

cis-Pt(DMSO)$_2$Cl$_2$, **34**

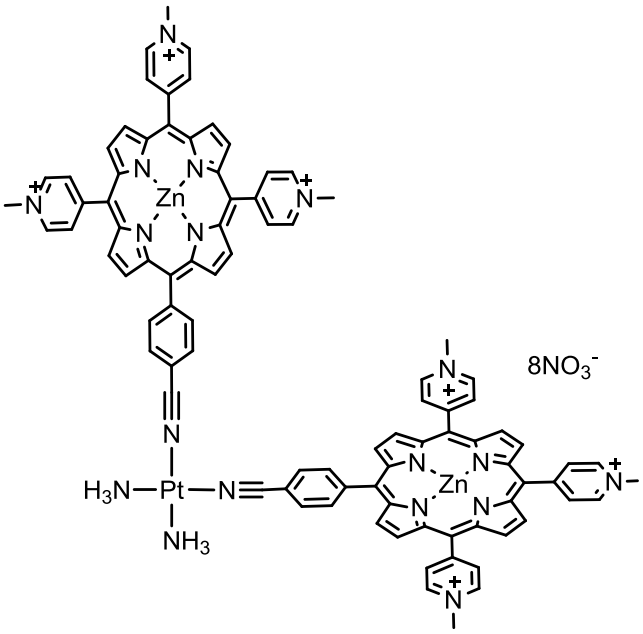

cis-Pt(NH$_3$)$_2$-di-5-cyanobenzol-10,15,20-methylpyridinium-zinc-porphyrin nitrate, **35**

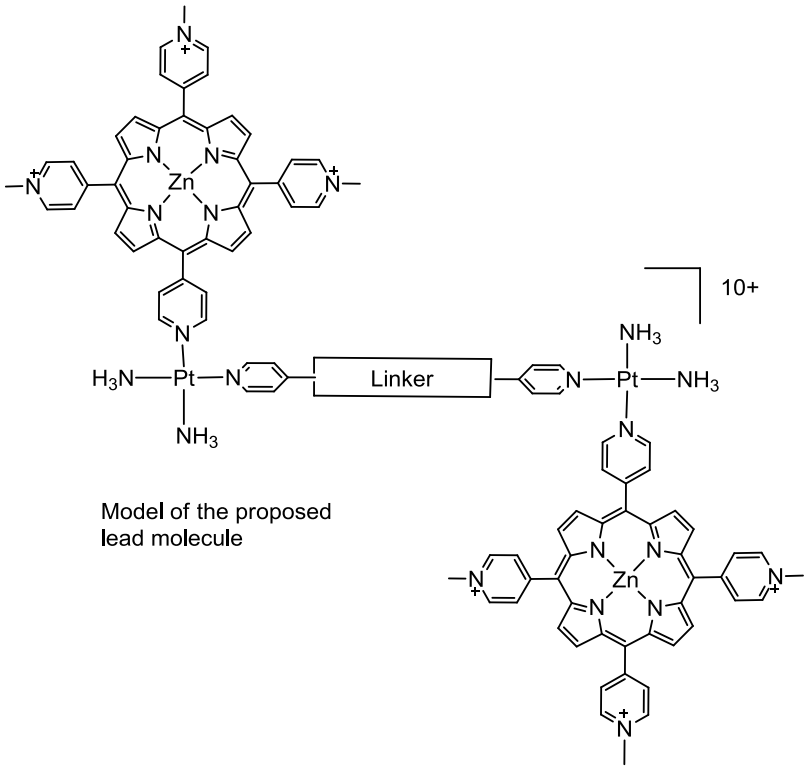

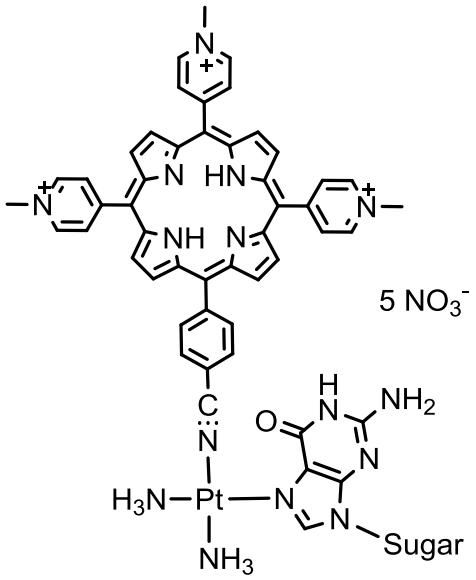

TriMePMCNP-*cis*Pt-G, **36**

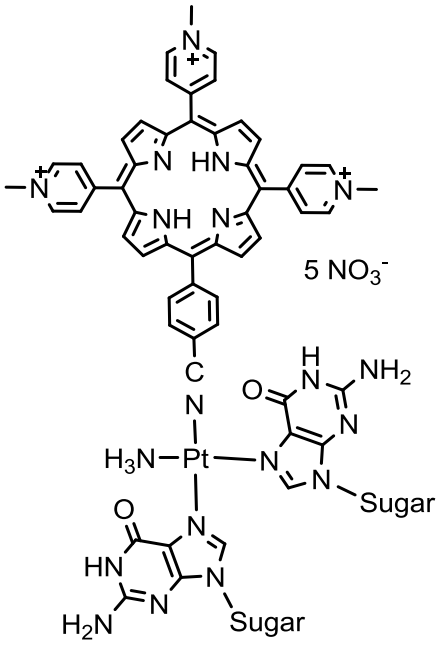

TriMePMCNP-*cis*Pt-2G, **37**

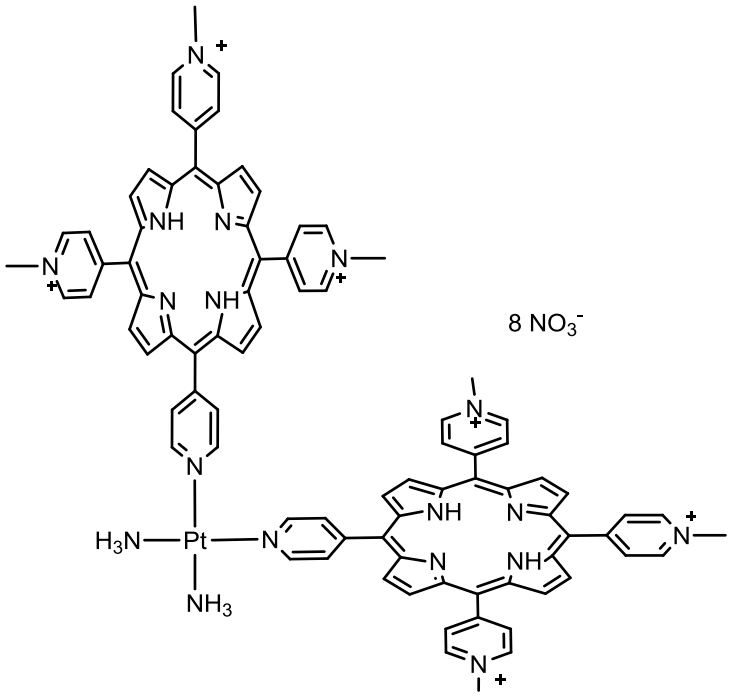

cis-Pt(NH_3)$_2$-di-5-cyanobenzol-10,15,20-methylpyridinium-porphyrin nitrate, **38**

2. Acknowledgements

I would like to thank colleagues, friends and family that supported me during the last 4 years. It has been an intense and interesting time at the University with a lot of new and exciting experiences, tasks, ups & downs and friendship. A lot of persons helped me in various aspects, personally and professionally. In the need of help, I could rely on a pre*cis*e and fair feedback, support and also some open ears. During the time at the University of Zurich, I received a lot of good ideas which made up my mind how I want to form my future.

Lots of persons joined in this part of my life and accompanied me for a while. I would like to thank all those for their great support. Especially the friendly help, constructive advices, ideas and patience of the members of the Inorganic Institute of the University of Zurich was very important for this work. Thank you!

I would also like to thank my friends for their persistence, patience and support. I am very happy and grateful that you supported me.

In particular, I would like to acknowledge the following persons…

PD Dr. Bernhard Spingler, for your patience, advice, and support. Thank you for giving me this interesting topic to work on and free hands to develop it further. Thank you for teaching me how to develop new ideas, working techniques and open thoughts in various topics, chemically and personally. Thanks for your friendship and the many discussions and for the correction of this supervision and work.

Prof. Dr. Roger Alberto, for giving me the opportunity to work in his group and giving me the freedom to develop and experiment on many ideas. I enjoyed a lot organizing our yearly Christmas lecture – it was a lot of fun. I enjoyed the Trin/Kandersteg meetings and the open atmosphere in your group. I appreciated a lot your direct way of communication, especially during the writing of my thesis. Thank you for helping me keeping my focus on my thesis and for your supervision.

Prof. Dr. Roland Sigel, for helping me in different aspects during my time as a PhD student. We built the CMSZH and had controversial discussion and common battles in various commissions. Thank you for helping me developing my profile and the many good discussions.

Prof. Dr. Eva Freisinger, for her support, patience, open doors for discussions. I always appreciated the time we discussed our various topics. Thanks.

My labmates and students: **Stefan Schnidrig,** for a great time in the lab synthesizing a lot of challenging molecules and combining them to functionality. **Michael Felber** and **Miriam Oberholzer** for their highly motivated, skilled work and support.

Dr. Benji Probst, for a great time and support from Vordiplom to PhD, lot of exchange of experience and some memorable moments throughout this time.

Dr. Pilar Sanchez for all her support in platinum chemistry and synthesis, cell culturing, and biotech questions. Thank you also for your friendship, lots of discussions and motivations that kept me going.

Barbara and Heinz Spring, for a great time during the Christmas, UZH 175 celebration, and University open days lectures. We had a good time finding and trying new and exciting experiments. Thanks for the coffee, friendship and good music. On the analysis side, thanks for the elementary analysis and pressure experiment supports.

ACI – Members, especially **Dr. Paul Schmutz** for his great repository of good advice and support and his kind friendliness; **Dr. Henrik Braband** for his help with all the machinery, his motivation and also bringing me down to earth from time to time; **Miguel Guttentag**, for his friendship, open ears and good discussions; **Dr. Felix Zelder**, for his help in MS and HPLC repair and supporting me with ideas how to build porphyrins; **Daniel Can** for synthetic questions and help on the Christmas lecture; **Dr. Fabio Zobi** for his ideas and joint brain storming; **Joachim Schnabl,** for the exchange on chemistry, entrepreneurship and friendship; **Dr. Sofia Gallo** for her help in

platinum chemistry and exchange of ideas towards the best cornerstone of my molecules.

I would also like to thank the following persons that helped me to learn other aspects of academic views such as leadership, strategic de*cis*ions, and diplomacy: **Dean Dr. Michael Hengartner, Dean and Pro-Rector Dr. Daniel Wyler, Prof. Dr. Peter Hamm, Vice-Dean Dr. Jay Siegel, and Vice-Dean Dr. Bernhard Schmid.** Thank you for respecting and supporting me in my function as the PhD representative during the last 3 years. I learned a lot.

Franziska Conrad, you know … thank you.

Natalie Fichter, for all your friendship, friendly smile and help during the last years in personal and professional matters. We had a great time.

Prof. Dr. Johan Malmstroem, my friend and colleague at Biognosys AG for all his support, help and trust in me during the last months. My colleague **Dr. Oliver Rinner** for his support, help, friendship, and trust.

My parents and **Manuela**, thank you for supporting me during the last 28, especially the last 4 years, and even more during the last half year when I was totally occupied with work and did not find the time to acknowledge everything you did for me. I must have been difficult to endure. Thank you for your help, support and love.

3. Abstract

3.1 Deutsche Zusammenfassung

Das Vorkommen und die Funktion von Z-DNA in Menschen wurde innerhalb der letzten Jahrzehnte erforscht und bestätigt[1-9]. Die Detektierbarkeit und damit ein tieferes Verständnis der Funktion von Z-DNA in lebenden Zellen oder gar ganzen Organismen wurde trotz vieler Forschungsarbeiten nicht erreicht. Man ist im Moment nicht in der Lage zu bestimmen, in welchem Zellstadium Z-DNA vorkommt und welche genaue Funktion es übernimmt. Der Fokus dieser Arbeit widmet sich dem Thema Detektierbarkeit von Z-DNA in lebenden Zellen über einen Ansatz, der durch rationelles Design von kleinen Molekülen diese speziellen Form Z-DNA darstellt.

Der erste Schritt dieser Arbeit war das Auffinden von funktionierenden Metallkomplexen und das Testen dieser in Modelsystemen. Das Ziel war, eine spezifische Interaktion zwischen DNA und dem Metallkomplex zu definieren welche einfach zu detektieren, reproduzierbar und auch *in vivo* anwendbar ist. Da DNA in wässriger und salzhaltiger Umgebung vorkommt, wurden ein stabiles und wasserlösliches Porphyrin, 5,10,15,20-Tetramethylpyridinium-porphyrin, als Grundbaustein gewählt. Die Eigenschaften der Porphyrine kann man durch verschiedene zentrale Metalle beeinflussen. Verschiedene Kombinationen dieser Porphyrine mit und ohne Metallzentren wurden in Modelsystemen getestet. Balaz *et al.* haben im Jahr 2005 eine Studie veröffentlicht, in welcher sie Z-DNA mit einem Zink(II) 5,10,15,20-(methyl-pyridinium)-porphyrin mittels CD Spektroskopie spezifisch nachweisen konnten[10, 11]. Wir haben diese Resultate kurze Zeit später bestätigen können und die Effekte verschiedener Metallzentren wie Kupfer und Nickel getestet. Dabei stellte sich heraus, das die Metallzentren eine wichtige Rolle spielen und verschiedene Interaktionen wie zum Beispiel Interkalation, partielle Interkalation, oder seitliche Koordination mit DNA bevorzugen. Ein Stacking der Porphyrine um die DNA wurde auch beobachtet, welches massgeblich bei Molekülen mit axialen Liganden am Metallzentrum einher ging.

Um dieses System spezifischer in kompetitiver Umgebung wie Zellen zu machen und elektrostatische Interaktionen zwischen den Porphyrinen zu vermeiden, wurde dieses System weiterentwickelt zu einem Porphyrin Netzwerk. Dieses sollte aus zwei Z-DNA detektierenden Einheit Metall-(methylpyridinium)-porpyhrin und einer starren Verbindung mit definiertem Abstand aufgebaut sein. Als Verbindungen der beiden Porphyrine wurde ein quadratisch planar koordinierendes Metallzentrum wie zum Beispiel *Cis*platin gewählt. Dieses Molekül könnte mit der Eigenschaft als side-on koordinierendes Metalloporphyrin die spezifischen Eigenschaften der Z-DNA wie Basenabstand, Durchmesser und die exponierten Koordinationsstellen (wie zum Beispiel das N7 des Guanosins) nutzen und nur an diese Konformation der DNA binden. Die Synthese dieser Moleküle wurde durch die positive Ladung der einzelnen Bauteile erschwert und erforderte einen neuen Ansatz. Dabei wurde aber eine interessante Entdeckung gemacht.

Fragmente dieser di-Porphyrin Systeme, ein Metalloporphyrin koordiniert an ein *Cis*platin (Verbindungen **17** – **22**) zeigten eine ausgeprägte Toxizität gegenüber humanen Krebszellen bei der Bestrahlung mit rotem Licht. Zwei menschliche Zelllinien wurden auf Toxizität der verschiedenen Verbindungen **17** – **22** getestet und mit Standards wie *Cis*platin verglichen. Viele Porphyrine sind fluoreszierende Verbindungen sind und werden als photoaktive Substanzen verwendet. Sie können Strahlung wie zum Beispiel rotes Licht, welches Melanoma durchdringen kann, nutzen, um Singlett Sauerstoff zu erzeugen, welches als hochaktive Spezies schweren Schaden in den Zellen anrichten kann. Die Bestrahlung für 10 Minuten mit gekühltem Licht vervielfachte die Toxizität um das bis zu 78 fache bei dem toxischsten Molekül **22** mit einer Konzentration IC_{50} von 0.08 μM. Um diesen Effekt besser zu verstehen und Verbesserungen am System vornehmen zu können wurden erste Zellstudien durchgeführt, welche auf den bleichenden Effekt durch die Entwicklung von Singlett Sauerstoff hindeuten.

3.2 English Abstract

The presence and function of left-handed Z-DNA in the human organism has been proved throughout the last two decades[1-9]. The detectability of Z-DNA in living cell has nevertheless not been achieved and one is not able to observe the processes that happen during and after the formation of Z-DNA. The focus of this work originated from the rational design of molecules able to interact with Z-DNA in living organisms.

Starting from studies of metal complexes interacting and inducing Z-DNA, the aim of this thesis was to develop a modular system that can interact with the Z-DNA and be observed for its specific interaction. Since DNA was the target and the interaction should occur in natural surroundings, the water-soluble porphyrin 5,10,15,20-tetramethylpyridinium-porphyrin with various central metal centers was chosen as a starting molecule and its properties tested in different model systems. Balaz *et al.* reported in 2005 the recognition of Z-DNA in a model CD spectrometry setup by the addition of Zinc (II) 5,10,15,20-(methyl-pyridinium)-porphyrin to a previously induced Z - DNA form of poly d(GC)[10, 11]. We reproduced these experiments with different central metals such as copper and nickel to find out that the central metal ion plays an important role in this interaction. The results revealed different behaviors of the porphyrins ranging from side-on coordination, intercalation or partial intercalation of the porphyrin system to stacking of the porphyrin around the DNA depending on the coordination sphere around the central metal ion.

To make this system more specific towards only Z-DNA recognition and also to avoid electrostatic interaction between the porphyrin and the DNA, we developed of a system based on a porphyrin array. This consisted of a two-(methyl-pyridinium)-porphyrins and a linker in between (for the compounds please refer to chapter 4, Figure 4.41). The idea was to build a molecule that could recognize the specific properties of Z-DNA like rigidity, base to base distance, coordination sites and sequence specific properties. The synthesis of this system turned out to be very difficult due to the highly charged molecules that had to be combined. A porphyrin

array consisting of a *cis*platin corner and two positively charged porphyrins was synthesized.

Fragments of this porphyrin system, one metalloporphyrins coordinated to a cisplatin (compounds **17** – **22**), showed very interesting characteristics when cancer cells were exposed to these compounds in the presence of red light. Two human cancer cell lines were treated with 6 lead compounds and the toxicity determined in various conditions. Since porphyrins are fluorescent and can act as photoactive compounds, the influence of red light that could penetrate skin was tested. The metal free porphyrin compound **19** was as toxic in the dark as the reference *cis*platin, a well-known anti-cancer agent. All compounds showed an increased toxicity when exposed to red light for 10 minutes. The Pt-porphyrin compounds **20** – **22** showed a significant toxicity towards both cell lines in the dark, which characterizes their behavior as *cis*platin analogs. When these compounds were exposed to red light for 10 minutes, the toxicity increased up to 78 times and reached IC_{50} concentrations down to 0.08 μM. The spectroscopic properties of the porphyrins absorbed the red light very effectively. To further understand the mechanism of these phototoxic effects, preliminary cell uptake studies showed a bleaching effect which could be due to the evolution of singlet oxygen.

4. Interaction of Metallo – Porphyrins with Different Conformations of DNA

4.1 DNA – an introduction

4.1.1 The early days of DNA research

Deoxyribonucleic acid (DNA) is a very unique molecule. DNA consists of numerous sequences of nucleobases that decode the genome. DNA represents the plan for all functionalities carried out in the human body. It possesses a high flexibility and thus can rotate around the sugar phosphate backbone, a process needed for the process called transcription, in which DNA is transcribed into RNA to further translate to proteins. In order to regulate the transcription process, DNA can constitute different conformations, which will be the topic in Chapter 5, which deals with the special left – handed Z-DNA.

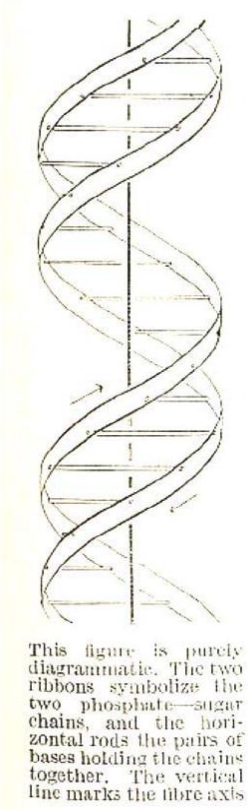

This figure is purely diagrammatic. The two ribbons symbolize the two phosphate—sugar chains, and the horizontal rods the pairs of bases holding the chains together. The vertical line marks the fibre axis

Figure 4.1 Schematic drawing of DNA in the 1953 as we know it today[12].

In the late 19th century, the discovery of our gene material was initiated by Mendel's work with common garden peas, *pisum sativum*. His discoveries led him to the

hypothesis that physical characteristics are the result of the interaction of discrete particles, which we now call genes. His theory was, however, widely disregarded by scientists at that time. In the last quarter of the 19th century, microscopists and cytologists, interested in the process of cell division, developed both the equipment and the methods needed to visualize chromosomes and their division in the processes of mitosis[13, 14] and of meiosis[15]. Shortly after, many scientists were convinced that the hereditary material (as defined by Mendel) and chromosomes must be the same. Later, chemical analysis of chromosomes showed them to be composed of both DNA and protein. The question arose, which substance carried the hereditary information? For many years most scientists favored the hypothesis that protein was the responsible molecule because of its vast complexity when compared with DNA. After all, DNA is only composed of 4 nucleobases while protein is composed of 21 amino acids, and DNA molecules are linear while proteins range from linear to multiple branched to globular.

It seemed clear that the relatively simple structure of a DNA molecule could not carry all of the genetic information needed to account for the so diversified life on earth. In the early 1950's, evidence showing that DNA must be the chromosomal component that carries hereditary information was observed. In 1952, Alfred Hershey and Martha Chase used radioactive labeling to grow a particular type of phage, known as T2, in the presence of two different radioactive labels so that the phage DNA incorporated radioactive phosphorus ^{32}P, while the protein incorporated radioactive sulphur ^{35}S. Their analysis showed that most of the ^{32}P-label was found inside of the cell, while most of the ^{35}S was found outside. This suggested to them that the proteins of the T2 phage remained outside of the newly infected bacterium while the phage-derived DNA stayed in the cell. They then showed that the phage derived DNA caused the infected cells to produce new phage chromosomes. This elegant work showed conclusively that DNA is the molecule which holds the genetic information.

The physical structure of the DNA molecule and its resulting functionality was subject to be discovered, since it was not clear how such a simple molecule could decode the full information on such a complex species as a human being.

In the late 1950s, only a few groups were working on determining the structure of DNA, among these was a group led by Linus Pauling[16, 17], and two groups in Britain from the University of Cambridge. A key inspiration in the work of all of these teams was the discovery in of Pauling in 1948 that many proteins included helices[12] which he found from X-ray patterns. Even in the initial crude diffraction data from DNA (see Figure 4.3 for a later version of a simple x-ray pattern), it was clear that the structure involved helices. Watson and Crick came up with a model that was restricted to what chemically and biologically was reasonable. In 1952, Chargaff discovered that two nucleotides pairs, adenine and thymine, guanine and cytosine, were always present in equal proportions.

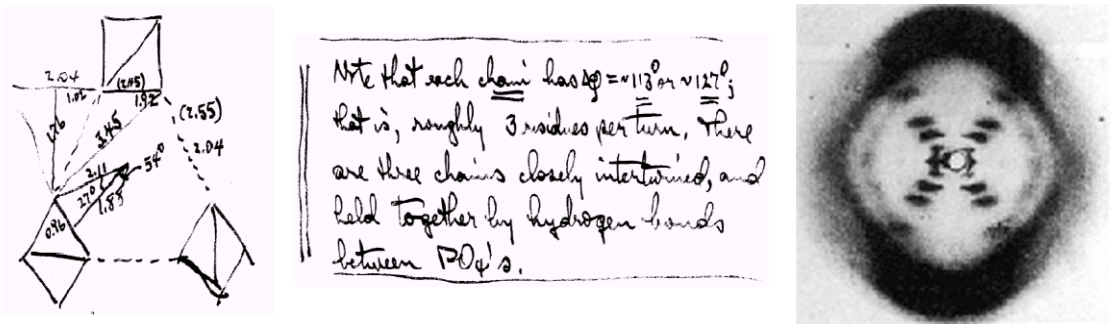

Figure 4.2 DNA structure prediction of Linus Pauling which turned out to be wrong. Taken from L. Pauling[12] later version of a simple x-ray pattern.

Watson and Crick began to postulate double helical arrangements, and concluded that reversing the directionality of one strand provides an explanation for Chargaff's results, which also had the effect of ensuring that the distance between the phosphate chains did not vary along a sequence. They could prove from an X-ray pattern obtained by Franklin that the constant distance between bases must have a value of 2 nanometers[18]. The same pattern also gave them the 3.4 nanometer-per-10 bases “pitch” of the helix. Watson, Crick and Wilkins were awarded the Nobel

Prize in medicine in 1962 for discovering the molecular structure of DNA. Figure 4.3 shows the DNA model presented by Watson and Crick in 1952[19].

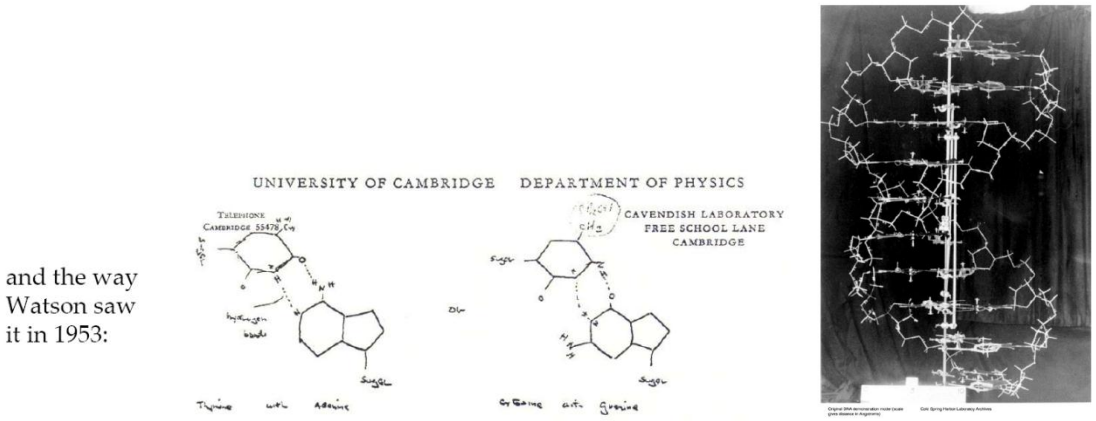

Figure 4.3 DNA model of Watson and Crick. Pictures taken from [19]. The hydrogen bonds the way Watson imagined them in 1953.

Today, DNA is well known and characterized. It is organized as two complementary strands which are made up of a phosphate-sugar backbone and a nucleobase in a periodic sequence. In between the bases of the two complementary strands are hydrogen bonds (Watson – Crick bonds) that can be separated[20-22]. In Figure 4.4, the phosphates (circles) are bound to the sugars (ribose – shown in black). In between the bases, the hydrogen bonds can be seen, whereas the number of the bonds depends on the bases (written inside of the bases, A – adenine, C – cytosine, G – guanine, T – thymine)[23]. DNA offers numerous possible binding sites for metals (Figure 4.3, right) whereas soft metals tend to coordinate to the nucleobases and hard metals to the backbone[24].

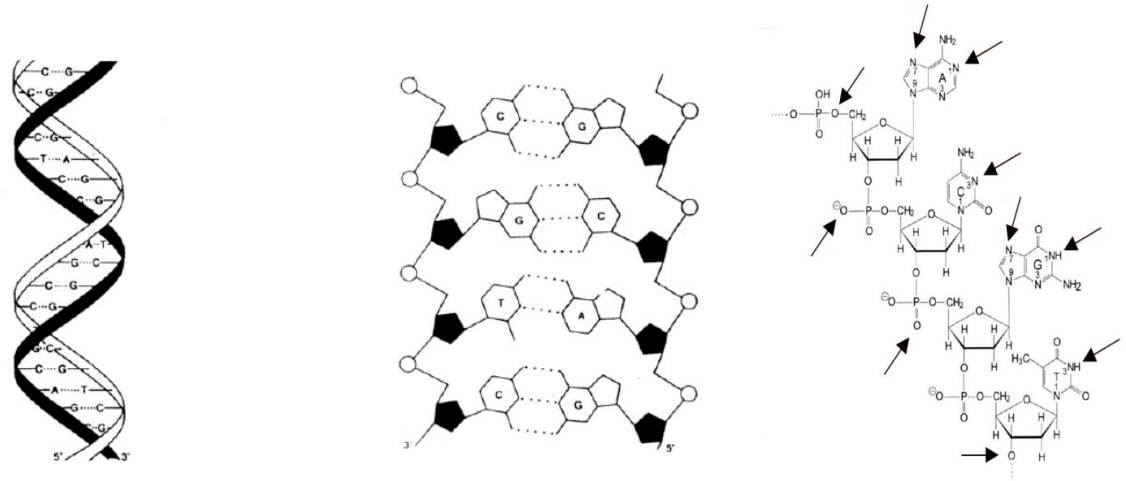

Figure 4.4 left: Hydrogen bonds in detail on the left and the double helical structure of B - DNA on the right. Picture taken from www.chemistrydaily.com; right: DNA strand presented as a chain of nucleotides, sugar and phosphate. The arrows present the possible binding sites for metals.

4.1.2 DNA and its role as a target of molecular chemistry

DNA, in its function as storage of the genes, has been a target for molecular approaches in medicine for a long time. The vision to control the function and expression of the genes and to block certain genes was the origin of personalized medicine. Since 25 years, several approaches were started to culminate in the decoding of the human proteome in 2001 by Celera and its founder Craig Venter[25]. Since that time, molecular diagnostics and direct target approaches towards certain regions or conformations of the DNA have been published[2, 3, 26-30]. The focus has always been the isolation and detection of a specific regions or conformations of DNA and later also of RNA.

The isolation of specific DNA targets within genomes is critical for a variety of research. Recently, considerable effort has been spent to isolating microsatellite sequences. Microsatellites are sequences containing a low level of sequence complexity comprised of short tandem repeats of two to five base pairs. They are often a marker of choice for population genetics studies mainly due to their higher mutation rate[26, 31].

Various approaches to target DNA were developed. DNA can be targeted via three different interactions: intercalation, groove (major or minor) binding or covalent binding[32-34]. The strongest interaction was found in the 1980s when Rosenberg discovered the interaction between platinum and DNA[35]. This topic is further discussed in Chapter 6.

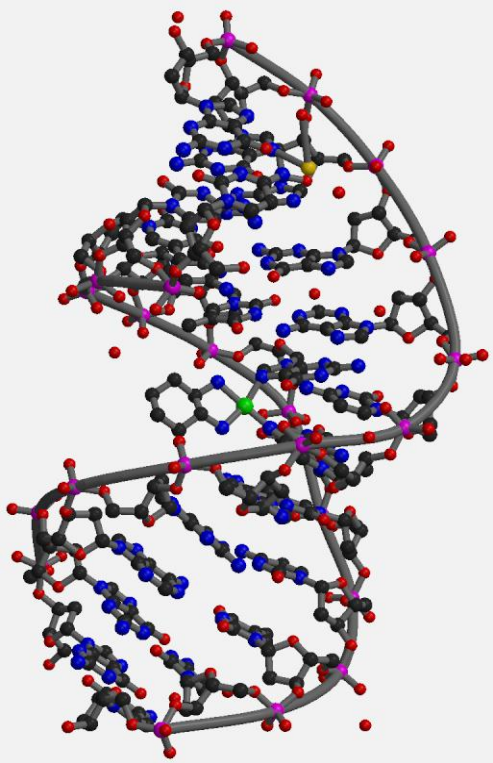

Figure 4.5 Interaction of oxaliplatin with a DNA fragment crystallized by Spingler et al.[36, 37]

DNA can also be targeted via a groove binding mode. Since the B- conformation of the DNA forms 2 kinds of deep and wide grooves, both major and minor grooves can be targeted. The major groove is a primary target which is also used for drugs such as methyl green[38] or DAPI[39-42], the Hoechst stain[43, 44]. The minor groove can be approached by proteins such as TBP[45-48] or small molecules such as Hoechst 33258 (Figure 4.7).

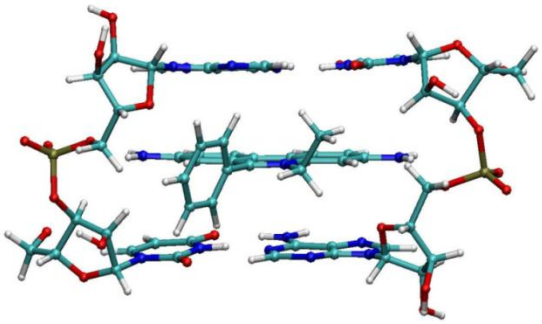

Figure 4.6 Molecular model of ethidium cation intercalating between two base pairs. This image was taken from http://en.wikipedia.org/wiki/File:DNA_intercalation2.jpg (created in 2005 using VMD software).

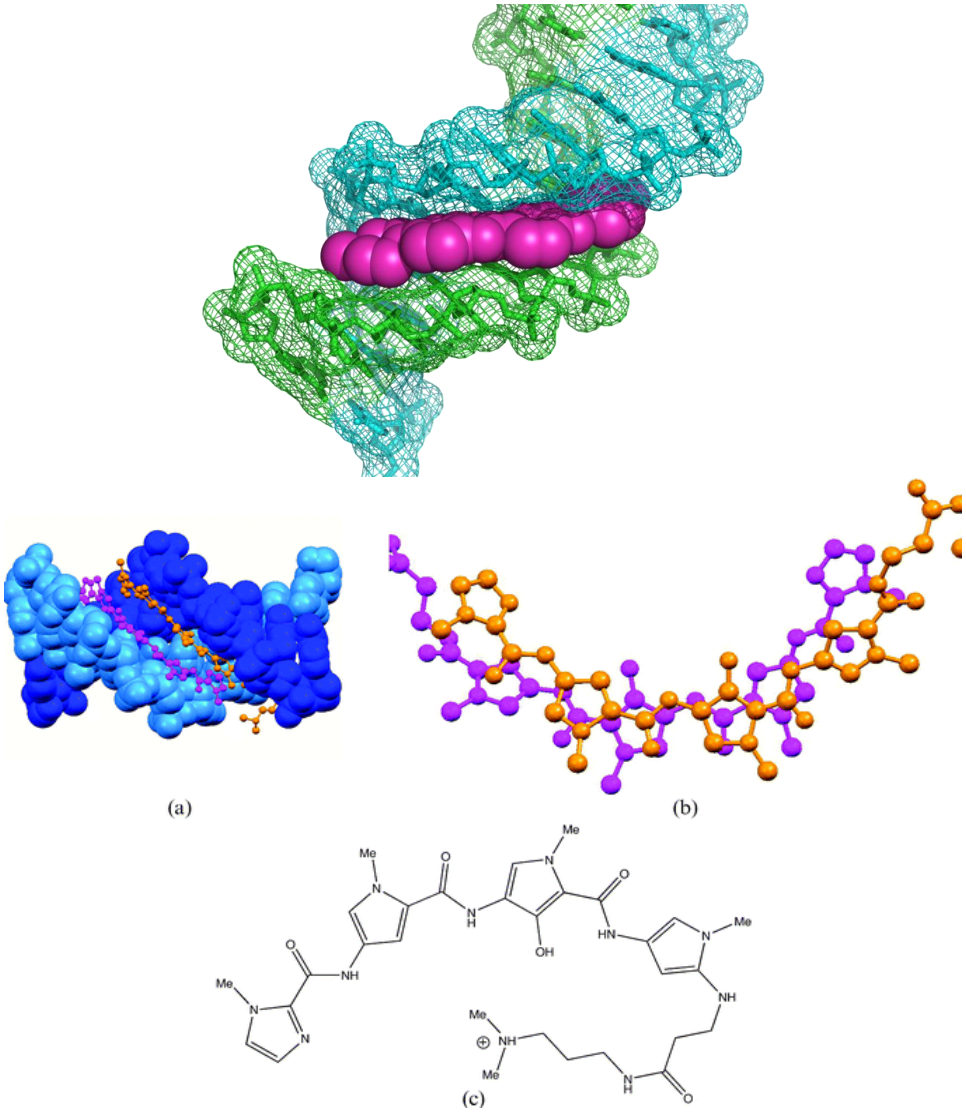

Figure 4.7 top: Hoechst molecule (magenta) bound to the major groove of DNA. Taken from PDB 264D "Three dimensional crystal structure of the A-tract DNA dodecamer" (picture http://en.wikipedia.org/ wiki/Hoechst_stain). Bottom: cylindrical structure binding to the minor groove. Below depicted is the organic structure [33, 44, 49, 50]. Picture taken from Hannon et al[49].

Another interaction type is most commonly used in biology for staining purposes – the intercalation. The most prominent intercalator is ethidium bromide [51-53] (see Figure 4.6). Intercalators have an appropriate size and chemical nature that fits in between base pairs of DNA. These ligands are commonly polycyclic, aromatic, and planar, and therefore often make good stains. Intensively studied DNA intercalators include berberine, proflavine, daunomycin, doxorubicin and thalidomine. They can be used for chemotherapeutic treatment to inhibit replication of DNA in fast growing cancer cells.

4.1.3 Different conformations of DNA

For many natural species, symmetry plays an important role. Symmetry can be observed in eukaryotic systems such as human beings as well as in simple prokaryotic systems such as algae. In the picture below, Japanese researchers produced an axial non-natural symmetry to a snail shell by modifying a set of genes of this snail.

Figure 4.8 Symmetrical snail shells produced by Japanese researchers in 2009 (taken from www.spiegel.de).

Even in the basic structures of living organisms, symmetry plays a vital role. It is observed in proteins forming symmetrically shaped ion channels, as well as in DNA. Double stranded DNA occurs in at least 3 different conformations of which all were

traced *in vivo*[54]. The most common conformation of the DNA *in vivo* is the B- form, a right – handed double helix characterized by a wide major groove and a narrow minor groove[55]. Its counterpart is the left handed Z-DNA. The major groove of the B-DNA is easily accessible to proteins which are important for the replication of DNA. The base pairs are situated perpendicularly to the helix axis and the sugar pucker is C2´ - endo. The bases are staked upon each other and the backbone forms a smooth curve. B-DNA is favored at low salt concentrations under physiological conditions, especially in a highly water containing environment (above 95%). It is believed to be the native conformation occurring in the chromosomes[3, 25, 56, 57]. The double helix is narrower and more elongated than the other right handed A-conformation. In B-DNA, the helix makes a turn every 3.4 nm, and the distance between two neighboring base pairs is 0.34 nm. Hence, there are about 10 pairs per turn. The antiparallel strands make two grooves of different widths, referred to as the major groove and the minor groove, which may facilitate binding specific proteins.

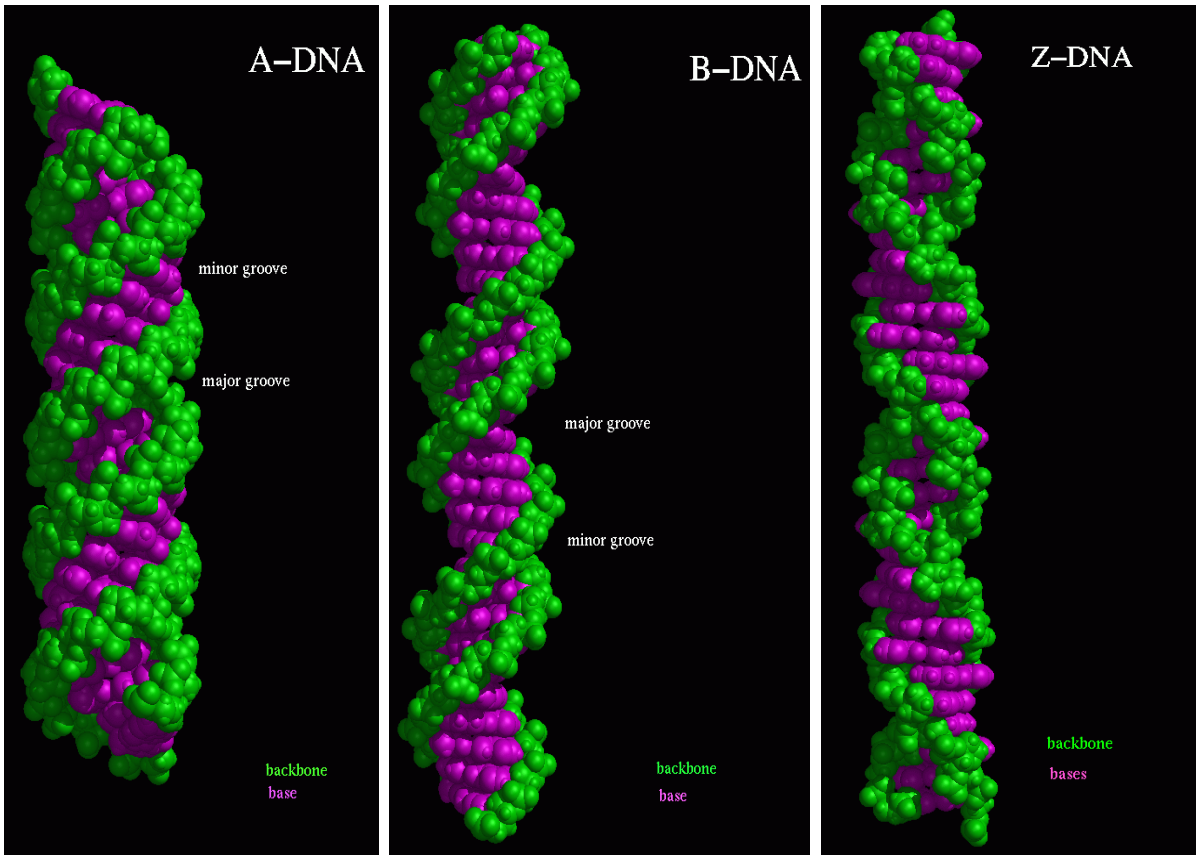

Figure 4.9 Comparison of the different types of DNA: A – DNA (left), B-DNA (middle) and Z-DNA (right). Pictures taken from the Image Library of Macromolecules of the University Jena.

The biological functions of the sequences of the nucleic acids are mainly based on the ability of the nucleic bases to undergo specific interactions. But DNA is a very flexible and dynamic molecule that can assume a variety of inter-converting forms. Figure 4.9 shows an overview of the three conformations. The A-form is found for the most RNA molecules and RNA – DNA duplexes [58]. It is characterized by a shorter, therefore wider helix with a deep and narrow major groove which cannot be easily accessed by proteins. The wide and shallow minor groove of the A-DNA is easier accessible to proteins, but the information content there is lower than in the major groove. The A-form is the favored conformation in low water concentrations. The alignment of the bases is not as perfect as with the B- form as the bases are tilted to the helix axis. The sugar pucker is C3´- endo because in RNA, the 2´- OH inhibits the C2´- endo conformation.

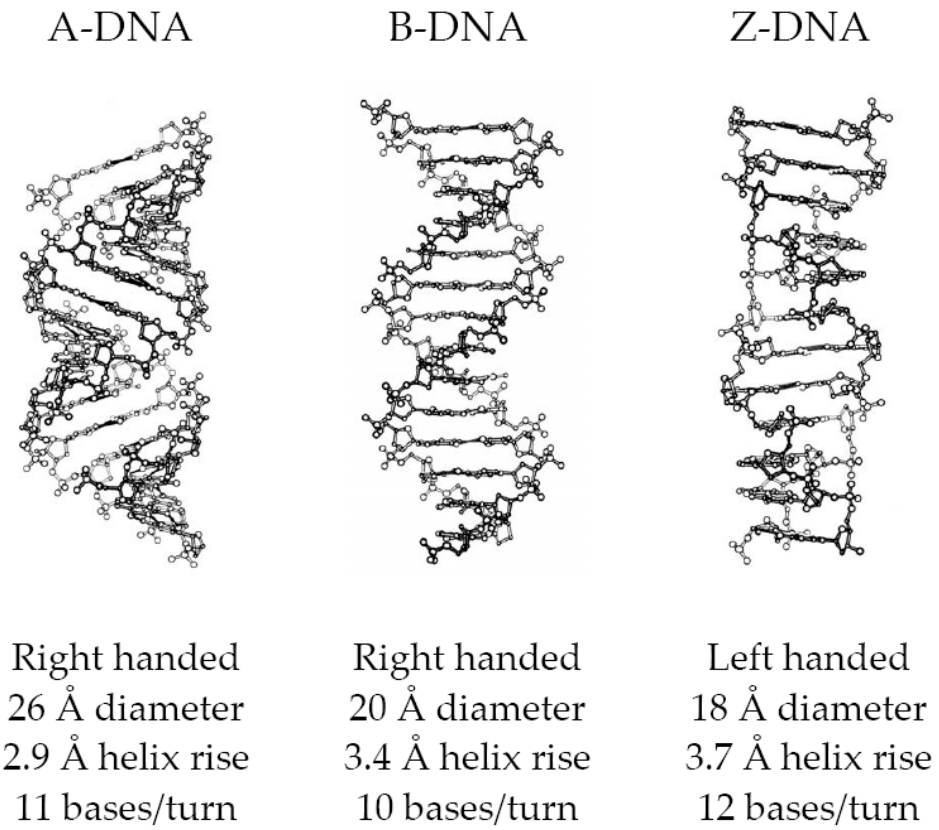

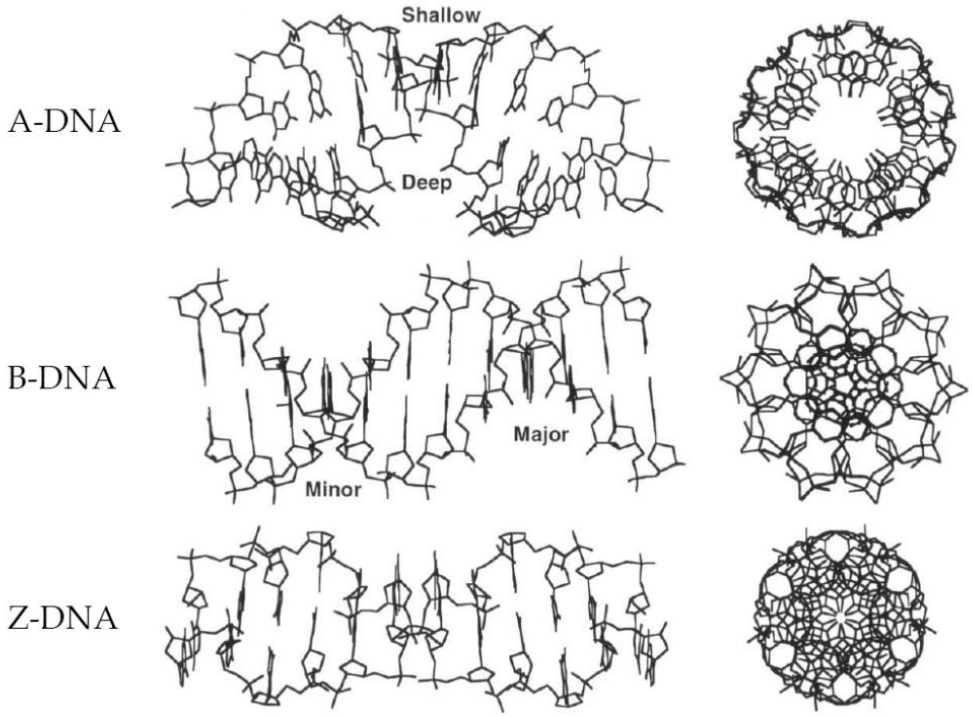

Figure 4.10 A comparison of A-, B- and Z-DNA. In the upper picture, the side view is presented with the data for the helix raise during one full turn and the number of bases needed for that. In the picture below, on the right side, the cross section of the DNA forms and, on the left, another side view is shown. Pictures taken from the lecture notes of Prof. Roland Sigel.

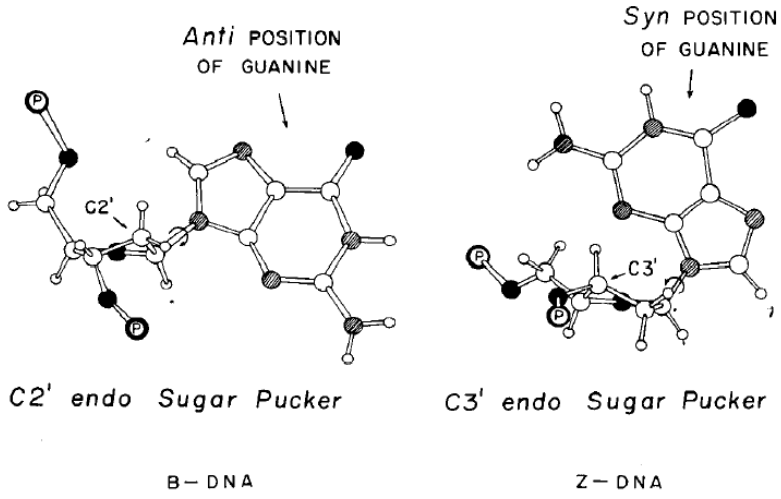

Figure 4.11 Sugar Pucker of B- (left) and Z- (right) DNA. The structure of guanosine in B-DNA and Z-DNA. The sugar is oriented so that the plane defined by C1'-O1'-C4' is horizontal. Atoms lying above this plane are in the endo conformation. In B-DNA (left), the glycosidic bond between the N9 position of the purine ring and C1' carbon of the ribose sugar is in the anti-position and the deoxyribose contains a C2' endo pucker. When Z-DNA (right) forms, the guanine rotates around the glycosidic bond into the syn position and the deoxyribose forms a C3' endo pucker. The sugar pucker change results in a different distance between the phosphate groups (Picture taken from Rich et al.[6]).

The most interesting DNA double helix structure is the Z-conformation. The name of this structure comes from the **z**ig – **z**agging of the phosphates. It is a left – handed double helix which is also found *in vivo*. It is much longer and narrower than the A- and B- conformation. This form of DNA is found especially for alternating purine - pyrimidine sequences in very high salt concentrations, some base substitutions or in alcohol [59]. The need for alternating purines and pyrimidines to form Z-DNA is due to the stacking of the bases. It is the dinucleotide unit, not the mononucleotide that is the repeating unit of this structure, for example there is good stacking within the GpC dinucleotide, but not between the (CpG). There is no real major groove found in this structure and the minor groove is very narrow[9, 60]. The bases are nearly perpendicular to the helix axis. The Zig – Zag backbone pattern arises from an alternating conformation of the bases relative to the deoxyribose sugar. In Z-DNA, the nucleotides alternate between the standard *anti* – conformation and the more compact *syn*-conformation with the base essentially sitting on top of the deoxyribose ring. This alternating pattern of *anti* / *syn* nucleotide conformations is strictly adhered in all the crystal structures of Z-DNA [61]. Thus, it is the alternation in the backbone and not the sequence that defines Z-DNA. Therefore, the guanine takes a *syn*-position and its sugar pucker is C3´- endo whereas cytosine takes the *anti* – position and its sugar pucker makes the C2´- endo conformation[62]. There is a slow exchange of the proton which should be provided for the guanine to form the Watson – Crick base pair because the hydrogen of the N2 – amine of guanine binds to the phosphate of the backbone (5´- PO)[63]. The syn – conformation of the guanine of Z-DNA and the anti – conformation of the B-DNA are shown in Figure 4.11[55].

The positions of the bases differ greatly in the different conformations of DNA. Since the position of the bases is essential for the ability of proteins or metals to bind on

the DNA strand, a closer look at the accessibility of the bases is shown

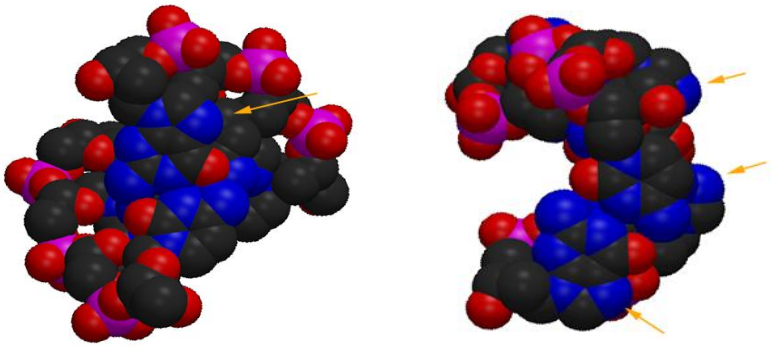

Figure 4.12. In the B- form (left), the location of the base pair is centered in the helix with the phosphate backbone organized around the periphery of the helix. The bases in Z-DNA are positioned towards the outside of the helix so that certain sites are more chemically reactive and easier accessible to metals than in B-DNA. The N7 and C8 positions of the guanine in Z-DNA, are exposed to the surrounding environment [61].

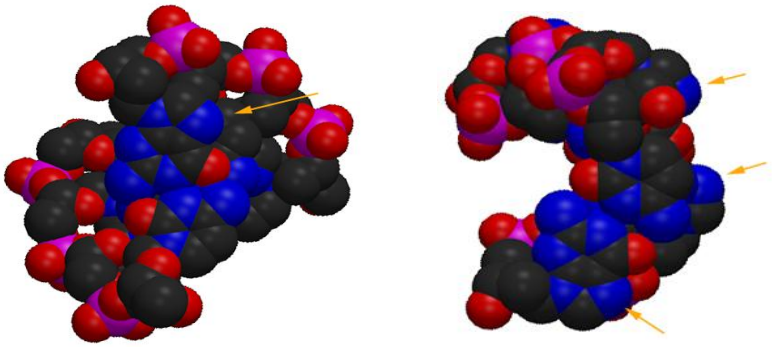

Figure 4.12 View along the axes of B- (left) and Z- (right) DNA each consisting of the sequence d(CGCG). The major groove is oriented to the right in both cases. The arrows point to the exposed N7 of guanine.

Several factors influence the B-Z equilibrium, which depends upon the DNA itself (intrinsic factors) and the environment (extrinsic factors)[64]. In the following section, both the intrinsic and extrinsic factors will be discussed.

Oligonucleotides containing alternating purine – pyrimidine sequences adopt the Z-conformation. The base sequence that favors Z-DNA is alternating poly d(GC), but also poly d(AT) can form the Z-DNA, although poly d(AT) is quite resistant to adopt

the left handed conformation. The tendency of alternating purines – pyrimidines to convert into the Z-form is d(GC) > d(AC) = d(GT) >> d(AT)[64-66]. Methylation of C5 of cytosine causes the Z-form to be more easily formed[67]. Since the methylation of cytosine occurs often in eukaryotic DNA as a form of regulating gene expression, this could be a hint of the function of Z-DNA[67-69].

The discovery of Z-DNA itself was unusual in that it was the first crystal structure of any double – stranded oligonucleotide. There had been spectroscopic evidence that there was something like a left – handed form, but this could not be proved until the crystal structure was solved. The Z-DNA conformation was first observed in very high concentration of salts (>2.5 M NaCl)[59]. The Z-form is destabilized by the charge repulsion of the negative phosphate groups. High concentrations of monovalent cations (Na^+, K^+, Li^+, etc.) can compensate the charge and therefore stabilize Z-DNA. More effective are multivalent cations such as polyamines or $[Co(NH_3)_6]^{3+}$, that are able to decrease the electrostatic repulsion and supply hydrogen bonding[70, 71]. Negative supercoiling has been found to be one of the most important factors in the stabilization of Z-DNA. To achieve the transcription of a particular gene, the polymerase goes along the DNA strand following its helical path. This movement would require a rotation of the transcription complex around the DNA axis. It was calculated that the rotation speed to of this transcription proteins would be too high to be reached by a complex structure like the transcription apparatus. In this case, the DNA has to be translocated past the stationary polymerase and rotate around its own axis while doing so. Both in eukaryotes and prokaryotes, the DNA is attached to cellular structures and the existence of these points of anchorage would prevent the free rotation of the DNA, resulting in the over winding of the DNA (positive supercoiling) ahead of the enzyme and the unwinding of the DNA (negative supercoiling) behind it (Figure 4.13)[72, 73].

Figure 4.13 The mechanism of transcription and the formation of negative supercoiling. R is the transcription ensemble consisting of the polymerase, the nascent RNA, and proteins bound to the RNA. When R is moving from left to right without turning around the DNA, the portion in front of the polymerase becomes over wound (positive supercoiling), the portion behind the enzyme becomes under wound (negative supercoiling) (Picture taken from Peck et al[72]).

4.1.4 Formation of Z-DNA

Fuertes reviewed the many molecular mechanisms proposed for the B- to Z-DNA transition. The considerable number of proposed models shows the high interest of the scientific research in the field and also shows how much it is still unknown[74].

One of these models for the transition from B- to Z-DNA involves flipping the base pairs upside down. During the process, deoxycytidine stays in its *anti*-conformation, due to the rotation of the sugar and the base; whereas deoxyguanosine changes into the *syn* conformation, since only the base rotates.

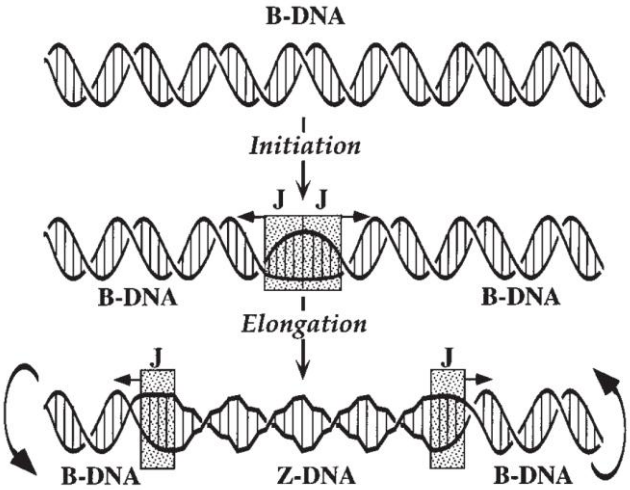

Figure 4.14 Zipper model for the B- to Z-DNA transition in negatively supercoiled closed circular DNA. The initiation step is the formation of the B-Z junction (J). Four melted base pairs can be found in these junctions[62].

Z-DNA is a higher energy conformation than B-DNA. Thus Z-DNA will only occur when plasmids are torsionally stressed, being stabilized by negative supercoiling[4, 73].

The analysis of 137 fully sequenced human genes demonstrated that sequences which could easily form Z-DNA were found in 98 cases. The most surprising was the fact that these sequences were 10 times more frequent in 5' than in 3' regions[75]. This would fit with the hypothesis that the energy to form Z-DNA *in vivo* is provided by the transcription[73].

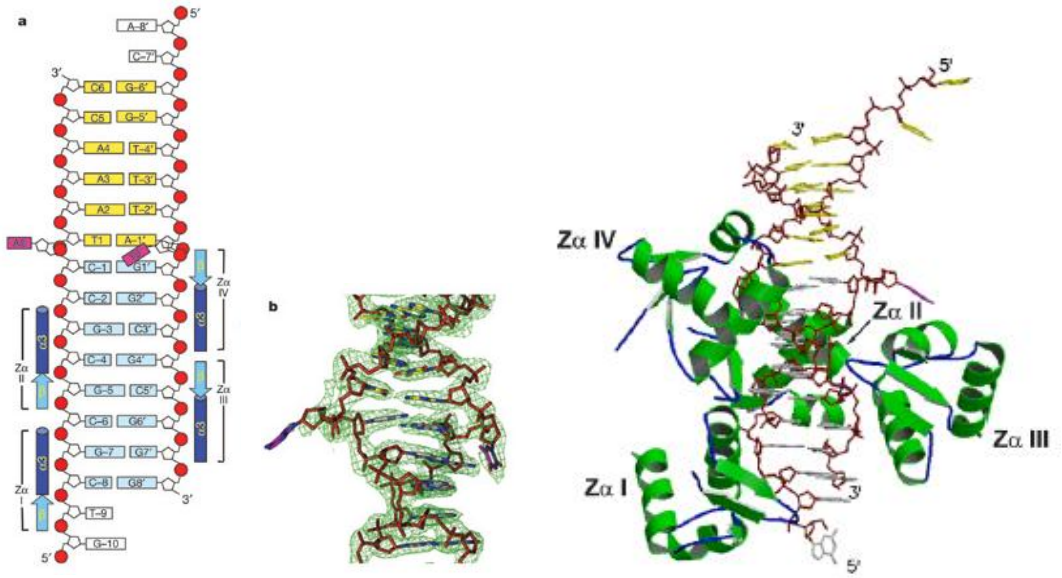

Figure 4.15 B- Z DNA junction was crystallized in the presence of the binding domain hZα_{ADAR1} from the human editing enzyme, double-stranded (ds)RNA adenosine deaminase (ADAR1), to stabilize the Z conformation. This crystal structure showed one base pair flipped out from the DNA helix. a) Schematic diagram of the DNA sequence and protein positions. Flipped out bases are A0 and T0´. b) $2F_o - F_c$ omit map of the DNA junction, calculated using native data at 2.6 Å[30].

Z-DNA can also be induced *in vitro*. The first factor influencing the Z-DNA formation is the selected DNA sequence, as mention above. Also, Z-DNA can be stabilized by high salt solutions[59]. Since in Z-DNA phosphates residues are closer to each other than in B-DNA, by introducing positively charged ions, the repulsion among phosphates is reduced. As a consequence, using multivalent cationic species lead to the formation of Z-DNA at lower concentrations of this species. Polyamines, such as spermine, or $[Co(NH_3)_6]^{3+}$ are good examples of cationic species inducing Z-DNA[70, 71].

Chemical modification of DNA can also influence the Z-DNA formation. Poly d(GC) can more easily adopt the Z- conformation by bromination or methylation of cytosine at C5 position or by bromination of guanine at the C8 position[8, 64-67]. It has to be mentioned that methylation of cytosine at the C5 is relatively common in eukaryotic DNA and there seems to be a correlation between methylation of a gene with the regulation of the transcription for that gene[6].

Several groups have studied the possible correlation between chromosomal breakpoints in human tumors to potential Z-DNA forming sequences[76, 77]. Vásquez *et al.* observed that the deletions or rearrangements generated in mammalian cells are mainly replication independent and are likely initiated by repair processing cleavages surrounding the Z-DNA forming sequence. Vásquez *et al.* proposed that these types of genomic alterations are related to the chromosome breaks and gene translocations that map near Z-DNA forming sequences in human leukemia and lymphoma[78].

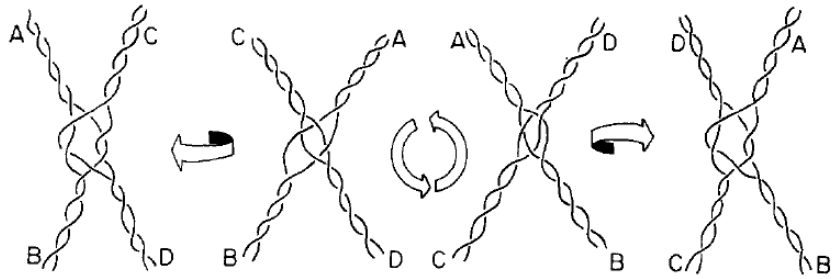

Figure 4.16 Isomerization of hemicatenated molecules. Molecules linked in a homologous sequence of d(GC) can invert one pair of arms with respect to the other by isomerization[79].

Kmiec observed that homologous pairing *in vitro* between plasmids requires the presence of Z-DNA in both plasmids, and the reaction seems to start within the Z-DNA stretches. At the region of homology, the two DNA rings become intertwined. The reaction is governed by superhelicity. The pairing starts within the $d(GC)_n$ sequence, in the Z-DNA form, and not at the unwound B-Z junction. A crucial observation was that a Z-DNA specific binding protein could block the whole process. Plasmids with $d(GC)_n{\cdot}d(CG)_n$ could be paired with plasmids with the same sequence.

However, these same plasmids could not be paired with plasmids containing $d(GT)_n \cdot d(CA)_n$ in the Z – conformation (Figure 4.16)[79].

4.1.5 Circular dichroism[80]

When light passes through an absorbing optically active substance, not only the left and right circularly polarized rays travel at different speeds, but also the two rays are absorbed to a different extend. The difference in absorption between the left and the right circularly polarized rays is called circular dichroism.

The bases are the chromophoric groups in DNA. The bases themselves have a plane of symmetry, therefore are not optically active. However, the sugar can induce a CD in the absorption bands of the chromophoric bases. Due to this, the intensity of the CD is low, since it is a secondary effect of the asymmetric sugar inducing a CD and not the bases themselves, which are symmetric. However, for nucleic acids, it is different. The hydrophobic planes of the bases tend to stack in water to minimize their exposure to the solvent. The electronic transitions of the chromophoric bases can interact with each other giving a CD spectrum of high intensity. As mentioned above, DNA can adopt different conformations. Since CD is dependent on base-base interactions, this technique can very easily discriminate among the different DNA conformations.

The intensity of the DNA CD bands in the long-wavelength (220-300nm) region is unexpectedly low. This is due to the cancellation of the many bands occurring in this region. Bands occurring at lower wavelengths (<200nm) have higher intensity and are much more sensitive to the DNA melting or the GC content of a specific sequence.

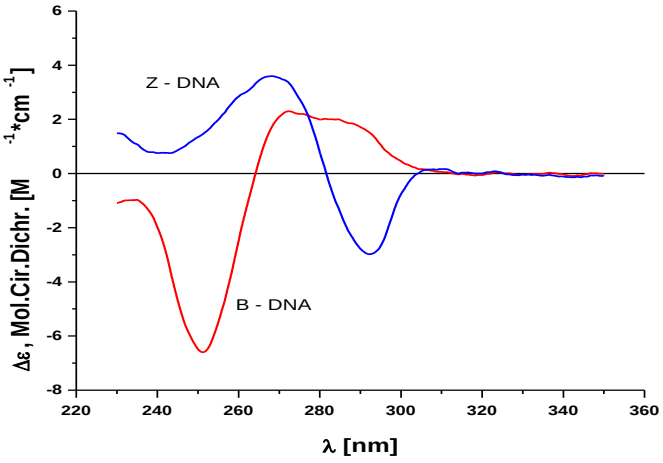

Figure 4.17 Circular dichroism of B-DNA (red) and Z-DNA (blue). Concentration of the DNA solution was 0.1 mM.

In the long-wave region, B-DNA presents a positive band at 275nm and a negative one around 250nm. The CD of Z-DNA is almost a mirror image of the B-DNA, with a negative band at 290nm and a positive one at 260nm. However this mirror image is just fortuitous and has nothing to do to the base to base interactions in Z-DNA compared with B-DNA (Figure 4.17).

4.1.6 Possible biological functions of Z-DNA.

Because the backbone chains of B- and Z-DNA run in opposite directions, B-DNA cannot be converted to Z-DNA by simply twisting on the two ends of the helix; a more elaborate mechanism must be involved. Figure 4.18 shows this conformation change from B- to Z-DNA including the intermediate stages[81]. DNA encodes biological information in at least two different ways: the sequence of the bases specifies the composition of proteins and its shape provides information to regulate the cell life. One of the biggest changes occurs when going from the right-handed B-DNA double helix to the slightly thinner and elongated left-handed Z-DNA conformation[4, 9]. It is established that DNA sequences that have the potential to adopt the Z-DNA conformation were found in biological systems[4]. Evidence of the existence of Z-DNA *in vivo* has been reported in recent years and it has been shown that the B- and Z-

form can coexist in an equilibrium of B- and Z- conformations in plasmids[82], in metabolically – active mammalian cells[83] and in polygene chromosomes from Drosophila[6, 84].

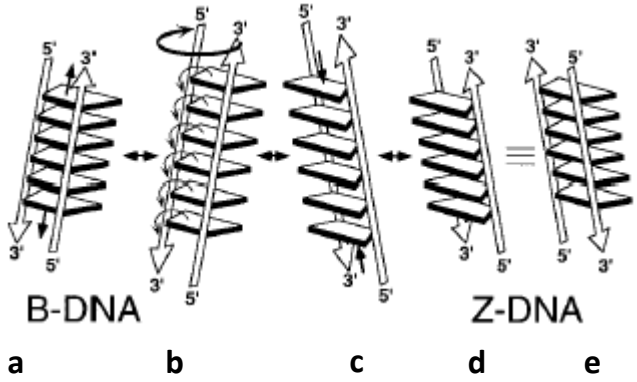

Figure 4.18 The transition from B- to Z-DNA and the reversal of the chain sense[62]. Starting from B-DNA (a): in the first step the phosphoribose backbone is extended. The bases are allowed to flip through the helix axis as the backbone is rotated from a right-handed to a left-handed direction (b). The helix then can be compacted again (c) to form Z-DNA (d and e) (Picture taken from Ho and Mooers[62]).

Z-DNA is a higher energy conformation than B-DNA and it is assumed that the energy necessary to form it *in vivo* is generated by the transcription process. The sequences that are able to induce Z-DNA, the alternating purine – pyrimidine sequence, are often found in eukaryotic genomes. For example Wolf *et al*.[85] showed that a long stretch of an alternating purine – pyrimidine sequence is found in the intron of the human corticotropin-releasing hormone (CRH) gene and that this sequence is found in the Z-DNA conformation in the transcribed gene.

Therefore Z-DNA is estimated to function as a regulator of gene expression[4]. This could become a new approach in anti-cancer therapy. Tumor cells are characterized by a higher replication rates than normal cells and require a higher reproduction of proteins and enzymes which can only be achieved by a higher rate of transcription of the DNA. Additionally to the regulatory function, the transcription – induced Z-DNA may provide information about the specific sequence where enzymes are located on the DNA.

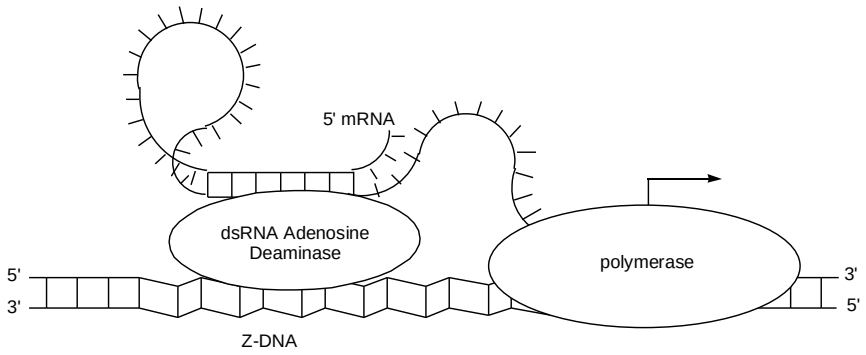

Figure 4.19 Example of Z-DNA occurring in a biological process. Interaction of ADAR1 with double-stranded RNA and Z-DNA. The Z-DNA binding site of the domain of ADAR1 is named Zab, and its subdomain, Zα, can recognize the characteristic features of left-handed DNA: the zig – zagging phosphates backbone, and the protruding C8 of the alternating syn *guanosine*[4, 86]*. Picture taken from Dr. Spingler.*

Each conformation of DNA has its own biological role in the regulation of the life of the cell[68, 73, 87]. To understand their biological effects, gathering information about any of these conformations is very important. DNA provides its genetic information in at least two different ways. The most important is given by the sequence of the nucleotides which specifies the composition of proteins. The second way of providing information is through its shape and conformation. DNA itself can regulate its own gene expression by enabling or blocking the transcription complexes to read the information of the sequence[4]. Z-DNA provides an interesting research area, since Z-DNA is such an unusual conformation of DNA with very controversial biological functions which are not yet proven. To selectively bind to Z-DNA and to be able to recognize the Z- conformation can be achieved since this form is different from all the other conformations. The special geometrical conformation of Z-DNA and its specific sequence of nucleobases can provide areas where complexes can strongly and specifically bind.

4.2 Abilities of Porphyrins to detect DNA

4.2.1 Interactions with Z - DNA

The interaction of porphyrins and related molecules with DNA was described as early as 1979 and followed by intensive studies by Pasternack *et al*[88-90]. He exposed DNA to different porphyrins and found in that positively charged porphyrins have unique behaviors. Apart from the obvious ability to intercalate in between the bases because of the flat nature of the molecules, two different *modi* of interaction were described early on.

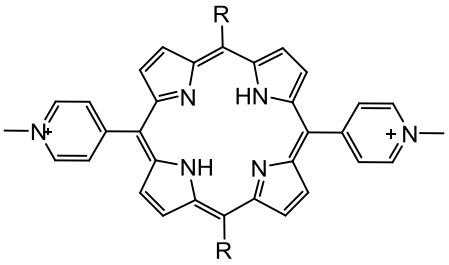

Figure 4.20 Example of an A_2B_2 – type porphyrin having three modi of interaction with DNA if moiety R is sterically non – demanding. The solubility of the porphyrins and thus ability to interact with components of the cells is due to the positive charge of the moieties.

The side on mode of interaction was mostly observed by symmetrical positively charged porphyrins, the attrition of porphyrins in the grooves of the DNA structure was mainly described for A_2B_2 - type porphyrins (Figure 4.20) in which the R moieties are sterically non – demanding[91-95]. Experiments with calf thymus DNA showed a substantial competition of positively charged porphyrins against ethidium bromide (a well-known intercalator and staining agent of DNA and cells) [91, 94, 96, 97]. These studies focused on fluorescence spectroscopic analysis as well as UV vis. Other studies in the late 80s and early 90s tried to determine the interaction of the various flat molecules, amongst these also phthalocyanines, porphyrins and acridines with DNA. X – Ray analysis and later on molecular modeling confirmed the interaction and also lead to several pharmaceutical applications based on these molecules[92, 98, 99]. For the interaction with B-DNA, it was found that the porphyrin has a pre*cis*e center of symmetry with the N-methylpyridinium groups inclined to the central porphyrin at

angles of 66-72°. It has been shown that only the CpG site can have full ligand intercalation, since the thymine methyl group sterically hinders intercalation at the TpA sites. Modeling also indicates the importance of electrostatic effects in the low-energy forms of intercalated and part-intercalated complexes at both sequences.

These molecules are also well studied towards their specific characteristics and widely used for other applications such as flat screens and are thus well understood. Nevertheless, synthesis studies of porphyrins and related molecules are still published due to the difficult steps involved to obtain a reasonable yield and to make more complex porphyrins accessible. Nature uses porphyrins as well in essential building blocks such as hemoglobin or chlorophyll. Balaz *et al.* proposed a side on binding mode for all non-intercalating porphyrins and coordination to N7 of the DNA's guanosine if the central metal center contains a vacant binding site.

4.2.2 Interaction of porphyrins with G – Quadruplexes

Porphyrins can also interact with different conformations of DNA. About 10 years ago, Wheelhouse *et al.* discovered that cationic porphyrins could stabilize G-quadruplex structures at the end of chromosomes and thereby inhibit the telomerase [100, 101]. They used extended porphyrins with bulky or long side arms as chromophores to fit on top of the quadruplex structure. At the ends of chromosomes are regions of DNA called telomeres which have the function to replicate chromosome ends using the enzyme telomerase, because the enzymes that replicate DNA cannot copy the extreme 3' ends of the chromosomes.

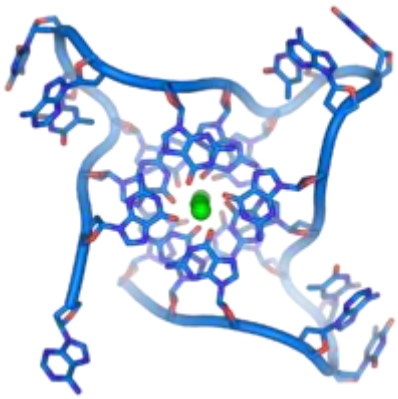

Figure 4.21 Top view on a G – Quadruplex structure with the central potassium ion in green. Picture taken from Wikipedia: Quadruplexes.

Human telomeres are nucleoprotein complexes containing the repeated DNA sequence $d(GGGTTA)_n$ (n = 100 - 3,000) that is paired with its complement strand, except for a short (24 - 400 base) single-stranded 3' overhang. Telomeric DNA gets shortened by each successive round of cellular replication, possibly resulting in a molecular clock that limits the total number of replication cycles a normal cell can undergo. These quadruplex structures have become an active field of the anti – aging and cancer research and several patents have been filed to protect various approaches to stabilize this unique conformation[100, 102-104]. Molecules that bind to G-quadruplex structures may inhibit cancer growth by at least two mechanisms which have a common basis: the stabilization of the G – quadruplex structure.

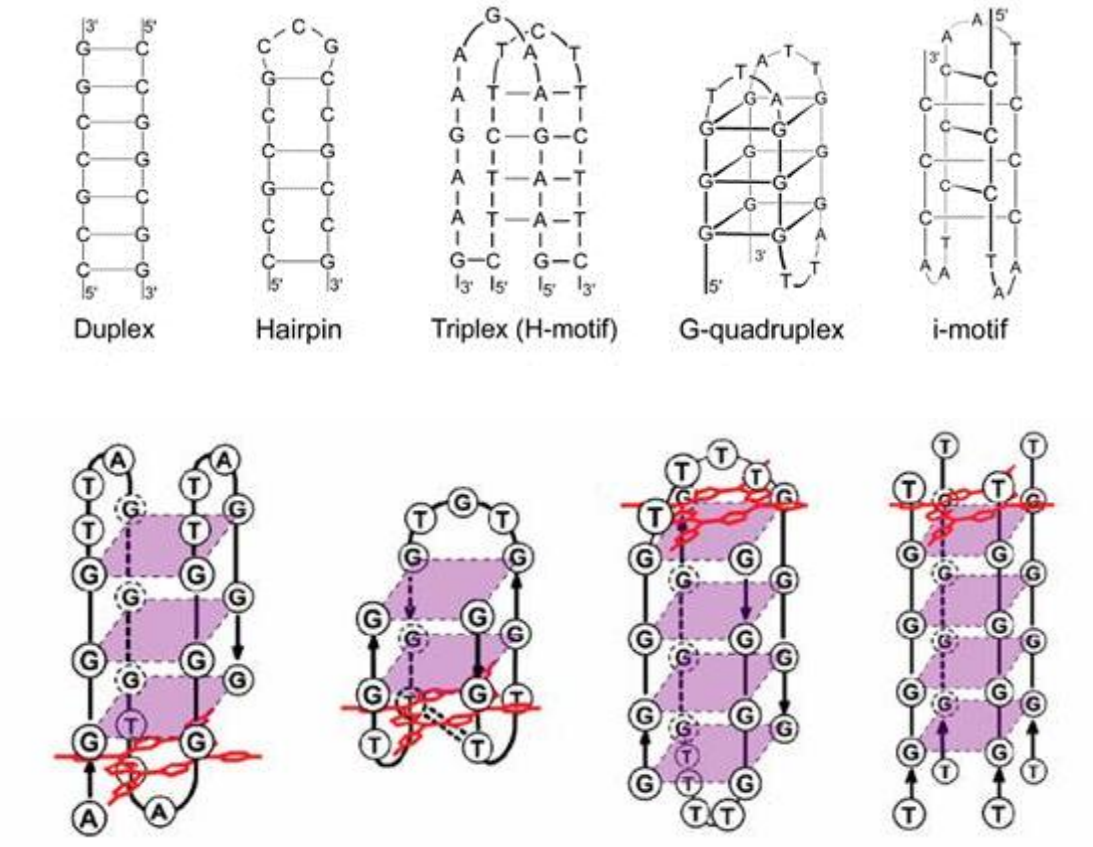

Figure 4.22 Comparison of different DNA motifs in G – rich sections of the DNA. Picture taken from http://www.bioorganic-chemistry.com/research.html. Possible interaction of porphyrins with quadruplex DNA.

4.3 Background and motivation for this work

Aim of the project was to detect the presence and location of the Z-DNA within the cells. Although sequences that can adopt Z-DNA are widely present in human DNA, the biological role for Z-DNA is not really understood yet. Short fragments of Z-DNA have been found in both prokaryote and eukaryote cells. These Z-DNA regions could have a crucial role in the expression of some genes[54, 87, 105-107]. The initial idea of the project was to find a specific binding molecule that would preferably interact only with Z-DNA also *in vivo*. Balaz *et al* proposed a zinc porphyrin to detect Z-DNA and a side on coordination of the central zinc towards N7 of the porphyrin[11]. This concept was taken as a basis to determine the location of Z-DNA in living cells. It is still not understood in which stage of the cell cycle, Z-DNA is occurring and how this effect the

expression level of certain proteins. It could become important for the specific treatment of cancer types to be able to block or stabilize or at least monitor some conformations of DNA such Z-DNA[26, 108-110].

4.4 Results and Discussion – Interaction of Porphyrins with DNA

4.4.1 Interaction of metallo – porphyrins with different conformations of DNA

The development of more complex porphyrins includes also the introduction of a core metal center. This metal determines whether an axial coordination hinders an intercalation (and therefore favors a side on coordination), but it also controls its spectroscopic properties. For example, the difference of the Q – band can shift up to 70 nm (from 550 nm to 620 nm) upon the exchange of cobalt to a zinc center. These changes can be observed via different methods. In Table 4.1, an overview of the interaction of porphyrins (visibly active) with DNA is summarized. These effects will be further discussed in the description of the results[111].

	Viscosity	**CD**	**Visible: Intensity of the Soret band**	**Visible: Shift of the Soret band**
Intercalator	Increase	Negative signal (near the Soret band)	Hypochromicity	Red
Outside stacking	Slight decrease	Conservative signal (= up and down peaks of almost equal intensity near the Soret band)	Hypochromicity	Slight red
Outside binding without stacking	Decrease	Positive signal (near the Soret band)	Hyperchromicity	Red

Table 4.1 Spectroscopic changes due to different porphyrin-DNA interactions according to Prof. Luigi G. Marzilli including a description of the different modes of interaction of porphyrins and DNA. The intercalation causes the greatest change in the visible UV spectra with a red shift of the Soret – and Q – band.

4.4.2 Interaction of lead porphyrins with guanosine

First, the interaction of the porphyrin molecules towards 5'-guanosine monophosphate (5'-GMP) was followed by UV titration. As shown in Figure 4.25, the types of coordination and electrostatic interactions are not quite as manifold compared to the interaction with DNA. Nevertheless, there are 3 different kinds of interaction and combinations of the three possible. This experiment was chosen to determine the most suitable molecules to be followed by a study with poly d(GC). As a simpler model system, the titration of porphyrin versus guanosine (G) was also carried out, but only weak interactions could be detected (see Table 4.2, left side).

Starting point was the synthesis of the DNA interacting moiety, the 5,10,15,20-tetrapyridyl-porphyrin, followed by a methylation and metallation step to obtain the 5,10,15,20-tetra-(4-methyl)pyridinium-porphyrin. The interaction of these molecules was tested as a model system towards the second step of this project, the formation of the Z-DNA specific porphyrin array. The synthesis of the basic porphyrin molecules and the following steps towards the water soluble [112-116], four fold methylated species was published[117, 118]. Nevertheless, optimization of the tedious workflow and the cleaning and separation of the final porphyrins was required. We choose a one-pot synthesis described by Lindsey *et al.* and Fleischer *et al.* for the porphyrin synthesis [117, 119]. The methylation was carried out as described in the literature using methyl iodide. The metallation was performed by reacting the water-soluble, tetra-methylated porphyrin with the acetate salts of either zinc, copper, or nickel (Scheme 4.1).

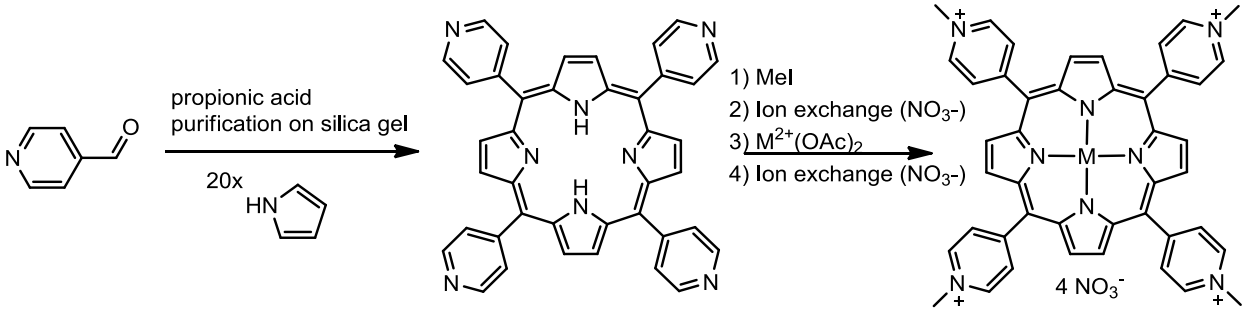

Scheme 4.1 Reaction scheme to obtain the 5,10,15,20-tetra-(4-methyl)pyridinium-porphyrin.

The methylation was carried out according to a slightly modified procedure described in literature, by treating the porphyrin with methyl iodide in DMF for 24h[120, 121]. After precipitation with acetone/ether and washing with acetone and cold water, the introduction of a metal into the porphyrin was carried out in water at 50°C using a water soluble metal salt (nitrate, tetrafluoroborate) and stirring for 24h. The yield in both reactions was almost quantitative yielding high purity as shown in the HPLC trace (Fig. 4.23).

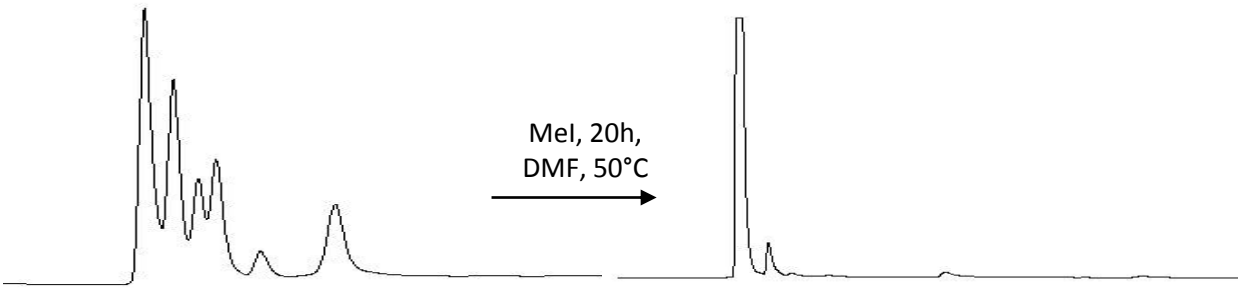

Figure 4.23 HPLC traces of the synthesis of 5,10,15,20-tetramethylpyridinium-porphyrin. After 1 hour (top) a vast variety of mono-, cis- & trans-di, tri-, and tetramethylated porphyrin is synthesized. After 20 hours, only a small fraction of the trimethylated species is seen, which will after an additional 4 hours turn fully react towards the tetramethylated porphyrin.

In the crystal structure below, porphyrin **10** was crystallized from water with the help of dioxane. The vacant space in the center of the porphyrin can nicely be seen. Only two counter ions are shown.

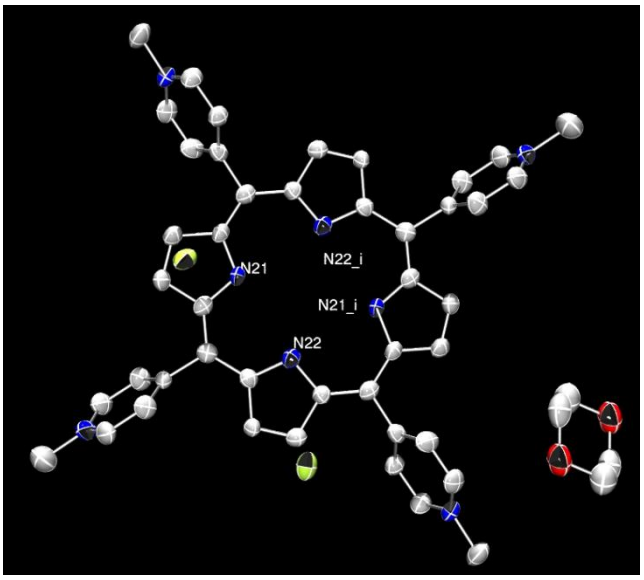

*Figure 4.24 Povray plot of porphyrin **10** crystallized from a dioxane/water mixture. Elipsoids are drawn at 50% probability. Hydrogen ions are omitted for clarity.*

These molecules were exposed under different conditions to bases, oligonucleotides and DNA in both the B- and Z- conformation. The stability constants (pK) were calculated according to the concentration G or 5'-GMP added (corrected by the dilution factor). Different central metal ions caused changes in the UV vis signal but were comparable for the stability constants. The Soret maxima of compounds **10** H_2TMPyP, **11**, NiTMPyP, and **14**, ZnTMPyP are shown in Table 4.2. All Soret bands lay in the region between 400 – 440 nm. The interactions of the porphyrins showed, as expected, different spectroscopic behaviors. For compounds **10** H_2TMPyP, and **11**, NiTMPyP, the Soret maxima shifted upon titration of 5'-GMP up to 6 – 8 nm into the red. The interaction of compound **10**, H_2TMPyP and compound **11**, NiTMPyP with the 5'-GMP can therefore be characterized as a mostly electrostatic driven interaction because there are no other interactions plausible. Compound **10**, H_2TMPyP does not have a vacant coordination site and compound **11**, NiTMPyP has two occupied axial binding sites. In the case of the compound **14**, ZnTMPyP, the situation is different since zinc can suit 2 axial coordinating ligands. The formation of a shoulder at 445 nm is an indication of a formation of a second species caused by a coordination of 5'-GMP towards the central metal ion of the porphyrin. The possible interactions

determined by this experiment are summarized in Figure 4.25. According to the axial ligands of the central ion, the electrostatic interaction gains importance.

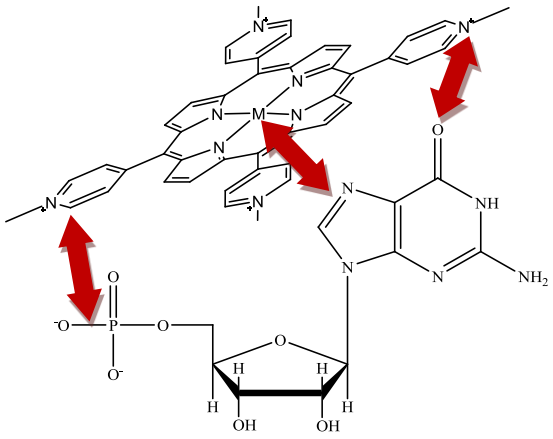

Figure 4.25 Possible interactions of zinc porphyrin with GMP, from left to right: electrostatic interaction of positively charged pyridinium moiety, coordinative interaction of the central zinc ion with N7 of guanine, electrostatic interaction of positively charged pyridinium moiety and oxygen(O6) of the base.

	Guanosine (G)	5’- guanosine – monophosphate (5’-GMP)
H_2TMPyP	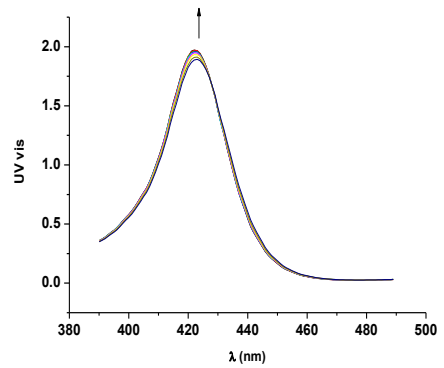 pK = 2.3	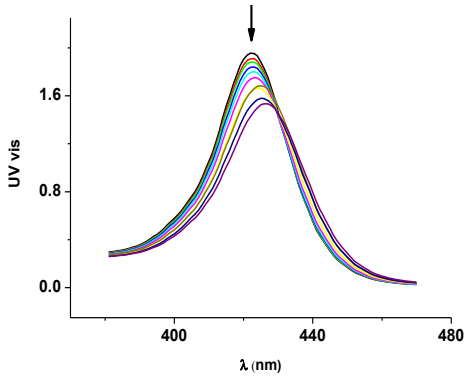 pK = 4.3
NiTMPyP	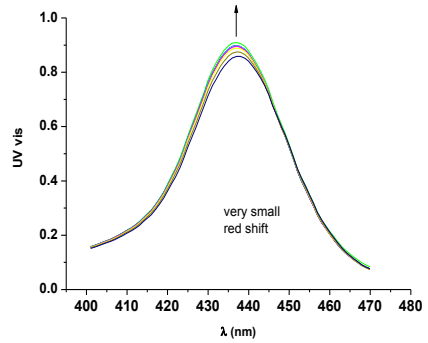 pK = 2.9	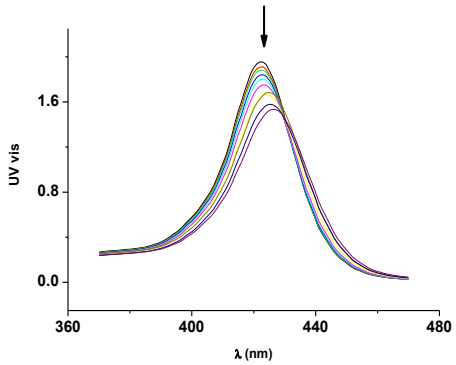 pK = 4.8
ZnTMPyP	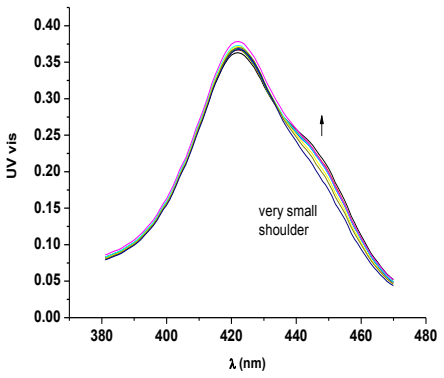 pK = 2.9	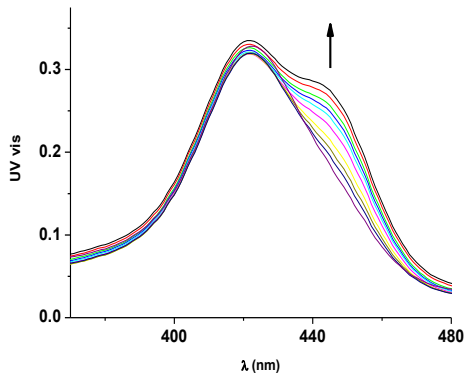 pK = 4.6

*Table 4.2 Comparison of the interaction of H_2TMPyP **10**, NiTMPyP **11**, and ZnTMPyP **14** with guanosine (left) and 5’-guanosine monophosphate (right). Conditions: 10^{-5} M **M(II)TMPyP** (M(II) = H_2, Ni, Zn) aq. was titrated with either G or 5´-GMP (0–40 eq.) at pH 6.5 (NaCac-Buffer). Dilution effects were corrected*

Surprisingly, in the case of the nickel porphyrin, the electrostatic effect dominated over the possible coordination of nickel towards the N7 of guanine. Obviously, the

nickel's axial ligands coordinated better than the guanosine. The formation of a shoulder beside the Soret band in case of the zinc porphyrin **14** can only be explained by the appearance of a new species, formed by the coordination of the zinc center to the N7 of guanine. Zinc porphyrins in most cases feature only one, but strong axial ligand building up a square planar pyramid. Even a water molecule can become a ligand (see chapter 5, Figure 5.14, and Table 5.2).

4.4.3 Interactions of porphyrin treated poly d(GC) with Z- inducing agent

Porphyrins are interacting in various modes with DNA as mentioned in Table 4.2. To discriminate in between the effect of the Z-inducing agent and the porphyrins **10**, **11**, and **14** towards the different conformations of DNA, two types of experimental setups were carried out. The Z-DNA inducing agent was chosen to be spermine rather than metals or high salt concentrations due to its non-binding properties. The pK_a values for spermine are 11.50, 10.95, 9.79 and 8.90[122], which makes it a four cation at pH = 7.0. It is the most effective and smallest (apart from metal ions such as zinc) inducing agent and it does not compete with the metal centers of the porphyrins. Spermine is a natural compound involved in cellular metabolism found in all eukaryotic cells and is an essential growth factor in some bacteria. Spermine is associated with nucleic acids and is thought to stabilize helical structure. As a buffer system, we chose the well-established sodium cacodylate buffer due to its non – coordinating character and reasonable buffer capacity at around pH 5.5 – 7.5[123]. In the first experiment, B-DNA was treated with the corresponding porphyrin followed by the attempt to induce Z-DNA. The experiment was monitored by CD spectroscopy to determine the change of the corresponding conformation of poly d(GC). In the second experiment, the DNA in its B-DNA form was treated with spermine to induce Z-DNA followed by the treatment of equivalents of the corresponding metal porphyrins.

The B-DNA treated with increasing amounts of the metal free porphyrin **10**, which can intercalate into DNA, resulted in a small uplift of the signal at 290 nm and developing a negative signal in the region of 435 nm. At a concentration of 0.2 equivalents porphyrin versus the number of base pairs, 0.1 equivalents spermine were added (Graph 4.1). The spectra strongly increased in both regions. The negative band at 435 nm further increased and an additional positive signal at 470nm appeared. Shortly after the addition of the potential Z-DNA inducing agent, the DNA precipitated although not yet neutralized. It is clear that the DNA remained in a right – handed helical conformation. Obviously the spermine caused some of the porphyrin to stack around the DNA.

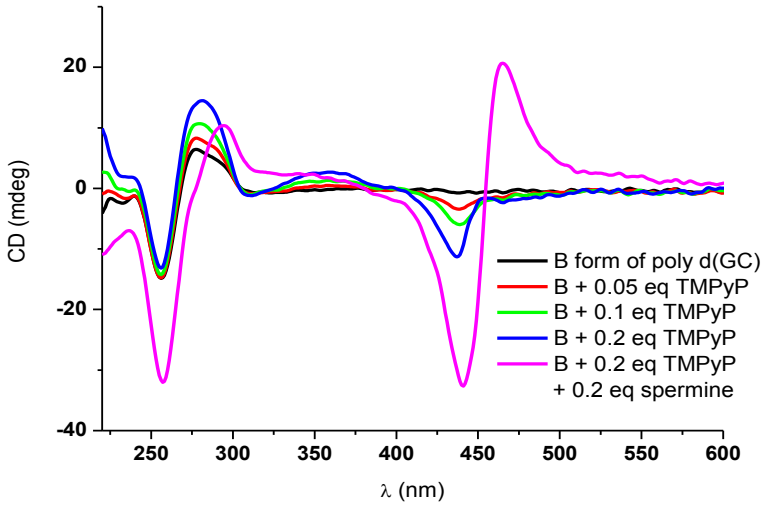

*Graph 4.1 CD spectra of poly d(GC) in its B- conformation (black), treated with molecule **10** followed by the addition of the Z-DNA inducing agent spermine. Concentration of poly d(GC) = 0.1mM (in base pair), Buffer: 1 mM sodium cacodylate pH 7.0.*

The same experiment with molecule **11** showed a different effect. After the addition of the porphyrin, the band at 425 nm of the porphyrin, which has become chiral, occurs without a large change in the region of the DNA (220 – 320 nm, see Graph 4.2). The only change is a slight decrease of the signal at 290 nm which indicates a distortion of the DNA (red, Graph 4.2) upon side on conformation or an intercalative mode. This would also explain the effect of the spermine towards the DNA: upon addition, only the DNA region is changed towards a more compact conformation of

the DNA (purple), the missing hump at 305 nm indicates a more narrow structure of the DNA.

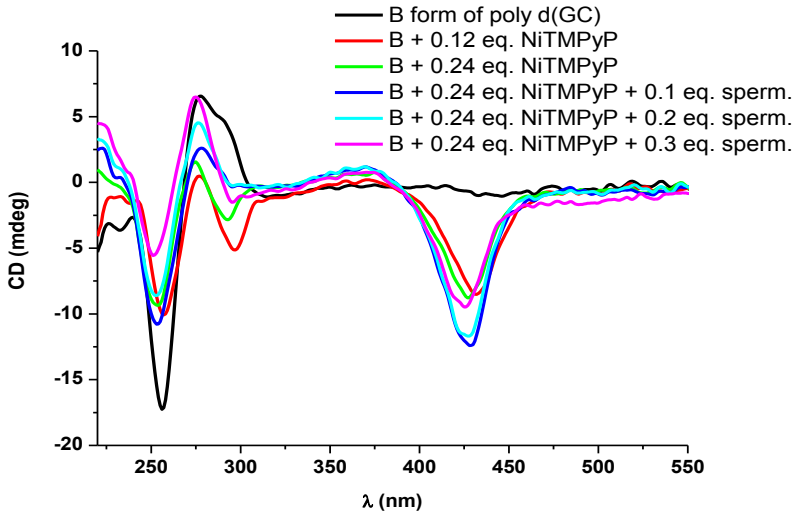

*Graph 4.2 CD spectra of poly d(GC) in its B- conformation (black), treated with molecule **11** followed by the addition of the Z-DNA inducing agent spermine. Concentration of poly d(GC) = 0.1mM (in base pair), Buffer: 1 mM sodium cacodylate pH 7.0.*

Spermine could not induce Z-DNA likely due to the semi – intercalative and side on conformation of the porphyrin towards the DNA. A different, even more complex result was obtained from the experiment carried out with the zinc porphyrin **14** (Graph 4.3). Upon addition of the porphyrin, no conformational change is observed in the DNA region. Also the band at 435 nm is very small and shows the characteristic up and down of the side on coordination. After adding spermine to the solution, the signal of the DNA flips completely (220 – 320 nm). Since the signal in the DNA region changes upside down, we assume left – handed helix. The weak signal around 435 nm remains. The exact interpretation of these results is difficult.

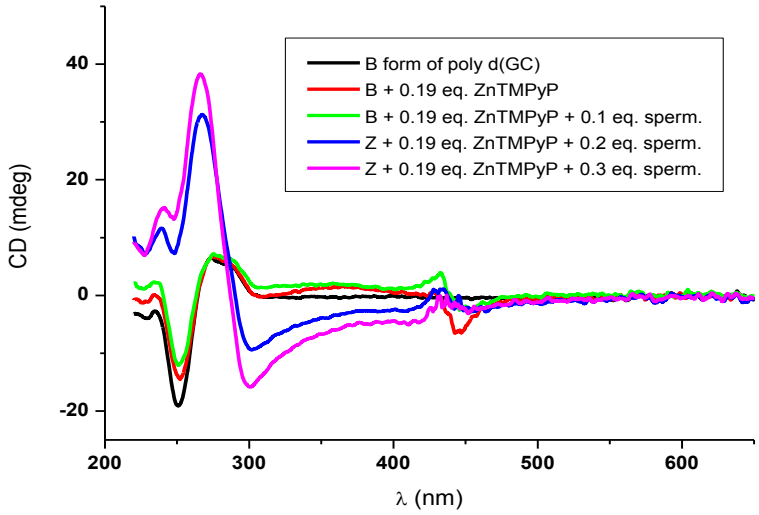

*Graph 4.3 CD spectra of poly d(GC) in its B- conformation (black), treated with molecule **14** followed by the addition of the Z-DNA inducing agent spermine. Concentration of poly d(GC) = 0.1mM (in base pair), Buffer: 1 mM sodium cacodylate pH 7.0.*

It shows that the effect of the porphyrin in combination with the Z- inducing agent spermine is not straight forward. The porphyrin can interact in various modi with the DNA and effect its conformation and ability to change this conformation. No Z-DNA could be induced with the pre – treatment of DNA with intercalative and semi – intercalative porphyrin, as expected. The zinc porphyrin cannot intercalate and favors a side on coordination or interaction with DNA and thus can allow a Z-DNA formation.

4.4.4 Interactions of lead porphyrins with previously induced Z- conformation of poly d(GC)

The interaction of molecules **10**, **11**, and **14** with poly d(GC) were carried out similarly compared to the experiments described above. Aim of these experiments was to a) identify which compound is able to detect Z-DNA conformation of poly d(GC), b) which type of interaction dominates, c) how the competition of positively charged inducing agents hinder the interaction of porphyrins with DNA, and d) if the results are comparable with the known literature examples.

When previously induced Z-DNA was treated with compound **10**, H_2TMPyP, it flipped back to its B- conformation[124, 125]. The intercalating molecule forces poly d(GC) back into its lower energetic state, because due to its higher strain on the backbone, the Z-form does not tolerate an intercalation and flips back into its more relaxed B-conformation. After this conformational change after the addition of surprisingly few 0.08 equivalents, more equivalents of **10** were added. A conformation was formed we interpret as a distorted right handed helix with porphyrins intercalating and stacking around the helix. Due to the high charge and maximum capacity of intercalation reached, the double stranded poly d(GC) might be forced to provide even more inter-base space and therefore distort itself. The poly d(GC) could not be forced back to its Z- conformation at the addition of spermine. After the addition of even more porphyrin (at 0.25 equivalents) the DNA precipitated. Nevertheless, a small signal at 445 nm upon addition of the porphyrin revealed a CD signal related to the change at the Soret band of the porphyrin. This indicates a distortion and change of the surrounding of the porphyrin.

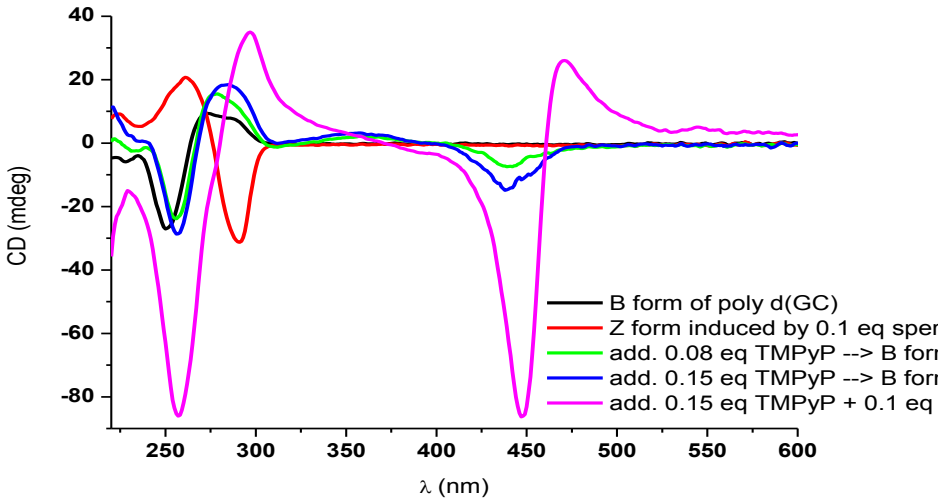

*Graph 4.4 CD spectra of poly d(GC) in its B-conformation (black), induced into its Z-conformation followed by the treatment of **10**. Concentration of poly d(GC) = 0.1mM, Buffer: sodium cacodylate pH 7.0.*

Nickel porphyrin **11** was added to a solution of previously induced Z-DNA. In Graph 4.5, the addition of the porphyrin can be followed, indicating a combination of a side

– on interaction and intercalation of the porphyrin with the DNA. The Z-DNA signal at around 290 nm becomes more positive upon addition of **11**. Also the positive signal at 255 nm undergoes a red shift and slightly changes in intensity. At 435 nm, the Soret band of **11**, a small negative signal occurs upon addition of around 0.15 equivalents of the nickel porphyrin. If the Z-form is still present is difficult to determine due to the party intercalative and thus reversing of the conformation back to the B- form. The fact that the central nickel atom does have a vacant coordination site creates multiple binding mode possibilities which cannot be sufficiently determined by CD spectroscopy. Nickel porphyrin **11** is only able to partly intercalate because it can coordinate an anion at its axial position. The raise of the band at 435 nm indicates though that the porphyrin might be suited for Z-DNA detection.

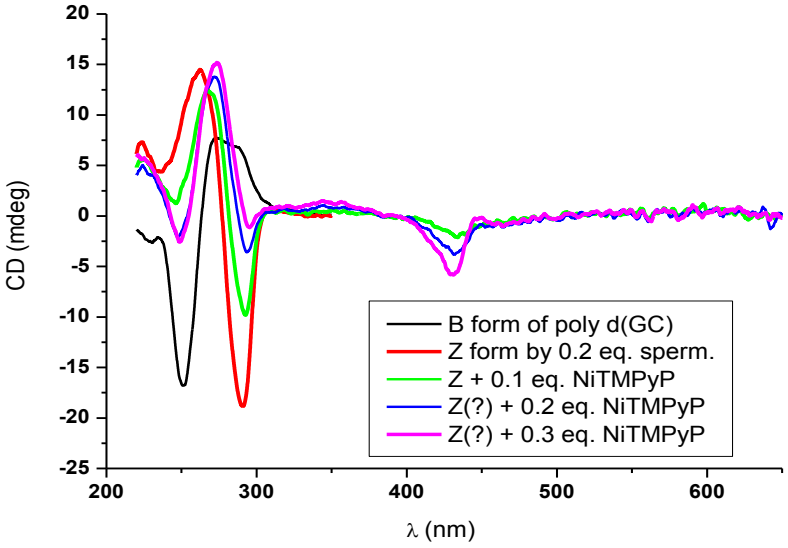

*Graph 4.5 CD spectra of poly d(GC) in its B- conformation (black), induced into its Z-conformation followed by the treatment of **11**. Concentration of poly d(GC) = 0.1mM, Buffer: sodium cacodylate pH 7.0.*

Following this pattern, the zinc porphyrin **14** was chosen as a non-intercalating molecule due to its axial water molecule (see Table 5.2)[11, 126-128]. Compound **14** was added to poly d(GC) in its Z- conformation and monitored via CD spectroscopy. Upon addition of 0.12 equivalents of **14**, a small band at 440 nm can be observed which correlates with the structural distortion and change of rotation angle and chirality of

the central metal of the porphyrin. The Z-DNA signal of the DNA is only undergoing small changes upon the addition of the porphyrin which proves the intact Z-conformation[11]. The DNA related CD signals from 220 – 320 nm are only changed a bit such as a small red shift of the signal at 255 nm and an increase of the signal at 290 upon addition of the signal. Apart from these small changes, the biggest change is the raise of the band at 440 nm which can be used as an internal probe for the detection of Z-DNA[10, 129-132]. The double signal (up and down) is an indicator of a side on conformation or even coordination to the DNA which is detected (statistically) equal with regard to its detection direction. The zinc porphyrin suits best to detect Z-DNA in a model solution and was chosen as the lead compound for the follow on studies[88-90, 95, 111, 133].

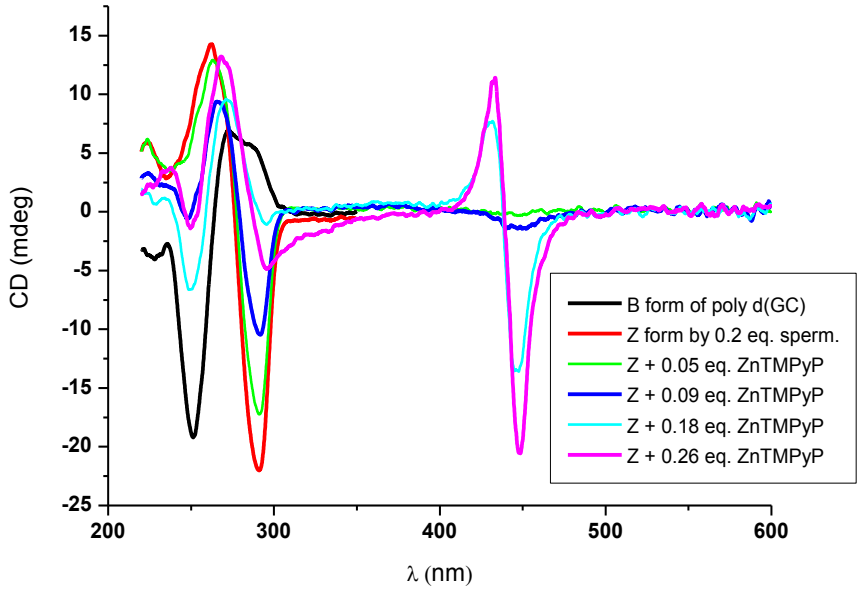

*Graph 4.6 CD spectra of poly d(GC) in its B- conformation (black), induced into its Z-conformation followed by the treatment of **14**. Concentration of poly d(GC) = 0.1mM, Buffer: sodium cacodylate pH 7.0.*

In comparing of the relevant Soret bands of the tested compounds shows, that the treatment of the zinc porphyrin with the Z-conformation of poly d(GC) shows the most significant changes which enable us to detect the presence of Z-DNA.

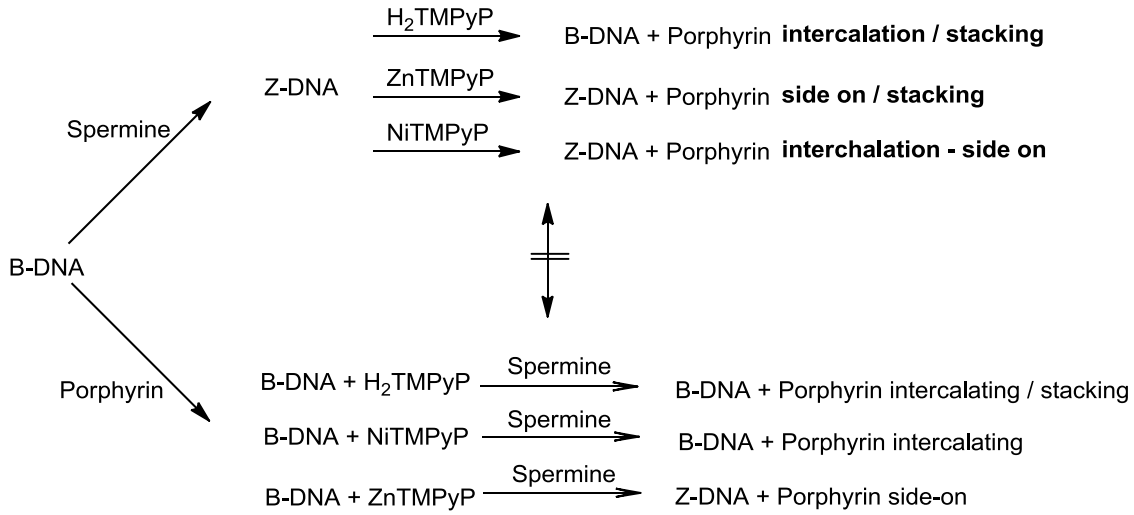

Figure 4.26 Overview of the different interactions of the lead porphyrins with B- and Z-DNA conformations after or before treatment with spermine.

4.4.5 Calculations of the coordination of zinc porphyrin towards DNA

Interestingly, very different interactions patterns of the different porphyrins interact with DNA were obtained. With the help of a computational model established in the lab of Prof. Dr. Jürg Hutter, the different electronic states of the porphyrins were modeled with different axial ligands. In a second step, the minimum repulsion of compound **14** interacting with different conformations of DNA was calculated.

Porphyrin **14** was modeled to determine the distances of the water molecule to the central zinc center. Surprisingly, the energetic lowest conformation of the porphyrin was a slightly distorted, non-planar conformation with a distortion angle of 7° between the pyrrole rings.

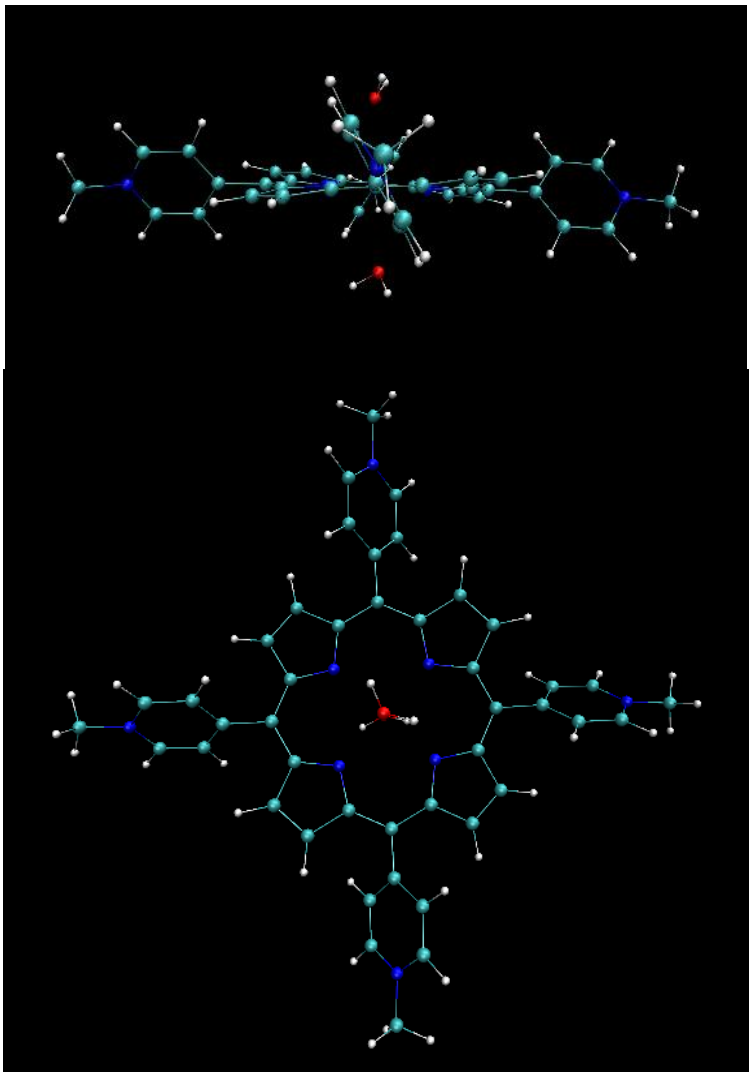

*Figure 4.27 Calculated structure of zinc porphyrin **14** with 2 water molecules in the axial position of the central metal ion. The distortion of the porphyrin is 7° within the pyrrole rings. The program CP2K was run with the following parameters: Marvin Sketch, Blyp-Funktional (Standard), triplez2p, Basis, Plainwave Density Cutoff: 280 Rydberg,* in vacuo*.*

The energetic HOMO and LUMO levels of porphyrin **14** were also calculated. The LUMO levels are located on the periphery of the molecule. This characteristic is mostly derived by the positive charge located at the methylated nitrogen atoms of the pyridines. Most electron density is located around the central porphyrin ring and the central metal ion (Figure 4.28).

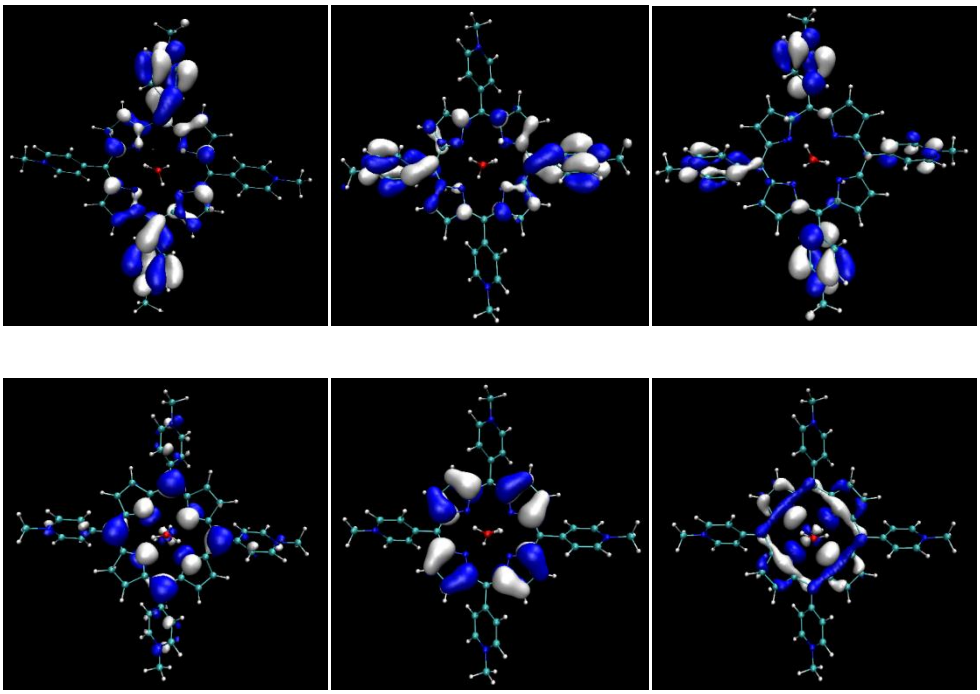

*Figure 4.28 Top: LUMO, LUMO -1, and LUMO -2 levels of porphyrin **14** with 2 axial water molecules calculated by CP2K. Bottom: HOMO, HOMO+1, HOMO +2 levels of porphyrin **14**. The red molecules in the middle represent the axial water molecules covering the central zinc atom.*

The same result was observed for porphyrin **14** with two axial chloride anions. The LUMO levels are located around the peripheral pyridyl residues and the HOMO levels in the center. The main difference is that the HOMO relocates around the axial chloride anions (Figure 4.29). The calculations towards a better understanding of the interaction of the porphyrin and the polyanion DNA are therefore leading towards the conclusion, that an electrostatic interaction between the negatively charged backbone of the DNA and the positively charged periphery of the porphyrin is the most likely scenario of interaction. This is contradictory to previous experimental evidence in the literature[99, 134-138].

In the literature, it is for example suggested, that a similar copper complexes, which contains leaner residues, can bind to DNA by different binding modes via electrostatic interaction and by intercalation of the aromatic ring into the base pairs of DNA. The functional groups on the side chain of the macrocycle play a key role in deciding the mode and extent of binding of the copper complexes to DNA[136]. A similar case can

be expected for the interaction of zinc and copper porphyrin **14** and **11** when exposed towards B- or Z-DNA.

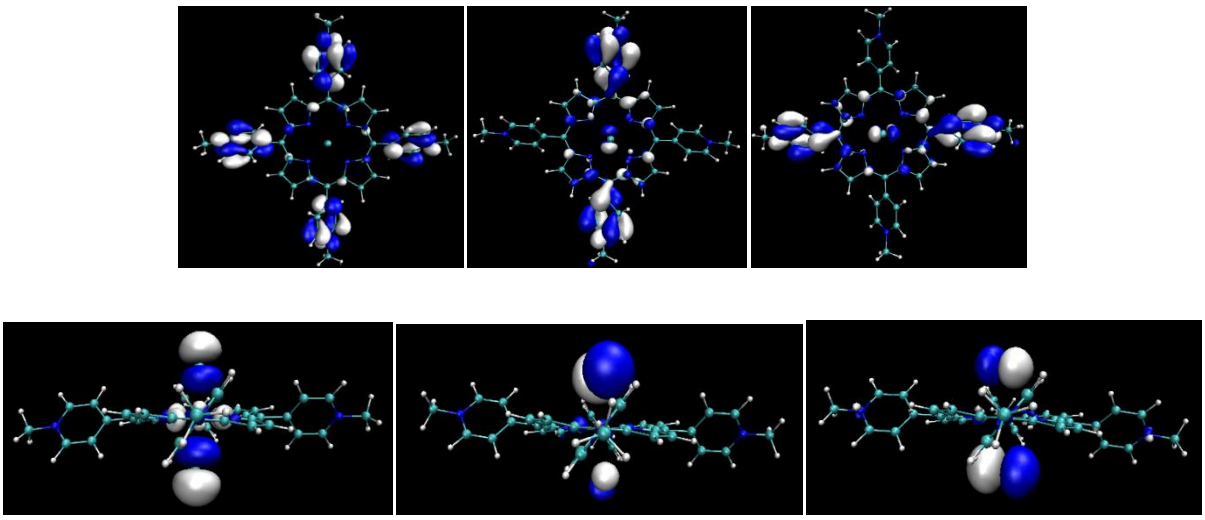

*Figure 4.29 Top: LUMO, LUMO -1, and LUMO -2 levels of porphyrin **14** with 2 axial chloride molecules calculated by CP2K. Bottom: HOMO, HOMO+1, HOMO +2 levels of porphyrin **14**. The red molecules in the middle represent the axial water molecules covering the central zinc atom.*

As Pasternack *et al.* already proposed in the 1990's, various interaction possibilities are possible[88-90, 95, 97, 111, 138-140]. The energetically lowest interaction of water – soluble zinc porphyrin **14** was calculated to be a side on electrostatic interaction (Figure 4.30. The porphyrin bridges 6 base pairs and thus can electrostatic interact with the phosphor-sugar backbone. The possible distance between the pyridinium residues and the phosphate varies around 3.15 to 3.3 Å. The occupancy of porphyrin vs. DNA base pairs can, in this mode of interaction reach a ratio of 1:5. The distance in between the central metal ion and the N7 or a phosphate is calculated to be too far for an interaction. Balaz *et al.* proposed a binding of the zinc to N7 of the guanine which seems to be incorrect[11]. The non-electrostatic interacting pyridyl residues are not interaction or even intercalating into the DNA which is interesting because the DNA would change conformation from Z- back to the B-form. A closer distance of the residue towards the deep groove can be estimated due to the proximity of the freely rotating, positively charged pyridinium groups and the negatively charged minor groove[141, 142].

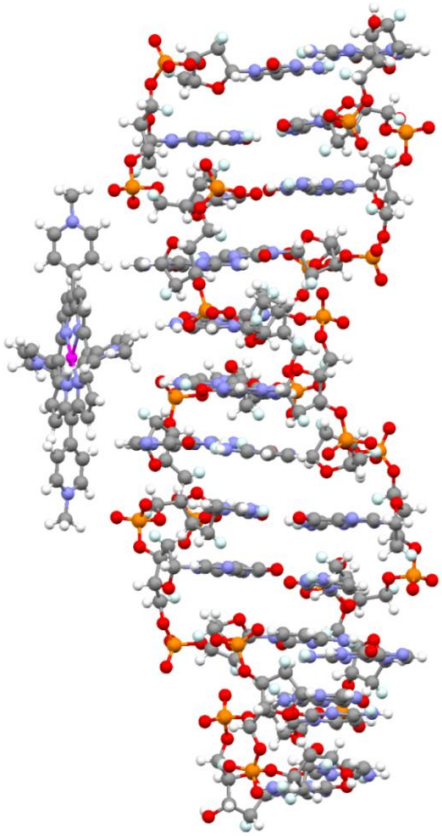

Figure 4.30 Calculated lowest repulsion of the energetic interactions of porphyrin with Z-DNA. The basic Z-DNA structure was derived from a crystal structure of Z-DNA.

4.4.6 Z-DNA detecting molecules

In order to combine the functionality of the porphyrins with a feature that would direct these multiple – charged molecules to the Z-form of the DNA rather than other conformations was the original main focus of this work. The concept chosen was to target a very specific differentiation between B- and Z-DNA: their diameter (see Figure 4.31).

The aim of this project is to synthesis a porphyrin – based molecule interacting only with the-form, ideally also in complex biological samples. The motivation was that there was no Z-form specific molecule proven to be specific *in vivo*. Balaz *et al.* could show that a model system based on a positively charged zinc porphyrin favors its interaction with Z-form over B- form[11, 142, 143]. It was also proven, that a

spectroscopic specificity towards the different conformations is given, when certain negatively charged nickel porphyrins are present at the conversion from B- to Z-DNA induced by spermine, which is a tetra – positively charged molecule[10]. We tested various combinations of metallated porphyrins and their interactions with both B- and Z-DNA. From that, a 3 dimensional approach was developed to enable an interaction with Z-DNA solely. Before that, the model system and its interaction with DNA was studied in experiment and calculated with the help of Prof. Hutter's Group (University of Zürich, see previous chapter)

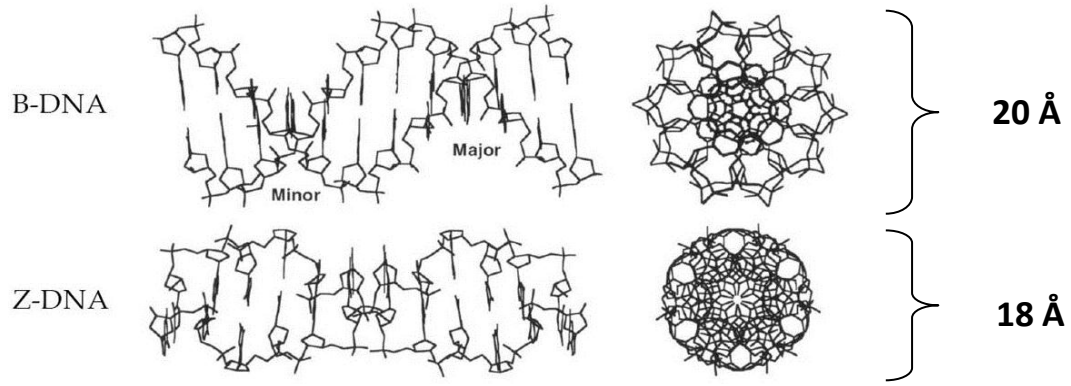

Figure 4.31 Comparison of diameter of B-DNA towards Z-DNA[2, 61]. The diameter is increasing to 23 Å and 19 Å respectively upon addition of the outer-sphere water molecules.

The idea was to build an array of two porphyrins bound to a peripherally coordinated metal center each and rigidly bridged in a right angle via an organic residue to form a U-formed structure that would only be able to enclose the Z-DNA but not a B-DNA structure due to its diameter (see Figure 4.31). The objective was to determine whether a small molecule can recognize Z-DNA in a complex biological mixture. The following features were defined as necessary to achieve the goal:

- positively charged
- recognized by Z-DNA by targeting its characteristic properties
- possible metal coordination to Z-DNA (N7 of guanine)
- detectable via CD, UV and fluorescence spectroscopy
- changes of environment detectable
- limited interaction with other molecules controlled by charge
- water-soluble

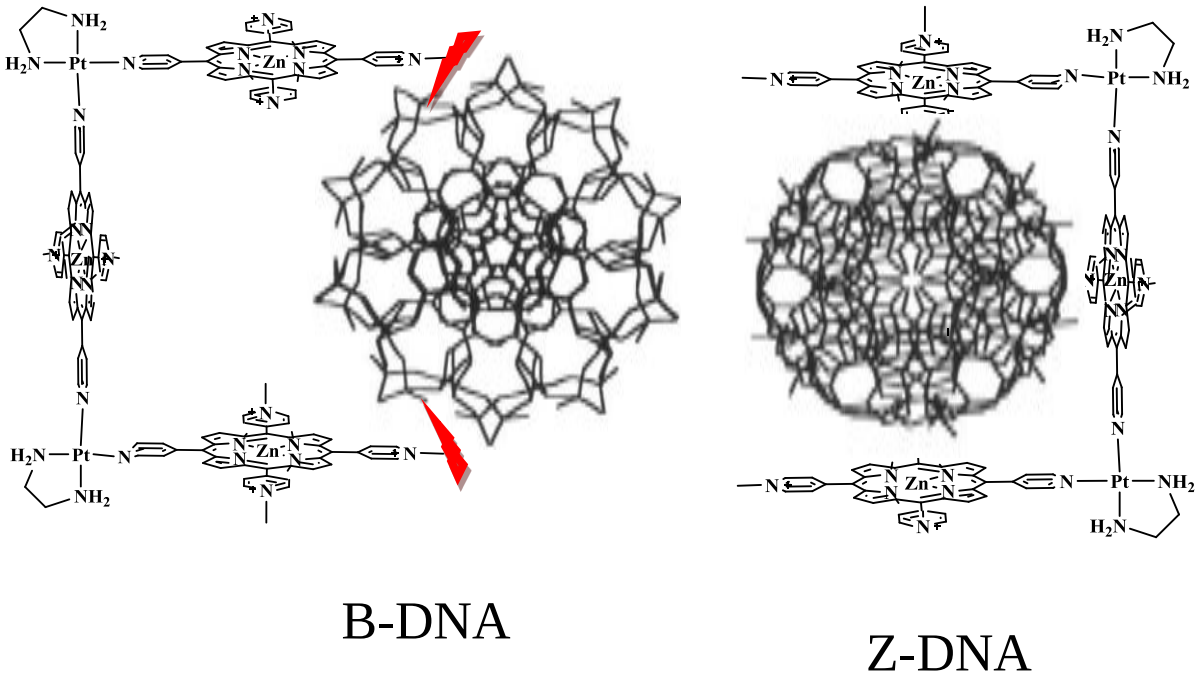

Figure 4.32 Schematic explanation for the diameter approach. The B-DNA does not fit in between the claws of the poly-porphyrin array.

The work of Balaz *et al.* showed that it was possible to find structures with these properties. As described above, the concept of the porphyrin arrays was developed according to the results previously obtained in the experiments with the mono porphyrin species. Thereby, the distance between the two flanking porphyrins and the rigidity of the molecule was the focus. We chose a platinum cornerstone in order to obtain a rigid right angle able to attach to various linker forms. The linker should be inert towards DNA (no charge, no coordination sites, no chirality) and rigid to keep the original 90° angle. The length of the linker determined the distance between the metal centers of the porphyrin, which was set to be 22 Å to fit only the Z-DNA conformation, and not around the B- form.

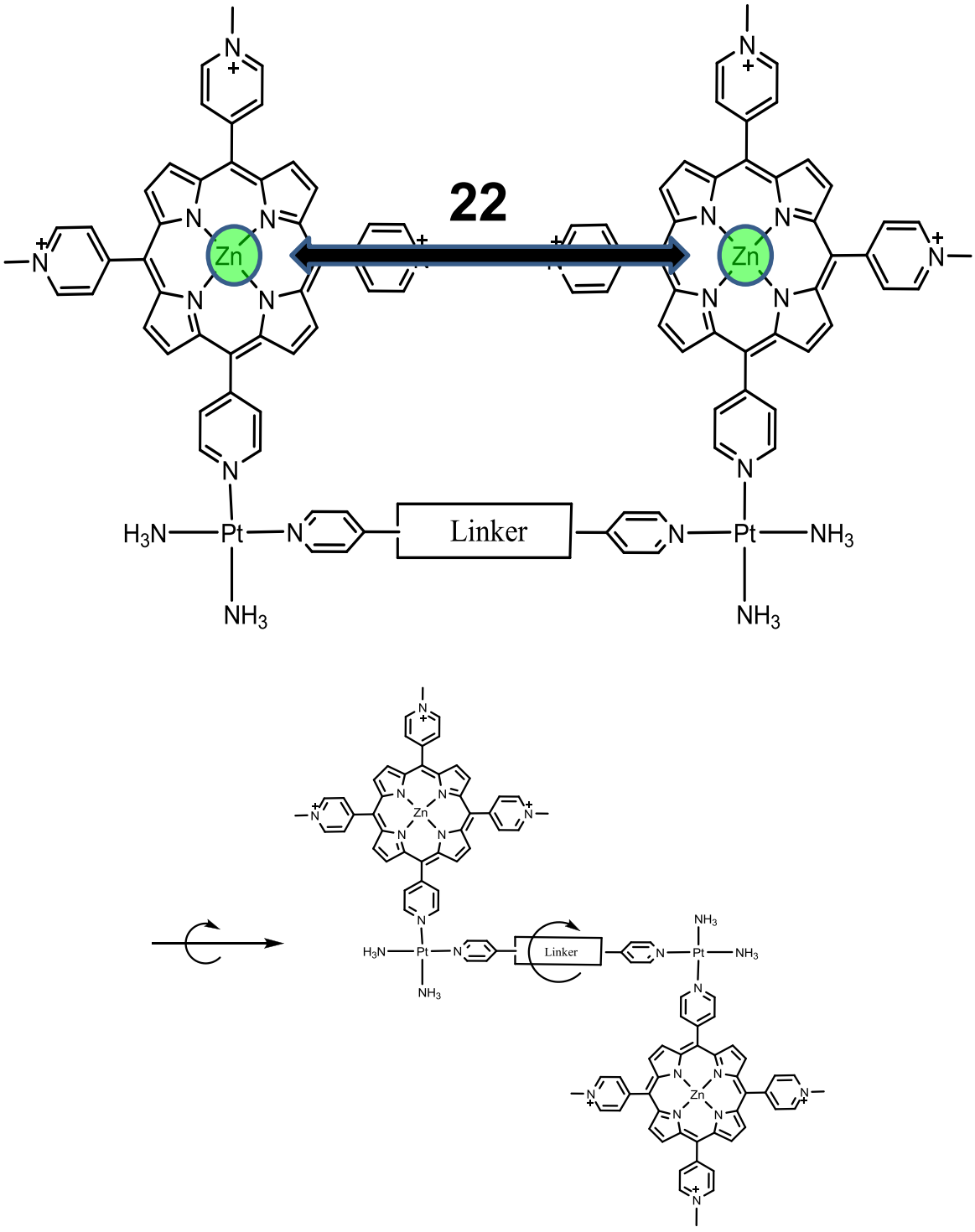

Figure 4.33 Schematic drawing of the lead molecule determining the distance between the metal centers of the corresponding neighboring porphyrins. The linker has to fulfill the task to keep the platinum centers at a given distance. Below: Different conformations of the proposed lead molecule due to the flexibility of the linker.

The arms or claws were chosen to be zinc porphyrins because of the known interactions with DNA, and the non – intercalation characteristics (see Figure 4.33). It was important to be able to follow the distance between the metals in the

porphyrins. We assumed that the different conformations and thus different distances of the metal cores of the porphyrins will be observable by fluorescence spectroscopy according to the Dexter energy transfer. The introduction of 2 different metal centers (nickel and zinc, or cobalt and zinc, copper porphyrins are non – fluorescent) and thus changed spectral properties will be observable.

The variability of the linker and the effect of the whole system was part of the investigation. It was assumed that a chiral linker or a linker that only allowed only one conformation by sterically hindering the other would have a different interaction with DNA. The synthetic challenge to assemble such molecules was simplified according to a modular system. The different units of the lead molecule were supposed to be exchangeable. The side arms were chosen to be porphyrins. The right angle unit choice was won by a platinum corner with different ligands completed by a variety of linking or bridging units. These had to be rigid, aromatic and ideally allow the right distance in between the corner and thus porphyrin units.

4.4.7 Porphyrins as side arms: an odyssey

Porphyrins chosen to fulfill the properties to interact with DNA (water soluble, positively charged) had to be rigidly bound to the Pt – unit. In this scenario, we first tried to synthesize a threefold methylated 5,10,15-tri-(methylpyridinium)-20-mono-pyridyl-porphrin **8** with zinc as a central metal ion. To fit this porphyrin and connect it to the corner building block, a vacant binding side was needed. As shown in Figure 4.33, we initially chose this to be a non-methylated pyridyl residue. The difficulty was to only tri – methylate a molecule that can be methylated four times. Since the methylation is kinetically dependant on the solubility of the thus successively more positively charged molecule, a non – methylatable, non – protic solvent like DMF was chosen. The methylation took from 20 min up to 24 h depending on temperature and solvent. Two different methylating agents could be used to perform the reaction in this conditions and solvents: methyl iodide and trimethyl oxonium.

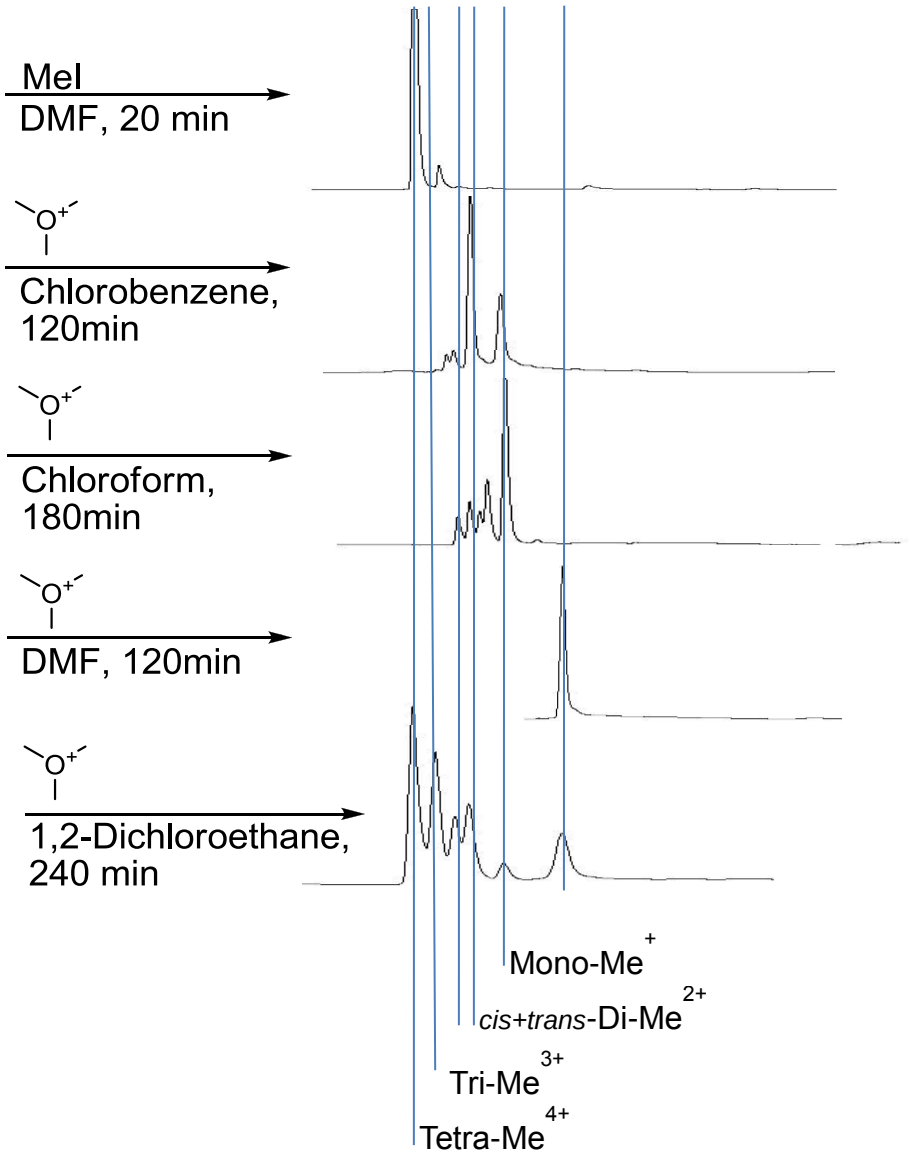

*Figure 4.34 Using different methylating agents to tri – methylate 5,10,15,20-pyridylporphrin **8**. Reactions were performed at 65°C to realize fast reaction times; for each reaction, 10 equivalents of the corresponding methylating agent were added.*

In all reactions, a complex mixture was resulting to form mono-, *cis* and *trans* di-, tri- and tetra- methylated species. This mixture was tried to be separated by HPLC protocols in preparative - and semi preparative – amounts. However, it was not possible to separate more than a few milligrams of the tri - methylated species from the mixture. This was not enough to exchange the counter anion and to proceed with the reaction with the platinum corner.

Other means of separation such as CPC (Centrifugal Partition Chromatography), thin layer chromatography as described the literature and thick layer chromatography could not separate this mixture as well[113, 144, 145]. The chemical approaches to block one pyridine residue by i.e. a cobalt pentamine complex were also accompanied by the difficult separation of multiply positive charged cations.

To overcome those separation issues, a different, chemical approach had to be found. We synthesized different A_3B porphyrins with A residues being able to methylate and B residues being not methylatable and have a vacant binding site. The most attractive B residue was the cyanophenyl building block which forms a strong coordination to platinum complexes.

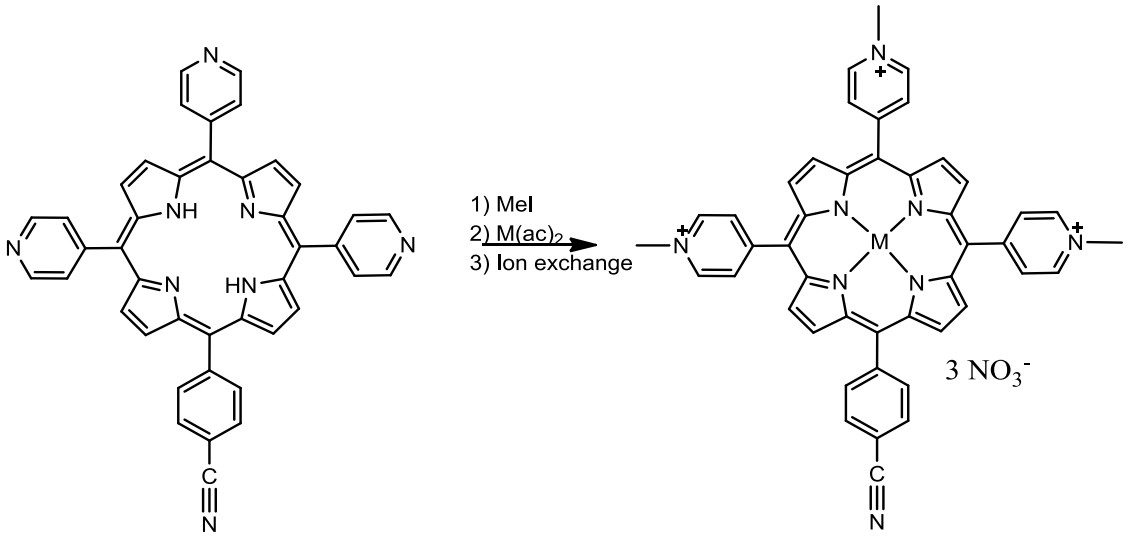

Figure 4.35 Synthesis of A_3B porphyrins to with a vacant binding site. Tri – methylation of porphyrins with a vacant coordination site to bind to the platinum cornerstone. The lead molecule with a central metal ion and a vacant tri-pyridyl-cyanophenyl-porphyrin.

As lead molecules, we synthesized the novel molecules **15**, **16** and **17** with different central metal ions which were linked to the corner building blocks (see also chapter 5 for further applications). These molecules feature a free rotating binding site which will linearly coordinate to a metal ion. The synthesis was performed via two different approaches. In the statistic approach, a 3:1:5 ratio of 4-pyridyl-aldehyde, 4-cyanobenzaldehyde, and pyrrole was stirred in propionic acid at 165°C followed a three step purification setup and chromatography to separate the 6 products[117, 146,

[147]. The second approach was a modified variety of a synthetic approach provided by Lindsey et al[148-151]. For a detailed description please refer to chapter 7. The yield of all reactions towards the porphyrins was porphyrin – like poor at around 0.5 – 3 %.

4.4.8 Corner Building Blocks

The corner building blocks had the task to form a 90° angle in between the side arm and the bridge in order to form a rigid structure. The molecule of choice was a platinum complex with square planar coordination sites of which 2 were occupied by strongly binding ligands. The vacant binding sites had to open up the right angle and keep the side arms in place.

Different ligands of the central platinum were chosen to modify the stability of the U – vs. S – shape of the porphyrin array.

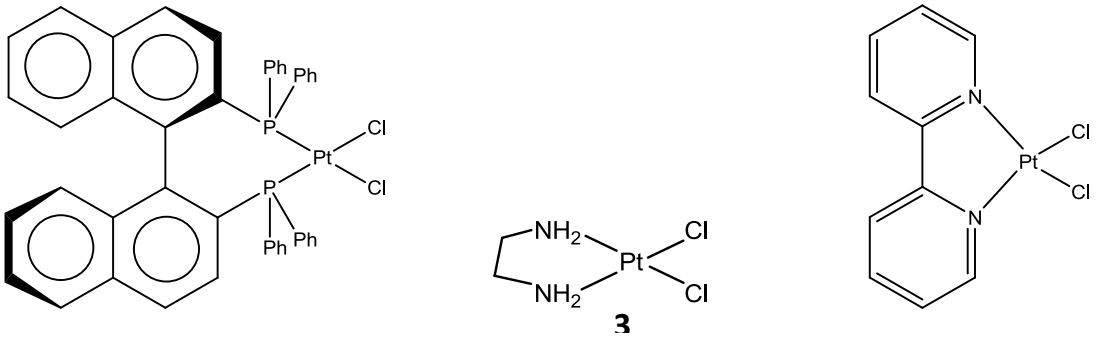

3

Figure 4.36 Selection of corner building blocks with different characteristic properties towards stabilizing a sterically hindered U shape.

The molecules and their ligands[152-155] were synthesized according to literature procedures[156-162]. The coordination towards the side arms was initiated by the precipitation of silver chloride. Different metals were tested but the kinetic stability of the platinum complexes (and palladium complexes) was superior towards other approaches[162-166].

4.4.9 Synthesis of the Bridges

To complete the lead molecule, an appropriate, straight bridging molecule had to be synthesized. Two different approaches were followed (see Figure 4.37)

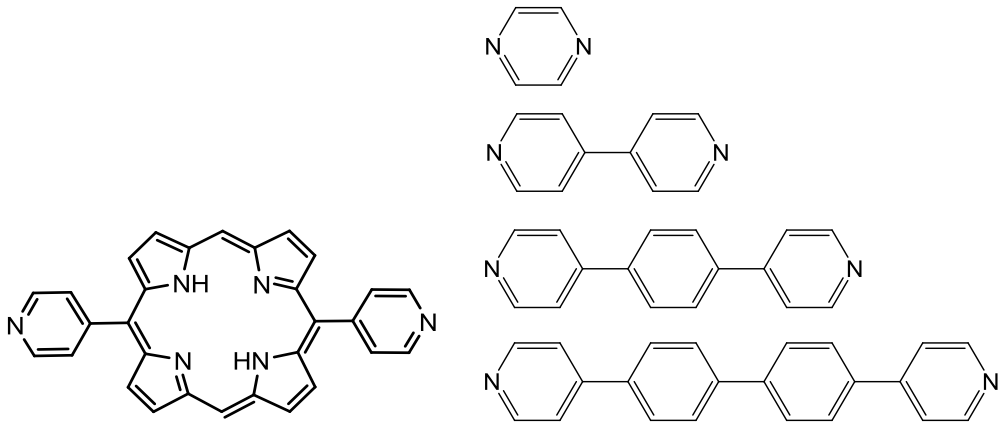

Figure 4.37 Two different, rigid bridging units to stabilize the lead molecule. Left: Slim porphyrin. Right: Series of (poly) – aryls having peripheral pyridyl residues.

In the first approach, an ABAB porphyrin with two *trans* to each other located coordination sites was synthesized. This slim porphyrin has a poor solubility and was synthesized according to literature proceeds starting form a 4-pyridyl-aldehyde to obtain a pyridyl-dipyrrole (PDP) which is then further reacted with trioxane (cyclic trimer of formaldehyde which is less reactive) to form the cyclic porphyrin[118, 167-170].

The second bridging unit, the linear 4,4'-biphenyl-4,4'-diyldipyridine **35**, was synthesized according to the Suzuki coupling reaction (see below) in which a boronic acid is reacted with diaryl-dihalogenide. The dipyridyl was obtained in overall yields between 0 – 71%. One possible reason for the failure of some of the reaction procedures could be obtained by crystallography. As shown in Figure 4.39 the 4-boropyridyl-pinacolester formed cross links to the neighboring boron atom which might explain the observed un-reactivity. This was previously mentioned in the literature[166, 177-179].

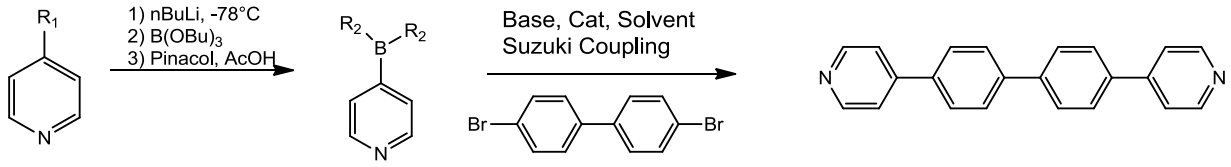

R_2	Solvent	Base	Catalyst	Yield
pinacol di-ester	MeOH / Toluene	Na_2CO_3, P(*t*-Bu)$_3$	$Pd(PPh_3)_4$	0
pinacol di-ester	Dimethoxyethane	KO^tBu	$Pd(PPh_3)_4$	0
pinacol di-ester	Toluene	K_3PO_4	$Pd(PPh_3)_4$	10[a]
OH	EtOH / HBr	$Bu_4N(OAc)$	$Pd(PPh_3)_4$	10[b]
OH	Ether	K_3PO_4	$NiCl_2(dppp)$	0
OH	Toluene	Na_2CO_3	$Pd(Cl)_2dppf$	71[a]

Figure 4.38 Suzuki reaction with different catalysts and with various reaction conditions. R_1 was in most cases I, in some Br with no influence on the following reactions. All reactions were carried out under argon [171-176]. [a]isolated yield, [b]non-isolated yield (by GC-MS).

We overcame this trouble by using the palladium catalyst $Pd(Cl)_2dppf$ together with the boronic acid of pyridine. The reaction times where somewhat longer but the yield much higher with this approach.

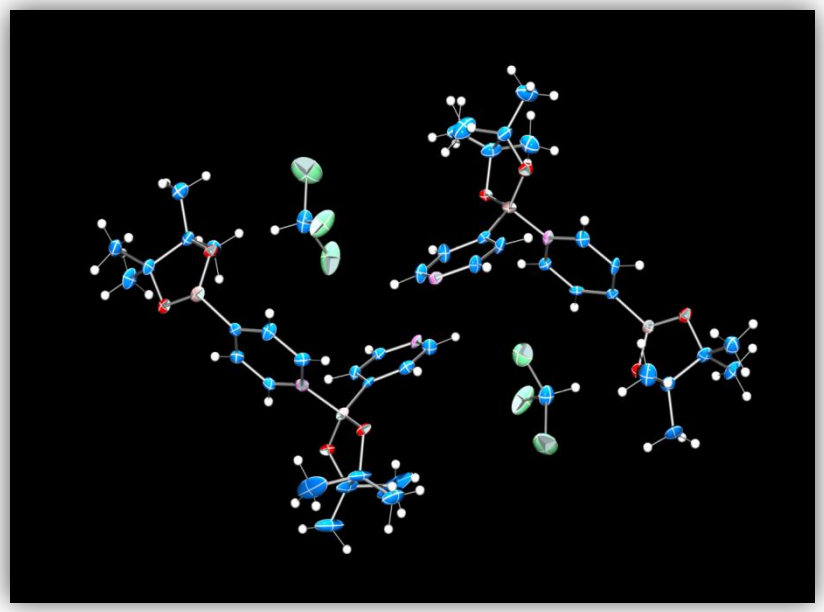

Figure 4.39 Crystal structure of 4-boropyridyl-pinacolester obtained after the catalytic reaction with the diaryl crystallized from chloroform/hexane solution. Boron of the pinacol ester is coordinated to the N of the pyridyl residue.

The coordination of these bridges was tested in a model system. According to Fujita *et al.*[173, 174, 180], a self – assembly upon addition of a *trans* – coordinating ligand can assemble towards a square. An activated en – palladium corner was added to a solution of 4,4'-bipyridyl and crystallized in an aqueous vs. methanol solution.

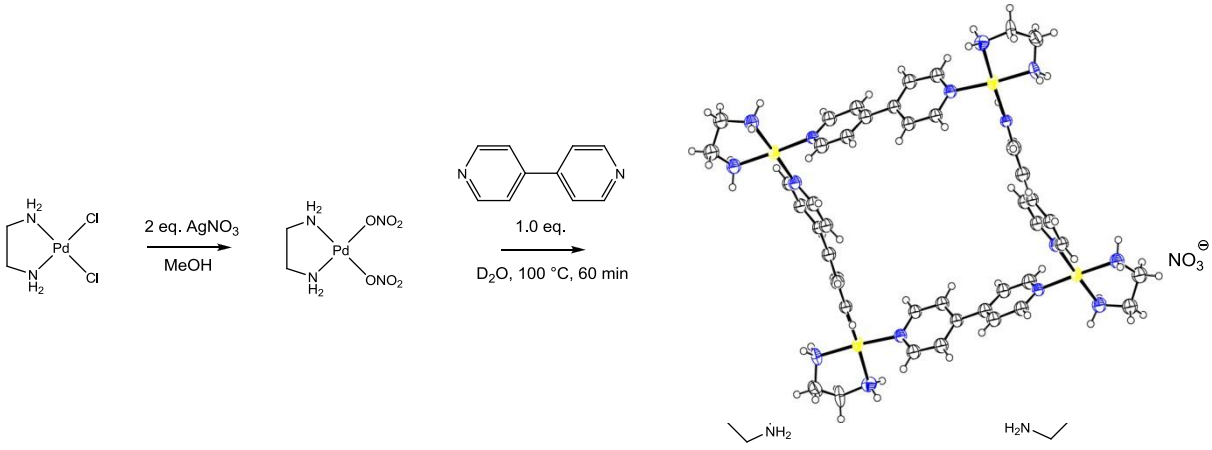

Figure 4.40 Reaction scheme and Pd_4(4,4'-bipyridyl)$_4$ square crystallized. Counter ion are 8 nitrates.

The assembly of the porphyrin array was sketched out as depicted in the synthesis plan. One problem difficult to overcome was the order of the successive reactions. First, the corner and bridge form a barbell followed by the addition of the side arm

porphyrin. The second option is a formation of a porphyrin – corner adducts and combines them with the bridge. In both synthetic approaches, several difficult steps have to be taken. There is a drastic difference of solubility of the flat, organic bridge and the water soluble, positively charged (activated) the platinum corners which have to become water soluble after the reaction in order to coordinate with the porphyrin. This coordination was crucial and made the first synthetic approach easier to tackle. It was not possible to form a water soluble tetra – aryl bridge coordinated to coordinated platinum corners. The follow on reaction was not possible. The same problem occurred when using the slim porphyrin **30** as bridge. The solubility was too poor.

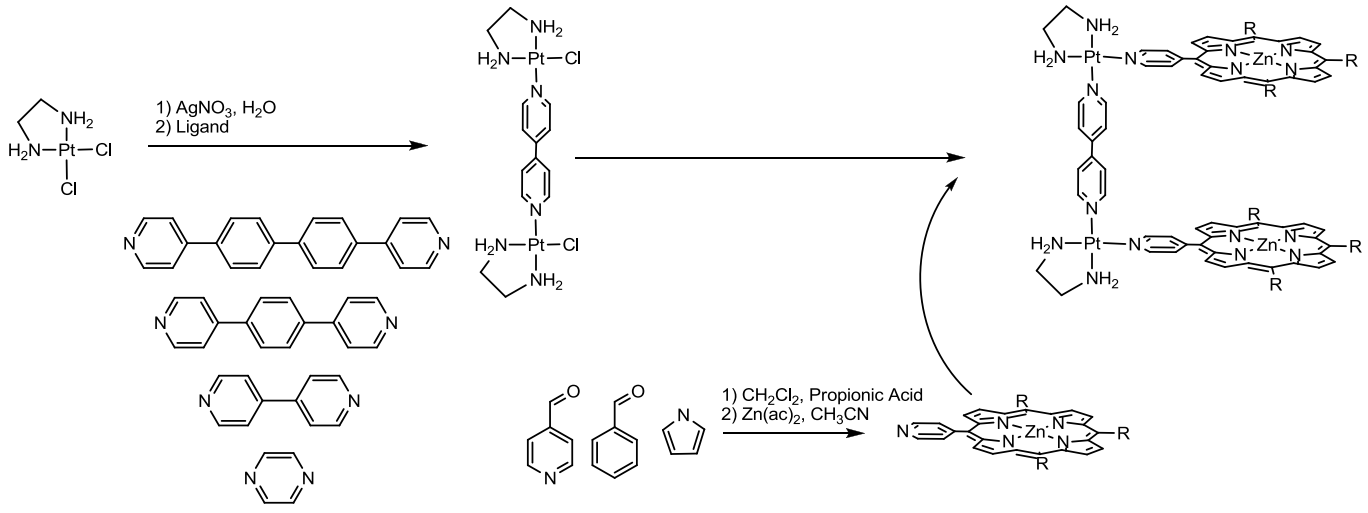

Figure 4.41 Synthesis plan for one way towards the lead molecule. All reactions were carried out in the dark.

It was possible to an L – shape with two side arm porphyrins and a platinum corner. The water soluble $[Pt(NH_3)_2(H_2O)2]2^+$ was added to an aqueous solution of porphyrin **19** to form molecule **31**, an L – shaped porphyrin array which has a charge of 8+. After purification via HPLC chromatography (see Figure 4.42), a yield of 26% could be obtained. Given the fact that the reaction took place between two highly positively charged molecules, this was surprising. Nevertheless, it was not possible to form a U – shaped molecule with a non – water soluble bridge.

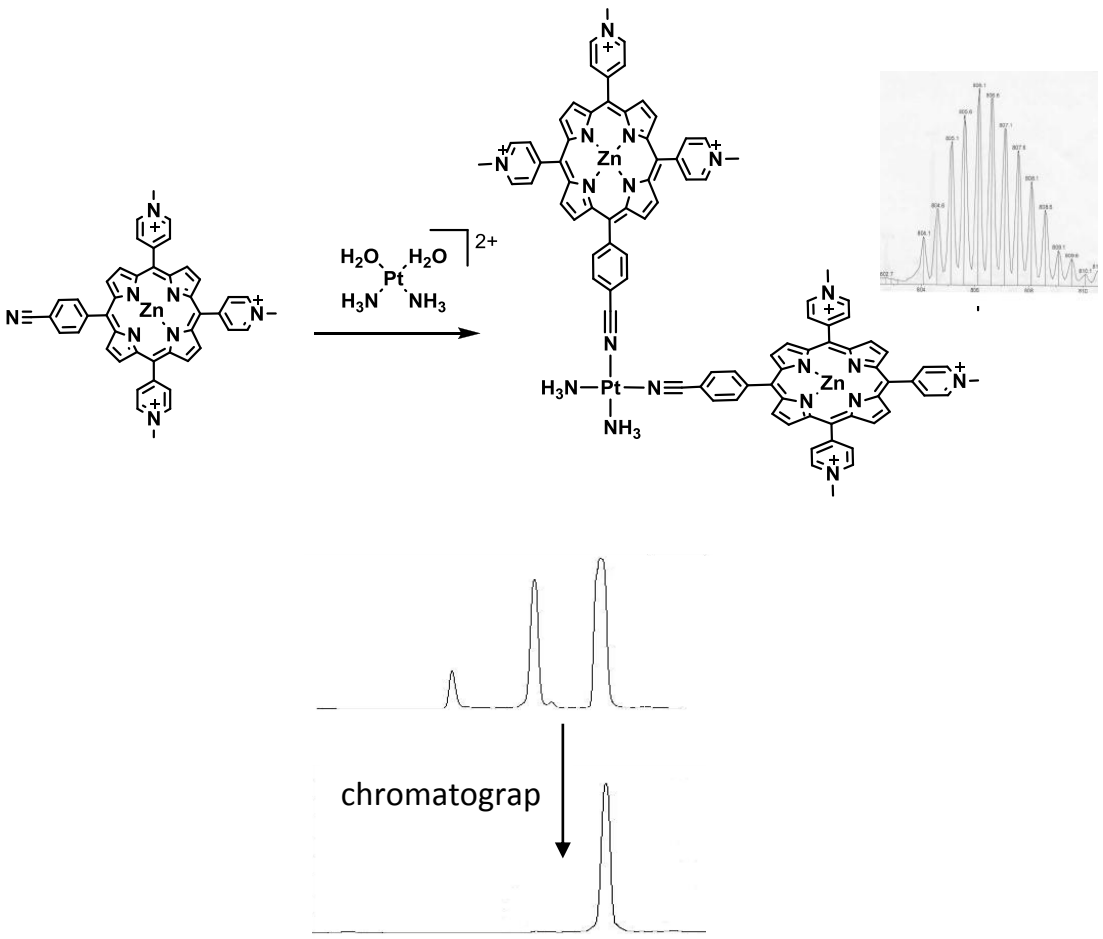

Figure 4.42 Reaction scheme and analytical data of the L – shaped porphyrin array which is eight fold positively charged. Ion exchange chromatography could separate the positively charged mixture.

4.5 Conclusion and Outlook

Metalloporphyrins interact in characteristic pattern with different conformations of DNA. Various metalloporphyrins were synthesized and exposed to different model systems to study their interaction with oligonucleic acids. It was found that the metal free porphyrins **10** and **17** do intercalate into DNA and thus stabilize the B- form. Other porphyrins containing central metal ions such as copper can intercalate or coordinate to DNA in a side – on fashion. A very unique behavior is observed when the interaction of porphyrins containing central metal ions with axial ligands was tested. Especially a central zinc ion in the porphyrin showed a unique behavior towards Z-DNA only.

The idea to demonstrate this in more difficult biological matrices with a combined approach unifying interaction specificity and sterically hindrances into one concept was unsuccessful due to chemical solubility issues. The foreseen lead molecule would have also combined the possibility to detect what the claws are reaching around due to their fluorescence properties.

To further test the properties of the porphyrins, the interaction of the metalloporphyrins coordinated to one corner building block *cis*platin (see molecules **20** – **22**) and the interactions towards cancer cells resulted in a new and exciting approach as described in chapter 5.

5. Photoactive Metalloporphyrins for a Combined Chemo- and Photodynamic Therapy

5.1 Abstract

We introduced a new class of photoactive platinum-porphyrin conjugates, with a light dependent cytotoxicity down to 0.08 μM (IC_{50}) for compound **22**. As photosensitizer of choice, cationic porphyrins were selected due to their water solubility, known cell and nucleus uptake, and the possibility to exchange the central metal to tune its characteristic absorption properties. Those complexes feature a very stable covalent bond between the photosensitizer and the *cisplatin* residue, and have a characteristic fluorescence behavior. We could convincingly show that their absorbance spectrum can be tuned to be useful for photodynamic therapy. The highly positively charged photo sensitizer makes the compounds water soluble and facilitates a cell uptake as was also shown for similar cationic porphyrin. The thus possible electrostatic or coordination to DNA (mitochondrial and well as chromosomal DNA) was studied in cell uptake studies.

We have prepared several novel porphyrin-*cisplatin* conjugates which were fully characterized and analyzed for their behavior towards different human cancer cell lines (Scheme 5.6.)[181]. In contrast to the already reported phthalocyanine-*cisplatin* conjugates[182], the platinum complexes **20 - 22** have two leaving groups: the one chloride and the ammine *trans* to the cyano-ligand, which is N-bound to the platinum metal center. In a recent publication, it could been shown that the cyanide anion (N- or C-bound to the platinum) has the stronger *trans* effect than the amine[157, 159]. This was also observed in the case of our platinum – containing conjugates using mass spectrometric measurements.

The cytotoxic effect of the molecules **17 - 22** was determined with and without irradiation of red, water-cooled light (3200 lux) at different durations and found to differ dramatically when irradiated. Shining light with a wavelength greater than 600 nm on the incubated cells increased cytotoxicity of the molecules up to a factor of 57!

The most effective photocytotoxic molecule, **22**, shows an IC_{50} value of 0.08 μM against the A2780 cell line.

Additionally to the classical determination of the physical properties, the stability of those molecules **17 - 22** in human serum was tested in a model system. This was carried out by monitoring the decomposition behavior and affinity of the molecules towards Human Serum Albumin (HSA) over time. It was shown that the non – platinum containing molecules **17 - 19** did not interact with HSA whereas the platinated conjugates **20 - 22** did show a significant coordination to HSA.

5.2 Introduction

Despite an impressive progress in the field of the chemotherapy, there is still the immediate need for multifunctional drugs that combines the advantages of photodynamic therapy and platinum based chemotherapy[38, 183-186]. In 2008, the pharmaceutical company Sanofi was selling the third generation drug oxaliplatin for more than 1.4 billion Euros[187-190]. Since the beginning of the 1990's photodynamic therapy has extended the medicinal possibilities to fight cancer, especially for cancer types that can be reached with red light. So far there are only few reports about combined photodynamic chemo therapies to enhance for a synergistic effect [191-197].

5.2.1 Cisplatin

The anti-cancer activity of *cis*-diaminedichloroplatinum(II) (*cis*platin, Figure 5.3) was accidentally discovered by the group of Barnett Rosenberg in 1969[35, 198]. They realized that certain platinum salts, which were accidentally formed from a platinum electrode, used to apply an electric field to bacterial Escherichia Coli, strongly inhibited cell division but had no influence on cell growth. Later they found out that this was also true for eukaryotic cells such as solid tumor cells. As a result, *cis*platin rapidly entered clinical trials and thus received FDA approval in 1979 for use as an anticancer drug[199]. Despite efforts to launch more platinum based anticancer

drugs[200], *cis*platin is the most widely used platinum anticancer drug and is especially effective against testicular[201], head, neck, non-small-cell lung, and cervical cancers[202]. *Cis*platin is cell cycle unspecific and often used in combination with other cytotoxic drugs to enhance its effect[35].

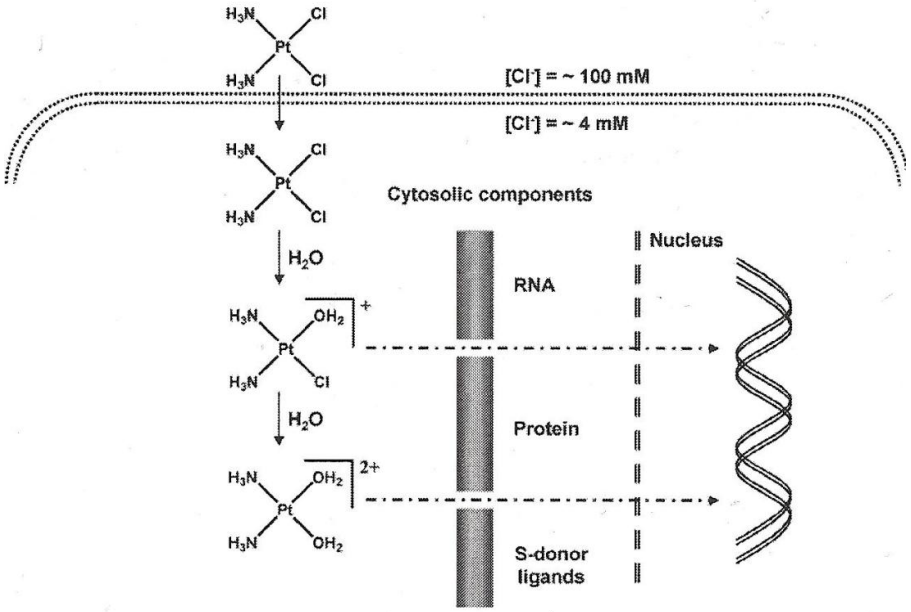

Figure 5.1 Cisplatin and its way into the cell. Different ligands are exchanged when entering a surrounding with a different chloride concentration.

5.2.2 Second and Third Generations of *cis*platin analogues

Although *cis*platin is a very effective anticancer drug, it has many undesirable side effects, in addition inherent and acquired resistances reduce its clinical efficacy. A number of less toxic second generation compounds have been synthesized, most notably carboplatin[203]. Carboplatin is less ototoxic but the neurotoxic effects are more prominent and are thus dose-dependent. 1R,2R-(diaminocyclohexane) oxalatoplatinum(II) (oxaliplatin, Figure 5.3) is a third generation platinum compound[204] that produces the same kind of inter- and intrastrand DNA cross-links as *cis*platin, but its neurotoxicity is the most common dose – limiting side effect[205].

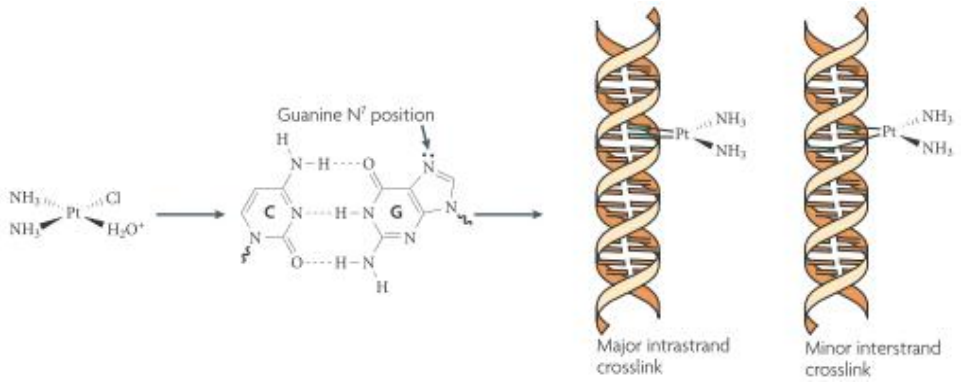

Figure 5.2 Cross-linking of the cisplatin with DNA and its coordination sites. Picture taken from a presentation of PD Dr. Bernhard Spingler.

Oxaliplatin, in combination with 5-fluorouracil, has been first approved in Europe, Asia, Latin America[206] and in 2002 in the USA[207] for the treatment of metastatic colorectal cancer[191, 208-210]. *Cis*-, carbo-, and oxaliplatin are the only three platinum based anti-cancer drugs that are applied worldwide. In some countries, heptaplatin[211], nedaplatin[212], and lobaplatin[213] have been additionally approved[188, 214].

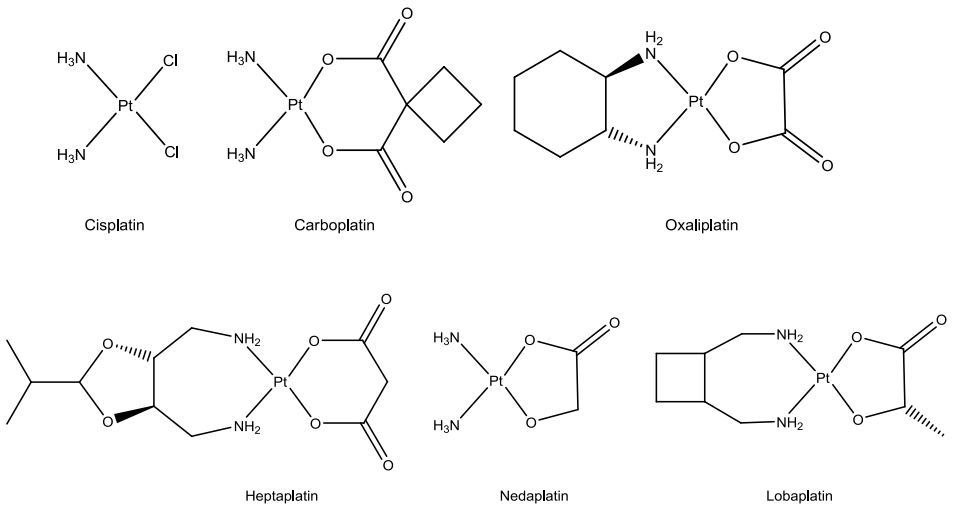

Figure 5.3 Worldwide (top) and regionally (bottom) used commercial platinum drugs.

Many research groups have trid, and some succeeded, to expand the success of these platinum drugs to different cancer types or the ones that have become resistant against e.g. *cis*platin[215-224]. Nevertheless, there is a great need to transfer the success of *cis*platin in treating a limited number of cancer types to other types of cancer. The long list of side effects further limits its field of use: one of the major concerns of

*cis*platin is its nephrotoxicity (kidney damage). The renal function of the patient has to be monitored via the patient's creatinine clearance. The renal damage is additionally counteracted with increased hydration and dieresis[187, 225, 226]. This dose limiting toxicity is derived from a reactive oxygen species which, in mouse models, were shown to be enhanced by the removal of free radical agents. The second major side effect of *cis*platin is its influence on the nervous system (neurotoxicity). A cost issue during the treatment with *cis*platin is the need to perform nerve conductivity measurements before and during the chemotherapy, since the neurotoxic effects are not understood and irreversible[227, 228]. Nausea and vomiting are additional side effects which occur since *cis*platin is one of the most emetogenic chemotherapy agents[229, 230]. The best solution against this side effect is the add-on of prophylactic aniemetics, i.e. granisetron, in combination with corticosteroids to enable treatment with the needed dosage. Other dramatic side effects of the drug are alopecia (hair loss), ototoxicity (loss of hearing)[231] and troubles with the electrolyte level[232].

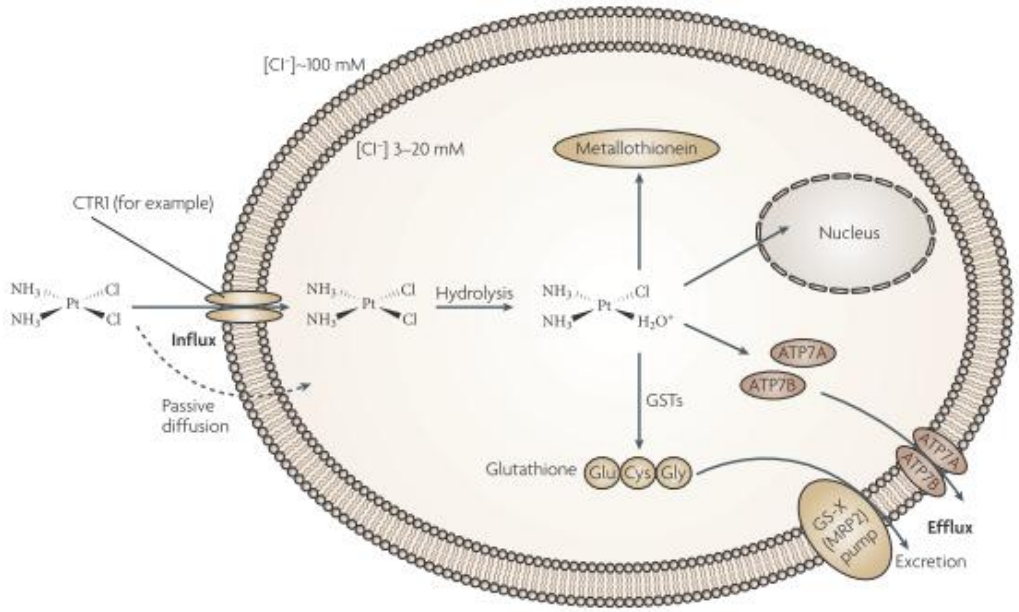

Figure 5.4 Way into cell of cisplatin and its possible targets within a cell. The transportation to the outside is also depicted. Picture taken from Nat. Rev. Cancer. 2007, 573.

The reasons for those side effects are not well understood, but the main concern about the treatment with *cis*platin is its cell unspecific uptake and damage. With the development of new platinum based drugs, chemists and physicians try to avoid

those side effects to make the treatment more cancer cell specific[233]. The chemistry of d8-Pt^{2+} compounds such as *cis*platin is a reason for its unspecific behavior towards DNA. It is constituted by a square planar geometry, with two amine and two chloride ligands each in *cis* coordination. *Cis*platin has a low solubility of only 1 mg / ml 0.9% aqueous saline solution[234] and is usually applied to the patient in a DMSO/saline solution. *Cis*platin is hydrolyzed in water by losing a chloride ligand and coordination of a water molecule to the platinum. This *cis*-$[(NH_3)_2PtCl(H_2O)]^+$ is highly reactive due to its pK_a of 6.55[235]. 80% of the mono-active form of *cis*platin is in the deprotonated (mono-hydroxo) form at the physiological conditions (pH 7.4)[192, 236-238]. Despite other possible binding sites, i.e. RNA, proteins, microfilaments, cellular DNA has been shown to be the primary target of *cis*platin. Due to its unique chemistry, *cis*platin is protected from early reaction in the bloodstream until its passage to the cell membrane by the relatively high concentration (>100 mM) of chloride which keeps it in the non-reactive dichloro form. With the uptake in the cell, the salt concentration of the new environment (<20 mM) enables *cis*platin to lose one chloride ligand to form the proposed active *cis*-$[(NH_3)_2PtCl(H_2O)]^+$ species, which binds preferably to the N7 of guanine rather than N7-adenine or N3-cytosine[209, 239-242]. First, the mono-adduct is formed, the major adduct being formed in the subsequent step to form a 1,2-intrastrand cross-link between the N7 of the adjacent purine residue, either in an d(GpG) - fashion or less frequently, d(ApG)[210, 243, 244]. Different coordination behavior is mostly known for *cis*platin binding to different types of RNA.[245-248] With the formation of those 1,2-intrastrand cross-links, the DNA conformation is altered to form a bend in the duplex helix and in some cases even an unwinding of the two strands[237, 249-255]. Those platinated regions and bends in the DNA duplex can be recognized by proteins, and can lead to cellular death by apoptosis or necrosis due to its interference with the normal functions of the proteins during transcription of the cells[256-258].

Cells can become resistant against *cis*platin, and either very high dosage has to be applied or an alternative treatment has to be found. There are several mechanisms

known that make cells drug resistant. Increased DNA repair is a mechanism to remove platinated DNA pieces or platinum induced lesions with the help of specific repair proteins, i.e. XPE-BF[215, 259, 260] which was found to increase *cis*platin resistance. Another example is ERCC1 which is expressed more frequently in *cis*platin resistant cells than in cells sensitive to *cis*platin. Another mechanism known is, that cells avoid uptake or even remove the drug, which results in a reduced accumulation of the drug in the cells. This is not fully understood, but different mechanisms of cell uptake can be a hint to understand this behavior: drugs pass into the cell either by passive diffusion or by active transport systems. In the cell membranes and the interior of cells, sulfur containing macromolecules, such as metallothioneins or glutathione are present. Heavy metals are known to trigger the production of metallothioneins and strongly bind to those proteins, which are believed to be one of the detoxification mechanisms of the cells[199, 242, 252, 261-266]. *Cis*platin binds to metallothioneins with a maximum of 10 platinum atoms per protein[267, 268].

The cytotoxicity of *cis*platin most likely involves the interaction of certain cellular proteins with the *cis*platin-modified DNA.[269] Several X-ray crystal structures of a *cis*platin-modified DNA complexed with HMG1, polymerase or histone proteins have been reported[255, 270, 271]. A novel feature of the first mentioned protein-DNA complex is the intercalation of a phenylalanine between the two cross-linked guanosine residues[270].

*Cis*platin is also used in combination therapy. Recent research directions have expanded the knowledge about these promising new therapies[272]. One study showed that there is low cross resistance of *cis*platin-sensitive and -resistant human ovarian cancer cells against *cis*platin in combination with intercalative drugs[224].

Furthermore, cis- and carboplatin have been covalently linked with functional molecules. These linkages can be permanent or intentionally hydrolytically labile[273]. Fluorescent *cis*platin conjugates allowed tracking of the platinum complexes in *cis*platin resistant and sensitive A2780 human ovarian carcinoma cells[219, 220]. The

group of Gibson has studied various conjugates of carboplatin with either folate[274] or a nucleus localizing sequence (NLS)[275]. Despite higher cancer cell uptake, the conjugates proved to be less cytotoxic than carboplatin. Gadolinium complexes have been tethered to platinum complexes via a substituted malonate linker, which hydrolysed with a half-life of 3 days. The conjugates had a comparable toxicity than carboplatin with less side effects[273].

5.2.3 Photodynamic Therapy with Porphyrins[197, 276-280]

Photodynamic therapy (also called PDT, photo radiation therapy, phototherapy, or photo chemotherapy) is a revolutionary treatment aimed at detecting and treating cancer without surgery or chemotherapy. It is based on the discovery that certain chemicals known as photosensitizing agents can kill cells when exposed to a particular type of light. Nowadays, PDT is mostly conducted in damaging cancer cells with fixed-frequency laser light in combination with a photosensitizing agent. Besides cancer, PDT has further developed to become an efficient therapy for other complications such as cardiovascular, chronic skin diseases, i.e. psoriasis. Advantages of the photodynamic therapy are that it is a well-defined surface treatment with no or few effects of the neighboring cells [183, 191, 193, 196, 197, 279, 281-283]. The treatment does not have to be invasive and can be repeated several times in contrast to radiotherapy. Limiting factors are that the surface or tumor has to be reached by a light source, so it is mainly used to treat areas on or just under the skin, or in the lining of internal organs. While the drug can travel throughout the body, the treatment only works when irradiated by light, so PDT cannot be used to treat extensive cancers. The current drugs available also leave people very sensitive to light for a time, requiring special precautions.

The first hint for a photodynamic therapy came with the increased knowledge of *"Porphyria"*, which is a collection of diseases in which pigments then called *porphyria* accumulate in the skin, bones, and teeth that turn caustic on exposure to light[284].

Many *porphyria*, are innocent in the dark but transferred by sunlight into caustic toxins. While struggling to find a cure for *porphyria*, scientist in the late 1850s came to realize that *porphyrias* could be not just a problem but also a tool for medicine[285-287]. If a *porphyria* is injected into cancerous tumor, it can be activated by light to destroy the tissue. As a consequence, scientists during the late 1850s began to unlock the puzzle as to why certain biological substances such as chlorophyll (chlorin) and heme show unique colors and behave like *porphyria*. Close structural similarity between heme and chlorin was demonstrated by Verdeil in 1844, followed by Hoppe-Seyer in 1880[94, 95, 104, 288-291]. Soon it became clear, that porphyrins (from the Greek word for purple) play a vital role in life's processes. Porphyrins were defined as bioinorganic components consisting of a cyclic tetrapyrrole macrocycle having 26 p - electrons. In nature, apart from their most prominent role as a carrier of oxygen in the hemin molecules, porphyrin-type molecules with a specific interior metal ion are found in cytochromes, peroxides and catalases, chlorophyll (involved in plant photosynthesis).

Photodynamic therapy (PDT) was first applied in 1900 when Raab *et al.* showed the cytotoxic effect of light towards infusoria when treated with acridines[292]. The first application to human skin cancer was performed by von Tappeiner and Jesionek in 1903[293], when applying white light to irradiate topical eosin. In 1924, Policard observed fluorescence of porpyhrins in cells and consequently, Auler and Banzer later described the cell uptake of porphyrins, first in plants and later, into human tumor cells in 1942[294]. Porphyrin containing compounds continued to be a major agent in the photodynamic therapy. In 1948, selective accumulation of porphyrins *in vivo* were described by Figge, followed by a report by Rassmussan-Taxdal observing a selective localization of porphyrin in tumors in 1955[295]. Porphyrins were also used for the detection of tumors and monitoring its growth as discovered by Lipson and Blades in 1960. Dougherty treated the first skin cancer patients with a porphyrin-based PDT drug in 1975[279], which came into clinical trials in 1978. This was the first PDT going for a drug approval. In 1990, Photofrin, a porphyrin based drug got FDA

approved and made it onto the market[162, 183, 185, 192, 238, 282, 296-300]. First only thought to be applicable for skin cancers and malignomal tumor cells, drugs were developed towards an application on various kinds of surface near cancers, such as early- and late-stage lung cancers, bladder cancer, colon or ovarian cancers to name a few[279, 285, 299, 301].

The most commonly used photo sensitizers are porphyrins or phthalocyanines, of which more than eighty different natural molecules are known. The fact that porphyrins can be used in combination with almost any metal opens a vast variety of electronic, spectral and structural properties. All porphyrin-like compounds have a strong absorption band around 400nm called Soret – band. Unfortunately this absorption band is not useful for PDT because blue light does not penetrate very deeply into tissue; thus the weaker satellite absorption bands (Q bands) between 500nm and 800nm are used for treatment. These Q bands equally contribute for fluorescence as the Soret – band does[10, 302-305].

The properties of porphyrins are ideal for photo sensitizers for PDT since they are non-toxic and a selective uptake in tumor cells in high concentrations is described. Margaron *et al.* have reported that prophyrins are, being amphiphilic, generally more photo dynamically active than symmetrically hydrophobic or hydrophilic molecules[306]. Due to the very strong absorbance of light and transfer this energy to surrounding oxygen molecules, toxic singlet oxygen species and free radicals are thus formed upon irradiation[279, 307-309]. Singlet oxygen, the predominant cytotoxic agent produced during PDT is a highly reactive form of oxygen that is produced by inverting the spin of one of the outermost electrons. These chemicals are very reactive and can damage proteins, lipids, nucleic acids and other cellular components.

5.2.4 Mechanism of Porphyrin Excitation

The generation of singlet oxygen can be described in the following steps: excitation of the porphyrin to the singlet excited state ($^1P^*$) made possible by the strong

absorption in the near red UV region (Figure 5.5, simplified Jablonski diagram)[284, 310-313]. The singlet excited porphyrin can decay back to the ground state with release of energy in the form of fluorescence - enabling identification of the tumor tissue. If the singlet state lifetime is suitable, which is the case for many porphyrins, the singlet state can be converted into the triplet excited state ($^3P^*$). This energy can be transferred to another triplet state (according to the spin-transfer rules). One of the very few molecules with a triplet ground state is dioxygen, which can be found in most cells. Energy transfer takes place to afford highly toxic singlet oxygen ($^1O_2$) from ground state dioxygen ($^3O_2$), provided the energy of the $^3P^*$ molecule is higher than that of the product $^1O_2$.

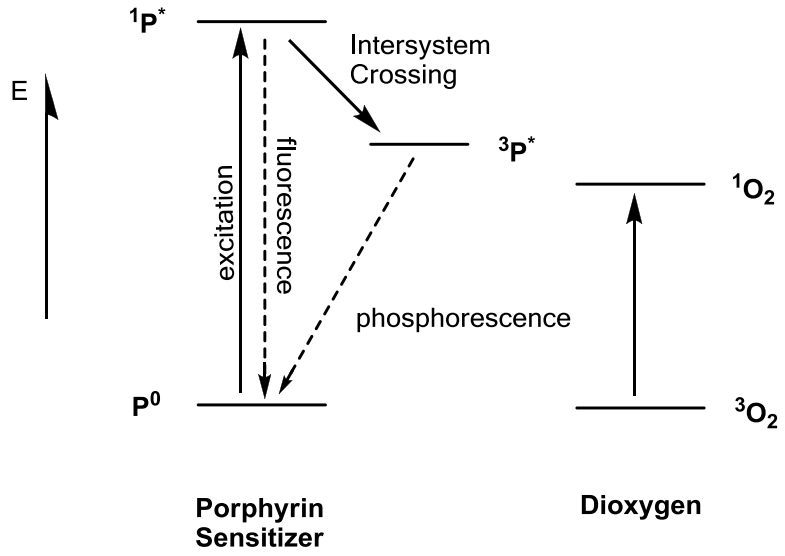

Figure 5.5 Simplified Jablonski diagram depicting the energy levels of the porphyrin on the left and dioxygen on the right, respectively.

There are 2 different types of photoreactions for the PDT (Scheme 5.1): Type-I photoreaction describes an electron transfer from the photo sensitizer to a substrate or directly to the dioxygen. The Type-II photoreaction is constituted of an energy transfer from the excited state of the photo sensitizer to the dioxygen to yield singlet oxygen.

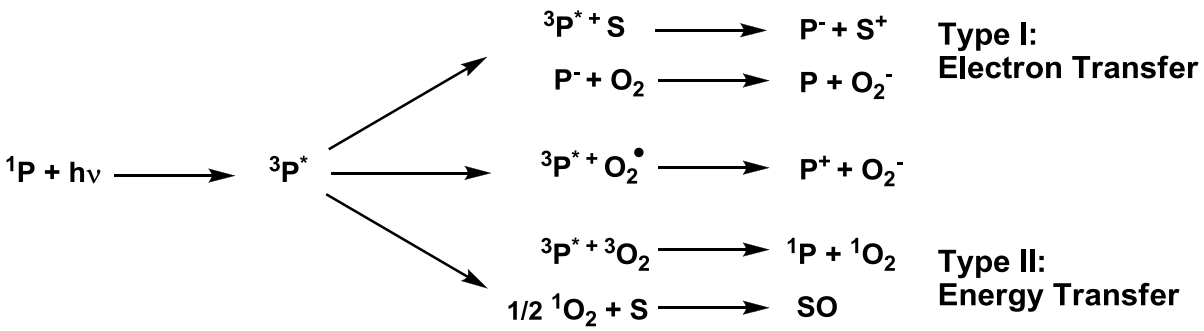

Scheme 5.1 An overview of type I and II photoreactions: P resembles the photo sensitizer, ^1P its singlet ground state, $^3P^*$ the triplet excited state, P^- is the reduced photo sensitizer, P^+ the oxidized form, S is a substrate molecule, S^+ its oxidized form, O_2 resembles dioxygen (triplet ground state), O_2^- is the superoxide anion, O_2. is the superoxide radical, $^3O_2$ is triplet ground-state oxygen , $^1O_2$ in a singlet excited state, and SO is an oxygen adduct of a substrate.

The general procedure of PDT includes the injection of the photosensitizing agent into the bloodstream of the patient. The drug is then absorbed by cells all over the body and later, the cancer cells are treated by exposing this surface to laser light (usually 10 – 30 minutes). The photosensitizing drug absorbs the light to form singlet oxygen that oxidizes the DNA, proteins, and membranes of the irradiated cells which are thus destroyed. Another application method is the treatment of a tumorous surface with a cream with is then locally irradiated after uptake of the photodynamic agent into the cells (up to 16h depending on the carrier substrate).

Mitochondria have become the central processing organelles in the majority of apoptotic pathways. Signals from cell surface receptors or from damaged sites converge on mitochondria, leading to permeabilization of both mitochondrial membranes, dissipation of the inner membrane potential and release of several apoptosis-related proteins, normally located inside the mitochondria. This process can also be triggered by targeted irradiation of the corresponding receptor proteins in proximity of the photo sensitizer (Figure 5.6). The release of apoptosis-related proteins results from the formation of a channel known as the permeability transition pore complex (PTPC). Another receptor, AIF is localized in the mitochondria and released in response to light stimuli. This apoptosis-inducing factor moves directly to the nucleus, where it produces chromatin. The hydrolytic reactions of apoptosis are catalyzed by a family of proteases termed *caspases*. The *caspases* are cysteine

proteases present in cytosol and activated by mitochondrial proteins. The combining effects of irradiation and the reaction of the surface receptors favor and accelerate the apoptotic behavior of mitochondrial protein cascades.

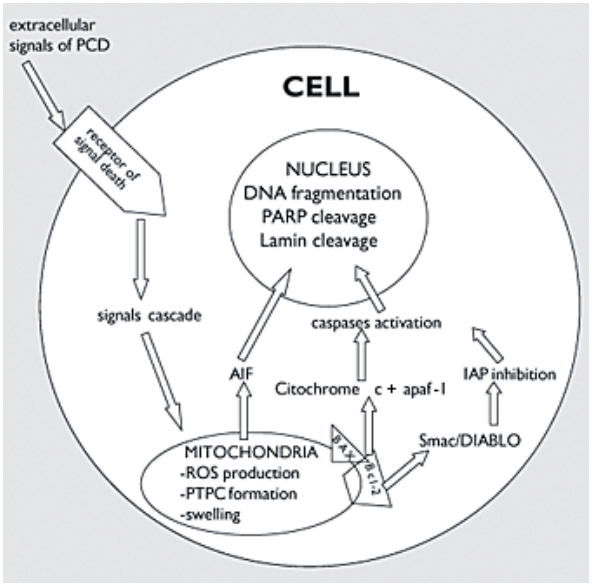

Figure 5.6 Apoptotic mechanism in mitochondiral membranes upon irradiation with light [225].

5.2.5 Porphyrins and their Biological Behavior

Porphyrins and metalloporphyrins possess a high binding-affinity to cellular components, membranes, proteins and DNA. Living cells as well as dead cells are stained rapidly by different porphyrins. Appropriate illumination at around 420 nm, in some cases of metalloporphyrins up to 550nm, generates an emission of red fluorescence and generates toxic oxygen species. *In vivo* administration of various porphyrin sensitizers to tumor bearing animals and humans resulted in uptake of the porphyrins in the tumors, while the normal surrounding tissues had a low comparable porphyrin concentration[90, 314-316].

As further developments, water soluble porphyrins were introduced, such as the tetra cationic 5,10,15,20-tetrakis(*N*-methyl-4-pyridinium)-porphyrin (Figure 5.7, TMPyP), which was found to localize in the nuclei of human leukemia cells. Furthermore upon UVA irradiation, it efficiently induces apoptosis[317]. Wu *et al.* claim

that some cationic porphyrins were killing HeLa cells with IC_{50} values down to 6 nM concentrations[183]. However, they did neither protect the cells from heating, as this is normally done[318] nor did they use any specified light source, since PDT is normally done with light that has a wavelength greater than 600 nm in order to penetrate deeper in the cancerous tissue.

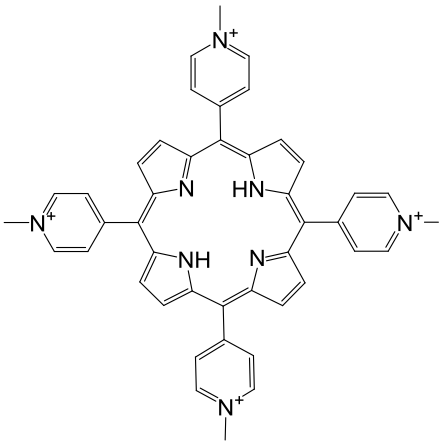

*Figure 5.7 Water soluble 5,10,15,20-tetrakis(*N*-methyl-4-pyridinium)-porphyrin used as a photo reactive reagent to damage DNA[317].*

5.2.6 Approved Drugs containing Porphyrins

In December 1995, the U.S. Food and Drug Administration (FDA) approved a photosensitizing agent called Porfimer sodium, or Photofrin (Figure 5.8), to relieve symptoms of esophageal cancer that is causing an obstruction and for esophageal cancer that cannot be satisfactorily treated with laser alone[162, 297, 300]. In January 1998, the FDA approved Porfimer sodium for the treatment of early non-small cell lung cancer in patients for whom the usual treatments for lung cancer are not appropriate. Still today, the most commonly used photo sensitizer is Photofrin. Recently, the FDA has recommended that BPDMA, marketed under the name Visudyne (injection), be approved for use in therapy, which is essentially a porphyrin based PDT to destroy the defined newly formed tissue in the retina. The ideal photo

sensitizer would have its absorption maxima at wavelengths longer than 600nm to achieve optimal penetration in deeper laying tissue and organs.

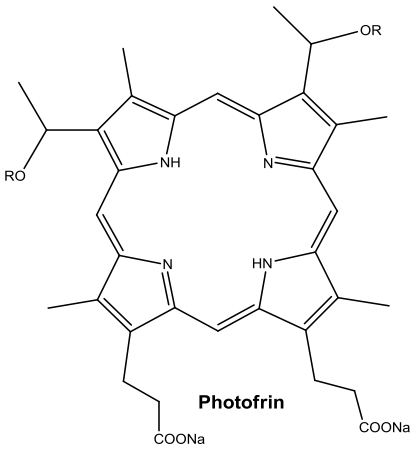

Figure 5.8 Commercial photo sensitizer Photofrin.

Different ways to apply this combinational therapy are tested, combining new laser types and photo sensitizers to treat potentially cancers that are located further below the skin or inside an organ. One important new aspect is also the combination of known classical chemotherapy and relatively new approaches like PDT to achieve optimal treatment of cancer with lesser side effects.

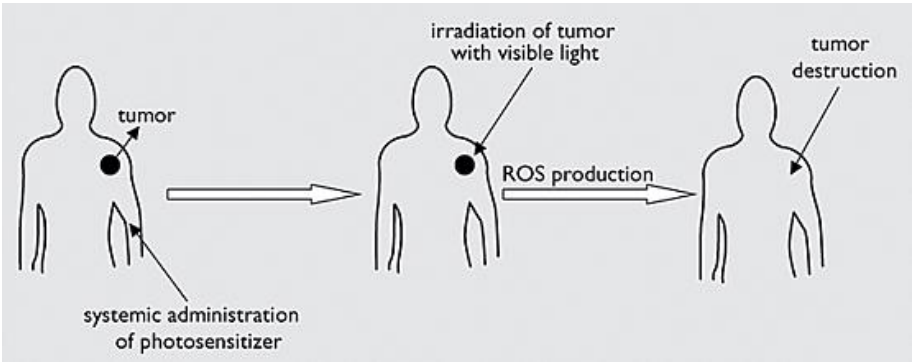

Figure 5.9 Schematic drawing of a possible application of the photo sensitizer via systemic administration with later irradiation of the tumor with light.

The market for photodynamic therapy is still rather small. Table 5.1 gives an overview on the cancer types which can be treated with the corresponding therapy including

the number of patients. The market estimate of approximately 250'000 suitable patients suggests that if safe and effective PDT treatments were available then annual sales well in excess of $100 million are possible.

Cancer Type	Patient Number	PDT suited
Head and Neck (oral cavity, esophagus)	150'000 based upon a US incidence of 17.7 per 100'000	10% = 15'000
Lung cancer	500'000 based upon a US incidence of 170'000	Estimated 10% = 50'000
Bladder	150'000 based upon a US incidence of 53'000	5% = 7'500
Gastric	Second most common cancer in Far East 120'000 pa. In the West around 300'000 pa	Estimated 10% = 30'000
Cervical	40'000 based upon a US incidence of around 13'000	Estimated 10% = 4'000
Non melanoma skin	500'000 based upon a US incidence	Estimated 80'000
Barrett's esophagus (pre-cancerous)	1 million based upon a US incidence	5% = 50'000
Total		**approx. 250'000**

Table 5.1 Overview on the number of patients estimated to benefit from a specific photodynamic therapy. Numbers derived from various sources of the official homepage of the NDA and NIH.

5.2.7 Combinatorial Therapies

There have been several studies evaluating the combination of PDT and "classical" chemotherapy[195]. First studies were done in the late nineties[319]. These and later studies could show that a combination of PDT and *cisplatin* was much more effective in killing murine tumors or mouse lymphoma cells respectively than any therapy alone[300]. Sadler et al. have introduced platinum(IV) diazide complexes, that upon UVA light irradiation are being activated to form the reactive Pt^{2+} complex (Scheme 5.2)[160, 186, 226, 286, 320, 321].

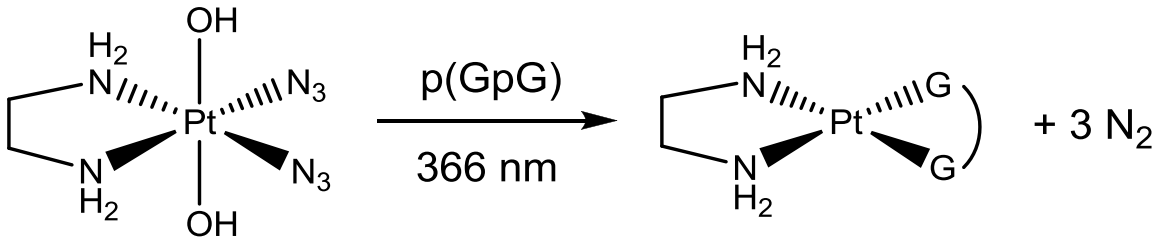

Scheme 5.2 Reaction of platinum(IV) diazide complexes and dinucleotides exposed to UVA light. Figure adopted from ref [226].

Another study showed that PDT combined with cytotoxic chemotherapy is well tolerated in mice bearing either the RIF-1 tumor or the EMT-6 tumor[191]. However, the Photofrin-induced photodynamic therapy-resistant cell line (RIF-1) is cross-resistant to *cisplatin*[192]. Another study showed that photodynamic therapy complements and enhances low-dose *cisplatin* cytotoxicity in MCF-7 breast cancer cells [38]. In the same line, mouse squamous cell carcinoma were exhibiting enhanced susceptibility to photodynamic therapy when they were treated simultaneously with low doses of *cisplatin*[296]. Mechanistic studies revealed that low doses of *cisplatin* together with a Photofrin based photodynamic therapy lead to disjointed cell cycle phase-related activity. This accounted for the synergistic outcome of the combination therapy[185]. There was also a report about an enhanced apoptotic effect of combined photodynamic therapy and carboplatin[225].

Many research efforts were evaluated to find photo sensitizer that were *covalently* linked to DNA damaging metal complexes[322]. Initial work mainly was performed in the group of Brunner. Their first conjugate failed to be more phototoxic than *cis*platin co-administrated with the porphyrin[238]. Follow-up compounds had phototoxicity down to the lower μM concentration[168, 323-328]. Munakata and co-worker synthesized water soluble tetrakis-(2-aminophenyl)-porphyrins that were coordinated to 4 *trans*-diamino-chloro-platinum units[329]. In Figure 5.10, the most recently published covalently conjugate between a photodynamic therapeutic agent (phthalocyanine) and *cis*platin is shown [182]. Their phototoxicity after a relatively long exposure of one hour is in the sub micro molar concentration range. It needs to be noted that these conjugates are actually di-platinum complexes with both metals having only one

leaving group. Whether these di-platinum complexes will result in mono-adducts to DNA, which are easily repaired, or di-adducts, which are much more difficult to be repaired in the cell, remains to be explored.

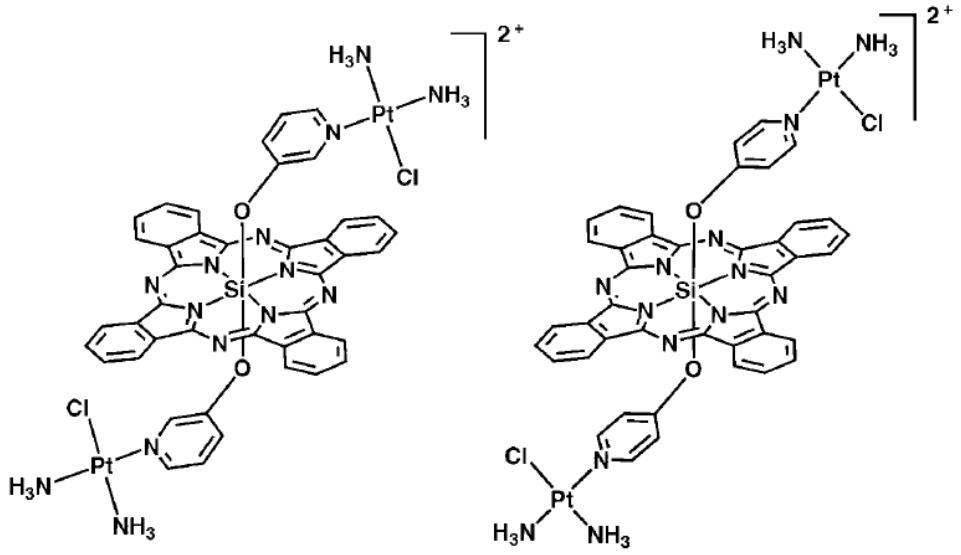

Figure 5.10 Example of a covalently linked cisplatin with a photodynamic therapeutic agent [182].

The cytotoxicity of conjugates of water-soluble porphyrins together with *cis*platin analogues was studied without evaluating a possible PDT effect[330-333].

5.3 Motivation and objective of this project

In order to successfully treat cancer that occurs near a surface, we combined the advantages of photodynamic therapy conducted via water-soluble porphyrins with the well-known behavior of *cisplatin*. On the one hand, the porphyrin residue contributes its properties to the complete system, by a) adding its ability to enter cells while functioning as a carrier system for the covalently bound *cisplatin*, b) as a very effective photo sensitizer with tunable excitation properties related to the central metal ion and c) its function (in case of the non-metal containing and the d^8-metal containing ones) as a possible intercalator, which is considered as a binding mechanism and d) it's tremendously improved water solubility[334]. It's highly positive charge contributes to its affinity towards negatively charged biological structures

such as DNA, deprotonated proteins and possibly cell membranes and the phospholipid bilayer. *Cisplatin* was attached to the porphyrin because of its known anticancer properties. When attached to i.e. DNA and irradiated, the generation of singlet oxygen in the proximity of biological molecules will create greater damage than in more remote areas in the cells. The same is true for the binding of *cisplatin* to the cell membrane or the mitochondria.

In Figure 5.11, the 6 lead molecules are shown. They all consist of a central porphyrin unit with 3 4-methyl-pyridinium and one *para*-cyanophenyl residues, which functions as a covalent link to platinum or stays innocent if no metal is attached. The prophyrins are aromatic, essentially flat, with a 3+ charge in case of the non-platinated and 4+ in case of the platinated species (no chloride dissociation assumed). From the organic synthesis, iodide species were received. These counter anions were exchanged using an anion exchange column and set to be nitrate due to high solubility and innocent behavior towards cells or DNA.

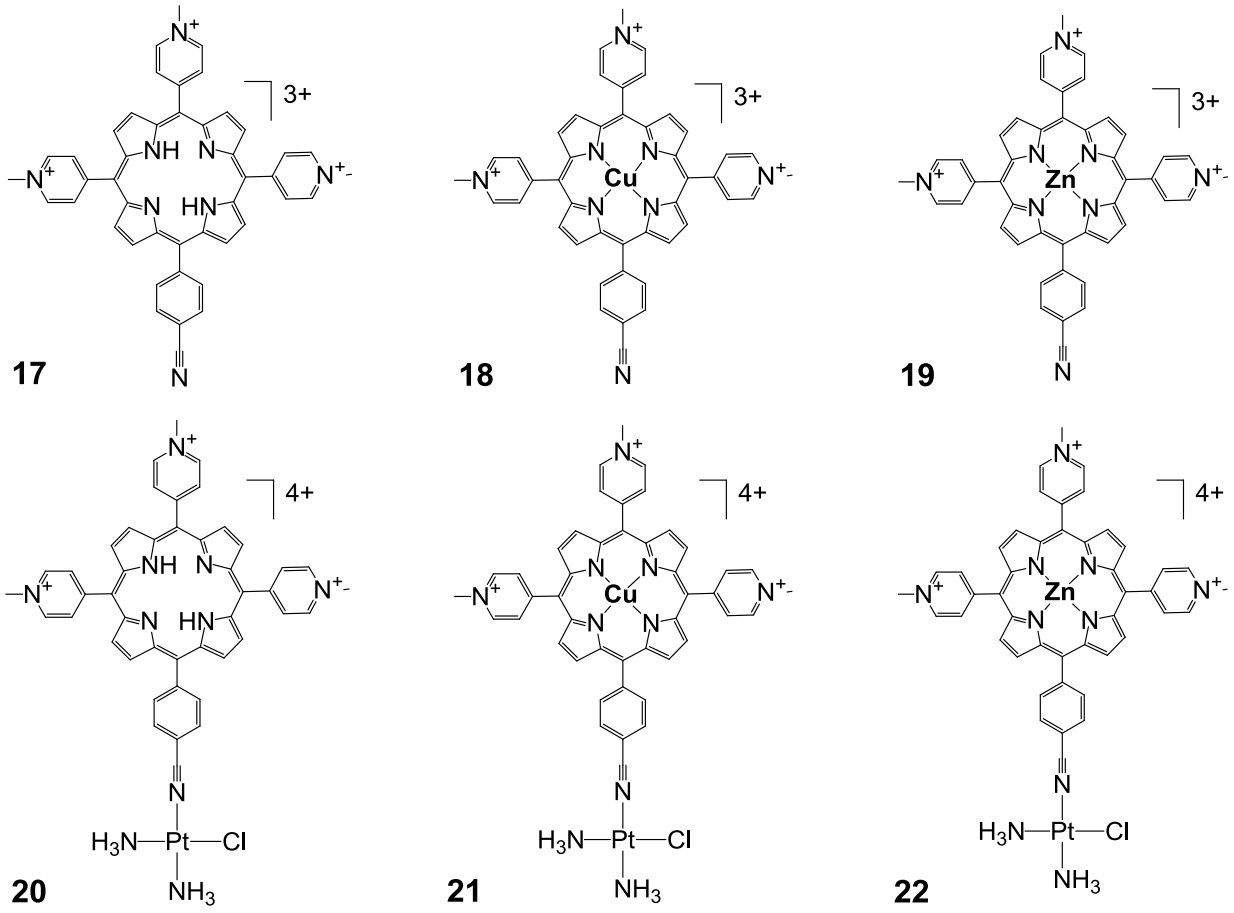

Figure 5.11 Synthesized cationic porphyrins without and with an attached cis-diamminechloroplatinum(II) unit and different central metal ions.[181]

5.4 Results and Discussion

5.4.1 Synthesis and Characterization

Despite a great number of well-known and previously synthesized porphyrins, the synthesis of the 5,10,15-methylpyridinium-20-*para*-benzonitrile-porphyrin nitrate was only described seldom in literature[335]. The synthesis of the porphyrins was carried out according to or slightly modified the known procedures in porphyrin chemistry. The first approach was the direct synthesis according to Adler and Longo starting with single components of the porphyrins (pyrrole, *para*-cyanobenzaldehyde, 4-pyridinaldehyde) and refluxing them in propionic acid under air for 40 minutes yielding a mixture of polypyrroles, 6 different porphyrins in statistical compositions of

their aromatic residues and other compounds which had to be separated *via* repeated column chromatography[147]. The yield was traditionally very low (~ 1%) and the clean-up very tedious.

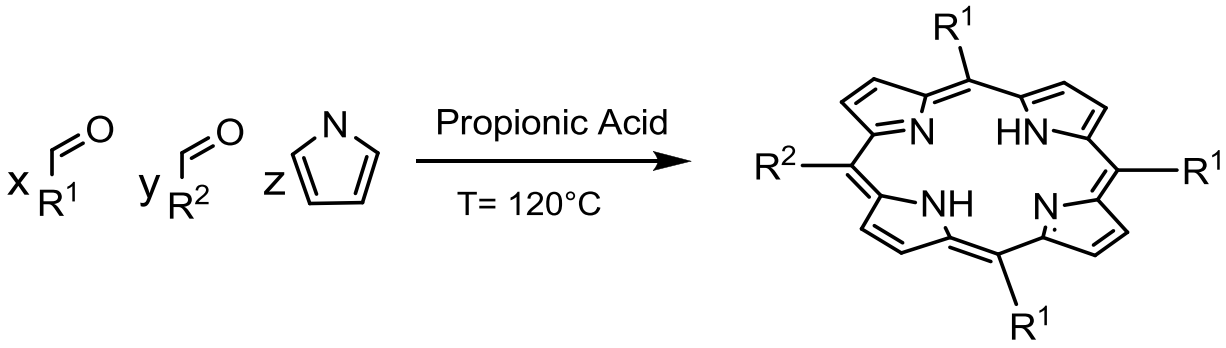

Scheme 5.3 Statistical Synthesis of A_3B - type Porphyrins.

The other, synthetically more challenging procedure was to go via the route described in Scheme 5.4. Starting from the dipyrromethane (DPM, if R^1=pyridine DPP), which is then reacted further in a Gringard promoted reaction with an aryl-chlorocarboxylic compound to the dipyrro-triaryl-diol[149, 336, 337]. This is processed to a stabilized tin – di(*n*-butyl) form which is thus reduced to the alcohol and instantly reacted to the closed ring porphyrin using again a dipyrromethane (DPM, if R^2= *para*-cyanobenzaldehyde DP*p*BN). This reaction yielded in each step around 30-50% of the desired product and totally yielded 12% of the porphyrin, although using a lot of purification and separation work.

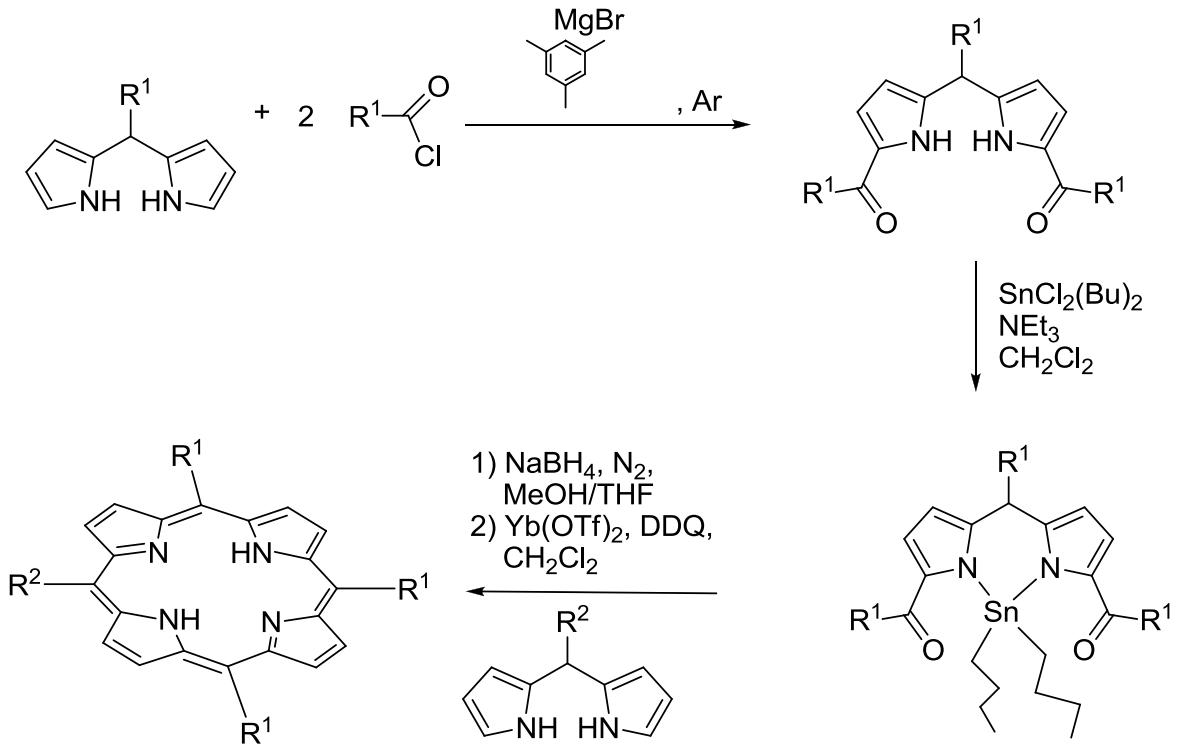

Scheme 5.4 Synthesis of the A_3B - type porphyrin via a stabilizing tin intermediate.

The synthesis of the *cisplatin*-porphyrin compounds was carried out according the general protocols used to prepare *cisplatin* adducts by activating *cis*platin by the precipitation of one chloride atom to produce a vacant site that is thus reacted with the cyano-group of the porphyrin. This reaction took several days or even weeks due to the two positively charged compounds that have to be reacted. The reaction was monitored via HPLC and the yield was high.

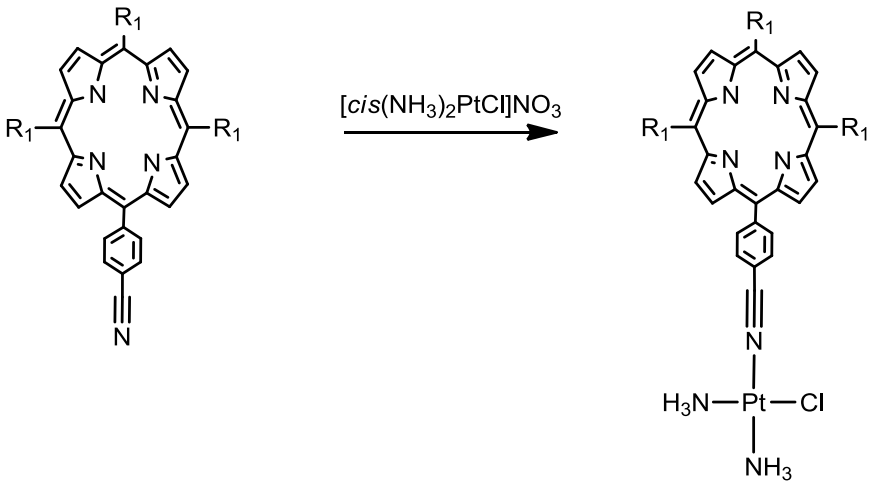

*Scheme 5.5 Reaction of the activated cis*platin *with a porphyrin residue (R_1 = 4-Me-pyridyl)*

We prepared porphyrin compounds **17 – 22** which were fully characterized according to standard methods, including ^{1}H-, ^{13}C-, ^{195}Pt-NMR, ESI-MS, HPLC, AAS, UVvis, and MALDI-MS. These compounds all originated from the 5,10,15-methylpyridinium-20-benzonitril-porphyrin nitrate and contained different central metal ions, i.e. Cu^{2+} or Zn^{2+} and/or a *cis*platin 4-methylpyridinium residue bound covalently to the nitrogen of the benzonitrile residue of the porphyrin. The seemingly simple preparation of mono activated *cisplatin* is rather low yielding as a survey of the literature shows[209, 266, 338-340]. The reaction times for those platinated porphyrins were up to 20 days until the complete conversion was obtained. Nevertheless, we succeeded in synthesizing the mono porphyrin *cisplatin* adducts **17 – 22** in 88-92% yield.

During the characterization of the compounds, it was found that these complexes have superior spectral properties upon previous porphyrin complexes regarding their absorption and fluorescence. The special absorption properties of these compounds culminated in compound **22** which had a standard Soret band at around 440 nm but a strong series of Q bands reaching form 565 to 680, a region which provides this compound **22** with good properties to be excited by irradiation through skin.

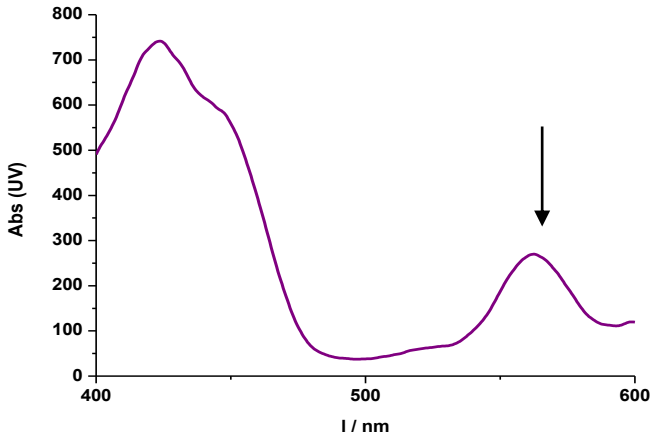

*Figure 5.12 Absorption spectrum of Porphyrin **22**. Arrow points to the large Q-band at 565 nm.*

Already in 1930, Reed and Bachem proposed, that UV light above 550 nm could reach the corium of the skin in their description of the skin penetration of children. The visible light can thus excite the porphyrin **22** to become an active photosensitizer.

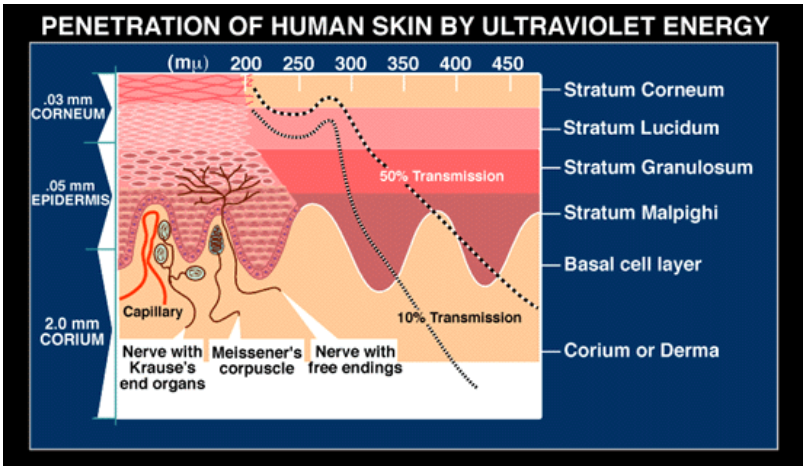

Figure 5.13 Schematic drawing of the skin layers and the UV energy travelling into the specific layers of the skin. Picture was taken from ***www.cambrige-campus.co.uk/skin-layer/UVtransmission***.

The spectral properties of the compounds did not change upon platination. Related DFT calculations showed that the influence of the central metal ion on the N (benzonitrile residue) is very small and thus the covalent platination does not have an influence on the electronic properties of the overall molecule. The HOMO and LUMO energy levels of compound **17** of the N atom of the CN show a minimal lower eV than the zinc containing compound **19**. The same is true for all metal containing porphyrins as well as for their solvated central metal ions. But the influence is rather small towards the N of the cyano residue. The different reaction times and kinetic properties for the platination reaction of the molecules **17** – **19** cannot be explained with the influence of the central metal ion. This happened to be rather due to solvatation effects of the porphyrin complexes. Since platinum complexes in general react rather slowly, the reaction times for the platination reached from 2 days to 14 days for a 100% platination. An anion effect can be neglected because the reaction was carried out once with nitrate and once with tetrafluoroborate as counter anion.

The DFT calculations do explain though why the UVvis spectrum for the sister compounds **17** & **20**, **18** & **21**, **19** & **22** are not different. The effect of the coordinated *cis*platin towards the spectral properties is too low.

A second observation related to chapter 4 could also be partly explained. The energies for the solvatation are showing a direct connection to the number of water molecules counted to the central metal ion. Compound **19** shows a large increase in ΔE for the dissolution of the first as well as for the second water molecule and thus 3 fold increased in stability from no to two coordinated water species (see Table 5.2). The first and second water molecule of copper compound **18** is not quite as strongly bound to the copper compared to the zinc containing compound. The copper molecule is known as an intercalator which was also observed for the compound **12** described in chapter 4.[11, 99, 111, 136, 302, 304, 314, 341] There the observed intercalative properties lead to the conclusion of a semi-intercalation or a combination of a side-on coordination and intercalation. The fact that compounds **19** and **22** are not intercalating but rather coordinating to DNA can also be explained with those numbers. The influence of the axially coordinated water molecules is rather strong as discussed previously[11].

		Porph-2H 17	**Porph-Cu 18**	**Porph-Zn 19**	**Porph-Cu(H_2O)**	**Porph-Zn(H_2O)**	**Porph-Cu(H_2O)$_2$**	**Porph-Zn(H_2O)$_2$**
Energies (Hartrees)	Electronic energy E_ε	-2172.65	-2367.68	-2237.15	-2444.12	-2313.60	-2520.54	-2390.02
	Solvent-corrected (H_2O) energy E_{solv}	-2173.05	-2368.08	-2237.56	-2444.52	-2313.99	-2520.95	-2390.43
	ΔE (kcal/mol)[a]	-	-	-	-3.96	-6.12	-4.73	-9.56
	[a] $\Delta E = E_{solv}[Porph\text{-}M(H_2O)_n] - E_{solv}[Porph\text{-}M] - n*E_{solv}(H_2O)$							
MO energy (eV) / % of N atom of CN	L+11	0.14 (36%)	0.14 (40%)	0.11 (41%)	0.15 (40%)	0.12 (41%)	0.17 (34%)	0.16 (41%)
	L+5	-1.88 (13%)	-1.86 (13%)	-1.87 (14%)	-1.83 (13%)	-1.85 (14%)	-1.79 (13%)	-1.79 (13%)
	LUMO (L)	-3.52	-3.4	-3.41	-3.37	-3.41	-3.31	-3.35
	HOMO (H)	-6.05	-6.1	-5.97	-5.93	-5.87	-5.74	-5.64
	H-1	-6.28	-6.15	-6.14	-6.04	-6.08	-5.93	-5.92
	H-2	-7.18	-7.08	-7.24	-6.88	-7.17	-6.62	-6.99
	H-6	-7.89	-7.66	-7.62	-7.47	-7.55	-7.36	-7.29
	Mulliken charge on N atom of CN	-0.115	-0.116	-0.116	-0.116	-0.107	-0.118	-0.113
	ΔE(HOMO-LUMO) [eV]	2.53	2.70	2.56	2.56	2.46	2.43	2.29

*Table 5.2 Selected DFT data for porphyrin compounds **17**, **18**, and **19** and their mono- and diaquated- species.*

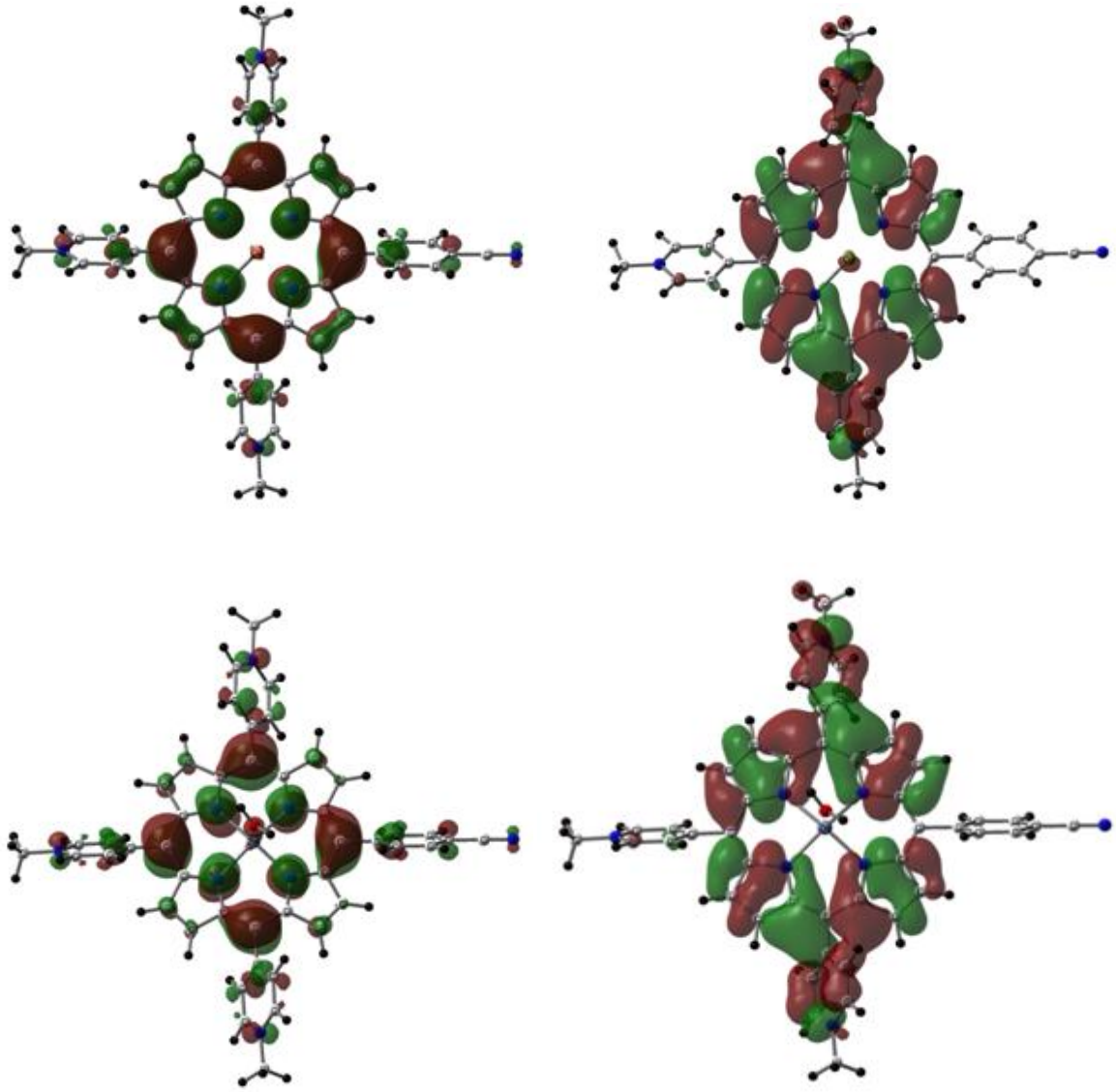

*Figure 5.14 HOMO (left) and LUMO (right) orbital level of Cu compound **18** (top, one axial water molecule) and Zn compound **19** (bottom, two axial water molecules).*

5.4.2 Stability of Platinum-Porphyrin Complexes in Water and Serum

For applications under biological conditions, it has to be secured, that the applied compounds are stable and not affected by the biological environment otherwise they might lose their functionality *in vitro* and *in vivo*. The serum stability is one important measure, as well as the internal stability of the compound itself.

The total concentration of albumin in plasma is around 60% of the total protein concentration, globulin (35%) and fibrinogen (4%) contribute to the rest of the highly abundant proteins. Lower abundant proteins only make up 1% of the total protein concentration. Albumin solutions are therefore taken as a model system to mimic cellular plasma conditions.

The covalent bond from the benzonitrile residue of the porphyrin to the platinum is strong and could not be broken upon the irradiation of light (>550 nm, 6000 lux, from a xenon lamp, up to 20 hours, with or without water cooling) nor exposure to oxygen. The stability tests were carried out in MEM medium, RPMI medium as well as in water. Additionally, to the standard characterization, the platinum content was determined by AAS (Atomic Absorption Spectroscopy) and found to be 1 equivalent compared to the molecule before and after the irradiation.

	Measured Abs.
Reference	0.215 (2)
20	0.213 (3)
21	0.219 (4)
22	0.209 (1)

Table 5.3 AAS Normalized standard and the corresponding averaged measured concentrations of 50 ppm after 3 repetitions of the measurement. Reference solution was taken from Sigma-Aldrich and diluted to 50 ppm.

It is known that *cisplatin*, especially in its activated form, binds rapidly and almost irreversible to human albumin present in its serum (HSA)[187, 342]. Since HSA contains cystein residues which are exposed to the solvent and it was shown in many studies that *cisplatin* binds to these covalently as shown, there are several binding modes possible towards HSA. Non-covalent linkage is usually a fast and reversible process detectable shortly after incubation. Electrostatic interactions are also reversible and

can thus be neglected due to slightly acidic conditions (pH = 5.0) during the experiments. Covalent coordination which is essentially irreversible and caused by a de-chlorination of the *cisplatin*-adduct and thus slow reaction evolves with time. Such covalent links can occur by either an unlikely separation of the platinum from the porphyrin or the combination and coordination of activated platinum toward a cystein, methionine, or histidine of the protein. The different resulting molecules could thus be observed due to their characteristic spectra via HPLC measurements. It was assumed, and later also tested, that the positively charged porphyrins alone regardless of the central metal center, do not interact with HAS ($pI_{HSA(25°C)}$ = 4.7). Thus, the electrostatic interaction could be neglected.

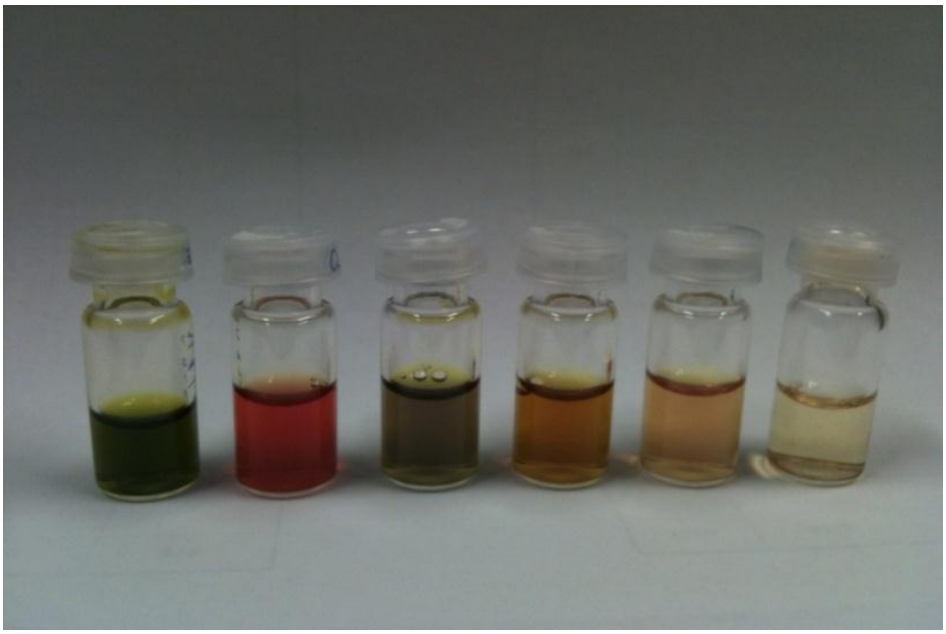

*Figure 5.15 Colorful porphyrins **17** - **22** (from left to right).HPLC probes taken during reaction.*

It should be noted, that all compounds **17** – **22** were stable in water, BSA media and also in acidic or saline solutions (up to pH1 and 1mM, respectively) over a period of weeks. Compounds **20**, **21**, and **22** showed a minor decomposition component when analyzed in a C18 – Nucleodur HPLC column with the typical 0.1% TFA buffer solution versus MeOH, which was due to the *cisplatin* – residue losing one chloride[181]. This behavior could be eliminated by the use of a saline solution (500 mg NaCl in 1l H_2O,

~10mM) which reverses the dechlorination. This behavior could also be observed during the stability test, which was carried out in a 0.1% TFA solution.

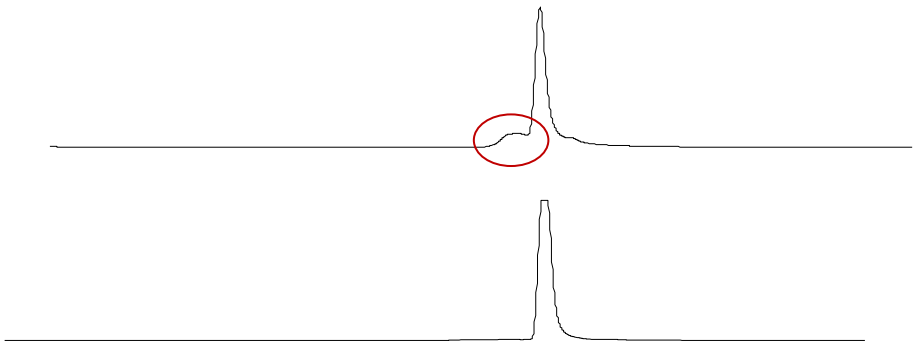

Figure 5.16 Comparison of HPLC properties of compound 22 run at a) normal 0.1% TFA buffer system and b) 10mM saline buffer system.

Size exclusion usually quantify the ratio of human serum albumin bound/unbound to substrates, but due to restrictions and complications during the use of the size exclusion columns with the highly positively charged porphyrin molecules, the stability tests were carried out as follows: a 1 : 1 solution of HSA (13 mg ml^{-1}) and a 0.1 mM solution of the compound were dissolved in a phosphate buffer (0.1 M, pH 7.4, 0.8% NaCl) and its reaction monitored over time with an HPLC system using a C18 – Nucleodur column (flow rate 0.7 ml/min, max. pressure 175 bar) with gradient 1[181, 343]. The effect of lipophilicity and size were taken into account to discriminate between the products. The traces were recorded with a photo diode array focusing at 280 nm to monitor the HSA to determine its relative concentration and at 420 nm in order to observe the free porphyrin (at around 6.5-8 min, depending on the metal and Pt – residue) and the reaction product formed from HSA and the porphyrin at around 10.9 minutes. The gradient was prolonged to 20 minutes for this experiment to re – equilibrate the column again at 10% MeOH/0.1% TFA/H_2O.

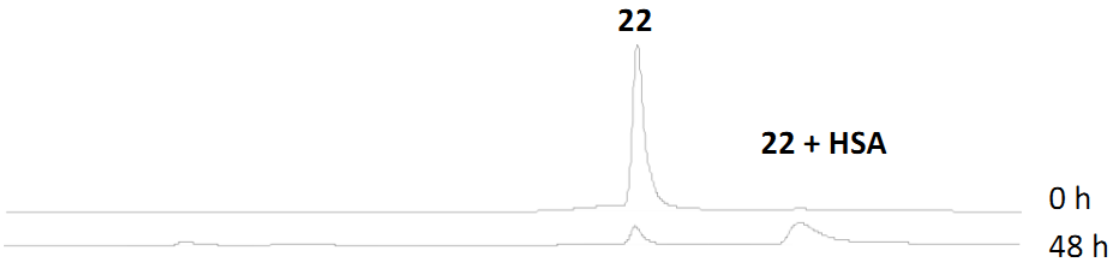

*Figure 5.17 HPLC at 420 nm traces of the lead molecule **22** and its interaction with HAS at a) start and b) 48h. Free **22** was observed as the first signal. The formation of the HSA – 22 adduct is visible by the second signal appearing.*

The observation of the reaction was carried out for 48 hours and monitored every 1 hour for the first 4 hours, then every 2 hours and later every 3 hours. The first rapid increase of bound Pt – Porphyrin (**20, 21, and 22**) towards HSA in the first 4 hours is due to hydrophilic interactions which accelerate the reaction. The latter process represents a covalent binding of the compounds to HSA. The compounds **20, 21,** and **22** showed a clear affinity and covalent bond to HSA but only 8% (**22**), 18% (**20**) and 25% (**21**) were covalently bound within 48 hours, which makes the compounds reasonable stable in HSA. All other compounds were stable apart from the loss of a chloride as discussed above.

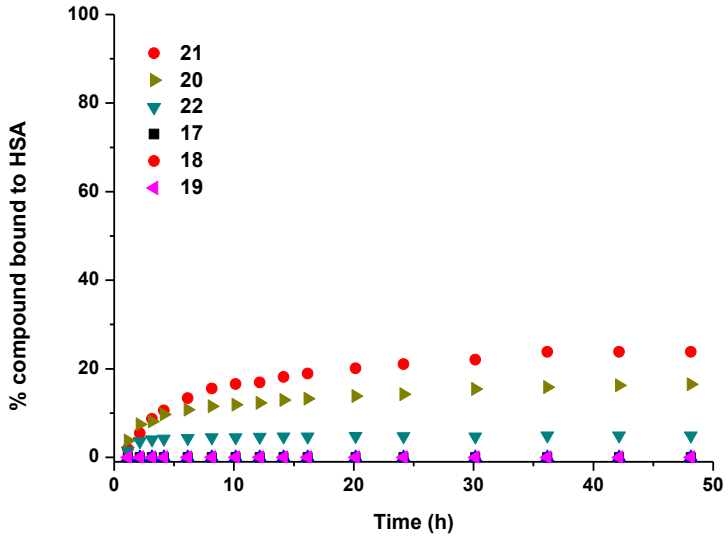

*Figure 5.18 Lead molecules **17** – **22** and their interaction with HSA at 480 nm. It was observed that the platinum – free molecules (**17**, **18**, and **19**) did not interact with HSA whereas the ones with a Pt – residue (**20**, **21**, and **22**) showed a slight amount of covalently bound Pt – HSA species.*

5.4.3 Porphyrin Complexes and their interaction with DNA

Porphyrins have a unique absorption characteristic with a strong absorption maximum called Soret band at around 420 nm for non-metallated and around 435 nm for metallated species. The Q – bands, absorbing light from 450 – 650 nm depend on the outer sphere of the porphyrin, are also very characteristic and contribute additional absorbing properties, which will be of importance hereof. This absorption characteristic makes all porphyrins highly light absorbing, enabling them to easily get into a higher excited (triplet) state from which they decay emitting a strong fluorescence at 650 – 720 nm, although a number of paramagnetic central metal ions, i.e. copper can quench the fluorescence totally and also limit the absorption properties. Non-paramagnetic metal ions make porphyrins highly fluorescent. In our example, Zn^{2+} compound **22** has a very intense series of Q – bands at 530 nm. Peripheral bound metals, such as *cisplatin* compounds in our case, do shift especially the Q – bands into the red, which improves the absorption in deeper skin layers. Zinc and Nickel porphyrins were showed a high fluorescence behavior, copper porphyrins did not. Platinated zinc porphyrin has an, for prophyrins, exceptional high first Q –

band absorbance (8.2×10^4 $cm^{-1}M^{-1}$) at a wavelength of 563 nm – which is a factor that contributes to the high photo – induced cytotoxicity of this complex when irradiated. Porphyrin compounds **17 - 21** have lower intrinsic absorbance bands intense enough to be used in photodynamic therapy, although copper porphyrins **18** and **21** are non-fluorescent as discussed in the literature for the related compound CuTMPyP (Fig. 5.19)[344].

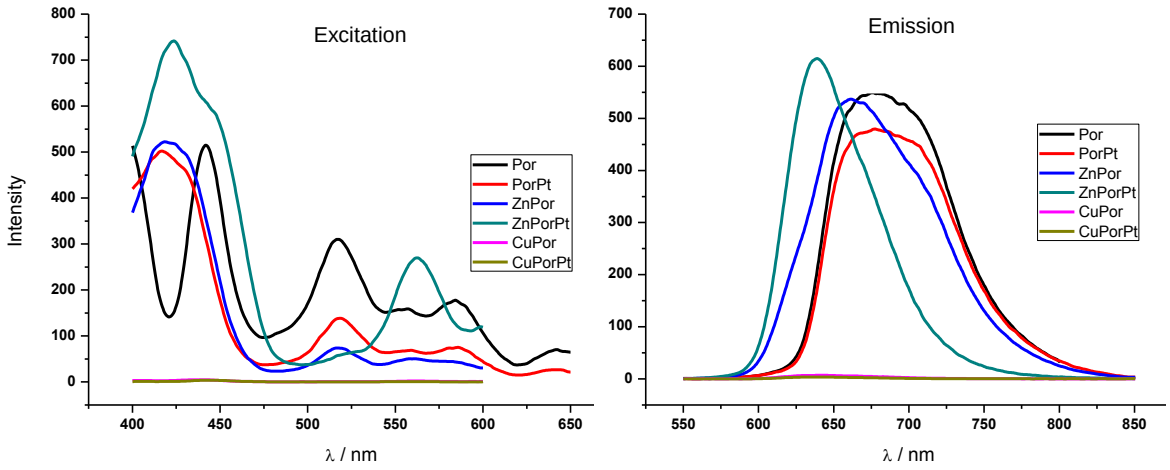

*Figure 5.19 Steady state excitation (λ_{em} = 680 for **17**-**21**, 640 for **22**) and emission (λ_{ex} = 420 for **17**-**21**, 430 for **22**) fluorescence spectra of porphyrins **17**-**22**.*[181]

Porphyrins are fairly flat molecules, which dominates their interactions with the environment. The effect of the central metal ions strongly affects the physical properties of the molecule. Some (mostly natural) porphyrins contain amine- or carboxy- residues that make them more versatile and capable of binding to various receptors. In most cases discussed, especially regarding aqueous chemistry, the charge of the porphyrin is de*cis*ive. We choose a positively charged system to facilitate the binding towards poly-anions such as DNA or RNA, the usual target when working with *cisplatin* – analogue. The ability to further bind to other molecules is limited for the simple porphyrin systems which only contain a central metal ion. Compound **17** cannot bind to any other species except to strong Lewis acids via its Lewis acceptor, the benzonitrile. A possible binding site is the interior of the porphyrin ring, which can be assessed by a metal ion such as i.e. Mg^{2+}. Other metals enter the center of the porphyrin and thus built very strong covalent linkages to the

porphyrin. Metallated porphyrins **18** and **19** are more versatile, including the possibility to exchange the central metal ion's axial ligands. In mass spectrometric measurements, only copper showed an adhesive behavior towards counter ions such as nitrate or chloride.

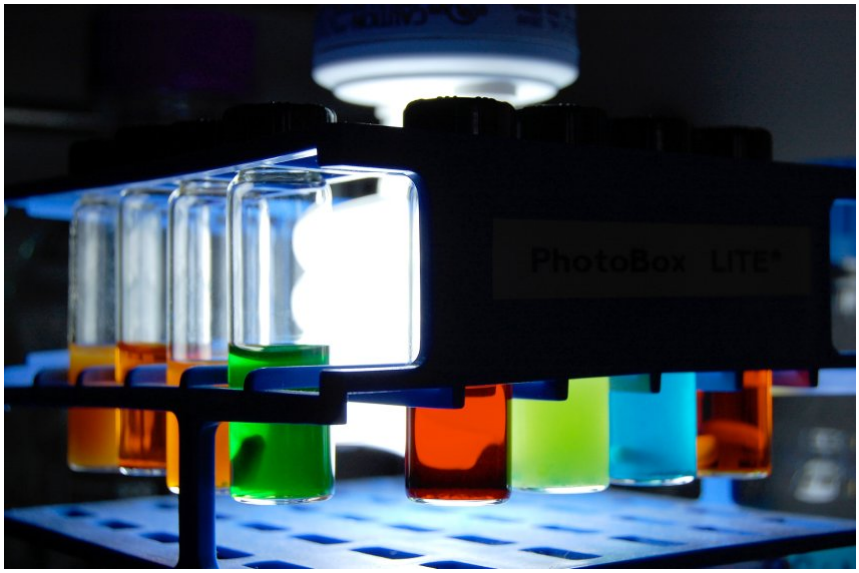

*Figure 5.20 Colorful play with porphyrin compounds **17** – **22** at various pH values and in different solvents.*

To study the activity of the compounds towards their *cisplatin* – like behavior, interaction of compounds **20**, **21** and **22** with 2'-desoxyguanosine was studied. Compounds **20**, **21** and **22** do have several vacant or accessible binding sites in aqueous conditions. The reaction was carried out in a solution containing 10mM phosphate buffer at a pH = 7.4 with 1% NaCl, in order to mimic physiological conditions. A tenfold excess of 2'-desoxyguanosine was applied to the compounds. The product formation was monitored by measuring ESI – MS spectra to determine the function of the binding versus time. The reaction time was well above 24h, which indicates a weak *trans*-effect of the benzonitrile – Pt complex. As shown in Figure 5.21 for the example of compound **21**, the first and easy accessible binding site is the previously discussed and well – known loss of a chloride which leads to the mono – adduct **21** – 2'-desoxyguanosine. In the consecutive step, the amine *trans* to the cyano – like bond of the Pt to the benzonitrile residue is broken and can further react with another 2'-desoxyguanosine.

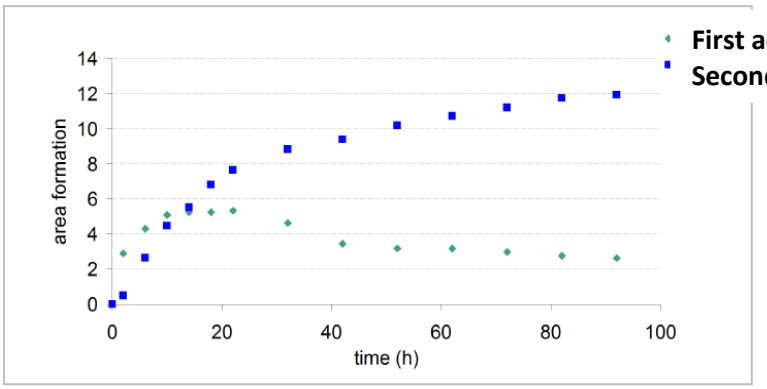

*Figure 5.21 Time – dependant reaction of **21** with 2'-desoxyguanosine.*

The reaction of the compounds follows the classical consecutive reaction profile A -> B -> C. The low solubility of 2'-desoxyguanosine prohibited a determination of the kinetics, which avoids a pseudo-first order condition in the first part of the reaction. The classical experiment with 2'-desoxyguanosine-monophosphate was also carried out, but the exposure to compound **20** caused immediate precipitation due to the positive charge of the porphyrin.

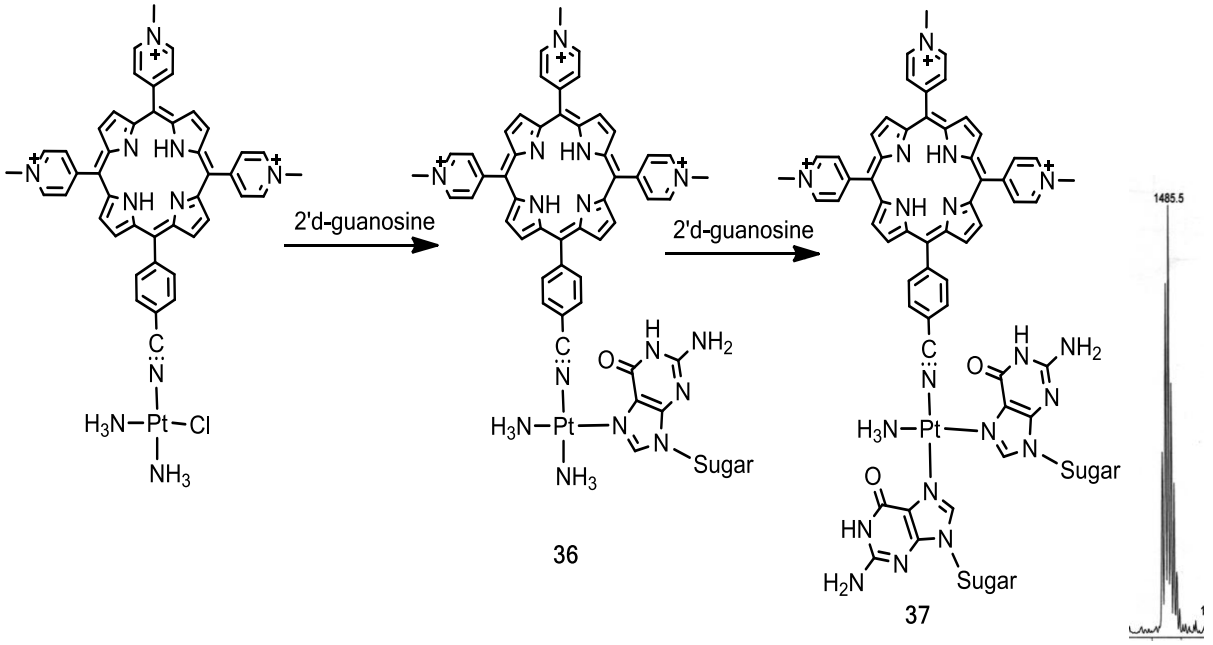

Scheme 5.6 Observed reaction behavior of cis-diammine-chloro-N-cyano-platinum(II)-porphyrin compounds and the corresponding MS spectrum in water with 2'-desoxyguanosine after 24h.

5.4.4 Cytotoxicity Studies in Carcinoma Cells

Most platinum drugs' cytotoxic effect is due to the formation of DNA – Pt – adducts. However, various possible mechanisms are mentioned in literature[187, 191, 238, 319, 345]. *In vitro* measurements of drug concentrations are related to the efficacy of drugs on inhibiting biological functions. The concentration of a drug needed to induce 50% cell death is called the IC_{50} value. One gold standard of determining this value is the MTT assay, another standard is the trypan blue assay[38, 346]. For our studies to determine the IC_{50} value, we carried out an MTT assay, which is a standard colorimetric assay for measuring the activity of enzymes that reduce MTT to formazan upon mitochondrial activity. MTT is a yellow colorant (3-(4,5-dimethylthiazol-2-yl)-2,5-diphenyltetrazolium bromide) that is reduced to purple formazan in the mitochondria of living cells. This reduction only takes place when the cells are alive and the mitochondrial reductase is active. By comparing the formation of the purple formazan, and untreated control cells, the activity of the drugs is monitored. The different absorbance of MTT and formazan can be monitored and quantified by using an ELISA plate reader to measure the absorbance at 570 nm[347].

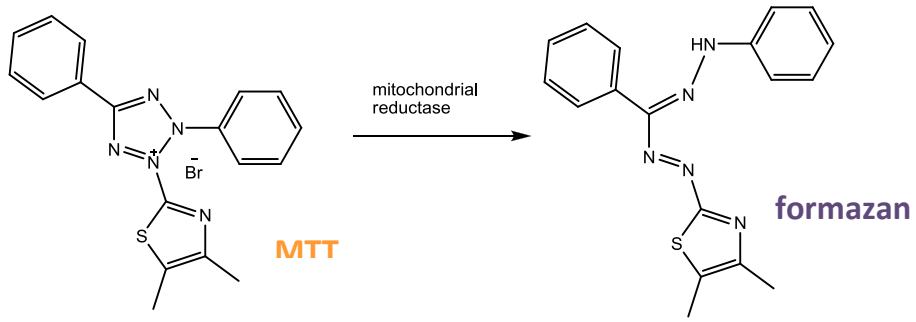

Scheme 5.7 Reduction of MTT to formazan.

To determine the cytotoxicity of the above mentioned compounds **17 - 22**, two different human cell lines, the human mama-carcinoma cells MCF-7 and the human ovarian cancer cells A2780, were exposed to the porphyrin compounds **17 – 22** under different conditions at concentrations ranging from below 0.1 to 200 μM.

Figure 5.22 96 well plate MTT assay. The outer wells are controls with no cells (0% survival), the second lowest row is occupied with untreated controls (100% survival), and in the internal rows each represents the dose response in statistical relevant data (5 experiments) at a given concentration.

The photodynamic effect of the compounds was monitored by exposing one set of the sample plates to light emitted from a water cooled xenon light (to avoid IR irradiation) covered with a cutoff filter 600 nm with an intensity of 3200 lux. The light was shone vertically on the plates with the help of a mirror in order to equally expose all wells in the same fashion. All experiments were carried out twice to avoid contamination errors of mistakes of handling the cells to influence the results. All graphs show a median of minimally 2 experiments.

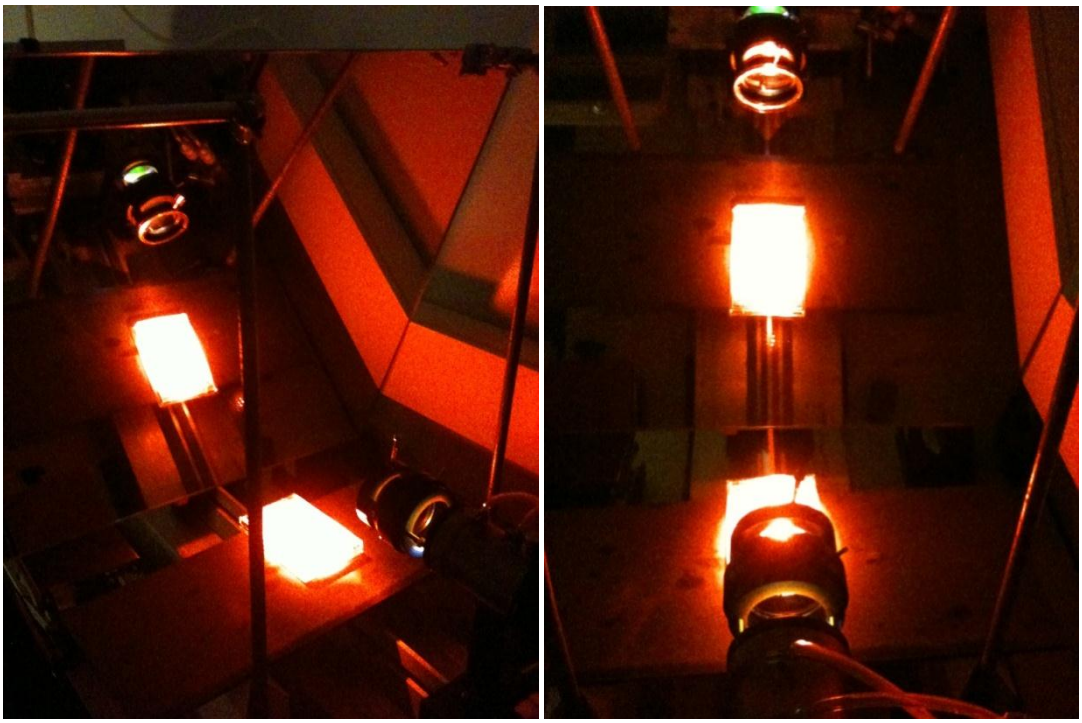

Figure 5.23 The experimental setup for the irradiation of the carcinoma cell lines. The beam of a water cooled light source equipped with a cutoff filter <600nm is directed via a mirror to the 96well plates in a 90° angle.

Compound **17**, a solely organic porphyrin did show a cytotoxic effect when exposed to light after incubation to the cells for 24 hours (green line, Figure 5.24). To determine the needed incubation time, two experiments with different incubation times were carried out. First, the cell plates were exposed to light after 4 hours with no prior exchange of the compound containing medium. This did not show any photo effect or enhancement on the cytotoxic effect (brown line). The photo effect only occurred, when the compounds could be taken up into the cell which takes about 16 – 24 hours. As depicted in Figure 5.24, compound **17** showed a phototoxic effect when exposed to light. The IC_{50} value drops to 1 μM in case of the MCF7 cell line and 0.55 μM in case of the A2780 cell line. Compared to the values obtained for the cytotoxic effects without irradiation to light, this is an increase in cytotoxicity of over 300%! The effect was comparable for both cell lines.

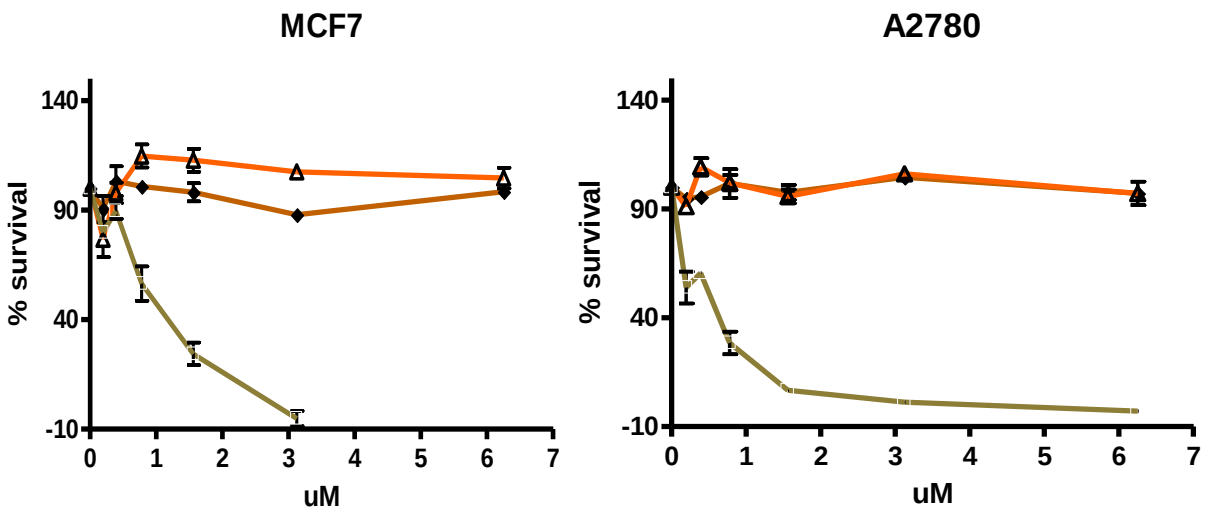

*Figure 5.24 MTT assay excerpt of compound **17**. Only the relevant region of the MTT assay is shown up to 100% cell death at the corresponding concentration. The data points are the median of two MTT assays. The orange line represents the MTT assays with no exposure to light. The brown one shows the survival rate of the cells after exposure to light 4 hours after incubation (no washing), the green line depicts the amount of living cells after exposure to light 24 hours after incubation (and washing) of the cells.*

In another experiment, the cell plate was incubated for 24 hours, then the medium was removed and the cells washed with medium to remove traces of compound which was not taken up by the cells. Afterwards, fresh, no-porphyrin containing, medium was given into the wells and then the plates with the cells were exposed to light. Like this, it could be avoided, that a possible photoreaction taking place outside of the cells and i.e. producing singlet oxygen could harm the cell membrane and thus cause cell death. This exposure to light was carried out at various exposures to light (5, 10, 20, 30, and 90 minutes) at a given concentration of 5 μM (Figure 5.25). These experiments were carried out for compounds **17** and **20**. As shown in Graph 5.25, the phototoxic effect did not increase during longer exposure times. After 10 minutes, the maximum was reached in case of platinated compound **20**.

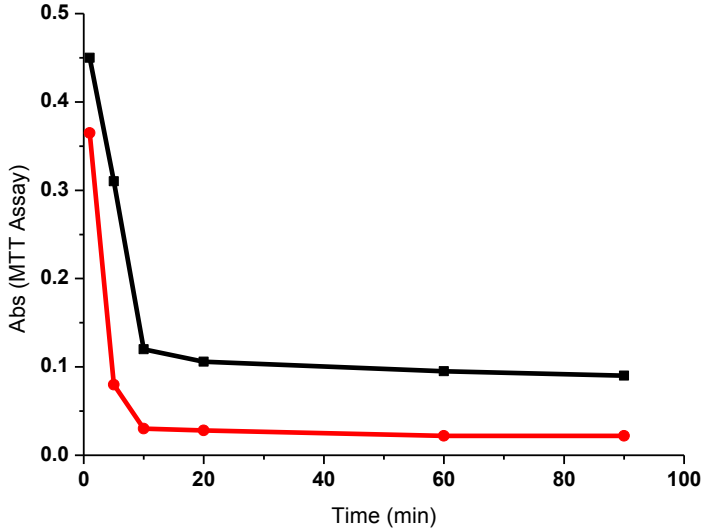

*Figure 5.25 Various light exposure times of cells treated with either compound **17** (black) or **20** (red) at 3200 lux.*

For convenience and since the plates could only be irradiated one at a time, 10 minutes exposure time were chosen to be the preferred exposure time for the following experiments.

A similar toxicity behavior was observed for compound **18**, a porphyrin with a central copper ion. See below for an overview of the IC_{50} values and IC_{90} values (Table 5.4). Again, a photodynamic effect is observed. The increase in cytotoxicity is caused by the irradiation of light. For both cell lines it is observed that the central copper is increasing the cytotoxicity of the compound compared with the metal free compound **17**. Comparable to compound **17** is also that copper compound **18** can as well act as an intercalator into DNA. This can tremendously disturb the biological function a block the cell metabolism and eventually lead to apoptotic effects.

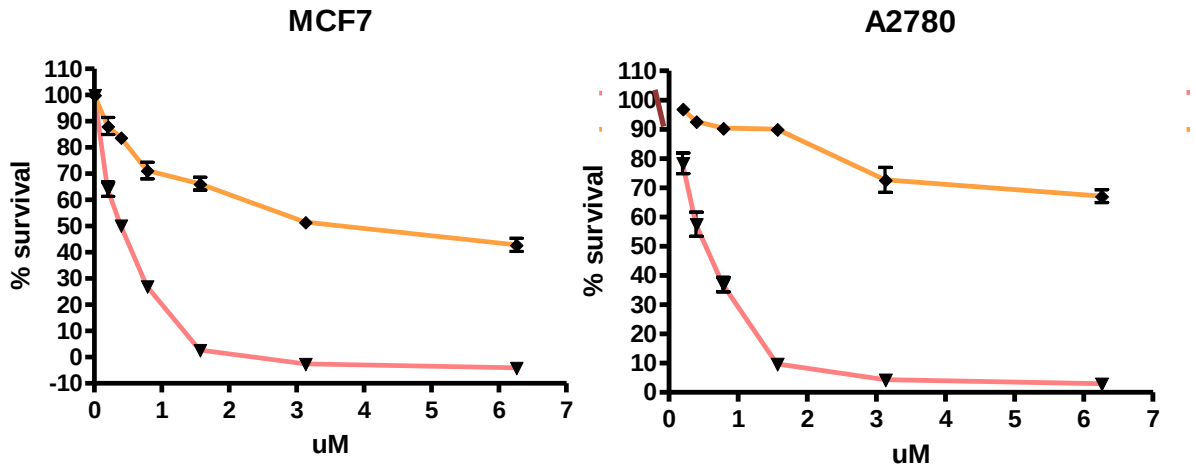

*Figure 5.26 MTT assay excerpt of Cu – compound **18**. Only the relevant region of the MTT assay is shown up to 100% cell death at the corresponding concentration. The data points are the median of two MTT assays. The orange line represents the MTT assays with no exposure to light (top). The light red one (bottom) shows the survival rate of the cells after exposure to light 24 hours after incubation (and washing) of the cells.*

Zinc porphyrin complex **19** shows a phototoxic effect (Figure 5.27). The non-platinated compound is also having a cytotoxic effect when no light is applied to the cells, but the effect is rather low. Interestingly, cell line A2780 showed a different behavior towards compound **19** compared to MCF7 when not irradiated. The phototoxicity is again very low (> 1μM). Zinc compound **19** is no intercalator due to one axial ligand that is fairly strong attached to the central metal ion.[10, 11, 143, 303] It can therefore not intercalate into DNA. This compound can, as described in Chapter 2, bind in a side-on mode towards biological molecules. It can also, being a flat molecule, occupy flat areas on the cell membrane causing damage by emerging singlet oxygen proximate to phospholipide bilayer.

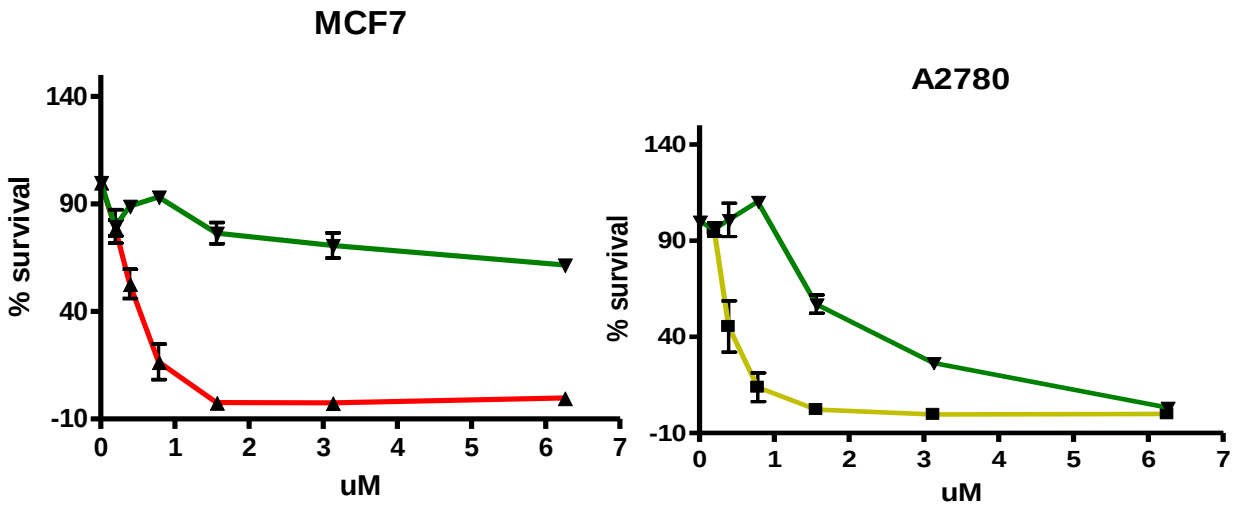

*Figure 5.27 MTT assay excerpt of Zn – compound **19**. Only the relevant region of the MTT assay is shown up to 100% cell death at the corresponding concentration. The data points are the median of two MTT assays. The green line represents the MTT assays with no exposure to light. The red (MCF7) or light green (A2780) line shows the survival rate of the cells after exposure to light 24 hours after incubation (and washing) of the cells.*

Compound **20**, a metal free porphyrin with a *cisplatin* residue, is a typical intercalator with an additional binding site (Figure 5.28). Interestingly and contrary to its non-platinated analog compound **17**, it does not show any phototoxic effect. It is very toxic regardless of light, nevertheless. This proves the proposed accessibility of the Pt – residue to biological relevant structures causing lower survival among the cells. The combined effect of intercalation and *cisplatin* – like behavior add up to a very toxic compound. Contrary to compound **17**, the externally bound platinum compound pulls out the electron density (as can also be observed in the absorption spectra) which prohibits a photoreaction.

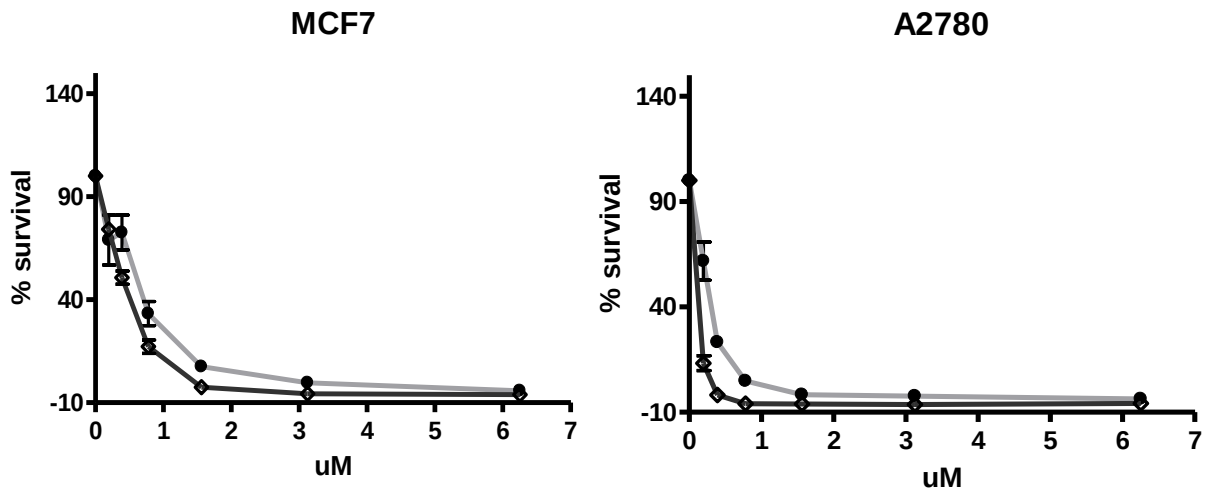

*Figure 5.28 MTT assay excerpt of Pt – compound **20**. Only the relevant region of the MTT assay is shown up to 100% cell death at the corresponding concentration. The data points are the median of two MTT assays. The grey line represents the MTT assays with no exposure to light. The dark grey red one shows the survival rate of the cells after exposure to light 24 hours after incubation (and washing) of the cells.*

Copper porphyrin with externally bound *cisplatin* **21** shows a similar behavior towards the two cell lines as copper compound **18** (Figure 5.29). There is a phototoxic effect, the cytotoxicity is high (see Table 5.4) and IC_{50} value is low. The possibilities of this compound are multiple ones: a possible binding via the *cisplatin* residue, an intercalation and also a photoactive compound able to induce singlet oxygen. Although there is no fluorescence of this compound, the absorption of this compound is well defined with a maximum at the Soret band around 430 nm and a prominent Q – band at 554 nm. This seems sufficient to excite the porphyrin to its singlet state to start the chain reaction to produce singlet oxygen.

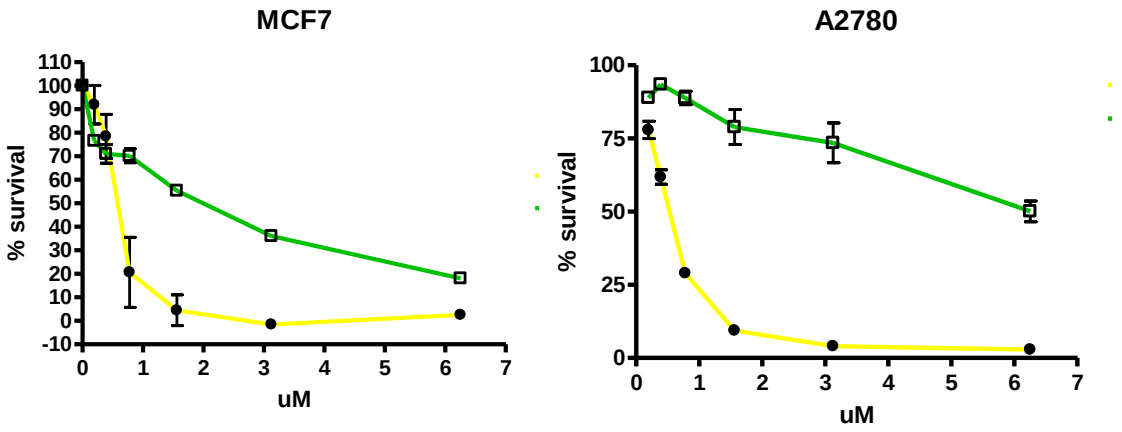

*Figure 5.29 MTT assay excerpt of Cu – compound **21**. Only the relevant region of the MTT assay is shown up to 100% cell death at the corresponding concentration. The data points are the median of two MTT assays. The green line represents the MTT assays with no exposure to light. The yellow line shows the survival rate of the cells after exposure to light 24 hours after incubation (and washing) of the cells.*

The non-intercalating zinc porphyrin **22** with a *cisplatin* coordinated on the outer sphere of the porphyrin was the most cytotoxic compound when irradiated (Figure 5.30). The very high cytotoxicity is related to the versatile binding modes this compound can participate in. The zinc porphyrin is not an intercalator since the axially bound water is preventing an intercalation[11]. The increased accumulation of zinc porphyrin in the mitochondria as well as in the cell nucleus was observed in preliminary cell uptake studies. The phototoxic effect was contributing 55 times to the cytotoxicity. This compound **22** is a good example of a limited toxicity compound triggered to become a highly toxic compound upon light irradiation. One important feature is its extraordinary high Q – band around 650 nm which contributes strongly to its fluorescence properties. Another effect of this characteristic is, that deeper skin sections treated with this compound can be reached to develop its phototoxic effect when irradiated with light. Compounds $IC_{50(hv)}$ value of 0.15 µM is comparable with the most cytotoxic compounds[114, 168, 194, 282, 324, 348]. The combined effect of the possibility to bind covalently via the platinum residue to DNA and to strongly evolve singlet oxygen resulted in a highly effective weapon against carcinoma cell lines.

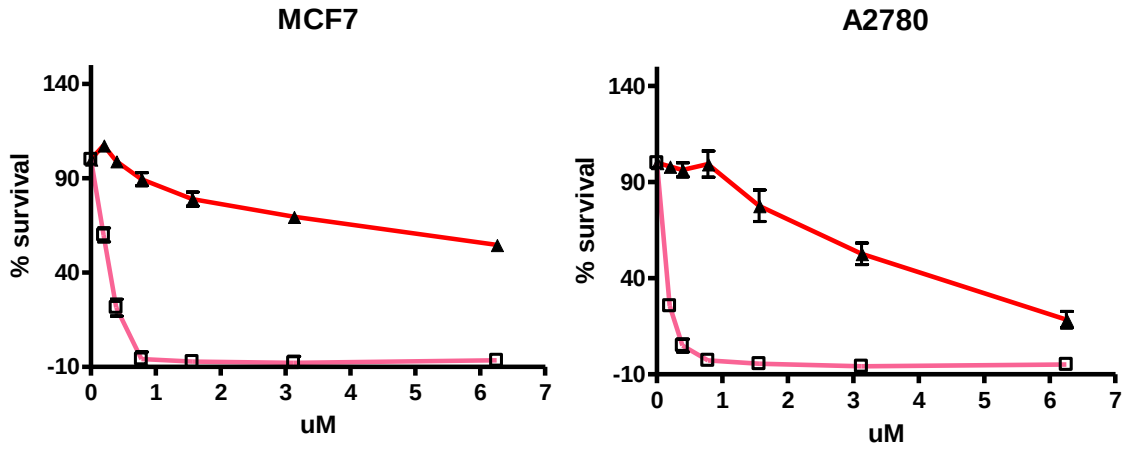

*Figure 5.30 MTT assay excerpt of Pt – compound **22**. Only the relevant region of the MTT assay is shown up to 100% cell death at the corresponding concentration. The data points are the median of two MTT assays. The red line represents the MTT assays with no exposure to light. The light red one shows the survival rate of the cells after exposure to light 24 hours after incubation (and washing) of the cells.*

An even more elevated cytotoxic effect for compound **22** was observed (Figure 5.31), when the counter ion was changed from nitrate to tetrafluoroborate and the compound dissolved in the medium with 50µl of DMSO. The observed IC_{50} value upon irradiation was down to 0.02 µM. It has to be further evaluated, which will be the most suitable conditions for a possible treatment of cancer cells (see chapter Outlook 5.5).

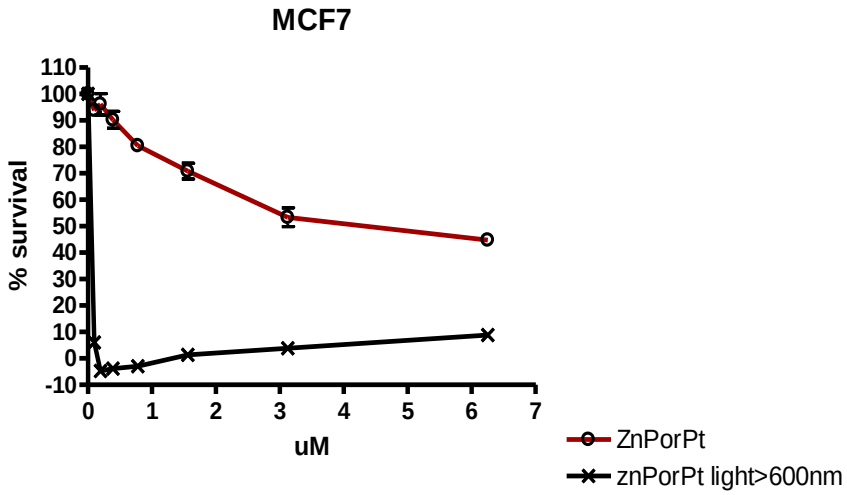

*Figure 5.31 MTT assay excerpt of Pt – compound **22**, with BF_4^- as a counter ion instead of the previously used NO_3^- dissolved in 1% DMSO medium.*

Cisplatin was chosen as a reference to compare the results and as internal standard for the cytotoxic test. It was shown, that the cells used in these experiments showed a standard cytotoxicity towards *cisplatin* as described in literature. To obtain comparable data on the behavior of *cisplatin* upon irradiation, an experiment with and without irradiation on the same conditions described before were carried out. In both cell lines, the cytotoxicity of the *cisplatin* was not particularly different upon irradiation. A small contrary effect was observed in the MCF7 cell line, in which the *cisplatin* decomposed during irradiation and showed a slightly minor cytotoxic effect (see below Figure 5.32, left).

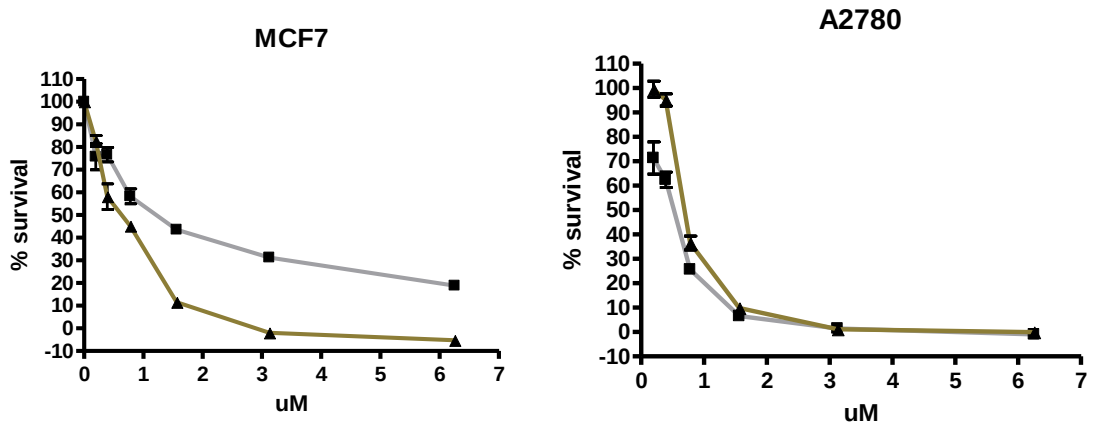

*Figure 5.32 MTT assay excerpt of cis*platin*. Only the relevant region of the MTT assay is shown up to 100% cell death at the corresponding concentration. The data points are the median of two MTT assays. The green line represents the MTT assays with no exposure to light. The grey one shows the survival rate of the cells after exposure to light 24 hours after incubation (and washing) of the cells.*

5.4.5 Calculated Interactions

To understand the mechanism of action, a possible model of the interaction between **17** – **22** and DNA was calculated. It was assumed that the *cisplatin* residue can coordinate as freely as if no porphyrin was coordinated. The model relied on an X-ray structure of cisplatin-modified DNA, one NH_3 ligand of the Pt complex was replaced by porphyrin **20** resulting in a depiction how such an interaction could happen. In comparisons studies, different scenarios such as intercalation, coordination and

partial side – on interaction were discussed. The distance in between the porphyrin and the *cis*platin enables the molecule to penetrate deep into the groove and coordinate in a classical cross-linking fashion with the bending of the DNA as depicted in Figure 5.33. For this type of interaction, *cis*platin residue would have to lose one of its *trans* located amine ligands. This is well possible due to the stronger *trans*-effect of the cyano – residue of the porphyrin towards the amine than vice versa.

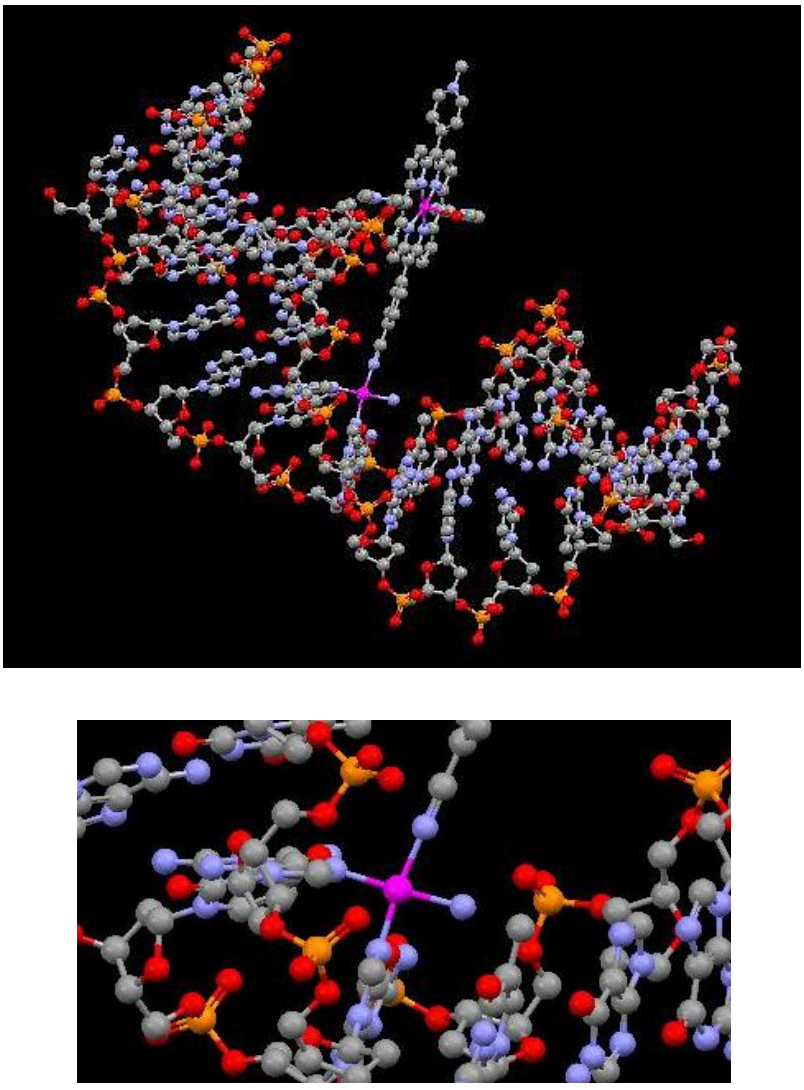

*Figure 5.33 Molecule **22** is cross-linking 2 neighboring guanosine residues in this calculated model system. Zoom to the coordination site below.*

Compound **22** could as well coordinate to one guanosine residue which would keep the helical structure of the DNA intact. This scenario is shown in Figure 5.34. The positive charge of the porphyrin causes an electrostatic interaction of the phosphate – sugar backbone towards the porphyrin. An intercalation of a zinc porphyrin is not

possible due to its strongly coordinated axial ligand. In Figure 5.35, a metal free porphyrin is chosen to depict the intercalation by a sterically not hindered porphyrin.

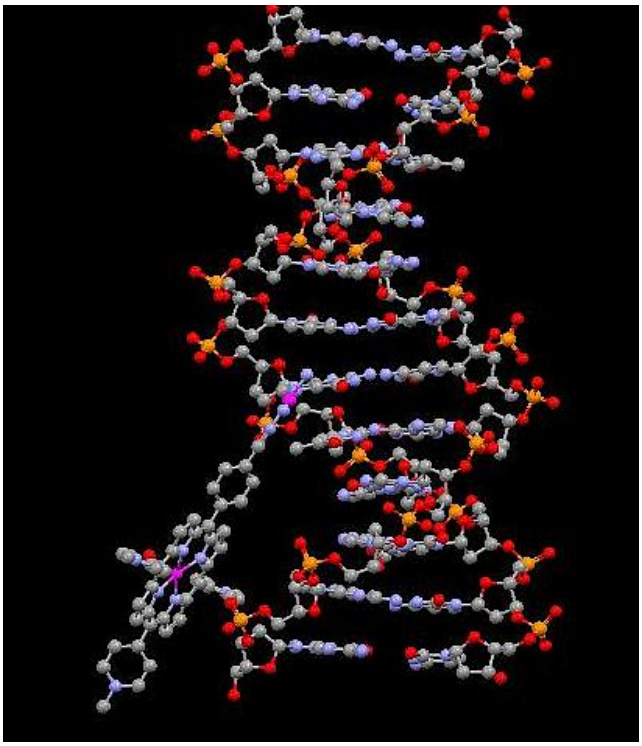

*Figure 5.34 Molecule **22** is coordinating to one guanosine residue of B - DNA in this calculated model system.*

By shortening the distance in between the porphyrin center and the *cis*platin residue, it is more likely to also intercalate into DNA (see Figure 5.35).

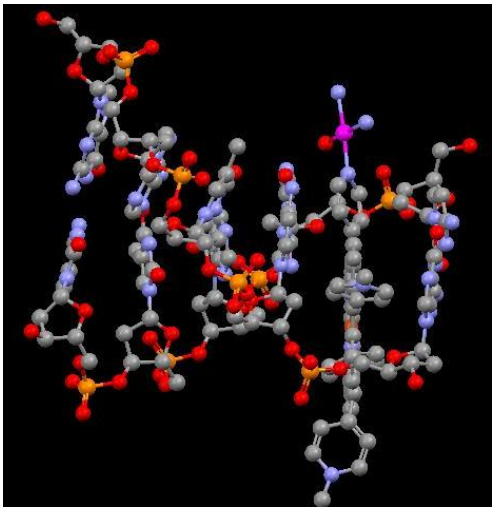

Figure 5.35 Porphyrin which is directly linked to a cisplatin via its pyridyl residue intercalating into DNA (side view). The shortened coordination disfavors a coordination of the platinum by a base.

5.5 Conclusion and Outlook

In the following Table 5.4, an overview of all compounds that were exposed to the carcinoma cell lines is listed. The ratio shown in the last column depicts the phototoxic effect and its impact on the photo- cytotoxicity – the higher the number the higher is the influence.

MCF7

Compound	IC_{50} (μM)		IC_{90}(μM)		Photoactive	~~hν~~/hν (IC_{50})
	~~hν~~	hν	~~hν~~	hν		
cisplatin	0.7	1.4	2.3	25	decomposition	0.5
17	38	1	85	2.5	yes	38
20	0.6	0.5	1.5	1.2	no	1.2
18	4	0.45	70	1.5	yes	8.9
21	2.5	0.7	13	1.3	yes	3.6
19	11.5	0.5	20	1.35	yes	23
22	8.5	0.15	60	0.45	yes	57

A2780

Compound	IC_{50} (μM)		IC_{90}(μM)		Photoactive	~~hν~~/hν (IC_{50})
	~~hν~~	hν	~~hν~~	hν		
cisplatin	0.8	0.65	1.7	1.8	no	1.2
17	43	0.55	80	1.4	yes	78
20	0.35	0.15	1	0.4	no	2.3
18	20	0.65	70	1.7	yes	31
21	6.5	0.55	60	1.5	yes	12
19	1.8	0.4	5.6	1.2	yes	4.5
22	3.2	0.08	10	0.3	yes	40

*Table 5.4 Comparison of the various tested compounds **17** – **22** in both cell lines. Values are given for the IC_{50} and IC_{90} values as well as for irradiated and a non-irradiated samples. The ratios ~~hν~~/hν for the IC_{50} values are given to compare the photo effect.*

The goal of this research project was to synthesize conjugates of *cis*platin and its analogs with photoactive molecules. The idea was to develop a combined chemo- and photodynamic therapy on the known basis of porphyrin and *cisplatin* chemistry.

The chosen synthetic concept of this publication has a major shortcoming, since the platinum metal centers have only one leaving group. Therefore, mainly the formation of mono-adducts to DNA, which are easily repaired, is expected to be formed. Preliminary cancer cell toxicity studies with novel conjugates were performed. IC_{50} values versus 2 human cancer cell lines down to 0.08 μM in the presence of red light could be found. The light irradiation increased the toxicity by a factor up to 55 compared with dark toxicity (factor 78 for porphyrin **21** which has no platinum bound to it). The proposal is based upon these exciting initial results. Follow up cell uptake studies revealed an accumulation of the porphyrins in the cell nucleus as well as in the mitochondria. In further cell uptake studies, time dependent uptake will be monitored and the development of toxicity within the cell determined.

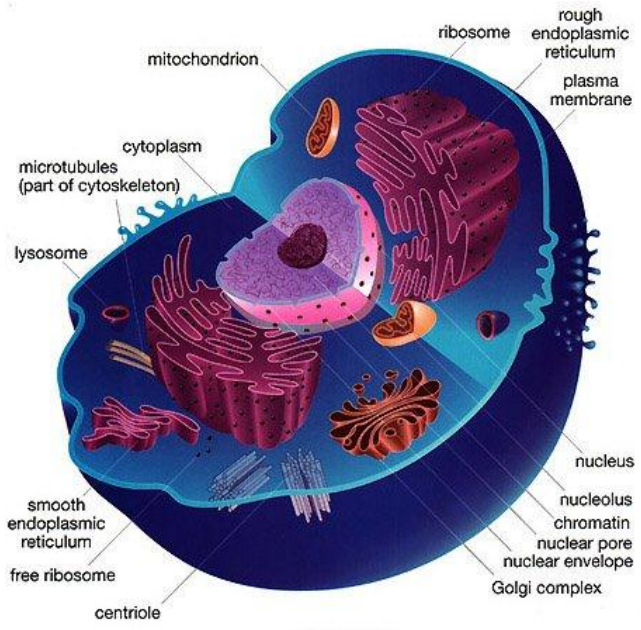

Figure 5.36 Schematic Drawing of the interior of a human cell.

Further studies on this class of porphyrins would include several changes on the link in between the porphyrin and the DNA binding platinum residue. In general, this should improve the properties of the cytotoxic platinum unit in terms of toxicity and selective cancer tissue uptake. Two concepts will be followed:

- with a **rigid** linker between the photosensitizer and the platinum center,
- with a **flexible** linker between the photosensitizer and the platinum center.

Potential biological targets are not easily reachable for rigid linkers and thus a series of flexible and variable sizes of Pt linkers will have to be tested (Figure 5.37). A cleavable linker containing one or several esters which will regulate the release of the platinum unit could be interesting to investigate the effects. Various ester-*cisplatin* analogs are known[267].

An expansion of the variety towards different photoactive units linked to a known cytotoxic platinum unit can open possibilities to fine tune the properties towards a better absorption of light in the tissue. Toxicity and selective cancer tissue uptake are a primary focus of the improvements as well. Possibilities are small peptide fragments like SV40, a nuclear localization signal (NLS) peptide to guide the molecule towards cancer cells[349].

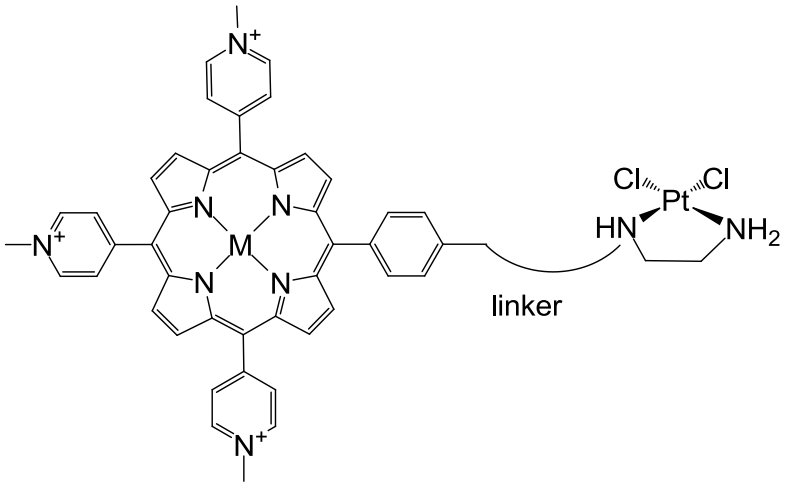

Figure 5.37 Porphyrin-platinum conjugates with a flexible linker to be synthesized and tested for their anti-cancer activity.

6. Conclusion and outlook

In the first part of this PhD thesis, the topic was driven by the question whether it was possible to locate and signal the Z-DNA conformation in cells. Therefore, a number of positively charged porphyrins were synthesized because the interactions of porphyrins with various conformations of DNA were studied and documented before [11, 88, 90, 99, 100, 124, 138, 145, 350-352].

The porphyrins synthesized contained different central metal ions such as nickel, copper, and zinc to tune their coordination spheres and their spectroscopic properties. The synthesis was carried out according to adjusted standard literature procedures starting either with the statistical approach formulated by Adler – Longo or the building block approach by Lindsey [117, 118, 146, 148, 169, 170, 353-355]. The yields of the syntheses for the porphyrins and the metalloporphyrins were expectedly low but could be improved after some iteration of the synthetic approaches. Compounds **10**, **11**, and **14** were tested for stability in saline and buffered solutions and exposed to different DNA model systems starting with DNA building block 5'-GMP followed by poly d(GC). The behavior towards different conformations of DNA, especially spermine - induced Z-DNA, was examined by CD spectroscopy. Different orders of exposures, either the Z-DNA inducing agent was added first followed by the treatment with porphyrin or *vice versa,* was used to simulate a competition between the molecules.

The wide range from flat, no axial containing ligands (H_2TMPyP **10**, NiTMPyP, **11**) to square pyramidal (ZnTMPyP, **14**) to octahedral (CuTMPyP, **18**) metal coordination spheres showed a significantly different behavior when reacted with DNA. The influences of the metal centers of the porphyrins towards the interaction and thus the ability to detect Z-DNA were tremendous. If the molecules can intercalate into DNA (H_2TMPyP **10**, and partly NiTMPyP, **11**), the previously Z-conformation flipped back into its B-form. Following this finding, DNA exposed to these porphyrins could not be transferred into its Z-form. Both molecules showed a tendency to stack around the DNA when the vacant intercalation sites are occupied.

The experiment revealed as well that the non – intercalating ZnTMPyP, **14** only showed a distinct CD signal when exposed to Z-DNA suggesting side-on coordination with a substantial stacking of the porphyrins upon increased concentrations. This signal was found to be specific only for the Z-form of the DNA since there was only a weak electrostatic interaction between B-DNA and compound **14**. This makes porphyrin **14** a suitable Z-DNA detecting molecule – which we wanted to improve.

The most prominent difference between the B- and the Z-conformation of DNA is, apart from its obvious left- and right-handedness, the different diameters. Zinc compound **14** was chosen as the flanking and thus DNA – interacting part in its function as a Z-DNA detecting molecule parallel connected to a second zinc compound **14** by a rigid bridge which would keep the flanks at a distance of 21 Å. This would enable the flanks to embrace only Z-DNA and not B-DNA. The porphyrins would be detectable via CD, UV or fluorescence spectroscopy and one could determine whether they are wrapped around DNA or just side-on coordinated due to its Dexter radius.

The synthesis of such a highly positively charged molecule was not achieved due to the vast differences in solubility of the different building units. Especially the synthesis of the bridging unit 4,4'-biphenyl-4,4'-diyldipyridine **35** and reaction with the corner unit *cis*platin was difficult. Another difficulty was the creation of a tri methylated species of a porphyrin which has 4 sides to be methylated. The exchange of the lead porphyrin to the novel compound **17**, an A_3B-type porphyrin with 3 sites which are methylatable and one free coordination site, which was synthesized by a modified novel procedure introduced by Lindsey solved the problem[148, 149]. The yield of the porphyrin synthesis was very low and the purification of the molecule difficult. The follow up reactions such as methylation and metallation were straight forward and gave high yields.

A fragment of the proposed lead molecule, one porphyrin **17** coordinated to a *cis*platin, caught our attention in the progress of this work. Since the exchange of one

of the ammonium ligands due to the *trans*-effect of the *de facto* cyano – ligand[157] was proven before, we tested the ability of this molecule **20** to bind N7 of guanine as well as the cytotoxic properties of this and its related metalloporphyrins in two human cancer cell lines. The compounds were tested to be stable in bovine serum and adhesive to HSA. The surprising results revealed not only that the molecules are toxic comparable to *cis*platin, but can also be activated upon irradiation of red light to become even more toxic. The best IC_{50} value was achieved by compound **22** being 0.08 μM when irradiated with red, water-cooled light for 10 minutes. This was 40 times more toxic compared to the non – irradiated sample. All porphyrins showed a phototoxic behavior which can be explained by the evolution of singlet oxygen derived from the spectral properties in the range from 550 – 680 nm.

Porphyrins are interesting targeting molecules for determining the different conformations of DNA. Combining the aspects of spectroscopic uniqueness, different modes of interaction and ability to fine-tune the coordination of the central metal ion and thus the spectroscopic properties creates a challenging but very interesting field for future research. Combining the phototoxic findings with the ability to detect Z-DNA in living cells could shed a new light on the Z-DNA research and produce interesting insights of the involvement of Z-DNA in the cell cycle and its properties in the metabolism.

7. Experimental

7.1 List of Abbreviations

Å	Angström
arom.	Aromatic
bs	Broad singlet
bt	Broad triplet
Calcd.	Calculated
CD	Circular dichroism
$CDCl_3$	Deuterated chloroform
CH_2Cl_2	Dichloromethane
CH_3CN	Acetonitrile
cm^{-1}	Unit of wave number (IR)
CO	Carbon monoxide
conc.	Concentrated
Cu	Copper
$CuCl_2$	Copper chloride
$Cu(NO_3)_2$	Copper nitrate
$Cu(BF_4)_2$	Copper tetrafluoroborate
D_2O	Deuterated water or deuterium oxide
DMF	N,N-Dimethyl formamide
DMSO-d_6	Deuterated methyl sulfoxide
DNA	Desoxyribonucleotide acid
EA	Elemental analysis
EDTA	Ethylenediaminetetraacetic acid
EI	Electron impact
eq.	Equivalent
ESI	Electrospray ionisation
Et_3N	Triethylamine
EtOH	Ethanol
FAB	Fast atom bombardment
g	Gram
G	Guanine
GC	Gas chromatography

h	Hour
H_2O	Water
H_2O_2	Hydrogen peroxide
HCl	Hydrochloric acid
Hepes	4-(2-Hydroxyethyl)-1-piperazineethanesulfonic acid
HPLC	High performance liquid chromatography
Hz	Hertz
IR	Infrared
J	Coupling constant (NMR)
K_2CO_3	Potassium carbonate
KBr	Potassium bromide
M	Molarity
m	mol
m	*meta*
Me	Methyl
MeOH	Methanol
MeOH-d_4	Deuterated methanol
mg	Milligram
$MgSO_4$	Magnesium sulfate
MHz	Megahertz
ml	Milliliter
mM	Millimolar
mmol	Millimole
mol	Mole
MS	Mass spectroscopy
MW	Molecular weight
N_2	Nitrogen gas
Na	Sodium
Na_2CO_3	Sodium carbonate
Na_2SO_4	Sodium sulfate
Ni	Nickel
nm	nanometer
NMR	Nuclear magnetic resonance
ORTEP	Oak Ridge thermal ellipsoid plot

p	*para*
pH	–log [H^+]
PPh_3	Triphenyl phosphine
ppm	Part per million
prep.	Preparative
R.T.	Retention time (HPLC)
r.t.	Room temperature
Ref.	Reference
R_f	Retention factor (TLC)
s	Singlet
t	Triplet
TAE EDTA)	Ethylenediaminetetracetic acid triethyl ester (Tri-Acetate-
TFA	Trifluoroacetic acid
THF	Tetrahydrofuran
TLC	Thin layer chromatography
Tris	Tris(hydroxymethyl)aminomethane
TsCl	Tosyl chloride
UV-Vis	Ultraviolet-visible
V	Volt
Zn	Zinc
δ	Chemical shift (NMR)
ε	Extinction coefficient (UV-Vis)
λ	Wavelength
ν	wavenumber (IR)
μl	microlitre
μM	Micromolar
˚C	Degree Celsius

7.2 Instrumentation and materials

All chemical were purchased from Aldrich, Molekula, Frontier Science or Fluka (Buchs, CH) and used without further purification. Biomolecules were purchased from Amersham Biosciences, Sigma - Aldrich or Operon and used without further purification unless otherwise described.

All the reactions were performed under nitrogen atmosphere unless otherwise described. The reactions were monitored by thin layer chromatography (TLC) or HPLC (see below). TLC was carried out on 0.25 mm Merck silica gel aluminum plates (60 F_{254}) or aluminum oxide pre-coated plastic sheets (alox N/UV_{254}) using UV light or staining solutions as visualizing agent:

Staining solutions:

Schlittler reagent [356]: Solution 1: 1g H_2PtCl_6 in 6 ml H_2O + 20 ml 1N HCl

Solution 2: 22.5 g KI in 225 ml H_2O

Solutions 1 and 2 were mixed and diluted with H_2O to a volume of 1000 ml.

Ce-P-Mo reagent: 10 g $Ce(SO_4)_2*4H_2O$ + 25 g $H_3[P(Mo_3O_{10})_4]$ + 60 ml conc. H_2SO_4 + 940 ml H_2O.

Column chromatography was performed on silica gel (particle size 0.040-0.063 mm) or aluminum oxide (0.05-0.15 mm, basic pH 9.5 ± 0.5, or neutral pH 7.5 ± 0.5).

HPLC analyses were performed on a VWR L-2130 system equipped with a diode array UV/vis spectrometer L-2430 and the following HPLC column, solvents and gradients:

Columns: Machery-Nagel C18 Nucleodur RP (5µm particle size, 100 Å pore size)

Solvent: 0.1% Formic Acid in Water (Solvent A), 10% MeOH in Water (Solvent B)

Gradient: 1 min 0% B, 0% B to 100% B within 8 min, keep at 100% B for 2 min, return to 100% A within 1 min, 2 min 0% B equilibration

Electrospray Ionization (ESI) Mass spectra were recorded either in the positive or negative mode on an Esquire HCT from Bruker (Bremen, Germany). Matrix-assisted laser desorption/ionization (MALDI) mass spectra were recorded on a Bruker Autoflex equipped with an ION Tech Ionizator.

Gas chromatography-mass spectra (GC-MS) were recorded on a Varian-Chrompack CP-3800 gas chromatograph equipped with a Saturn 2000 electron impact mass spectrometer (EI-MS). The samples were carried by He through a CP-SIL 8 CB-MS column (30 m X 0.25 mm).

UV/Vis spectra were recorded on a Varian Cary 50 spectrometer equipped with a temperature controlled cuvette holder. All experiments were carried out at 25°C if not stated otherwise.

IR spectra were recorded on a Perkin Elmer BX FT-IR spectrometer using samples in KBr pellets.

NMR spectra were recorded on a Varian Mercury 200 MHz or Gemini 300 MHz spectrometer. The chemical shifts are relative to residual solvent protons as reference.

Circular dichroism measurements were performed using a Jasco J-810 spectropolarimeter equipped with a Jasco PFD-4255 Peltier temperature controller.

Elemental analyses were performed on a Leco CHNS-932 elemental analyzer.

MTT Assays and fluorescence measurements were carried out on a fluorescence spectrophotometer Varian Cary Eclipse equipped with a temperature controlled cuvette holder. All experiments were carried out at 37°C. Light source used was a slide projector lamp with a cut-off filter at 600 nm.

Crystallographic data were collected at 183(2) K on an Oxford Diffraction Xcalibur system with a Ruby detector using Mo K_α radiation (λ = 0.7107 Å) that was graphite-monochromated. Suitable crystals were covered with oil (Infineum V8512, formerly known as Paratone N), mounted on top of a glass fiber and immediately transferred to the diffractometer. The program suite CrysAlis^{Pro} was used for data collection, semi-empirical absorption correction and data reduction.[357] Structures were solved with direct methods using SIR97[358] and were refined by full-matrix least-squares

methods on F^2 with SHELXL-97.[359] The structures were checked for higher symmetry with help of the program Platon.[360] Data were collected for Lorentz and polarization effects as well as for absorption (numerical). Structures were solved with direct methods using SHELXS-97 [361] or SIR97 [358] and were refined by full-matrix least-squares methods on F^2 with SHELXL-97[359].

7.3 Synthesis of Porphyrin and their Building Blocks

Statistic Synthesis of 5,10,15,20-tetraphenylporphyrin (TPP, 1) to 5,10,15,20-tetrapyridylporphyrin (TPyP, 6) and its intermediates *[104, 114, 119, 147, 167, 169, 362, 363]*

Pyrrole (7.0 ml, 100 mmol, freshly distilled), benzaldehyde (7.5 ml, 74 mmol), and 4-pyridine-carboxaldehyde (2.5 ml, 26 mmol) were refluxed in 250 ml propionic acid for 1 hour under air. The reaction mixture was cooled and allowed to stand open overnight. Filtration and methanol washing afforded 2.74 g of a purple crystalline product. TLC (98% $CHCl_3$ / 2% ethanol) showed 6 different products with the following R_f-values: 5,10,15,20-tetraphenylporphyrin (TPP, **1**) 0.88, 5-pyridyl-10,15,20-triphenylporphyrin (MPyTPP, **2**) 0.6, trans-5,15-dipyridyl-10,20-diphenylporphyrin (trans-DPyDPP, **3**) 0.42, *cis*-5,10-dipyridyl-15,20-diphenylporphyrin (*cis*-DPyDPP, **4**) 0.22, 5,10,15-tripyridyl-20-phenylporphyrin (TPyMPP, **5**) 0.12, 5,10,15,20-tetrapyridylporphyrin (TPyP, **6**) 0.08. These isomers were separated by silica gel chromatography using 5% isopropanol / 95% dichloromethane solvent system which was gradually ending with 100% methanol. After separation, the following yields of the resulting porphyrins were obtained: 260 mg TPP, 185 mg MPyTPP, 16 mg *trans*-DPyDPP, 46 mg *cis*-DPyDPP, 44 mg TPyMPP, 222 mg TPyP.

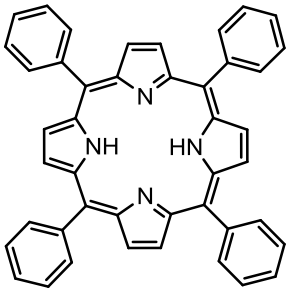

TPP, **1**

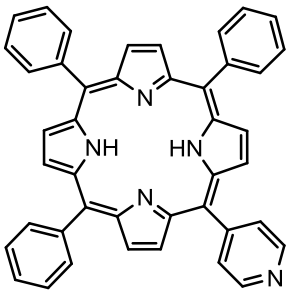

MPyTPP, **2**

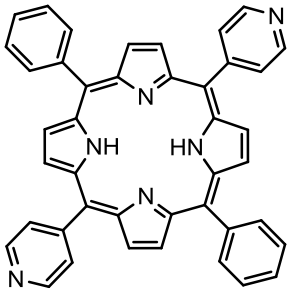

trans-DPyDPP, **3**

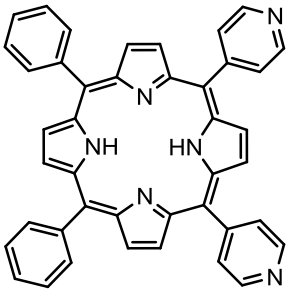

cis-DPyDPP, **4**

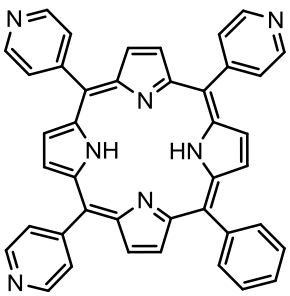

TriPyMPP, **5**

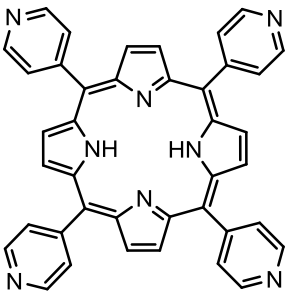

TPyP, **6**

5,10,15,20-tetraphenylporphyrin TPP 1 [$C_{44}H_{30}N_4$, M = 614.75 g/mol], purple powder. EA: calculated: C, 85.97; H, 4.92; N, 9.11; found: C, 85.88; H, 4.88; N, 9.20. ^{1}H-NMR (200 MHz, $CDCl_3$): δ = -2.81 (s, 2H, $NH_{pyrrole}$), 7.62-7.88 (m, 12 H, *m*- and *p*-phenyl), 8.08-8.32 (m, 8H, *o*-phenyl), 8.63-8.96 (m, 8H, pyrrole). UV vis spectrum [λ, nm, in $CHCl_3$, (ε x 10^4, $cm^{-1}M^{-1}$)]: 418 (Soret band, 100), 516 (Q1, 20), 550 (Q2, 13), 590 (Q3, 20), 646 (Q4, 5). MS (ESI): m/z (%) = 614 (100) $[M]^+$, 637 (40) $[M+ Na]^+$.

5-pyridyl-10,15,20-triphenylporphyrin MPyTPP 2 [$C_{43}H_{29}N_5$, M = 615.24 g/mol], purple powder. EA: calculated: C, 83.88; H, 4.75; N, 11.37; found: C, 83.82; H, 4.80; N, 11.29. ^{1}H-NMR (200 MHz, $CDCl_3$): δ = -2.73 (2H, s, $NH_{pyrrole}$), 7.77 – 7.85 (10 H, m, *m*- and *p*-phenyl), 8.08 – 8.12 (9H, m, *o*-phenyl and 3,5-pyridyl), 8.16 – 8.32 (6H, m, pyrrole), 9.04 (2H, d, 2,6-pyridyl). MS (ESI): m/z (%) = 615.3 (100) $[M]^+$, 638.7 (20) $[M+Na]^+$.

5,15-dipyridyl-10,20-diphenylporphyrin *trans*-DPyDPP 3 [$C_{42}H_{28}N_6$, M = 616.17 g/mol], purple powder. EA: calculated: C, 81.80; H, 4.58; N, 13.63; found: C, 82.00; H, 4.45; N, 13.77. ^{1}H-NMR (200 MHz, $CDCl_3$): δ = -2.86 (2H, s, $NH_{pyrrole}$), 7.79 (6 H, m, *m*- and *p*-phenyl), 8.17 - 8.22 (8H, m, *o*-phenyl and 3,5-pyridyl), 8.90 (8H, d, pyrrole), 9.06 (4H, d, 2,6-pyridyl). MS (ESI): m/z (%) = 617 (100) $[M+H]^+$, 639 (60) $[M+ Na]^+$, 544 (30)$[M-py]^+$.

5,10-dipyridyl-15,20-diphenylporphyrin *cis*-DPyDPP 4 [$C_{42}H_{28}N_6$, M = 616.17 g/mol], purple powder. EA: calculated [M+ HCl + 3 C_3H_8O]: C, 73.49; H, 6.41; N, 10.08; found: C, 73.37; H, 6.46; N, 9.78. ^{1}H-NMR (200 MHz, $CDCl_3$): δ = -2.86 (2H, s, $NH_{pyrrole}$), 7.76 – 7.81 (6 H, m, *m*- and *p*-phenyl), 8.20 – 8.25 (8H, m, *o*-phenyl and 3,5-pyridyl), 8.90 (8H, d, pyrrole), 9.06 (4H, d, 2,6-pyridyl). MS (ESI): m/z (%) = 617(100) $[M+H]^+$.

5,10,15-pyridyl-20-phenylporphyrin TriPyMPP 5 [$C_{41}H_{27}N_7$, M = 617.70 g/mol], purple powder. EA: calculated: C, 79.72; H, 4.41; N, 15.87; found: 79.68; H, 4.55; N, 15.66. ^{1}H-NMR (200 MHz, $CDCl_3$): δ = 7.80 – 7.85 (3H, m, *m*- and *p*-phenyl), 8.15 – 8.19 (8H, m, *o*-phenyl and 3,5-pyridyl), 8.86 (8H, d, pyrrole), 9.07 (6H, d, 2,6-pyridyl). MS (ESI): m/z (%) = 618 (100) $[M+H]^+$, 639 (40) $[M+ Na]^+$.

5,10,15,20-tetrapyridylporphyrin TPyP 6 [$C_{40}H_{26}N_8$, M = 618.17 g/mol], purple powder. EA: calculated: C, 77.65; H, 4.24; N, 18.11; found: C, 77.67; H, 4.17; N, 18.13. ^{1}H-NMR (200 MHz, $CDCl_3$): δ = 8.14 – 8.18 (8H, m, 3,5-pyridyl), 8.82 (8H, d, pyrrole), 9.04 (8H, d, 2,6-pyridyl). UV vis spectrum [λ, nm, in $CHCl_3$,]: 418, 512, 546, 588, 646. MS (ESI): m/z (%) =618 (100) $[M]^+$.

Statistic Synthesis of 5,10,15,20-tetrapyridylporphyrin (TPyP, 6) to 5,10,15,20-tetra-para-benzonitrile-porphyrin (TBNP, 7) and its statistic intermediates

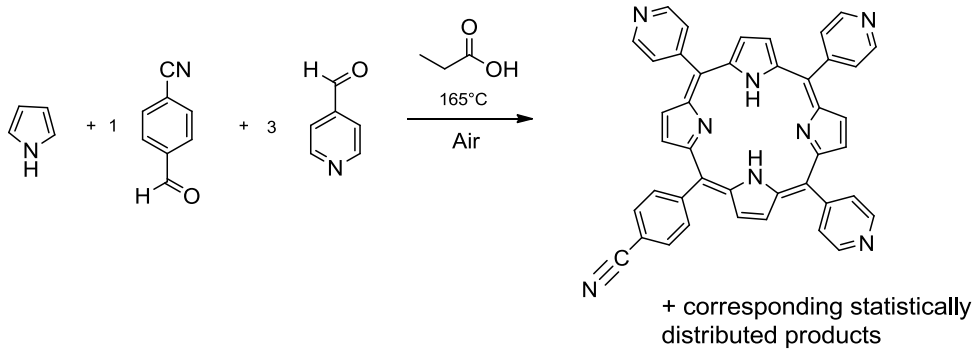

To a 100 ml round-bottom flask equipped with a magnetic stirring bar, a reflux condenser and a dropping funnel (100 ml) attached to the reflux condenser, 2.01g (15.3 mmol) 4-cyanobenzaldehyde and 5.16g (46 mmol) pyridine-4-carbaldehyde and 40ml propionic acid were added. The suspension was heated to reflux (165°C oil bath). The suspension turned into a homogeneous solution while heating. Under reflux of the propionic acid, 4.13g (61.6 mmol) pyrrole was added drop wise with the help of the dropping funnel within 1h. The reflux increased considerably because the boiling point of pyrrole is below the boiling point of propionic acid. The reaction was stirred for 2h under reflux after complete addition of the pyrrole. The black solution was cooled down to room temperature. The propionic acid was evaporated (75°C, 1 mbar). The crude black solid product was further dried under high vacuum at 70°C for 24h. The crude product was purified over multiple silica gel columns (gradient 0:100 -

2:98 MeOH: CH_2Cl_2) to afford 85 mg (0.9% yield) of the pure product **7**, the other fractions were not separated and afforded 143 mg of a porphyrin mixture.

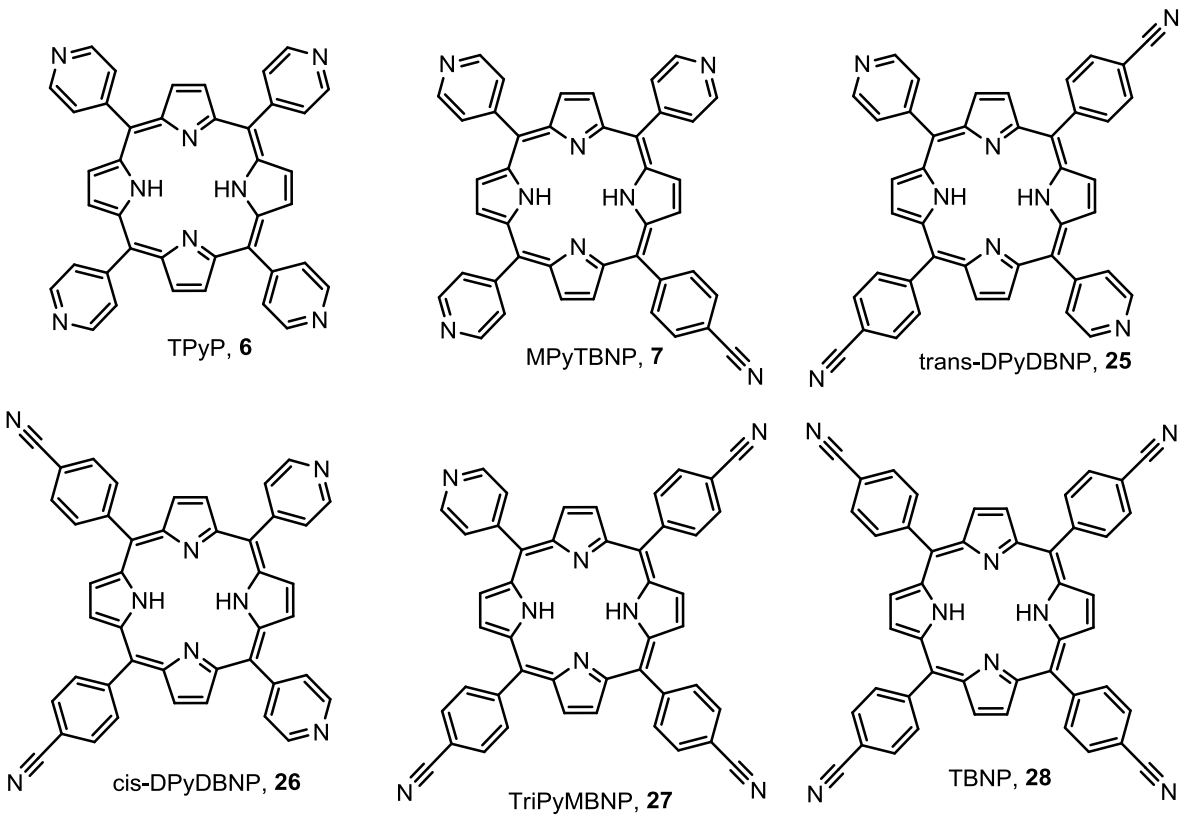

5,10,15-pyridyl-20-*para*-benzonitrile-porphyrin (7) [$C_{42}H_{26}N_8$, M = 642.23 g/mol], HPLC: 10.86 min (100%). EA: calculated: C, 79.58; H, 4.08; N, 16.29; found: C, 79.37; H, 4.46; N, 16.38. ^{1}H NMR ($CDCl_3$, 300 MHz): δ 9.06 (d, *J* = 4.5 Hz, 6H, 2'), 8.87 (s, 4H, 12, 13, 17, 18), superimposed by 8.85 (d, 2H, 2, 8), 8.80 (d, *J* = 4.8 Hz, 2H, 3, 7), 8.33 (d, *J* = 8.4 Hz, 2H, 1"), 8.16 (d, *J* = 1.5 Hz, 6H, 3'), 8.09 (d, *J* = 6.3 Hz, 2H, 2"), –2.92 (s, 2H, 3", 4"). MALDI-MS (dithranol) 643.2 $[M+H]^+$.

trans-5,15-pyridyl-10,20-*para*-benzonitrile-porphyrin **25,** *cis*-5,10-pyridyl-15,20-*para*-benzonitrile-porphyrin **26,** 5-pyridyl-10,15,20-*para*-benzonitrile-porphyrin **27,** and 5,10,15,20-*para*-benzonitrile-porphyrin **28** were not separated and characterized.

5,10,15-tri-methylpyridinium-20-pyridyl-porphyrin nitrate (8)

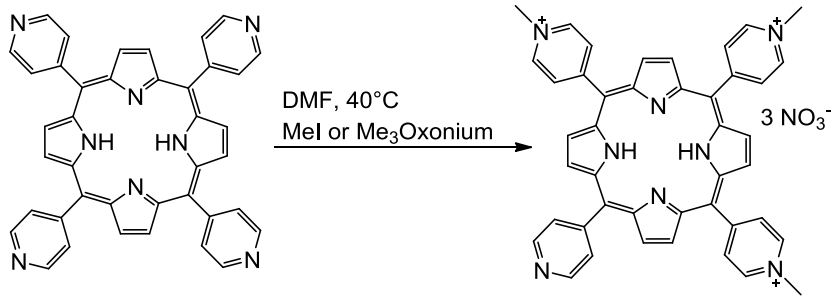

TriMe PyMPP, **8**

5,10,15,20-tetrapyridyl-porphyrin (**6**) (140 mg, 0.226 mmol) was dissolved in 40 ml DMF given into a 100 ml flask and about 10 equivalents of MeI (156 μl, 2.18 mmol) added. The solution was stirred for 2 – 6 hours at 40°C and followed by HPLC. After a ratio between the tetra and tri methylated species of around 4:3 was detected, a 1:1 mixture of acetone : diethyl ether was added to the solution and the precipitate filtered, washed with cold acetone and diethyl ether and charged onto a Amberlyte A-26 ion-exchange resin column charged with a saturated solution of NH_4NO_3 in water to exchange the I^- ions with NO_3^- ions. The resulting solution was dried, weight to afford 152 mg and attempted to be separated using the following techniques:

Preparative HPLC with C_{18} Nucleosil column: Several flat gradients over the time period of 55 min were tested for separation. The separation could not afford pure product **8**.

Preparative HPLC with C_{18} Nucleodur semi preparative column: Several flat gradients over the maximum time period of 63 min were tested. The separation could not afford pure product **8**.

Semi - Preparative HPLC with a cation exchange column (Machery Nagel, strongly or weakly exchanging columns): Several gradients were tested with different buffer systems. The separation could not afford pure product **8**.

Thick Layer Chromatography (TLC): on a 1.5 or 2 mm TLC silica plate, an aqueous solution containing the porphyrin mixture was given and the plate given into a developing chamber containing the mobile phase (aqueous solution of ammonium nitrate, ethanol, n-butanol; 10:6:1). After 35 minutes, the plate was removed and the silica containing the different bands cut off the glass. The silica gel was dissolved in water/methanol to extract the corresponding porphyrin which was determined by HPLC. The separation was moderate, but never clean and always contained the corresponding neighboring porphyrins up to 20%[364].

CPC (Centrifugal Partition Chromatography) was tested with the help of Armen, France, because a separation was described in the literature before[120]. Different solvent mixtures such as water/n-butanol and aq. propionic acid/n-butanol , were tested with this method, but only very few showed a separation behavior. The testing will be continued with other solvent mixtures.

Another approach was carried out by demethylation of the tetra methylated species. The demethylating agent was 1-methylimidazole which reacted to 1,3-dimethylimidazole cation. The reaction was carried out in water and monitored via HPLC. A defined mixture of a 4:2 tetra:tri methylated species was obtained repeatedly after 3h at 45°C. Upon further reaction, the mixture got more complex.

The most material was afforded by the thick layer chromatography. The solution was lyophilized at 0.2 mbar overnight and afforded a purple product yielding 8 mg (0.1%).

5,10,15-methylpyridinium-20-pyridyl-porphyrin nitrate, **8** [$C_{45}H_{41}N_8$, M = 663.79 g/mol], HPLC[343]: 7.21 min (100%). MS (ESI): m/z (%) = 664.7 (100) $[M+H]^+$.

5,10,15,20-tetra-methylpyridinium-porphyrin nitrate (10)

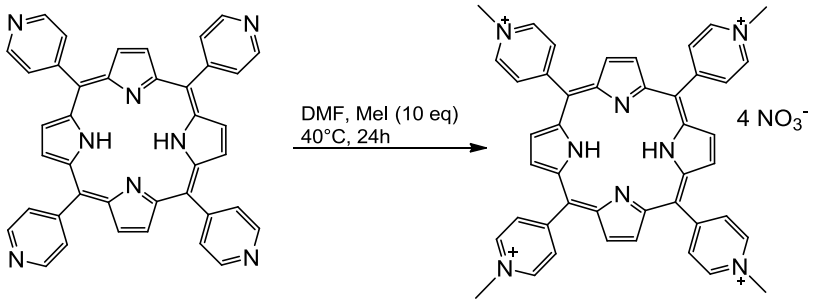

5,10,15,20-tetrapyridyl-porphyrin **(6)** (140 mg, 0.226 mmol) were dissolved in 40 ml DMF given into a 100 ml flask and around 10 equivalents of MeI (156 μl, 2.18 mmol) added. The solution was stirred overnight at 40°C and the process of the reaction followed by HPLC. After completion of the reaction, a 1:1 mixture of acetone : diethyl ether were added and the precipitate filtered, washed with cold acetone and diethyl ether and charged onto a Amberlyte A-26 ion-exchange resin column charged with a saturated solution of NH_4NO_3 in water to exchange the I^- ions with NO_3^- ions. The resulting solution was lyophilized at 0.2 mbar overnight and afforded a purple product yielding 165 mg (95%).

5,10,15,20-methylpyridinium-porphyrin nitrate (10) [$C_{44}H_{38}N_{12}O_{12}$, M = 926.85 g/mol, porphyrin alone 678.32 g/mol], HPLC[343]: 6.65 min (100%). EA: calculated: C, 57.02; H, 4.13; N, 18.13; found: C, 57.41; H, 4.26; N, 17.89. H-NMR (200 MHz, H_2O): δ = -2.76 (2H, s, $NH_{pyrrole}$), 2.86 – 2.89 (12H, m, methyl) 7.76 – 7.80 (8H, m, *m*-pyridyl), 8.19 – 8.23 (8H, m, o-pyridyl), 8.90 (8H, d, pyrrole). MS (ESI): m/z (%) =, 169.7 (100) $[M(por)]^{4+}$, 226.3 (80) $[M(por)]^{3+}$, 339.4 (30) $[M(por)]^{2+,}$ 678.9 (100) $[M(por)]^+$. UVvis spectrum [λ, nm, in H_2O]: 420 (Soret), 515 (Q1), 545 (Q2), 588 (Q3), 624 (Q4).

5,10,15-methylpyridinium-20-benzonitrile-porphyrin nitrate (17)

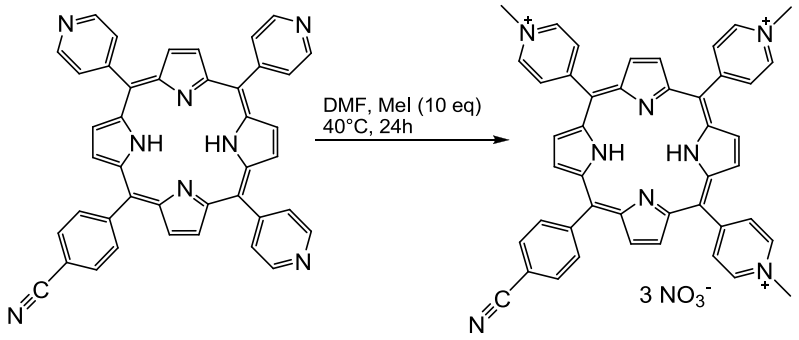

5,10,15-pyridyl-20-*para*-benzonitrile-porphyrin **(7)** (200 mg, 0.311 mmol) were dissolved in 40 ml DMF given into a 100 ml flask and about 15 equivalents of MeI (156 µl, 2.18 mmol) added. The solution was stirred overnight at 40°C and followed by HPLC. After completion of the reaction, a 1:1 mixture of acetone:diethylether were added and the precipitate filtered, washed with cold acetone and diethylether and charged onto an Amberlyte A-26 ion-exchange resin column charged with a saturated solution of NH_4NO_3 in water to exchange the I^- ions with NO_3^- ions. The resulting solution was lyophilized at 0.2 mbar overnight and afforded a purple product yielding 245 mg (91%).

5,10,15-methylpyridinium-20-benzonitrile-porphyrin nitrate (17) [$C_{45}H_{35}N_{11}O_9$, M = 873.8 g/mol], HPLC[343]: 8.15 min (100%), EA: calculated: C, 61.85; H, 4.04; N, 17.63; found: C, 61.66; H, 4.25; N, 17.72. ^{1}H-NMR (200 MHz, H_2O, 294 K): δ = 2.80 – 2.86 (9 H, m, methyl), 8.34 (2H, 2 d, 3-cyanobenzol), 8.46 (2H, 2 d, 2-cyanobenzol), 9.30 (6H, d, 10-pyridinium), 9.37 – 9.40 (2H, m, 1-pyrrole) 9.42 (2H, d, 2'H-pyrrole of 4-pyrrole residue), 9.55 (4H, dd, 2'H-pyrrole of 2- and 3-pyrrole residues). 9.70 (4H, d, 3-pyridinium of 5,15-pyridinium), 9.75 (2H, d, 3H of 10-pyridinium). MS (ESI): m/z (%) = 343.3 (100) $[M\text{-}3NO_3\text{-}H]^{2+}$, 686.3 $[M\text{-}3NO_3\text{-}2H]^+$. UV vis spectrum [$\lambda$, nm, in H_2O]: 424 (soret, 100), 516 (Q1, 20), 551 (Q2, 13), 591 (Q3, 20), 644 (Q4, 5).

Synthesis of 5-(4-Phenyl)-dipyrromethane (PDP) [169, 363]

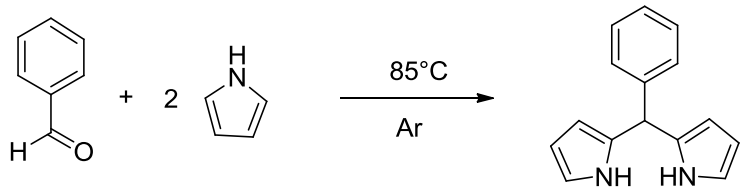

10 g (92.8 mmol) 4-phenyl-carboxaldehyde and 84 ml (~1300 mmol) freshly distilled pyrrole were combined and the solution was degassed with argon for 10min. The reaction was carried out under argon. The reaction solution was heated to 85 °C. After 15h the solution was cooled to room temperature. After an additional 4h stirring at room temperature the pyrrole was removed *in vacuo*. The remaining dark violet oil was further dried by high vacuum overnight to afford a sticky dark oil which was solved in CH_2Cl_2 and cleaned by filtration over basic Alox (pH=9.5). The main fractions were combined to afford 11.9 g of crude product as a black solid. The black solid was purified by bulb to bulb distillation to afford 7.84 g colorless crystals ($2*10^{-2}$mbar and 210°C). Yield: 34%. The compound was stored at -20 °C.

5-(4-Phenyl)-dipyrromethane ^{1}H NMR (200MHz, $CDCl_3$): δ 5.46 (s, 1H), 5.88-5.90 (m, 2H), 6.15-6.19 (m, 2H), 6.72-6.75 (m, 2H), 7.11-7.14 (m, 2H), 8.11 (bs, 2H), 8.49-8.52 (m, 2H). ESI-MS: m/z (%) 221.6 $[M+H]^+$. EA (calc): C 81.4, H 5.92, N 12.66; (found): C 81.64, H 5.82, N 12.51.

Synthesis of (4-Pyridyl)-dipyrromethane (PyDP) [167, 169, 363]

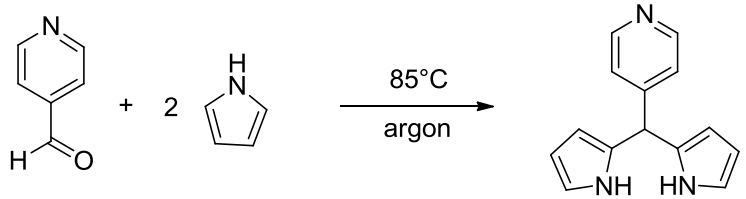

A 250ml flask was charged with 10 g (93.4 mmol) 4-pyridine-carboxaldehyde and 84 ml (~1300 mmol) freshly distilled pyrrole. The resulting yellow solution was degassed by bubbling argon through the solution for 10min. The reaction was carried out under

nitrogen and the solution heated to 85°C. After 15h, the solution was cooled to room temperature. After an additional 4h stirring at room temperature, pyrrole was removed *in vacuo*. The remaining dark violet oil was further dried by high vacuum overnight to afford a sticky oil. The oil was solved in CH_2Cl_2 and cleaned by filtration over a basic Alox pad (2 cm height, pH = 9.5). The resulting oil was purified by bulb to bulb distillation to afford 6.24 g (25% yield) as colorless crystals ($2*10^{-2}$mbar and 210°C). The compound was stored at -20 °C.

(4-Pyridyl)-dipyrromethane MS (ESI): m/z (%) = 462.3 (100) $[3M]^+$, 245.0 (100) $[M+Na]^+$, 223.0 (80) $[M+H]^+$, 156.0 (40) $[M\text{-pyrrole}]^+$. The compound was crystallized from a chloroform solution.

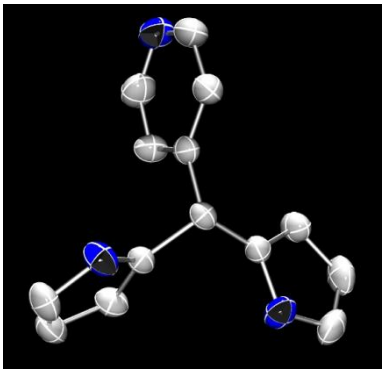

Figure 7.1 Povray representation of an ORTEP plot of DPyP crystallized from chloroform. Ellipsoids are drawn at 50% probability. Hydrogen ions are omitted for clarity.

Synthesis of 5-(4-Methyl-pyridinium)dipyrromethane (MPyDP) [167, 353]

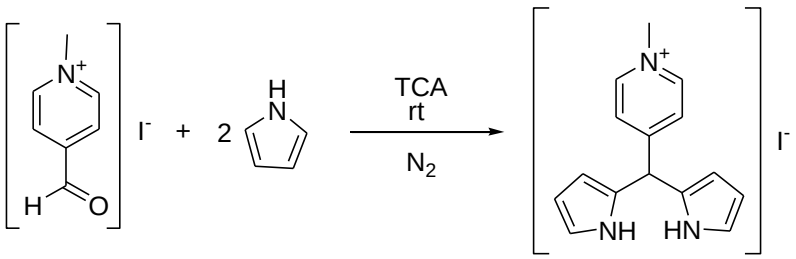

1.37 g (5.5mmol) Pyridinium-N-methyl-4-carboxaldehyde iodide was added to a 100ml one-necked round-bottom flask equipped with a magnetic stirring bar. 36.9 g (550 mmol) pyrrole was added and the system was degassed by passing nitrogen

through the solution. After 5 min, 0.899g (5.5mmol) TCA were added and the flask was closed with a plug. Analysis with MS showed almost complete reaction and almost no by-product was formed after 20 h stirring at room temperature. The pyrrole was removed at room temperature by suction (high vacuum) to afford highly viscous brown oil. The crude product was dissolved in $CHCl_3$ and evaporated at room temperature to remove remaining pyrrole. 2.834g crude green solid product could be obtained consisting of the favored product and the TCA starting material. Because of stability reasons the TCA wasn't separated from the crude material. A theoretical yield of 96% (5.28mmol) could be obtained if the TCA was subtracted from the yield. ^{1}H NMR (200MHz, $CDCl_3$): δ 4.205 (s, 3H), 5.82-5.84 (m, 2H), 6.04-6.09 (m, 2H), 6.73-6.75 (m, 2H), 7.75-7.76 (d, J = 6.6Hz, 2H), 8.46-8.49 (d, J = 6.6Hz, 2H), 9.43 (bs, 2H) ESI-MS: m/z 238.5 $[M-I]^+$

Synthesis of 5-(4-chloro-pyridyl)dipyrromethane (ClPyDP) *[169, 170, 365, 366]*

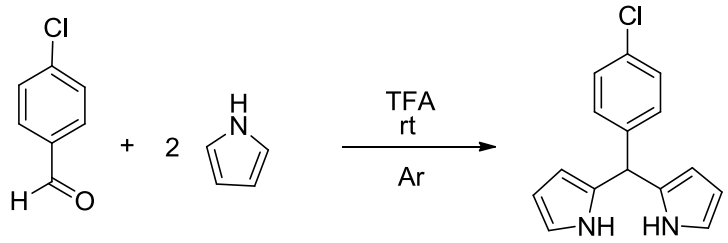

To a two-necked round-bottom flask equipped with 5 g (35.6 mmol) 4-chloro-benzaldehyde, 59.7 g (62 ml, 890 mol) pyrrole was added. The system was closed with a septum and degassed by passing argon through the solution for 10min. Under argon atmosphere 0.59 g (5mmol) TFA were added by syringe. After 10 min the now brown solution was quenched with 30ml 0.2M aqueous NaOH solution. The brown solution cleared up slightly and turned brown-orange. The organic phase was separated and extracted with EtOAc and washed twice with water. The combined organic phases were evaporated to dryness over night at high vacuum to afford a brown solid. The crude product was purified by bulb to bulb distillation (<1*10^{-3}mbar, 140°C) to afford 4.0 g (44% yield) of the colorless crystals. The colorless crystals were

stored at -20 °C. ^{1}H NMR (200MHz, $CDCl_3$): δ 5.44 (s, 1H), 5.90 (s, 2H), 6.16-6.20 (m, 2H), 6.70-71 (m, 2H), 7.12-7.17 (d, 2H), 7.26-7.32 (m, 2H), 7.88 (s, 1H) ^{13}C NMR (50 MHz, $CDCl_3$): δ 43.35, 107.43, 108.56, 117.51, 128.73, 129.75, 131.98, 132.73, 140.65 ESI-MS: m/z 279.5 $[M+Na]^+$

Synthesis of 5-(4-phenyl)-di-(5-pyrro-1-carboxyphenyl)methane ***[118, 170, 337, 366-368]***

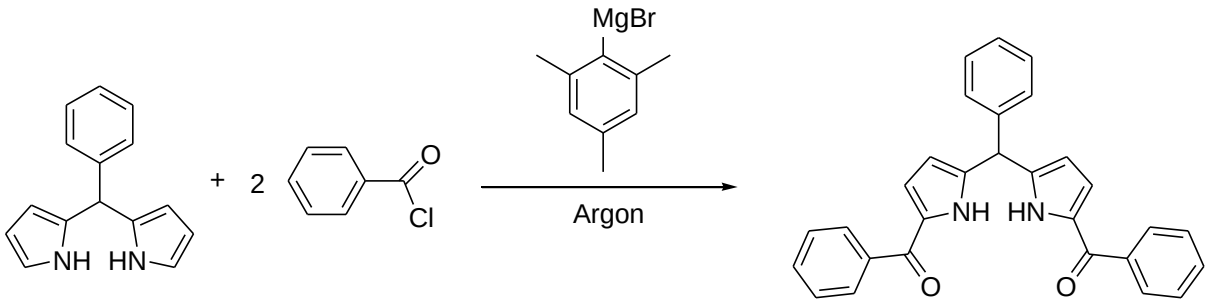

A 1l three-necked round-bottom flask, equipped a 100 ml dropping funnel was flushed with a constant flow of argon via the reflux condenser. The dropping funnel was closed by a septum. 3 g (13.5 mmol) phenyldipyrromethane and 270 ml dry toluene were added to the flask. 45 ml (~1.5 M, ~67.2 mmol) of the prior synthesized mesitylene magnesia bromide solution were added into the dropping funnel. Under an argon atmosphere the mesitylene magnesia bromide solution was added drop wise within 20min. The colorless solution in the flask turned slightly black. The reaction mixture was cooled down after 30min with external heating (85 °C). The dropping funnel was quickly exchanged with another 100ml dropping funnel containing 4.7 g (33.6 mmol) benzoylchloride dissolved in 34ml toluene. The benzoylchloride solution was added drop wise to the reaction mixture within 10min. The mixture turned darker. The reaction was a little exothermic. After an additional 10min the reaction mixture was quenched with 200 ml saturated aqueous NH_4Cl solution. The organic phase changed to an intensive red color while the brine phase stayed colorless under precipitating white salt crystals. After 35 min stirring the solution was extracted. Therefore 270ml EtOAc were added. The organic phase was further washed with 200ml brine and 200ml water. The combined organic phases

were dried over Na_2SO_4. The red solution was stored overnight under argon in the fridge. Overnight a few colorless needles were formed in the flask. The solvent was evaporated under light protection at 25 °C via high vacuum to afford 8.84 g (20.5 mmol, 153% yield) of dark red oil. The crude product was used directly for the next reaction, because of stability reasons.

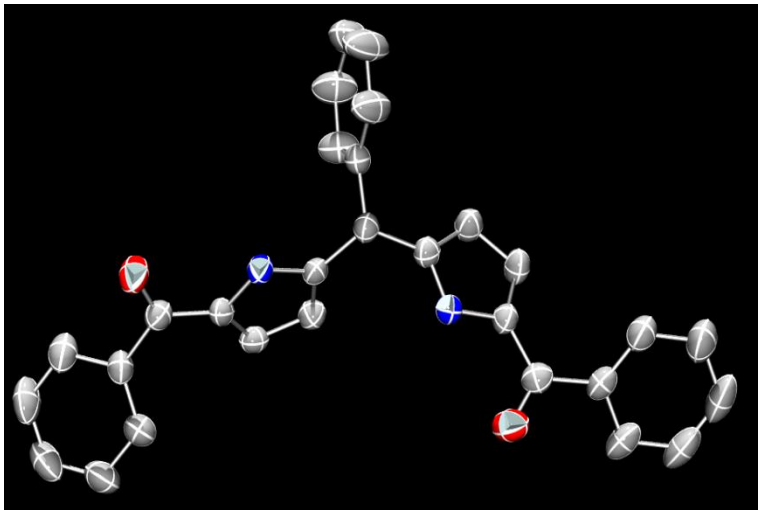

*Figure 7.2 Povray representation of ORTEP plot of **10** crystallized from chloroform. Ellipsoids are drawn at 50% probability. Hydrogen ions are omitted for clarity.*

Synthesis of tin di-butyl 5-(4-phenyl)-di-(5-pyrro-1-carboxyphenyl)methane [337, 367-369]

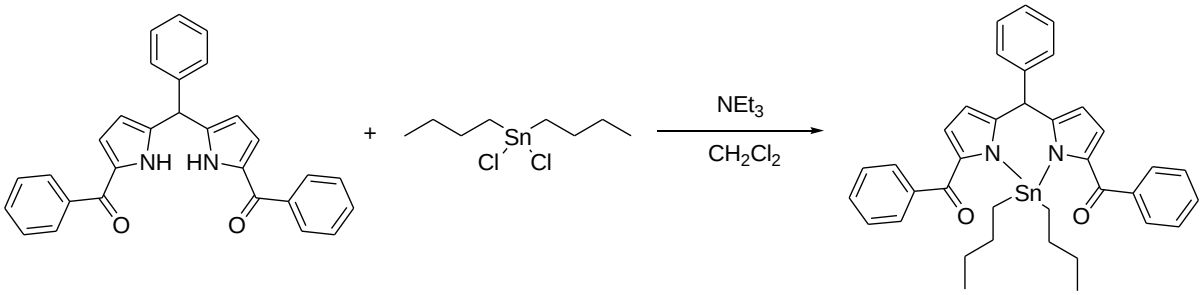

The crude 5-(4-phenyl)-di-(5-pyrro-1-carboxyphenyl)methane (≤5.81 g, ≤13.5 mmol) was suspended in 200 ml CH_2Cl_2. 4 g (40.3 mmol) NEt_3 and 4 g (13.4 mmol) $SnCl_2Bu_2$ were added. The suspension was stirred for 30 min at room temperature. The crude product was filtered over 70 g silica gel and washed with 0.5 l CH_2Cl_2. The solvent was removed *in vacuo* to afford 10.8 g crude product. The crude product was purified

over a silica column (97.5:2.5 hexane:EtOAc; 1 % NEt_3) to afford a total of 5.3 g (8 mmol, 60 % yield regarding the overall yield of the whole synthesis starting from the dipyrromethane). ^{1}H NMR (200MHz, $CDCl_3$): δ 0.66-0.78 (m, 6H), 1.49-1.55 (m, 12H), 5.60 (s,1H), 6.19 (d, J = 3.6 Hz, 2H), 7.09 (d, J = 3.8 Hz, 2H), 7.20-7.29 (m, 9H), 7.43-7.61 (m, 6H), 7.88-7.92 (m, 4H), ^{119}Sn NMR (74.5MHz, $CDCl_3$), -269.70 (s) ESI-MS: m/z 661.2 $[M+H]^+$.

Synthesis of (4-pyridiyl)-di-(5-pyrro-1-carboxyphenyl)methane [337, 367, 368]

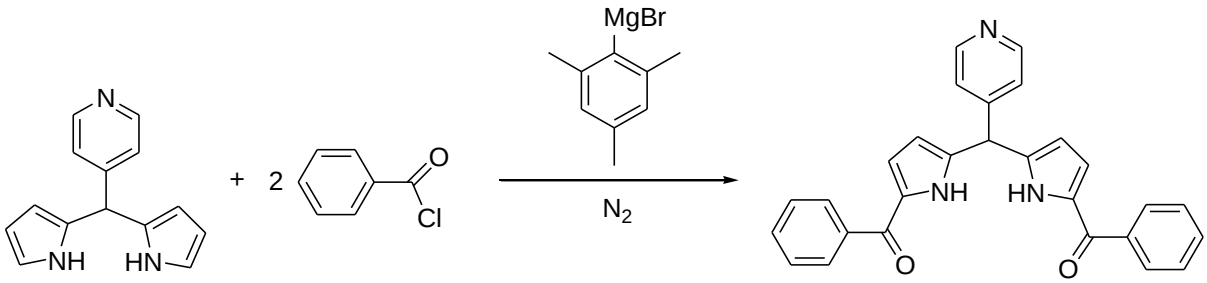

A 1l three-necked round-bottom flask, equipped a 100ml dropping funnel was flushed with a constant flow of nitrogen via the reflux condenser. The dropping funnel was closed by a septum. 3 g (13.4 mmol) 4-pyridinedipyrromethane and 270 ml dry toluene were added to the flask. The 4-pyridinedipyrromethane was not completely soluble. 45 ml (~1.5 M, ~67.2 mmol) of the prior synthesized mesitylene magnesia bromide solution were added into the dropping funnel. Under a nitrogen atmosphere, the mesitylene magnesia bromide solution was added drop wise within 10min. The yellow suspension in the flask turned into a dark brown suspension. The reaction mixture was heated up to 85 °C. After 60 min the three-necked round-bottom flask was held into an ultra-sonic bath for a few minutes to obtain smaller insoluble crystals. The dropping funnel was quickly exchanged with another 100ml dropping funnel containing 4.7 g (33.6 mmol) benzoylchloride dissolved in 34 ml dry toluene. The benzoylchloride solution was added drop wise to the reaction mixture within 15 min. After an additional 10 min the black reaction solution was quenched with 200 ml saturated aqueous NH_4Cl solution. After 10 min stirring the solution was

extracted with 270 ml EtOAc. The organic phase was further washed with 200 ml brine and 200 ml water. The combined organic phases were dried over Na_2SO_4. The brown solution was stored overnight under argon in the fridge. The solvent was evaporated under light protection at 30°C *in vacuo* to afford a dark brown oil. The crude product was used directly for the next reaction, because of stability reasons.

Synthesis of tin di-butyl 5-(4-pyridyl)-di-(5-pyrro-1-carboxyphenyl)methane [337, 367, 368]

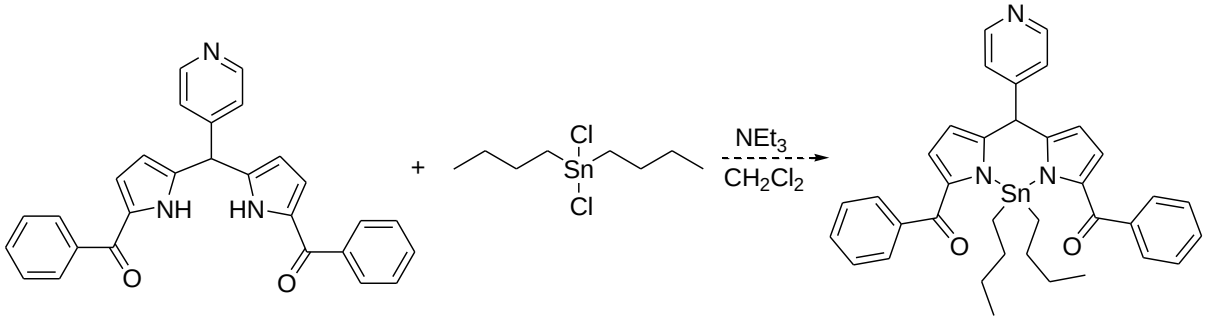

Crude 5-(4-phenyl)-di-(5-pyrro-1-carboxyphenyl)methane (≤5.78 g, ≤13.4 mmol) was suspended in 200 ml CH_2Cl_2. 4 g (40.3 mmol) NEt_3 and 4 g (13.4 mmol) $SnCl_2Bu_2$ were added. The suspension was stirred for 30 min at room temperature. The solvent was removed *in vacuo* to afford 16 g crude product. The crude product was purified over a silica column (95:5-8:2 hexane:EtOAc; 1% NEt_3) to afford a total of 1.6 g product. The analytical results of the product showed discrepancies to the desired product. ^{1}H NMR (500MHz, $CDCl_3$): δ 0.64-0.71 (m), 1.08-1.19 (m), 1.26-1.33 (m), 1.42-1.57 (m), 1.98-2.02 (d), 2.25 (s), 2.52 (bs), 4.79-4.80 (d), 5.00 (s), 5.43 (s), 6.33 (d), 6.48 (d), 6.79-6.92 (t), 7.12-7.15 (dd), 7.27-7.35 (m), 7.47-7.50 (t), 7.54-7.57 (t), 7.89-7.92 (d) ^{13}C NMR (126 MHz, $CDCl_3$): δ 13.75, 13.80, 19.86, 20.37, 20.58, 21.02, 24.57, 24.67, 26.14, 26.45, 27.40, 27.54, 44.99, 115.43, 115.45, 124.32, 128.61, 129.23, 131.82, 135.99, 136.12, 136.75, 137.89, 149.48, 149.82, 184.57, 184.71. ^{119}Sn NMR (74.5MHz, $CDCl_3$): -276.52 (s).

Synthesis of 5-pyridin-10,15,20-phenyl-porphyrin via 5-(4-phenyl)-di-(5-pyrro-1-phenolyl)methane *[337, 367, 368]*

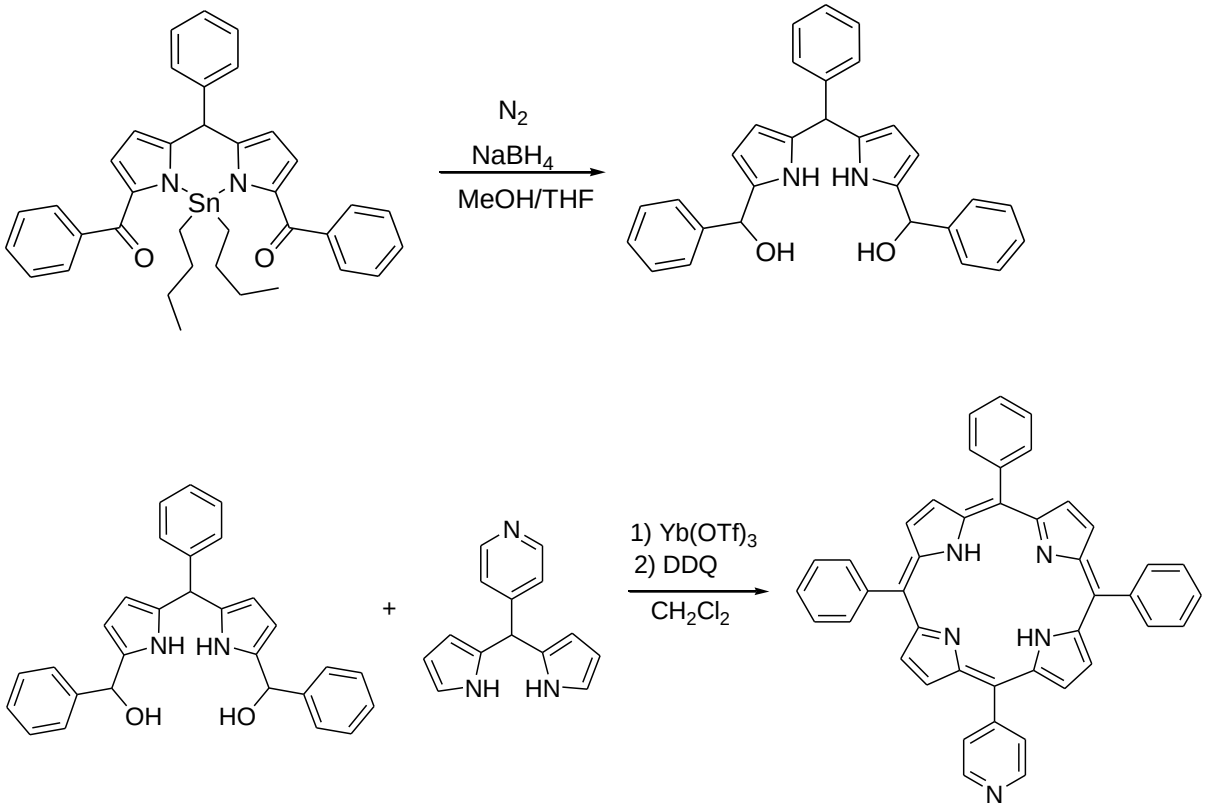

A 100ml flask was equipped with 1 g (1.5 mmol) tin di-butyl 5-(4-pyridyl)-di-(5-pyrro-1-carboxyphenyl)methane. The system was flushed with nitrogen, then 60ml dry THF/MeOH (10:1) was added. The 2.27 g (60 mmol) $NaBH_4$ was added rapidly in small portions within 10 min. The solution was foaming while and afterwards adding the $NaBH_4$. Only a small part of the added $NaBH_4$ was dissolved. TLC indicated complete conversion after 1 h 30 min. The reaction was quenched with 100ml saturated aqueous NH_4Cl solution. Strong foaming lead to a loss of 1/4 to 1/3 of the product. The product was extracted once with 100 ml CH_2Cl_2. The organic phase was dried over Na_2SO_4 and concentrated *in vacuo* at 40 °C to afford the instable intermediate. 0.652 g (1.5 mmol) 4-Pyridinedipyrromethane were dissolved in 600 ml CH_2Cl_2 with the help of an ultra-sonic bath. The solution of 600 ml 4-pyridinedipyrromethane was added to the intermediate. Under nitrogen (passing through the solution) 1.19 g (1.92 mmol) $Yb(OTf)_3$ were added. The yellow solution turned black slowly. After 30 min 1.02 g (4.5 mmol) DDQ was added and the nitrogen disconnected. After 1h stirring at

room temperature the solution was filtered over 2cm silica gel pads. The silica pad was washed with 500 ml CH_2Cl_2 (1% TEA) and 500ml CH_2Cl_2/MeOH (9:1, 1% TEA) to afford 217 mg (first 500ml) and 2.79 g (second 500ml) crude product (black sticky tan solid). The crude product was purified by silica column (increasing gradient CH_2Cl_2:MeOH 10:0 up to 9:1, 1% TEA). 82 mg (0.13 mmol) pure violet crystals and 39mg (0.06 mmol) less pure black crystals could be obtained (13% yield).

^{1}H NMR (200MHz, $CDCl_3$): δ -2.801 (s, 2H), 7.74-7.79 (m, 9H), 8.16-8.24 (m, 8H), 8.79-8.89 (m, 8H), 9.02-9.05 (m, 2H). ESI-MS: m/z (%) 661.2 (100) $[M+HCOOH]^+$.

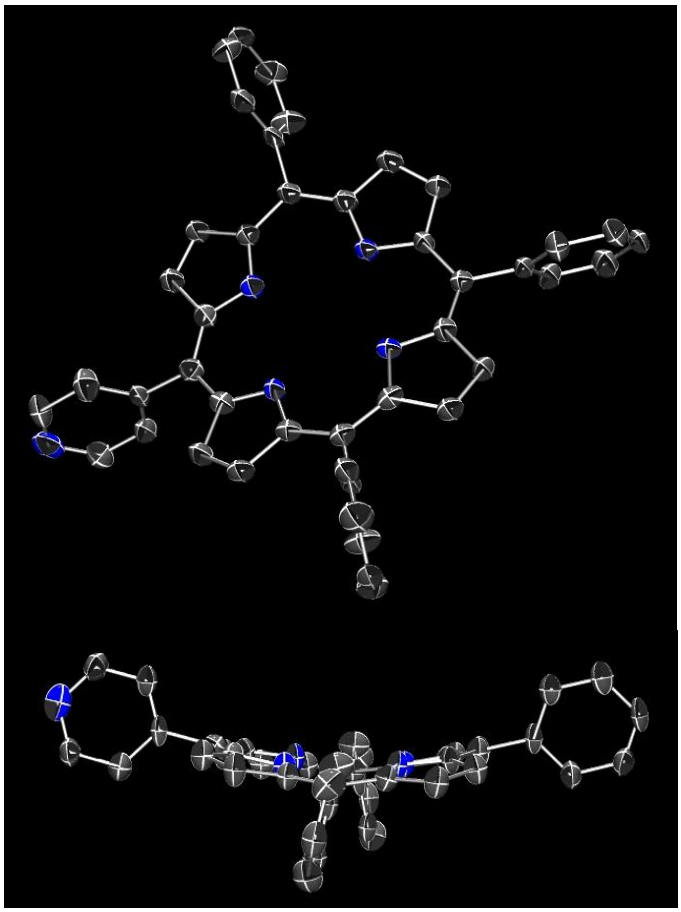

*Figure 7.3 Povray representation of ORTEP plot of porphyrin **2** crystallized from a chloroform/MeOH mixture. Ellipsoids are drawn at 50% probability. Hydrogen ions are omitted for clarity.*

7.4 Synthesis of Metallo - Porphyrin Complexes

5,10,15,20-methylpyridinium-nickel(II)-porphyrin nitrate (11) [133, 146, 370-372]

To a solution of 50 mg (0.058 mmol) 5,10,15,20-methylpyridinium-porphyrin nitrate **(10)** in 25 ml H_2O, 14.2 mg (1 eq.) of nickel(II)acetate were added and the solution stirred for 24h at 45 °C. The reaction was monitored by HPLC. After the completion of the reaction, the solvent was removed *in vacuo*. The crude product was loaded onto an Amberlyte A-26 ion-exchange resin column charged with a saturated solution of NH_4NO_3 in water to obtain the pure nitrate product. Yield: 52 mg, 0.055 mmol, 94%.

HPLC[343]: 7.28 min (100%), MS calc: 982.2; obtained (ESI^+): m/z (%) = 183.6 $[M(por)]^{4+}$ (100), 244.5 $[M(por)]^{3+}$ (100), 367.1 $[M]^{2+}$ (40), 352.5 $[M-(CH_3)_2]^{2+}$ (80).

5,10,15,20-methylpyridinium-copper(II)-porphyrin nitrate (12) [133, 146, 370-372]

To a solution of 50 mg (0.058 mmol) 5,10,15,20-methylpyridinium-porphyrin nitrate **(10)** in 25 ml H_2O, 15.6 mg (1eq.) of copper(II)tetrafluoroborate were added and the solution stirred for 24h at 45 °C. The reaction was monitored by HPLC. After the completion of the reaction, the solvent was removed *in vacuo*. The crude product was loaded onto an Amberlyte A-26 ion-exchange resin column charged with a saturated solution of NH_4NO_3 in water to exchange the BF_4^- ions with NO_3^- ions and obtain the pure nitrate product. Yield: 49 mg, 0.053 mmol, 98%.

HPLC[343]: 7.16 min (100%), MS (ESI): m/z (%) = 184.8 $[M]^{4+}$ (100), 241.4 $[M-CH_3]^{3+}$ (80).

5,10,15,20-methylpyridinium-cobalt(II)-porphyrin nitrate (13) [146, 372]

To a solution of 50 mg (0.058 mmol) 5,10,15,20-methylpyridinium-porphyrin nitrate **(10)** in 25 ml H_2O, 14.2 mg of cobalt(II)acetate were added and the solution stirred for 24h at 45 °C. The reaction was monitored by HPLC. After the completion of the

reaction, the solvent was removed *in vacuo*. The crude product was loaded onto an Amberlyte A-26 ion-exchange resin column charged with a saturated solution of NH_4NO_3 in water to obtain the pure nitrate product. Yield: 50 mg, 0.055 mmol, 96%.

HPLC[343]: 7.39 min (100%), MS (ESI): m/z (%) = 240.4 $[M\text{-}CH_3]^{3+}$ (100).

5,10,15,20-methylpyridinium-zinc(II)-porphyrin nitrate (14) [133, 146, 371-373]

To a solution of 50 mg (0.058 mmol) 5,10,15,20-methylpyridinium-porphyrin nitrate **(10)** in 25 ml H_2O, 14.2 mg of zinc(II)acetate were added and the solution stirred for 24h at 45 °C. The reaction was monitored by HPLC. After the completion of the reaction, the solvent was removed *in vacuo*. The crude product was loaded onto an Amberlyte A-26 ion-exchange resin column charged with a saturated solution of NH_4NO_3 in water to obtain the pure nitrate product. Yield: 52 mg, 0.056 mmol, 97%.

HPLC[343]: 7.18 min (100%), MS (ESI): m/z (%) = 185.4 $[M]^{4+}$ (100)

5,10,15-methylpyridinium-20-para-benzonitrile-copper(II)-porphyrin nitrate (18)

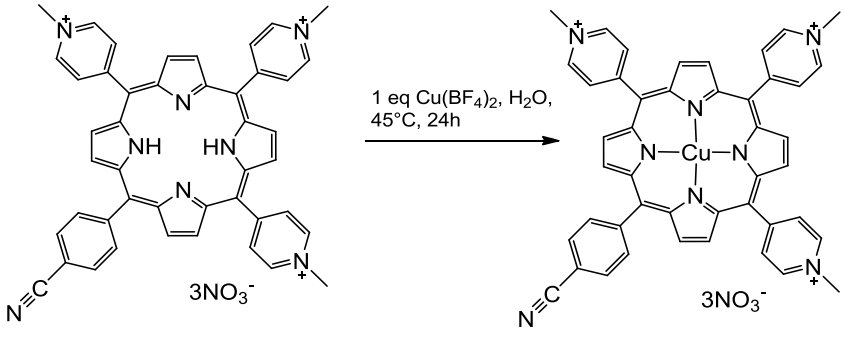

To a solution of 17 mg (0.023 mmol) 5,10,15-methylpyridinium-20-*para*-benzonitrile-porphyrin nitrate **(9)** in 15 ml H_2O, 3.28 mg of $Cu(BF_4)_2$ were added and the solution stirred at 45 °C. The reaction was monitored by HPLC. After the completion of the reaction, the solvent was removed *in vacuo*. The crude product was loaded onto an

Amberlyte A-26 ion-exchange resin column charged with a saturated solution of NH_4NO_3 in water to exchange the BF_4^- ions with NO_3^- ions and obtain the pure nitrate product. Yield: 52 mg, 0.056 mmol, 97%.

18, [$C_{45}H_{33}N_{11}O_9Cu$, M = 935.36 g/mol]: HPLC[343]: 8.12 min (100%), MS (ESI): m/z (%) = 250.1 $[M]^{3+}$ (100), 373.9 $[M]^{2+}$ (90), 748.5 $[M(CuPor)]^+$ (40). UVvis spectrum [λ, nm, in H_2O]: 315, 424 (Soret, 100), 542 (Q1, 30), 582 (Q2, 13).

5,10,15-methylpyridinium-20-para-benzonitrile-zinc(II)-porphyrin nitrate (19)

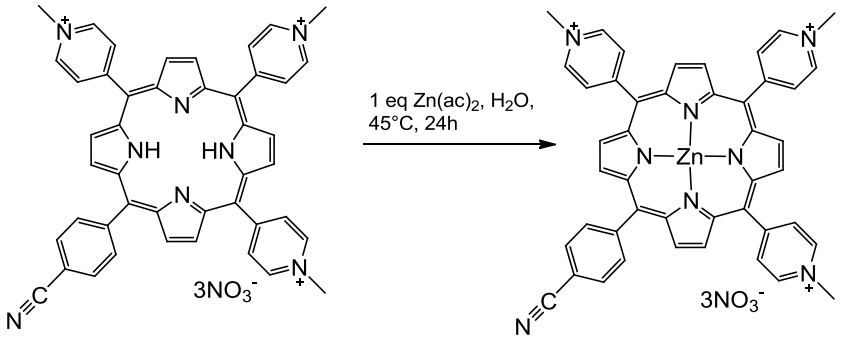

To a solution of 19 mg (0.025 mmol) 5,10,15-methylpyridinium-20-*para*-benzonitrile-porphyrin nitrate **(9)** in 15 ml H_2O, 3.58 (1.1 eq.) mg of zinc(II)acetate were added and the solution stirred at 45 °C. The reaction was monitored by HPLC. After the completion of the reaction, the solvent was removed *in vacuo*. The crude product was loaded onto a Amberlyte A-26 ion-exchange resin column charged with a saturated solution of NH_4NO_3 in water to certify the presence of only NO_3^- ions. Yield: 23 mg, 0.024 mmol, 92%.

19, [$C_{45}H_{33}N_{11}O_9Zn$, M = 937.19 g/mol]: HPLC[343]: 7.16 min (100%), MS (ESI): m/z (%) = 249.7 $[M]^{3+}$ (100), 274.1 $[M]^{2+}$ (15). MS (MALDI) m/z (%) = 687.3 $[M\text{-}Zn]^+$ (100), 749.2 $[M]^+$ (70). UVvis spectrum [λ, nm, in H_2O]: 322, 438 (Soret), 563 (Q1), 613 (Q2).

***cis*-$(NH_3)_2$PtCl-5,10,15-methylpyridinium-20-*para*-benzonitrile-porphyrin nitrate (20)**

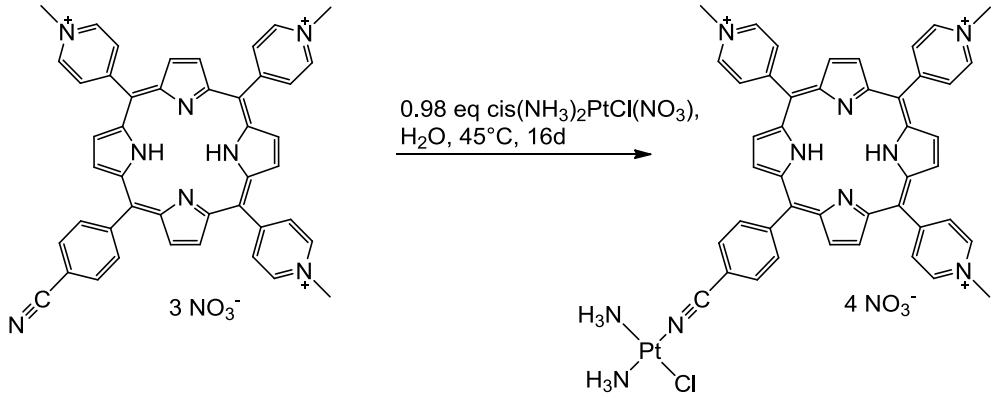

20 mg (0.023 mmol) 5,10,15-methylpyridinium-20-*para*-benzonitrile-porphyrin nitrate **(17)** were given in 25 ml H_2O, then 50 ml of a filtered aqueous solution of 6.86 mg (0.023 mmol) *cis*-$(NH_3)_2PtCl(NO_3)$ (see platinum building blocks) were added and the solution stirred for 16 days at 45 °C in the dark. The reaction was monitored by HPLC, and stopped after completion. After cooling the solution to room temperature, it was treated with a 0.01 M KCl solution. Then, the solution was dried *in vacuo* and the purple precipitate washed with acetone, iced water and methanol. After dissolving it again in water, the solution was lyophilized at 0.2 mbar overnight to afford the purple product. Yield: 23 mg, 0.019 mmol, 83%.

cis-$(NH_3)_2$PtCl-5,10,15-methylpyridinium-20-para-benzonitrile-porphyrin nitrate ***(20***) [$C_{45}H_{41}ClN_{14}O_{12}Pt$, M = 1200.43 g/mol]: HPLC[343]: 7.54 min (100%), gradient 1 and 2. MS (ESI): m/z (%) = 229.8 (100) [M-*cis*$(NH_3)_2PtCl$-$4NO_3$]$^{3+}$, 233.8 (70) [M-Cl+OH-$4NO_3$]$^{4+}$, 234.9 (40) [M-$4NO_3$]$^{4+}$, 316.8 (20) [M-H-$4NO_3$]$^{3+}$, 335 (60) [M-H-*cis*$(NH_3)_2$PtCl-CH_3]$^{2+}$, 343.5 [M-H-*cis*$(NH_3)_2PtCl$]$^{2+}$ (100). MS (MALDI): m = 705.3 (100) [M-*cis*$(HN_3)_2PtCl+OH_2$]$^+$, 897.2 (5) [M-NH_2-Cl-3H]$^+$. ^{195}Pt-NMR (129 MHz, H_2O, 293 K): δ = -2300.56 (Pt(3N)(Cl)).

***cis*-$(NH_3)_2$PtCl-5,10,15-methylpyridinium-20-para-benzonitrile-copper(II)-porphyrin nitrate (21)**

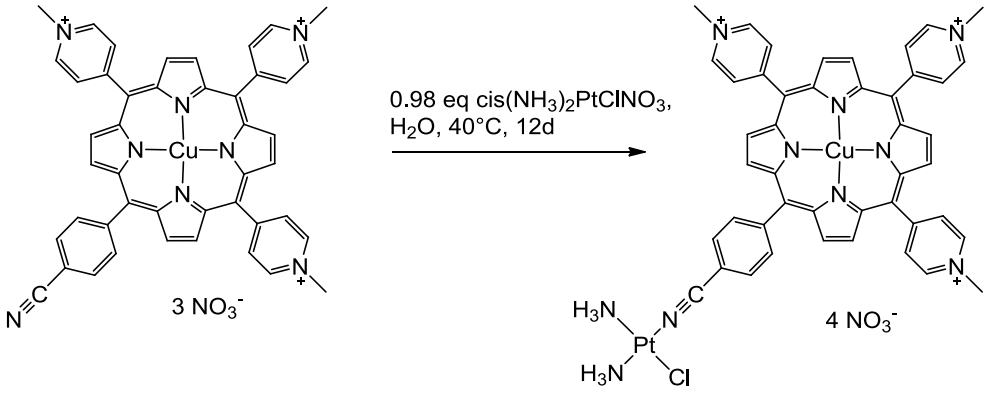

15 mg (0.015 mmol) 5,10,15-methylpyridinium-20-*para*-benzonitrile-copper(II)-porphyrin nitrate **(18)** were given in 10 ml H_2O, then a filtered aqueous solution of 3.43 mg (0.0152 mmol) *cis*-$(NH_3)_2PtCl(NO_3)$ was added and the solution stirred for 12 days at 40 °C. The reaction was monitored by HPLC. After cooling the solution to room temperature, it was treated with a 0.01 M KCl solution. Then, the solution was dried *in vacuo* and the purple precipitate washed with acetone, iced water and methanol. After dissolving it again in water, the solution was lyophilized at 0.2 mbar overnight to afford the reddish product. Yield: 16.4 mg, 0.013 mmol, 86%.

cis-$(NH_3)_2$PtCl-5,10,15-methylpyridinium-20-para-benzonitrile-copper(II)-porphyrin nitrate (**21**) [$C_{45}H_{39}ClCuN_{14}O_{12}Pt$, M = 1261.96 g/mol]: HPLC[343]: 7.43 min (100%) with gradient 1, and 7.77 (96%) with gradient 2. MS (ESI): m/z (%) = 250.3 [M-*cis*$(NH_3)_2PtCl]^{3+}$ (100), 373.8 [M-H-*cis*$(NH_3)_2PtCl]^{2+}$ (50). ^{195}Pt-NMR (129 MHz, H_2O, 293 K): δ = -2340.12 (Pt(3N)(Cl)).

***cis*-$(NH_3)_2$PtCl-5,10,15-methylpyridinium-20-para-benzonitrile-zinc(II)-porphyrin nitrate (22)**

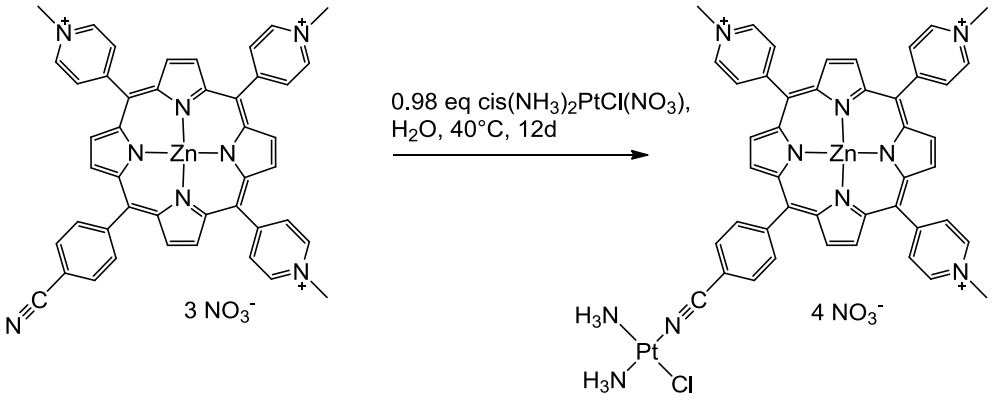

30 mg (0.032 mmol) 5,10,15-methylpyridinium-20-*para*-benzonitrile-zinc(II)-porphyrin nitrate **(19)** were given in 10 ml H_2O, then a filtered aqueous solution of 8.11 mg (0.0342 mmol) *cis*-$(NH_3)_2PtCl(NO_3)$ was added and the solution stirred for 12 days at 45 °C. The reaction was monitored by HPLC. After cooling the solution to room temperature, it was treated with a 0.01 M KCl solution. Then, the solution was dried *in vacuo* and the purple precipitate washed with acetone, iced water and methanol. After dissolving it again in water, the solution was lyophilized at 0.2 mbar overnight to afford the purple product. Yield: 34 mg, 0.027 mmol, 84%.

cis-$(NH_3)_2$PtCl-5,10,15-methylpyridinium-20-para-benzonitrile-zinc(II)-porphyrin nitrate (**22**) [$C_{45}H_{39}ClN_{14}O_{12}PtZn$, M = 1263.80 g/mol]: HPLC[343]: 7.69 min with gradient 1 and 8.14 min with gradient 2 (100%). MS (ESI): m/z (%) = 250.3 [M-*cis*$(NH_3)_2$PtCl-$4NO_3$]$^{3+}$ (100), 251.8 [M-CH_3-$4NO_3$]$^{4+}$ (30), 253.9 [M-$4NO_3$]$^{4+}$ (50), 338.3 [M-$4NO_3$]$^{3+}$ (20), 367.5 [M-*cis*$(NH_3)_2$PtCl-CH_3-$4NO_3$]$^{2+}$ (40), 375 [M-*cis*$(NH_3)_2$PtCl-$4NO_3$]$^{2+}$ (80). MS (MALDI): m = 770.3 [M+Na-*cis*Pt-$4NO_3$]$^{+}$ (100), 897.2 [M+Pt+NH_2-3H-$4NO_3$]$^{+}$(5). ^{195}Pt-NMR (129 MHz, H_2O, 293 K): δ = -2393.97 (Pt(3N)(Cl)).

cis-$(NH_3)_2$PtCl-para-benzonitrile

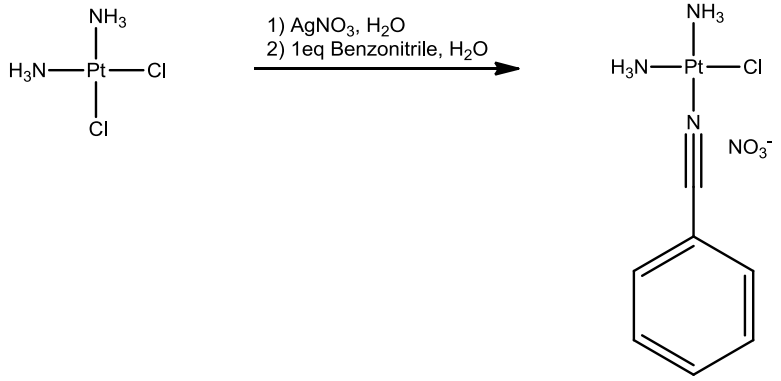

In order to test the affinity and kinetic stability of the Pt-NC coordination, 10 mg (0.04 mmol) of *cis*-[$(NH_3)_2PtCl(NO_3)$] was reacted with the 4.2 µl benzonitrile (1eq.) in 10 ml n-butanol. The resulting blue solution was stirred for 12 hours in the dark and the solvent removed. 11.4 mg of the bluish powder were obtained (0.038 mmol). Yield: 89%.

MS (ESI): m/z (%) = 231.1 $[Pt\text{-}(NH_3)_2+2H]^+$ (10), 266.1 $[M\text{-benzonitrile-}Cl]^+$ (10), 367.2 $[M\text{-}NO_3]^+$ (100), 435.2 $[M\text{-}Cl\text{+benzonitrile-}NO_3]^+$ (10).

7.5 Organic Bridges

The preset characteristics of the organic bridges were simple – able to coordinate to two metal corners on both ends via a nitrogen atom, rigid, keeping the distance and innocent towards DNA. Only organic, non-charged and aromatic structures were chosen such as the 5,15-pyridyl-porphyrin. In the course of these studies, the simple to synthesis 5,15-phenyl-porphyrin was obtained and crystallized from a $CHCl_3$ versus hexane vapor diffusion. The distance in between the both terminal (*para*) C's of the phenyl was 17.4 Å, which fit perfectly to the above outlined strategy.

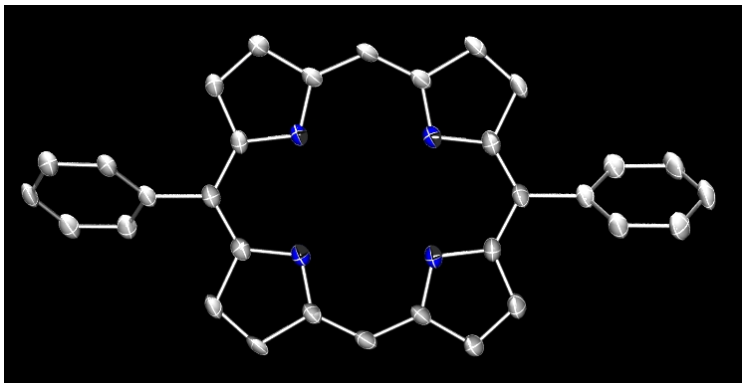

Figure 7.4 Povray plot of 5,15-phenyl-porphyrin crystallized from a $CHCl_3$ versus hexane vapor diffusion. Ellipsoids are drawn at 50% probability. Hydrogen ions are omitted for clarity.

5,15-pyridyl-porphyrin, 29[363]

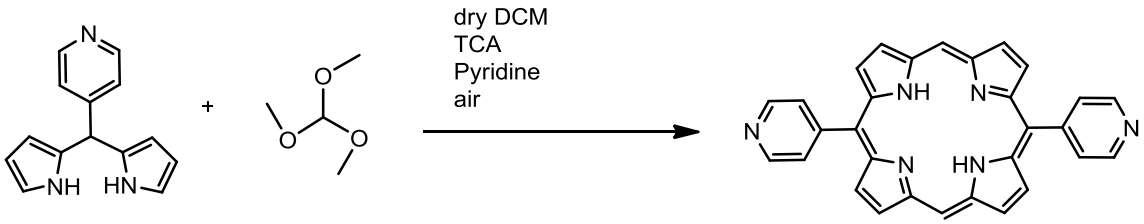

120 mg 5-(4-Pyridyl)-dipyrromethane (PyDP, 0.54 mmol) were dissolved in dry CH_2Cl_2 (1l) under argon atmosphere. To this solution, trimethyl orthoformate (1.2 eq., 68.7 mg) was added and the reaction solution cooled to stay below 25 °C for 4 hours. Then, trichloroacetic acid was added (10 ml of 0.1 mM solution), after 2 hours, pyridine was added to neutralize the solution, then air was bubbled through the solution. The solvent was removed and the resulting dark compound purified on a silica gel column (3 runs) to yield 68.1 mg of 5,15-pyridyl-porphyrin (32%).

MS (ESI): m/z (%) = 463.3 $[M]^+$ (100). ^{1}H NMR (200MHz, $CDCl_3$): δ -2.54 (2H, s, inside porphyrin NH pyrrole), 7.81 (4H, dd, 3-pyridyl), 8.25 (4H, 2 dd, 3-pyridyl), 9.07 (4H, d, pyrrole proximate to 10,20-position), 9.37 (4H, d, pyrrol proximate to 5,15-position), 10.29 (4H, s, 10,20-porphyrin H). UV vis spectrum [λ, nm, in $CHCl_3$]: 416 (Soret), 512 (Q1), 540 (Q2), 585 (Q3). EA calc.: C 77.57, N 18.09, H 4.34; found: C 77.33, N 18.94, H 4.58.

Synthesis of 1,4-bis(4',4''-pyridyl)benzene, 30 [374]

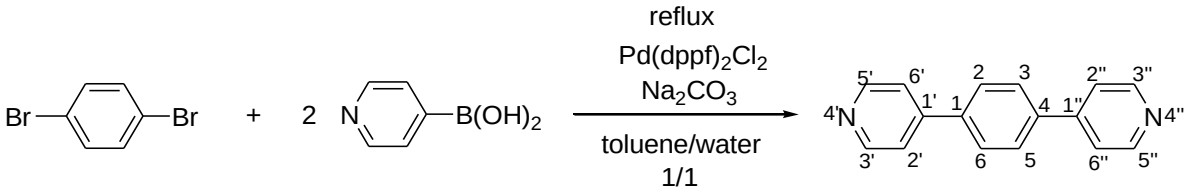

A 100ml two-necked round-bottom flask was equipped with 1.65 g (7 mmol) 1,4-dibrombenzene, 2.73 g (24.5 mmol) pyridine-4-boronic acid, 1.49 g (14 mmol) Na_2CO_3 dissolved in 40 ml toluene/water (1:1; degassed by passing nitrogen through the solution) and 0.51g (0.7mmol) $Pd(dppf)_2Cl_2$. The system was degassed for 15 min by passing nitrogen through the suspension. The reaction was heated to reflux and allowed to react for 72 h under a nitrogen atmosphere. The solvent was removed *in vacuo* and the resulting residue was extracted with ethyl acetate and washed with water (three times). The combined organic phases were dried over anhydrous Na_2SO_4. The Na_2SO_4 was filtered off. The solvent was evaporated to afford 1.97 g of a dark brown solid, which was further purified by silica gel column chromatography (CH_2Cl_2/MeOH(10% NH_3) (99:1 V/V up to 97.5:2.5 V/V) to afford a fine grey crystalline solid of 1,4-bis(4',4''-pyridyl)benzene (Yield: 1.27g, 78%).

1,4-bis(4',4''-pyridyl)benzene. ^{1}H NMR (200MHz, $CDCl_3$): δ 7.53-7.56 (4H, m, H-2, H-3, H-5, H-6), 7.8 (4H, s, H-2', H-2'', H-6', H-6''), 8.69-8.72 (4H, d, J = 5.8Hz, H-3', H-3'', H-5', H-5'') ^{13}C NMR (50 MHz, $CDCl_3$): δ 121.6, 127.7, 138.8, 147.3, 150.4 ESI-MS: m/z 233.1 $[M+H]^+$, 255.5 $[M+Na]^+$ Anal. Calcd (%) for $C_{16}H_{12}N_2$: C 82.73, H 5.21, N 12.06. Found: C 82.58, H 5.26, N 11.95.

Synthesis of 1,1'-bis(4'',4'''-pyridyl)-4,4'-biphenyl, 31 [176]

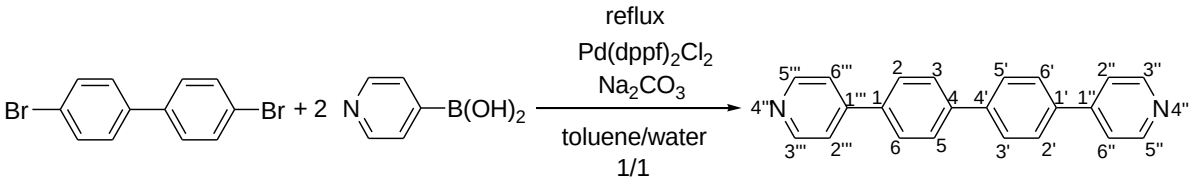

1.56 g (5mmol) 4,4'-dibromobiphenyl, 2.15 g (17.5 mmol) pyridine-4-boronic acid, 1.06 g (10 mmol) Na_2CO_3 dissolved in 40 ml toluene/water (1:1; degassed by passing nitrogen trough the solution) and 0.37 g (0.5 mmol) $Pd(dppf)_2Cl_2$. were combined in a 100 ml flask. The system was degassed for 10min with passing nitrogen trough the suspension. The reaction was heated to reflux and allowed to react for 72 h under nitrogen atmosphere. The solvent was evaporated and the resulting residue was extracted with CH_2Cl_2 and washed with water (three times). The combined organic phases were dried over anhydrous Na_2SO_4. The solvent was evaporated to afford a black solid. The crude product was elutriated with MeOH. The MeOH was removed by suction and the crystalline residue was washed several times with MeOH to afford 1.10g (Yield: 71%).

1,1'-bis(4'',4'''-pyridyl)-4,4'-biphenyl. ^{1}H-NMR (200MHz, $CDCl_3$): δ 7.56-7.59 (m, 4H, H-2'', H-2''', H-6'', H-6'''), 7.75-7.80 (m, 8H, H-2, H-2', H-3, H-3', H-5, H-5', H-6, H-6'), 8.69-8.75 (m, 4H, H-3'', H-3''', H-5'', H-5''') ^{13}C NMR (50 MHz, $CDCl_3$): δ 121.71 (4C, C-2'', C-2''', C-6'', C-6'''), 127.77 (4C, C-3, C-3', C-5, C-5'), 127.99 (4C, C-2, C-2', C-6, C-6'), 137.64 (2C, C-1, C-1'), 141.18 (2C, C-4, C-4'), 147.94 (2C, C-1'', C-1'''), 150.53 (4C, C-3'', C-3''', C-5'', C-5''') ESI-MS: m/z 309.4 $[M+H]^+$. EA calc (%): $C_{22}H_{16}N_2$: C 85.69, H 5.23, N 9.08. found: C 82.51, H 5.19, N 8.81.

Synthesis of 4-(4-bromophenyl)-pyridine [176]

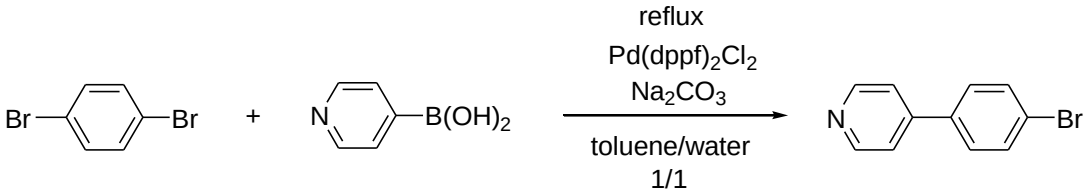

A 100ml flask was equipped 1.65 g (7 mmol) 1,4-dibrombenzene, 0.86 g (7 mmol) pyridine-4-boronic acid, 0.74 g (7 mmol) Na_2CO_3 dissolved in 35 ml toluene/water (1:1; degassed by passing nitrogen through the solution) and 0.26 g (0.35 mmol) $Pd(dppf)_2Cl_2$. The system was degassed for 10min by passing nitrogen trough a suspension. The reaction was heated to reflux and allowed to react for 104 h under nitrogen atmosphere. The solvent was evaporated and the resulting residue was extracted with five times 100 ml CH_2Cl_2 and washed with water (two times). The combined organic phases were dried over Na_2SO_4. The solvent was evaporated to afford 1.18 g of a brown solid, which was further purified by alox column chromatography (pH=9.5, 1:1 CH_2Cl_2/EtOAc) to afford a grey crystalline solid (yield, 294mg, 18%).

4-(4-bromophenyl)-pyridine. ^{1}H NMR (200MHz, $CDCl_3$): δ 7.43-7.53 (m, 4H), 7.59-7.65 (m, 2H), 8.65-8.68 (d, 2H) ESI-MS: m/z 234.5 $[M+H]^+$.

4-methylpyridinium-4'-pyridine iodide[375]

15 mg 4,4'-bipyridine (0.12 mmol) were dissolved in $CHCl_3$ and 1 eq (14.1 mg, 620 µl) methyliodide at 4°C and stirred for 30 minutes, then allowed to return to room temperature. The resulting precipitate was obtained by cooling the solution to -10°C and filtering it. Yield 15.2 mg (73 %). MS (ESI): m/z (%) = 171.7 $[M]^+$(100).

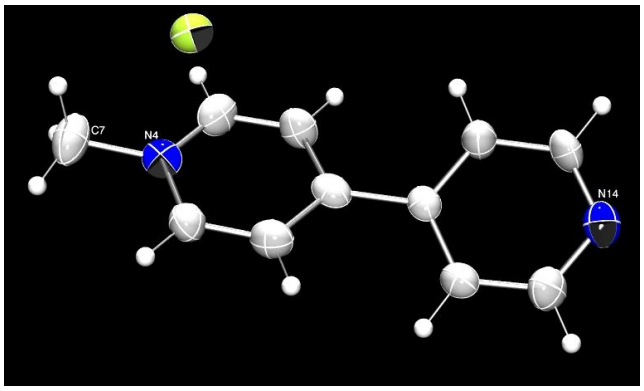

Figure 7.5 Povray plot of 4-methylpyridinium-4'-pyridide iodine crystallized from a methanol/n-pentane mixture. Ellipsoids are drawn at 50% probability.

The crystal structure above was obtained by reacting 4,4'-bipyridine with one equivalent of methyliodide in $CHCl_3$ at 4°C and slowly allowing it to reach room temperature. The resulting pale yellow crystal was obtained by vapor diffusion of an aqueous solution versus dioxane. The two neighboring pyridine rings are twisted against each other in a 60° angle for minimal overlap of its dislocated aromatic orbitals. The following crystal structure shows one of the decomposition products of 4-chloropyridinium bromide in methanol and crystallizing the colorless powder from water versus dioxane.

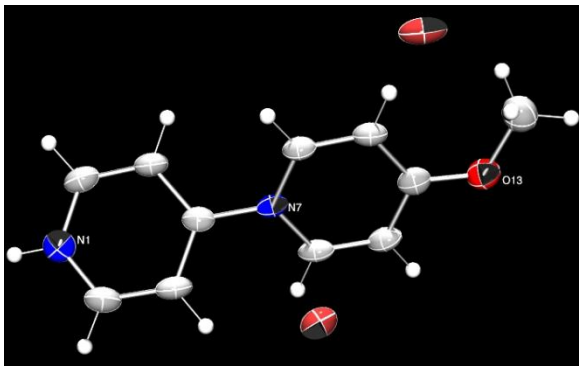

Figure 7.6 Povray plot of 1-(4-pyridine)-4-methoxy-pyridinium dibromide crystallized from a methanol solution. Ellipsoids are drawn at 50% probability.

7.6 Platinum building blocks

$Pt(NH_3)_2Cl_2$, Cisplatin [156, 376]

An aqueous solution (120 ml) of 11.95 g (28.8 mmol) K_2PtCl_4 was treated with 30 ml of a saturated solution of potassium iodide (18.8 g, 113.3 mmol) and heated to 40°C in 5 minutes and kept at that temperature for another 15 minutes. Then, 30 ml 8N NH_3 (aq.) were added to generate a yellow crystalline precipitate and a colorless solution. After 2h, the precipitate was filtered followed by washing with cooled water, MeOH, Et_2O and dried at 50°C to yield 12.7 g of a pale yellow crystalline powder (88%). This *cis*-$Pt(NH_3)_2I_2$ was suspended in 100 ml water and stirred for 30 min at 80°C with 8.97 g $AgNO_3$ (52.8 mmol). After 90 min at RT and 2.5 h at 4°C without stirring, a yellow precipitate of AgI was filtered over a cellite pad. To the yellow filtrate, 4.53 g of KCl (60.8 mmol, 2.3 eq) were given and the solution stirred for 10 min at 80°C. The solution was left at 4°C overnight, the precipitate filtered, washed with cooled water and MeOH, and then dried to yield 6.25 g (20.8 mmol, 72.4% yield).

^{195}Pt-NMR (129 MHz, $CDCl_3$, 293 K): δ = - 2112.7 (Pt(2N)(2Cl)). EA: calculated: H, 2.02; N, 9.34; found: H, 2.08; N, 9.29.

$Pt(NH_3)_2Cl^+NO_3$, $Pt(NH_3)_2^{2+}$, activated cisplatin

All platinum compounds were activated by removing one or two equivalents of the chlorides with the help of silver ions (from $AgNO_3$, $AgBF_4$, silver(I)acetate). The precipitate was removed by centrifugation, filtering through cellite and drying the filtrate *in vacuo* and conserving the powder for a maximum of 2 days at -20°C in the dark. In most cases, the filtrate was directly used for the following reaction without further analysis or purification assuming 100% yield.

Pt(en)I_2, Dhara Synthesis[156]

An aqueous solution (120 ml) of 11.95 g (28.8 mmol) K_2PtCl_4 was treated with 30 ml of a saturated solution of potassium iodine (18.8 g, 113.3 mmol) and heated to 40°C for 5 minutes. The solution turned from light red to dark red to form K_2PtI_4. To this, 2.47 ml (34.4 mmol, 1.2 eq) ethylenediamine (en) were added to leave behind 11.5 g (28.0 mmol) yellow crystalline Pt(en)I_2 and a colorless solution. Isolated yield: 88.1%

[Pt(en)I_2 [$C_2H_8I_2N_2Pt$, M = 508.99 g/mol]. EA: calculated: C, 4.72; H, 1.58; N, 5.50; found: C, 4.76; H, 1.28; N, 5.46. ^{195}Pt-NMR (200 MHz, $CDCl_3$): δ = -2133.4. MS (ESI): m/z (%) = 531.8 (100) $[M + Na]^+$, 469.5 (15) $[M – I + MeOH]^+$. ^{195}Pt-NMR (129 MHz, H_2O, 293 K): δ = -2967.32 (Pt(3N)I).

cis-Pt(en)Cl_2[325, 329, 377, 378]

200 mg (0.48 mmol) K_2PtCl_4 and 38.6 µl (0.58 mmol, 1.2 eq) ethylenediamine (en) were given in 5 ml H_2O and the solution heated to 50 °C and stirred for 14 hours in the dark. The reaction was stopped and the yellow precipitate filtered to yield 157.2 mg. Yield: 96%

cis-Pt(en)Cl_2 [$C_2H_8Cl_2N_2Pt$, M = 326.08 g/mol]. EA: calculated: C, 7.37; H, 2.41; N, 8.59; found: C, 7.37; H, 1.92; N, 8.50. MS (ESI): m/z (%) = 349.1.8 (100) $[M + Na]^+$. ^{195}Pt-NMR (129 MHz, H_2O, 293 K): δ = -2123.72 (Pt(3N)(Cl)).

7.7 Multi – porphyrin and Platinum Arrays

cis-Pt(NH$_3$)$_2$(TriMPyP)$_2$ nitrate, 38

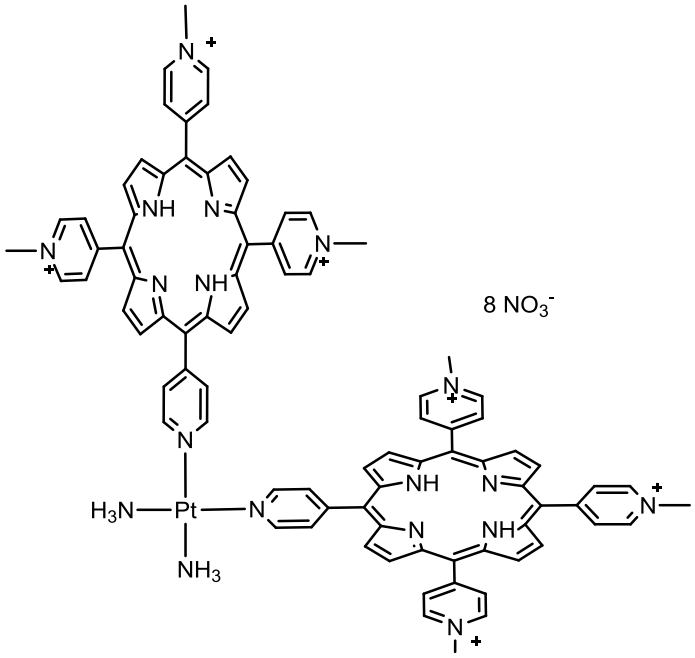

40.9 mg (0.1 mmol) *cis*-[Pt(NH$_3$)$_2$(DMSO)$_2$](NO$_3$)$_2$ were dissolved in 5 ml chloroform and given into a 5 ml chloroform solution containing 155 mg (0.2 mmol) TriMPyP. After 1 day of stirring and mild heating to 45 °C, 4 ml of water were added. The aqueous solution turned deep green. The two solvents were separated, the aq. solution washed with chloroform and dried *in vacuo* to yield 96 mg (0.055 mmol, 55 %)

cis-Pt(NH$_3$)$_2$(TriMPyP)$_2$ nitrate [$C_{86}H_{76}O_{24}N_{26}Pt$, M = 2051.52 g/mol] HPLC : 6.42 min[190, 378]. EA: calc. C, 50.32; H, 3.72; N, 17.74; found: C, 50.55; H, 3.58; N, 18.02. MS (ESI): m/z (%) = 197.5 $[M-8NO_3+H_2O]^{8+}$ (100), 369.3 $[M-8NO_3-5CH_3]^{3+}$ (90).

***cis*-Pt(NH$_3$)$_2$(MPyTPP)$_2$ nitrate**

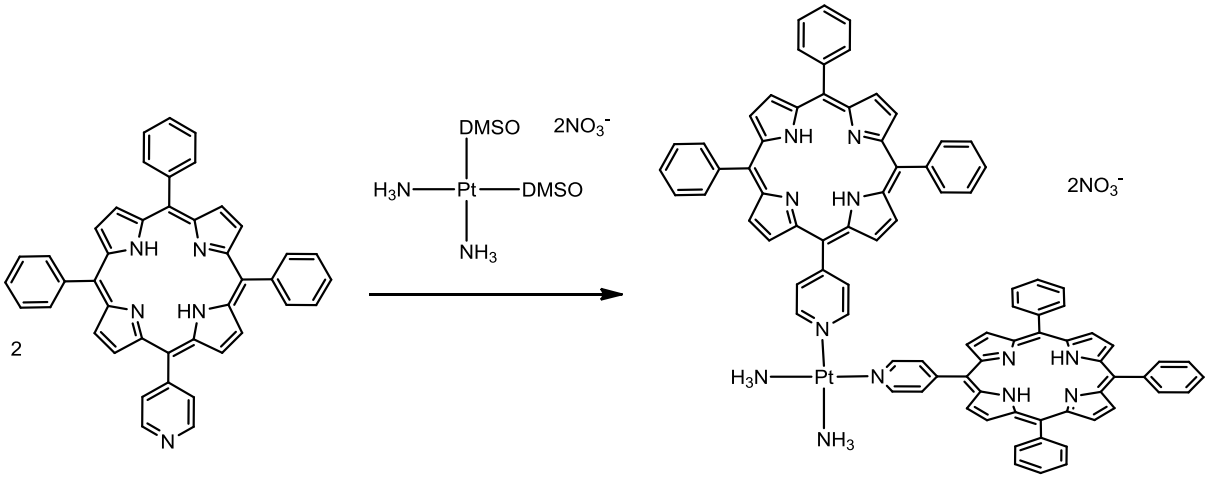

40 mg (0.12 mmol) *cis*-Pt(NH$_3$)$_2$Cl$_2$ were dissolved in 5 ml DMSO, 2 eq. AgNO$_3$ (40.8 mg, 0.24 mmol) were added and stirred for 1 hour. The solution was separated by centrifugation from the precipitation, dried *in vacuo* and the resulting light yellow product dissolved in 5 ml dichlormethane. To this solution, 150 mg (0.24 mmol) MPyTPP were added and the mixture stirred for 1 day at 42 °C. Yield: 55 %

cis-Pt(NH$_3$)$_2$(MPyTPP)$_2$ nitrate [$C_{86}H_{64}N_{14}O_6Pt$, M = 1584.6 g/mol] EA: calc. C, 65.19; H, 4.07; N, 12.37; found: C, 65.22 H, 4.31; N, 12.22. MS (ESI): m/z (%) = 792 $[M\text{-}NO_3]^{2+}$ (70).

***cis*-$(NH_3)_2$Pt-di-5,10,15-methylpyridinium-20-*para*-benzonitrile-zinc(II)-porphyrin nitrate, 35**

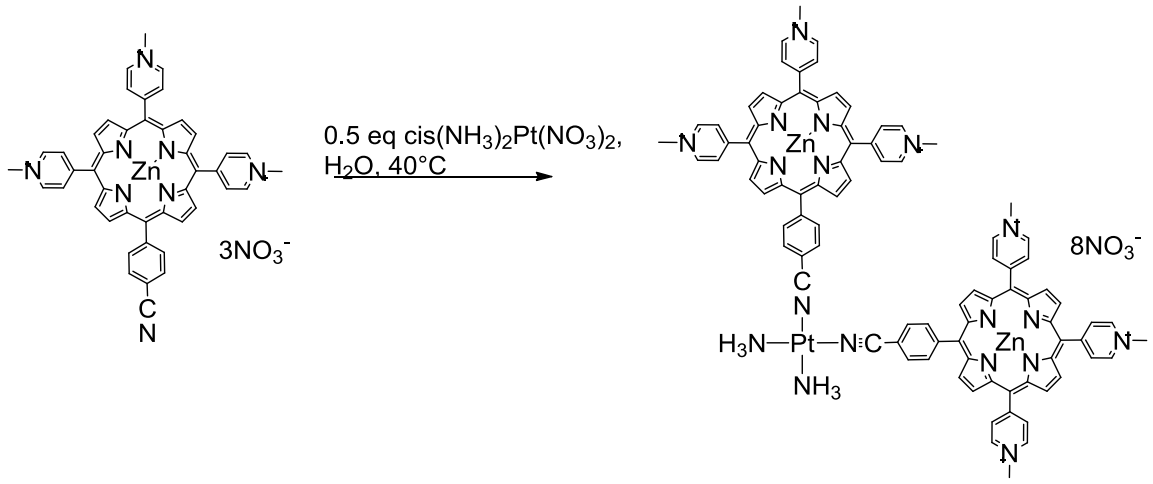

30 mg (0.02 mmol) 5,10,15-methylpyridinium-20-*para*-benzonitrile-zinc(II)-porphyrin nitrate (**35**) were given in 5 ml H_2O, then a filtered aqueous solution of 4.6 mg (0.019 mmol) *cis*-$(NH_3)_2Pt(H_2O)_2$ were added and the solution stirred for 10 days at 40 °C. The reaction was monitored by HPLC. After cooling the solution to room temperature, it was treated with a 0.01 M KCl solution. Then, the solution was dried *in vacuo* and the purple precipitate washed with acetone, iced water and methanol. After dissolving it again in water, the solution was lyophilized at 0.2 mbar overnight to afford the greenish product. Yield: 34 mg, 0.028 mmol, 88%.

cis-$(NH_3)_2$Pt-di-5,10,15-methylpyridinium-20-para-benzonitrile-zinc(II)-porphyrin nitrate. HPLC: 7.39 min (100%). MS (ESI): m/z (%) = 250.3 $[\mathbf{35}]^{3+}$ (100), 251.8 $[\mathbf{35}+Pt(NH_3)_2+(H_2O)]^{4+}$ (30), 253.9 $[\mathbf{35}+Pt(NH_3)_2+(H_2O)]^{4+}$ (50), 338.3 $[M]^{3+}$ (20), 367.5 $[\mathbf{35}-CH_3]^{2+}$ (400), 375 $[\mathbf{35}]^{2+}$ (80). ^{195}Pt-NMR (129 MHz, $CDCl_3$): δ = -2662.43.

(cis-[Pt(NH$_3$)$_2$Cl]$_2$ 5,15-dipyridylporphrin nitrate

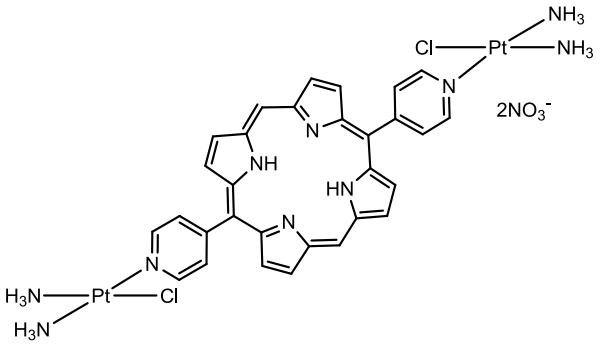

An activated *cis*platin solution (25mg, 0.1mmol in 30 ml DMF) was added to a solution of (23.4 mg, 0.5 eq.) 5,15-dipyridylporphrin in DMF and the solution stirred for 3 days. The reaction was followed by TLC. The resulting purple compound was soluble in ethanol or dichloromethane, but not in water although it has 2 positive charges.

MS (ESI): m/z (%) = 1081.2 (9.5) $[M\text{-}Cl]^+$. ^{195}Pt-NMR (200 MHz, $CDCl_3$): δ = -2326.3.

(cis-[Pt(NH$_3$)$_2$Cl]$_2$ trans-DPyDPP nitrate, reaction of cisplatin with 3.

An activated *cis*platin solution (25mg, 0.1mmol in 30 ml DMF) was added to a solution of (30.5 mg, 0.5 eq.) trans-DPyDPP, **3** in DMF and the solution stirred for 3 days. The reaction was followed by TLC. The resulting purple compound was soluble in $CHCl_3$, CH_2Cl_2, but not in water although it has 2 positive charges located on the platinum. The analysis was not conclusive due to solubility issues.

[cis-Pd(en)$_2$(4,4'-bipyridyl)]$_4$ nitrate [175, 176]

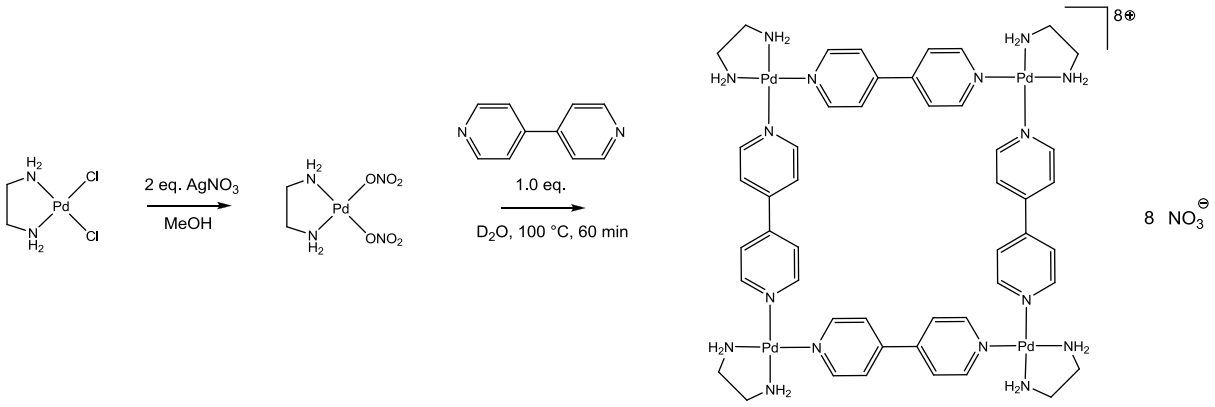

Ta a solution of $Pd(en)Cl_2$ (40 mg, 0.17 mmol) in dry MeOH (5 ml), $AgNO_3$ (57.2 mg, 0.34 mmol) were added and the precipitate was filtered off. The solvent was removed in vacuo and the activated palladium salt dissolved in D_2O (4 ml). Then, 4,4'-bipyridine (21.8 mg, 0.14 mmol) were added and the mixture stirred at 10 °C for 1h. The square was isolated as a white precipitate (73.8 g, 41.3 μmol) by addition of ethanol in 93 % yield.

^{1}H-NMR (200 MHz, D_2O): δ 8.76 (8H, d, J = 6.6 Hz), 7.77 (8H, d, J = 6.6 Hz), 2.84 (16H, d, J = 6.0 Hz).

[cis-Pt(en)$_2$(4,4'-bipyridyl)]$_4$ nitrate

Ta a solution of $Pt(en)I_2$ (40 mg, 0.08 mmol) in dry MeOH (5 ml), $AgNO_3$ (26.8 mg, 0.16 mmol) were added and the precipitate was filtered off. The solvent was removed in vacuo and the activated palladium salt dissolved in D_2O (4 ml). Then, 4,4'-bipyridine (12.8 mg, 0.08 mmol) were added and the mixture stirred at 10 °C for 1h. The square was isolated as a white precipitate (41.6 g, 19.4 μmol) by addition of ethanol in 95 % yield.

^{1}H-NMR (200 MHz, D_2O): δ 8.81 (8H, d, J = 6.0 Hz), 7.80 (8H, d, J = 6.0 Hz), 2.76 (16H, d, J = 6.2 Hz).

7.8 CD titration of poly (dG-dC) - poly (dG-dC) with Cu^{2+}, Ni^{2+} and Zn^{2+} porphyrins

7.8.1 UV, Fluorescence, and CD titration of 5'-GMP with (metallo)-porphyrins

800 µl of a 0.1 mM aqueous (1 mM sodium cacodylate buffer solution (pH = 7.0)) solution of 5'-GMP were given into a 1ml CD quartz cuvette. To this solution, aliquots of a 1 mM solution (buffered sodium cacodylate solution (pH = 7.0) of the corresponding (metallo)-porphyrin solution were added. The corresponding measurements were carried out in a quartz cuvette with a magnetic stirrer. All measurements were taken at 25 °C unless otherwise described. The data obtained were processed in Windows Excel and Origin 7.0.

7.8.2 UV, Fluorescence, and CD titration of poly d(GC) with (metallo)-porphyrins[379]

The DNA solution (concentration of approximately 0.1 mM) in an aqueous 1 mM sodium cacodylate buffer solution (pH = 7.0) was determined by UV vis spectroscopy (ε_{260} = 8400 1/cm*M for 1 base)[379]. To this solution, aliquots of a 1 mM solution (buffered sodium cacodylate solution (pH = 7.0) of the corresponding (metallo)-porphyrin solution were added. The corresponding measurements were carried out in a quartz cuvette with or without a magnetic stirrer. All measurements were done at 25 °C unless otherwise described. The data obtained were processed in Windows Excel and Origin 7.0.

7.8.3 HPLC Measurements[343]

Gradient 1 (13 min, for 26 min gradient double the times indicated) starting with 0% methanol in a 0.1% TFA aqueous solution ramping up to 100% methanol within 8 minutes, holding at 100% methanol for 2 minutes, going back to 100% aqueous solution within 1 minute and washing.

Gradient 2 (13 min) starting with 0% methanol in a 0.1% TFA and 5% NaCl aqueous solution ramping up to 100% methanol within 8 minutes, holding at 100% methanol for 2 minutes, going back to 100% aqueous solution within 1 minute and washing.

7.9 MTT Cytotoxicity Studies

7.9.1 Cell Lines [380, 381]

A2780 cell line (human ovarian cancer) were grown in RPMI-1680 (Gibco) supplemented with 10% FBS, 60 μg mL^{-1} streptomycin (Gibco) and 60 units (0.66 μg per unit) penicillin. MCF-7 cell line (human mama-carcinoma) were grown in MEM-10370 (Gibco) supplemented with 10% FBS, 60 μg mL^{-1} streptomycin (Gibco) and 60 units (0.66 μg per unit) penicillin. HeLa cell line (cervical cancer) is one of the oldest and most commonly used human cell lines. The line was grown in DMEM-41966 (Gibco) supplemented with 10% FBS, 60 μg mL^{-1} streptomycin (Gibco) and 60 units (0.66 μg per unit) penicillin.

7.9.2 MTT Cytotoxicity assay [38, 347, 382, 383]

Five hundred cells/well were plated in 96-well plates kept at 5% CO_2 at 37 °C, treated the next day with various concentrations of *cisplatin*, porphyrin or Pt-porphyrin derivative (**17** - **22**) with a final volume of 100μl. After 18 hours incubation, one set of cells treated with **17** - **22** was exposed to light (slide projector, 3200 lux, cut off filter >600nm, IR free and water-cooled light source, 10 minutes). After an additional 3 days, 20 μL of MTT solution (5mg/ml, Sigma, in PBS filter-sterilize) were added, the plates were incubated for 5 h at 37° C. 100 μl of lyses solution were added (10 g SDS, 25 mL DMF, 25 ml ddH_2O, pH <4.7 (phosphate buffer), and the plates were incubated overnight at 37 °C. The soluble formazan was quantified at 570 nm using an ELISA reader. All specific growth rates are expressed as the mean of quintuplets of three independent experiments.

7.9.3 Crystallographic Data

Code, Nr.	**bs020510, 10**	**pa071109**	**pa101107**
Empirical formula	$C_{48}H_{46}I_4N_8O_2$	$C_{32}H_{22}N_4$	$C_{14}H_{18}I_2N_2O_3$
Formula weight	1274.53	462.54	516.10
Crystal system	Monoclinic	Monoclinic	Triclinic
Space group	$P2_1/n$	$P2_1/c$	P-1
a [Å]	17.0290(9)	14.5305(7)	8.0284(2)
b [Å]	6.7744(5)	16.8710(7)	9.3576(3)
c [Å]	21.0200(11)	9.6388(4)	12.6851(3)
α [°]	90	90	104.858(2)
β [°]	90.731(5)	105.324(4)	103.816(2)
γ [°]	90	90	91.525(2)
Volume [$Å^3$]	2424.7(3)	2278.89(17)	890.55(4)
Z	2	4	2
Density (calculated) [Mg/m^3]	1.746	1.348	1.925
Absorption coefficient [mm^{-1}]	2.617	0.081	3.541
F(000)	1236	968	492
Crystal size [mm^3]	0.15 x 0.13 x 0.02	0.41 x 0.09 x 0.03	0.34 x 0.06 x 0.06
Crystal description	dark red plate	purple needle	yellow needle
Theta range for data collection [°]	3.06 to 25.68	2.59 to 25.35	2.26 to 30.51
Index ranges	-20<=h<=17 -7<=k<=8 -25<=l<=22	-12<=h<=17 -20<=k<=17 -11<=l<=9	-11<=h<=11 -13<=k<=13 -17<=l<=18
Reflections collected	11410	10831	18547
Independent reflections	4605 [R(int) = 0.0591]	4176 [R(int) = 0.0637]	5437 [R(int) = 0.0275]
Reflections observed	2821	2149	3818
Criterion for observation	>2sigma(I)	>2sigma(I)	>2sigma(I)
Completeness to theta	99.8 % to 25.68°	99.9 % to 25.35°	99.9 % to 30.51°
Absorption correction	Semi-empirical from equivalents	Semi-empirical from equivalents	Semi-empirical from equivalents
Max. and min. transmission	0.9618 and 0.3990	0.9976 and 0.7168	0.8156 and 0.5132
Data / restraints / parameters	4605 / 0 / 282	4176 / 0 / 325	5437 / 1 / 207
Goodness-of-fit on F^2	0.967	0.886	1.022
Final R indices [I>2sigma(I)]	R1 = 0.0683 wR2 = 0.1619	R1 = 0.0594 wR2 = 0.1110	R1 = 0.0296 wR2 = 0.0588
R indices (all data)	R1 = 0.1079 wR2 = 0.1729	R1 = 0.1356 wR2 = 0.1268	R1 = 0.0567 wR2 = 0.0628
Largest diff. peak and hole [$e.Å^{-3}$]	2.513 and -0.942	0.223 and -0.361	0.973 and -0.727

Name, Nr.	**pa101209, 2**	**pa110209**	**ss191109**
Empirical formula	$C_{43}H_{29}N_5$	$C_{23}H_{33}B_2Cl_3N_2O_4$	$C_{14}H_{13}N_3$
Formula weight	615.71	529.48	223.27
Crystal system	Monoclinic	Orthorhombic	Monoclinic
Space group	C2	$Pna2_1$	$P2_1$
a [Å]	20.042(14)	18.7419(4)	8.1252(5)
b [Å]	14.977(7)	11.9472(3)	6.1476(2)
c [Å]	13.605(9)	24.9145(6)	12.0015(6)
α [°]	90	90	90
β [°]	131.71(2)	90	100.960(5)
γ [°]	90	90	90
Volume [$Å^3$]	3049(3)	5578.7(2)	588.55(5)
Z	4	8	2
Density (calculated) [Mg/m^3]	1.341	1.261	1.260
Absorption coefficient [mm^{-1}]	0.080	0.359	0.077
F(000)	1288	2224	236
Crystal size [mm^3]	0.30 x 0.30 x 0.02	0.22 x 0.11 x 0.09	0.43 x 0.13 x 0.10
Crystal description	dark red plate	colourless needle	colourless needle
Theta range for data collection [°]	1.92 to 26.37	2.18 to 24.11	2.55 to 30.51
Index ranges	-25<=h<=25 -16<=k<=16 -16<=l<=16	-21<=h<=21 -13<=k<=13 -28<=l<=28	-11<=h<=11 -8<=k<=8 -17<=l<=12
Reflections collected	10871	29488	5796
Independent reflections	3004 [R(int) = 0.0682]	8641 [R(int) = 0.0764]	1947 [R(int) = 0.0208]
Reflections observed	2630	4057	1509
Criterion for observation	>2sigma(I)	>2sigma(I)	>2sigma(I)
Completeness to theta	92.4 % to 26.37°	99.9 % to 24.11°	99.9 % to 30.51
Absorption correction	None	Semi-empirical from equivalents	Semi-empirical from equivalents
Max. and min. transmission		0.9684 and 0.9282	0.9923 and 0.8766
Data / restraints / parameters	3004 / 1 / 433	8641 / 94 / 629	1947 / 1 / 154
Goodness-of-fit on F^2	1.039	0.806	1.006
Final R indices [I>2sigma(I)]	R1 = 0.0771 wR2 = 0.2091	R1 = 0.0528 wR2 = 0.1078	R1 = 0.0457 wR2 = 0.1058
R indices (all data)	R1 = 0.0849 wR2 = 0.2171	R1 = 0.1300 wR2 = 0.1218	R1 = 0.0603 wR2 = 0.1109
Absolute structure parameter		0.13(8)	
Largest diff. peak and hole [$e.Å^{-3}$]	0.369 and -0.382	0.584 and -0.302	0.190 and -0.162

Name, Nr	**pa301009**	**ss150110**	**ss111009**
Empirical formula	$C_{11}H_{11}IN_2$	$C_{11}H_{12}Br_2N_2O$	$C_{29}H_{22}N_2O_2$
Formula weight	298.12	348.05	430.49
Crystal system	Orthorhombic	Monoclinic	Orthorhombic
Space group	Pbca	C2/c	Pbca
a [Å]	16.4984(4)	14.4906(4)	13.3655(3)
b [Å]	7.40945(16)	10.4674(3)	17.3425(4)
c [Å]	18.6719(6)	17.1762(7)	19.7854(5)
α [°]	90	90	90
β [°]	90	101.806(3)	90
γ [°]	90	90	90
Volume [$Å^3$]	2282.53(10)	2550.16(15)	4586.10(18)
Z	8	8	8
Density (calculated) [Mg/m^3]	1.735	1.813	1.247
Absorption coefficient [mm^{-1}]	2.770	6.339	0.079
F(000)	1152	1360	1808
Crystal size [mm^3]	0.32 x 0.06 x 0.02	0.17 x 0.06 x 0.04	0.43 x 0.33 x 0.14
Crystal description	colourless needle	colourless block	colourless prism
Theta range for data collection [°]	2.51 to 29.13	2.42 to 28.28	2.82 to 27.10
Index ranges	-19<=h<=22 -9<=k<=10 -25<=l<=22	-19<=h<=19 -13<=k<=13 -22<=l<=22	-17<=h<=17 -14<=k<=23 -26<=l<=16
Reflections collected	11561	14089	19356
Independent reflections	3066 [R(int) = 0.0554]	3149 [R(int) = 0.0496]	5050 [R(int) = 0.0302]
Reflections observed	1841	1918	2984
Criterion for observation	>2sigma(I)	>2sigma(I)	>2sigma(I)
Completeness to theta	99.9 % to 29.13°	100.0 % to 28.28°	99.9 % to 28.28°
Absorption correction	Semi-empirical from equivalents	Semi-empirical from equivalents	Semi-empirical from equivalents
Max. and min. transmission	0.9467 and 0.8378	0.7856 and 0.7238	0.9891 and 0.9358
Data / restraints / parameters	3066 / 0 / 128	3149 / 0 / 146	5679 / 0 / 298
Goodness-of-fit on F^2	0.915	0.822	0.950
Final R indices [I>2sigma(I)]	R1 = 0.0413 wR2 = 0.0893	R1 = 0.0325 wR2 = 0.0485	R1 = 0.0573 wR2 = 0.1491
R indices (all data)	R1 = 0.0826 wR2 = 0.0991	R1 = 0.0746 wR2 = 0.0526	R1 = 0.1183 wR2 = 0.1671
Largest diff. peak and hole [$e.Å^{-3}$]	0.950 and -0.646	0.717 and -0.390	0.553 and -0.155

8. Literature

[1] N. Kresge, R. D. Simoni, R. L. Hill, *J. Biol. Chem.* **2009**, *284*, e23.
[2] R. R. Sinden, *Nature* **2005**, *437*, 1097.
[3] A. Rich, S. Zhang, *Nat. Rev. Genet.* **2003**, *4*, 566.
[4] A. Herbert, A. Rich, *J. Biol. Chem.* **1996**, *271*, 11595.
[5] K. Tomita, T. Hakoshima, K. Inubushi, S. Kunisawa, H. Ohishi, G. A. v. d. Marel, J. H. v. Boom, A. H.-J. Wang, A. Rich, *J. Mol. Graphics* **1989**, *7*, 71.
[6] A. Rich, A. Nordheim, A. H.-J. Wang, *Annu. Rev. Biochem.* **1984**, *53*, 791.
[7] E. M. Lafer, A. Möller, A. Nordheim, B. D. Stollar, A. Rich, *Proc. Natl. Acad. Sci. USA* **1981**, *78*, 3546.
[8] A. Nordheim, M. L. Pardue, E. M. Lafer, A. Möller, B. D. Stollar, A. Rich, *Nature* **1981**, *294*, 417.
[9] A. H. J. Wang, G. J. Quigley, F. J. Kolpak, J. L. Crawford, J. H. van Boom, G. van der Marel, A. Rich, *Nature* **1979**, *282*, 680.
[10] M. Balaz, K. Bitsch-Jensen, A. Mammana, G. A. Ellestad, K. Nakanishi, N. Berova, *Pure Appl. Chem.* **2007**, *79*, 801.
[11] M. Balaz, M. De Napoli, A. E. Holmes, A. Mammana, K. Nakanishi, N. Berova, R. Purrello, *Angew. Chem. Int. Ed.* **2005**, *44*, 4006.
[12] L. Pauling, R. B. Corey, *Proc. Natl. Acad. Sci. USA* **1953**, *39*, 84.
[13] A. Schneider, *Jahresber. Oberhess. Gesells. Nat. Heilkde. Gießen* **1873**, *14*, 69.
[14] H. M. Berman, W. K. Olson, D. L. Beveridge, J. Westbrook, A. Gelbin, T. Demeny, S.-H. Hsieh, A. R. Srinivasan, B. Schneider, *Biophys. J.* **1992**, *63*, 751.
[15] E. van Beneden, *Arch. Biol.* **1883**, *4*, 265.
[16] J. D. Dunitz, *Angew. Chem. Int. Ed.* **2001**, *40*, 4167.
[17] D. Eisenberg, *Proc. Natl. Acad. Sci. USA* **2003**, *100*, 11207.
[18] R. E. Franklin, R. G. Gosling, *Nature* **1953**, *172*, 156.
[19] J. D. Watson, F. H. C. Crick, *Nature* **1953**, *171*, 737.
[20] G. M. T. Cheetham, T. A. Steitz, *Curr. Opin. Struct. Biol.* **2000**, *10*, 117.
[21] S. Neidle, *Nat. Prod. Rep.* **2001**, *18*, 291.
[22] K. H. Reddy, *J. Indian Chem. Soc.* **2003**, *80*, 69.
[23] D. Voet, J. G. Voet, *Biochemistry*, 2nd ed., **1995**.
[24] L. Stryer, *Biochemistry*, 4th revised ed., **1996**.
[25] J. C. Venter, M. D. Adams, E. W. Myers, P. W. Li, R. J. Mural, G. G. Sutton, H. O. Smith, M. Yandell, C. A. Evans, R. A. Holt, J. D. Gocayne, P. Amanatides, R. M. Ballew, D. H. Huson, J. R. Wortman, Q. Zhang, C. D. Kodira, X. Q. H. Zheng, L. Chen, M. Skupski, G. Subramanian, P. D. Thomas, J. H. Zhang, G. L. G. Miklos, C. Nelson, S. Broder, A. G. Clark, C. Nadeau, V. A. McKusick, N. Zinder, A. J. Levine, R. J. Roberts, M. Simon, C. Slayman, M. Hunkapiller, R. Bolanos, A. Delcher, I. Dew, D. Fasulo, M. Flanigan, L. Florea, A. Halpern, S. Hannenhalli, S. Kravitz, S. Levy, C. Mobarry, K. Reinert, K. Remington, J. Abu-Threideh, E. Beasley, K. Biddick, V. Bonazzi, R. Brandon, M. Cargill, I. Chandramouliswaran, R. Charlab, K. Chaturvedi, Z. M. Deng, V. Di Francesco, P. Dunn, K. Eilbeck, C. Evangelista, A. E. Gabrielian, W. Gan, W. M. Ge, F. C. Gong, Z. P. Gu, P. Guan, T. J. Heiman, M. E. Higgins, R. R. Ji, Z. X. Ke, K. A. Ketchum, Z. W. Lai, Y. D. Lei, Z. Y. Li, J. Y. Li, Y. Liang, X. Y. Lin, F. Lu, G. V. Merkulov, N. Milshina, H. M. Moore, A. K. Naik, V. A. Narayan, B. Neelam, D. Nusskern, D. B. Rusch, S. Salzberg, W. Shao, B. X. Shue, J. T. Sun, Z. Y. Wang, A. H. Wang, X. Wang, J. Wang, M. H. Wei, R. Wides, C. L. Xiao, C. H. Yan, et al., *Science* **2001**, *291*, 1304.
[26] A. Bacolla, R. D. Wells, *Mol. Carcinogen.* **2009**, *48*, 273.
[27] P. W. Davis, R. W. Adamiak, I. Tinoco Jr., *Biopolymers* **1990**, *29*, 109.
[28] Y. A. Shin, J. J. Butzow, L. D. Sinsel, P. Clark, R. P. Pillai, W. C. Johnson, G. L. Eichhorn, *Biopolymers* **1988**, *27*, 1415.
[29] R. D. Wells, *Trends Biochem. Sci.* **2007**, *32*, 271.
[30] S. C. Ha, K. Lowenhaupt, A. Rich, Y. G. Kim, K. K. Kim, *Nature* **2005**, *437*, 1183.
[31] S. Rothenburg, F. Koch-Nolte, A. Rich, F. Haag, *Proc. Natl. Acad. Sci. USA* **2001**, *98*, 8985.
[32] A. C. G. Hotze, N. J. Hodges, R. E. Hayden, C. Sanchez-Cano, C. Paines, N. Male, M. K. Tse, C. M. Bunce, J. K. Chipman, M. J. Hannon, *Chem. Biol.* **2008**, *15*, 1258.
[33] M. J. Hannon, V. Moreno, M. J. Prieto, E. Moldrheim, E. Sletten, I. Meistermann, C. J. Isaac, K. J. Sanders, A. Rodger, *Angew. Chem.* **2001**, *113*, 904.

[34] A. Rodger, K. J. Sanders, M. J. Hannon, I. Meistermann, A. Parkinson, D. S. Vidler, I. S. Haworth, *Chirality* **2000**, *12*, 221.
[35] B. Rosenberg, L. VanCamp, T. Krigas, Research Corp., USA, *US4177263*, **1979**, pp. 4.
[36] B. Spingler, D. A. Whittington, S. J. Lippard, *Inorg. Chem.* **2001**, *40*, 5596.
[37] B. Spingler, D. A. Whittington, S. J. Lippard, *J. Inorg. Biochem.* **2001**, *86*, 440.
[38] E. Crescenzi, L. Varriale, M. Iovino, A. Chiaviello, B. M. Veneziani, G. Palumbo, *Mol. Cancer Ther.* **2004**, *3*, 537.
[39] T. P. Silverstein, *J. Chem. Educ.* **2008**, *85*, 1192.
[40] F. Barcelo, M. Ortiz-Lombardia, J. Portugal, *Biochim. Biophys. Acta* **2001**, *1519*, 175.
[41] F. G. Albert, T. T. Eckdahl, D. J. Fitzgerald, J. N. Anderson, *Biochemistry* **1999**, *38*, 10135.
[42] A. K. Eggleston, N. A. Rahim, S. C. Kowalczykowski, *Nucleic Acids Res.* **1996**, *24*, 1179.
[43] J. M. C. A. Kerckhoffs, J. C. Peberdy, I. Meistermann, L. J. Childs, C. J. Isaac, C. R. Pearmund, V. Reudegger, S. Khalid, N. W. Alcock, M. J. Hannon, A. Rodger, *Dalton Trans.* **2007**, 734.
[44] A. Oleksy, A. G. Blanco, R. Boer, I. Uson, J. Aymami, A. Rodger, M. J. Hannon, M. Coll, *Angew. Chem. Int. Edit.* **2006**, *45*, 1227.
[45] J. B. Chaires, *Biopolymers* **1997**, *44*, 201.
[46] J. A. Subirana, N. G. A. Abrescia, *Biophys. Chem.* **2000**, *86*, 179.
[47] D. S. Daniels, T. T. Woo, K. X. Luu, D. M. Noll, N. D. Clarke, A. E. Pegg, J. A. Tainer, *Nat. Struct. Mol. Biol.* **2004**, *11*, 714.
[48] R. S. Edayathumangalam, P. Weyermann, J. M. Gottesfeld, P. B. Dervan, K. Luger, *Proc. Natl. Acad. Sci. USA* **2004**, *101*, 6864.
[49] I. Meistermann, V. Moreno, M. J. Prieto, E. Moldrheim, E. Sletten, S. Khalid, P. M. Rodger, J. C. Peberdy, C. J. Isaac, A. Rodger, M. J. Hannon, *Proc. Natl. Acad. Sci. USA* **2002**, *99*, 5069.
[50] F. Tuna, J. Hamblin, A. Jackson, G. Clarkson, N. W. Alcock, M. J. Hannon, *Dalton Trans.* **2003**, 2141.
[51] S. C. Jain, H. M. Sobell, *J. Biomol. Struct. Dyn.* **1984**, *1*, 1161.
[52] S. C. Jain, H. M. Sobell, *J. Biomol. Struct. Dyn.* **1984**, *1*, 1179.
[53] M. K. Pal, J. K. Ghosh, *Spectrochim. Acta A* **1995**, *51*, 489.
[54] S. Rothenburg, F. Koch-Nolte, F. Haag, *Immunol. Rev.* **2001**, *184*, 286.
[55] R. E. Dickerson, H. R. Drew, B. N. Conner, R. M. Wing, A. V. Fratini, M. L. Kopka, *Science* **1982**, *216*, 475.
[56] H. Li, J. Xiao, J. M. Li, L. Lu, S. Feng, P. Dröge, *Nucleic Acids Res.* **2009**, *37*, 2737.
[57] C. Morrison, E. Wagner, *Nucleic Acids Res.* **1996**, *24*, 2053.
[58] R. Chattopadhyaya, S. Ikuta, K. Grzeskowiak, R. E. Dickerson, *Nature* **1988**, *334*, 175.
[59] F. M. Pohl, T. M. Jovin, *J. Mol. Biol.* **1972**, *67*, 375.
[60] R. Wing, H. Drew, T. Takano, C. Broka, S. Tanaka, K. Itakura, R. E. Dickerson, *Nature* **1980**, *287*, 755.
[61] R. R. Sinden, *DNA: Structure and Function*, Academic Press, San Diego, **1994**.
[62] P. S. Ho, B. H. M. Mooers, *Biopolymers* **1997**, *44*, 65.
[63] R. E. Dickerson, *Methods Enzymol.* **1992**, *211*, 67.
[64] B. H. Johnston, *Methods Enzymol.* **1992**, *211*, 127.
[65] T. M. Jovin, L. P. Mcintosh, D. J. Arndt-Jovin, D. A. Zarling, M. Robert-Nicoud, J. H. van de Sande, K. F. Jorgenson, F. Eckstein, *J. Biomol. Struct. Dyn.* **1983**, *1*, 21.
[66] A. Moller, A. Nordheim, S. A. Kozlowski, D. J. Patel, A. Rich, *Biochemistry* **1984**, *23*, 54.
[67] M. Behe, G. Felsenfeld, *Proc. Natl. Acad. Sci. USA* **1981**, *78*, 1619.
[68] D. B. Tippin, B. Ramakrishnan, M. Sundaralingam, *J. Mol. Biol.* **1997**, *270*, 247.
[69] O. Mauffret, C. El Amri, F. Santamaria, G. Tevanian, B. Rayner, S. Fermandjian, *Nucleic Acids Res.* **2000**, *28*, 4403.
[70] D. Bancroft, L. D. Williams, A. Rich, M. Egli, *Biochemistry* **1994**, *33*, 1073.
[71] R. V. Gessner, G. J. Quigley, A. H. J. Wang, G. A. van der Marel, J. H. van Boom, A. Rich, *Biochemistry* **1985**, *24*, 237.
[72] L. J. Peck, A. Nordheim, A. Rich, J. C. Wang, *Proc. Natl. Acad. Sci. USA* **1982**, *79*, 4560.
[73] L. F. Liu, J. C. Wang, *Proc. Natl. Acad. Sci. USA* **1987**, *84*, 7024.
[74] M. A. Fuertes, V. Cepeda, C. Alonso, J. M. Perez, *Chem. Rev.* **2006**, *106*, 2045.
[75] G. P. Schroth, P. J. Chou, P. S. Ho, *J. Biol. Chem.* **1992**, *267*, 11846.
[76] M. Steinmetz, D. Stephan, K. F. Lindahl, *Cell* **1986**, *44*, 895.
[77] A. Weinreb, D. R. Katzenberg, G. L. Gilmore, B. K. Birshtein, *Proc. Natl. Acad. Sci. USA* **1988**, *85*, 529.
[78] G. Wang, L. A. Christensen, K. M. Vasquez, *Proc. Natl. Acad. Sci. USA* **2006**, *103*, 2677.
[79] E. B. Kmiec, W. K. Holloman, *Cell* **1986**, *44*, 545.

[80] K. Nakanishi, N. Berova, R. W. Woody, *Circular Dichroism: Principles and Applications*, **1994**.
[81] S. C. Harvey, *Biophys. J.* **1983**, *41*, A159.
[82] W. Zacharias, A. Jaworski, J. E. Larson, R. D. Wells, *Proc. Natl. Acad. Sci. USA* **1988**, *85*, 7069.
[83] B. Wittig, T. Dorbic, A. Rich, *Proc. Natl. Acad. Sci. USA* **1991**, *88*, 2259.
[84] D. J. Patel, S. A. Kozlowski, A. Nordheim, A. Rich, *Proc. Natl. Acad. Sci. USA* **1982**, *79*, 1413.
[85] W. Zacharias, J. E. Larson, J. Klysik, S. M. Stirdivant, R. D. Wells, *J. Biol. Chem.* **1982**, *257*, 2775.
[86] S. Wölfl, C. Martinez, A. Rich, J. A. Majzoub, *Proc. Natl. Acad. Sci. USA* **1996**, *93*, 3664.
[87] G. Wang, K. M. Vasquez, *Front. Biosci.* **2007**, *12*, 4424.
[88] R. F. Pasternack, E. J. Gibbs, J. J. Villafranca, *Biochemistry* **1983**, *22*, 5409.
[89] R. F. Pasternack, E. J. Gibbs, A. Gaudemer, A. Antebi, S. Bassner, L. Depoy, D. H. Turner, A. Williams, F. Laplace, M. H. Lansard, C. Merienne, M. Perree-Fauvet, *J. Am. Chem. Soc.* **1985**, *107*, 8179.
[90] R. F. Pasternack, D. Sidney, P. A. Hunt, E. A. Snowden, E. J. Gibbs, *Nucleic Acids Res.* **1986**, *14*, 3927.
[91] M. A. Sari, J. P. Battioni, D. Mansuy, J. B. Le Pecq, *Biochem. Biophys. Res. Commun.* **1986**, *141*, 643.
[92] K. G. Ford, L. H. Pearl, S. Neidle, *Nucleic Acids Res.* **1987**, *15*, 6553.
[93] L. G. Marzilli, *New J. Chem.* **1990**, *14*, 409.
[94] M. A. Sari, J. P. Battioni, D. Dupré, D. Mansuy, J. B. Le Pecq, *Biochemistry* **1990**, *29*, 4205.
[95] R. F. Pasternack, E. J. Gibbs, in *Met. Ions Biol. Syst., Vol. 33* (Eds.: A. Sigel, H. Sigel), **1996**, pp. 367.
[96] W. J. Jin, Y. S. Wei, C. S. Liu, G. L. Shen, R. Q. Yu, *Spectrochim. Acta A* **1997**, *53*, 2701.
[97] R. F. Pasternack, M. Caccam, B. Keogh, T. A. Stephenson, A. P. Williams, E. J. Gibbs, *J. Am. Chem. Soc.* **1991**, *113*, 6835.
[98] M. Bennett, A. Krah, F. Wien, E. Garman, R. Mckenna, M. Sanderson, S. Neidle, *Proc. Natl. Acad. Sci. USA* **2000**, *97*, 9476.
[99] L. A. Lipscomb, F. X. Zhou, S. R. Presnell, R. J. Woo, M. E. Peek, R. R. Plaskon, L. D. Williams, *Biochemistry* **1996**, *35*, 2818.
[100] R. T. Wheelhouse, L. H. Hurley, Board of Regents, the University of Texas System, USA, *WO9833503A1*, **1998**, pp. 136.
[101] D. F. Shi, R. T. Wheelhouse, D. Y. Sun, L. H. Hurley, *J. Med. Chem.* **2001**, *44*, 4509.
[102] Y. H. Du, J. Huang, X. C. Weng, X. Zhou, *Curr. Med. Chem.* **2010**, *17*, 173.
[103] B. Gatto, M. Palumbo, C. Sissi, *Curr. Med. Chem.* **2009**, *16*, 1248.
[104] D. P. N. Goncalves, S. Ladame, S. Balasubramanian, J. K. M. Sanders, *Org. Biomol. Chem.* **2006**, *4*, 3337.
[105] J. A. Kwon, A. Rich, *Proc. Natl. Acad. Sci. USA* **2005**, *102*, 12759.
[106] Y.-G. Kim, M. Muralinath, T. Brandt, M. Pearcy, K. Hauns, K. Lowenhaupt, B. L. Jacobs, A. Rich, *Proc. Natl. Acad. Sci. USA* **2003**, *100*, 6974.
[107] D. B. Oh, Y. G. Kim, A. Rich, *Proc. Natl. Acad. Sci. USA* **2002**, *99*, 16666.
[108] B. Spingler, F. Zobi, P. M. Antoni, A. Medina-Molner, R. Alberto, *Chimia* **2005**, *59*, 826.
[109] Y. Qu, A. Harris, A. Hegmans, A. Petz, P. Kabolizadeh, H. Penazova, N. Farrell, *J. Inorg. Biochem.* **2004**, *98*, 1591.
[110] H. Zhang, G. A. van der Marel, J. H. van Boom, A. H. J. Wang, *Biopolymers* **1992**, *32*, 1559.
[111] R. F. Pasternack, R. A. Brigandi, M. J. Abrams, A. P. Williams, E. J. Gibbs, *Inorg. Chem.* **1990**, *29*, 4483.
[112] H.-P. Yuan, L. Thomas, L. K. Woo, *Inorg. Chem.* **1996**, *35*, 2808.
[113] E. Alessio, M. Macchi, S. L. Heath, L. G. Marzilli, *Inorg. Chem.* **1997**, *36*, 5614.
[114] T. Gianferrara, I. Bratsos, E. Iengo, B. Milani, A. Ostric, C. Spagnul, E. Zangrando, E. Alessio, *Dalton Trans.* **2009**, 10742.
[115] E. Iengo, E. Zangrando, E. Alessio, *Eur. J. Inorg. Chem.* **2003**, 2371.
[116] C. V. K. Sharma, G. A. Broker, G. J. Szulczewski, R. D. Rogers, *Chem. Commun.* **2000**, 1023.
[117] J. S. Lindsey, I. C. Schreiman, H. C. Hsu, P. C. Kearney, A. M. Marguerettaz, *J. Org. Chem.* **1987**, *52*, 827.
[118] P. D. Rao, S. Dhanalekshmi, B. J. Littler, J. S. Lindsey, *J. Org. Chem.* **2000**, *65*, 7323.
[119] E. B. Fleischer, A. M. Shachter, *Inorg. Chem.* **1991**, *30*, 3763.
[120] D. W. Dixon, G. M. Pu, H. Wojtowicz, *J. Chromatogr. A* **1998**, *802*, 367.
[121] D. Z. Fan, M. Taniguchi, Z. Yao, S. Dhanalekshmi, J. S. Lindsey, *Tetrahedron* **2005**, *61*, 10291.
[122] K. D. Stewart, T. A. Gray, *J. Phys. Org. Chem.* **1992**, *5*, 461.
[123] B. Spingler, P. M. Antoni, *Chem. Eur. J.* **2007**, *13*, 6617.
[124] J. Novy, M. Urbanova, *Biopolymers* **2007**, *85*, 349.
[125] J. K. Barton, Columbia University, USA, *US4721699*, **1986**, pp. 101.
[126] A. Onoda, M. Igarashi, S. Naganawa, K. Sasaki, S. Ariyasu, T. Yamamura, *Bull. Chem. Soc. Jpn.* **2009**, *82*, 1280.

[127] G. Proni, G. Pescitelli, X. F. Huang, K. Nakanishi, N. Berova, *J. Am. Chem. Soc.* **2003**, *125*, 12914.
[128] S. G. Dimagno, V. S. Y. Lin, M. J. Therien, *J. Org. Chem.* **1993**, *58*, 5983.
[129] J. A. Strickland, L. G. Marzilli, W. D. Wilson, G. Zon, *Inorg. Chem.* **1989**, *28*, 4191.
[130] S. Matile, N. Berova, K. Nakanishi, J. Fleischhauer, R. W. Woody, *J. Am. Chem. Soc.* **1996**, *118*, 5198.
[131] A. Mammana, T. Asakawa, K. Bitsch-Jensen, A. Wolfe, S. Chaturantabut, Y. Otani, X. X. Li, Z. M. Li, K. Nakanishi, M. Balaz, G. A. Ellestad, N. Berova, *Bioorg. Med. Chem.* **2008**, *16*, 6544.
[132] H. M. Ma, X. Chen, N. Zhang, Y. Y. Han, D. Wu, B. Du, Q. Wei, *Spectrochim. Acta A* **2009**, *72*, 465.
[133] R. F. Pasternack, L. Francesconi, D. Raff, E. Spiro, *Inorg. Chem.* **1973**, *12*, 2606.
[134] M. Goto, T. Matsumoto, M. Sumimoto, H. Kurosaki, *Bull. Chem. Soc. Jpn.* **2000**, *73*, 97.
[135] T. D. McGregor, W. Bousfield, Y. Qu, N. Farrell, *J. Inorg. Biochem.* **2002**, *91*, 212.
[136] J. Liu, H. Zhang, C. H. Chen, H. Deng, T. B. Lu, L. N. Ji, *Dalton Trans.* **2003**, 114.
[137] S. Ramakrishnan, M. Palaniandavar, *Dalton Trans.* **2008**, 3866.
[138] J. A. Strickland, D. L. Banville, W. D. Wilson, L. G. Marzilli, *Inorg. Chem.* **1987**, *26*, 3398.
[139] R. F. Pasternack, E. J. Gibbs, J. J. Villafranca, *Biochemistry* **1983**, *22*, 2406.
[140] G. Dougherty, R. F. Pasternack, *Inorg. Chim. Acta* **1992**, *195*, 95.
[141] S. Geremia, L. Di Costanzo, G. Nardin, L. Randaccio, R. Purrello, D. Sciotto, R. Lauceri, F. Pichierri, *Inorg. Chem.* **2004**, *43*, 7579.
[142] A. D'Urso, A. Mammana, M. Balaz, A. E. Holmes, N. Berova, R. Lauceri, R. Purrello, *J. Am. Chem. Soc.* **2009**, *131*, 2046.
[143] M. Balaz, A. E. Holmes, M. Benedetti, P. C. Rodriguez, N. Berova, K. Nakanishi, G. Proni, *J. Am. Chem. Soc.* **2005**, *127*, 4172.
[144] F. C. Skrobot, I. L. V. Rosa, A. P. A. Marques, P. R. Martins, J. Rocha, A. A. Valente, Y. Iamamoto, *J. Mol. Catal. A Chem.* **2005**, *237*, 86.
[145] L. G. Marzilli, G. Petho, M. F. Lin, M. S. Kim, D. W. Dixon, *J. Am. Chem. Soc.* **1992**, *114*, 7575.
[146] A. D. Adler, F. R. Longo, V. Varadi, in *Inorg. Synth., Vol. 16* (Ed.: F. Basolo), **1976**, pp. 213.
[147] A. D. Adler, F. R. Longo, J. D. Finarelli, J. Goldmacher, J. Assour, L. Korsakoff, *J. Org. Chem.* **1967**, *32*, 476.
[148] J. S. Lindsey, *Acc. Chem. Res.* **2010**, *43*, 300.
[149] D. K. Dogutan, M. Ptaszek, J. S. Lindsey, *J. Org. Chem.* **2008**, *73*, 6187.
[150] D. K. Dogutan, J. S. Lindsey, *J. Org. Chem.* **2008**, *73*, 6728.
[151] A. Z. Muresan, P. Thamyongkit, J. R. Diers, D. Holten, J. S. Lindsey, D. F. Bocian, *J. Org. Chem.* **2008**, *73*, 6947.
[152] J. A. Raskatov, A. L. Thompson, J. M. Brown, *Tetrahedron: Asymmetry* **2010**, *21*, 1737.
[153] H. U. Blaser, F. Spindler, A. Studer, *Appl. Catal. A: Gen.* **2001**, *221*, 119.
[154] C. G. Frost, P. Mendonca, *Tetrahedron: Asymmetry* **1999**, *10*, 1831.
[155] J. Fan, J. A. Whiteford, B. Olenyuk, M. D. Levin, P. J. Stang, E. B. Fleischer, *J. Am. Chem. Soc.* **1999**, *121*, 2741.
[156] S. C. Dhara, *Indian J. Chem.* **1970**, *8*, 193.
[157] P. Ruiz-Sanchez, C. König, S. Ferrari, R. Alberto, *J. Biol. Inorg. Chem.* **2011**, *16*, 33.
[158] J. B. Mangrum, N. P. Farrell, *Chem. Commun.* **2010**, *46*, 6640.
[159] P. Ruiz-Sanchez, University of Zürich (Zürich), **2009**.
[160] F. S. Mackay, N. J. Farrer, L. Salassa, H. C. Tai, R. J. Deeth, S. A. Moggach, P. A. Wood, S. Parsons, P. J. Sadler, *Dalton Trans.* **2009**, 2315.
[161] L. Yang, F. L. Wimmer, S. Wimmer, J. X. Zhao, P. S. Braterman, *J. Organomet. Chem.* **1996**, *525*, 1.
[162] S. S. Kamath, S. Shukla, T. S. Srivastava, *Bull. Chem. Soc. Jpn.* **1991**, *64*, 1351.
[163] K. Takahashi, T. Nihira, *Bull. Chem. Soc. Jpn.* **1992**, *65*, 1855.
[164] S. B. Kunze, R. Alberto, H. H. Knight Castro, S. Mundwiler, University Zürich, Switz., *WO2005068483*, **2005**, pp. 38.
[165] S. Ghosh, S. R. Batten, D. R. Turner, P. S. Mukherjee, *Organometallics* **2007**, *26*, 3252.
[166] S. K. Schneider, P. Roembke, G. R. Julius, H. G. Raubenheimer, W. A. Herrmann, *Adv. Synth. Catal.* **2006**, *348*, 1862.
[167] D. Lahaye, K. Muthukumaran, C. H. Hung, D. Gryko, J. S. Reboucas, I. Spasojevic, I. Batinic-Haberle, J. S. Lindsey, *Bioorg. Med. Chem.* **2007**, *15*, 7066.
[168] C. Lottner, K. C. Bart, G. Bernhardt, H. Brunner, *J. Med. Chem.* **2002**, *45*, 2079.
[169] D. Gryko, J. S. Lindsey, *J. Org. Chem.* **2000**, *65*, 2249.
[170] B. J. Littler, M. A. Miller, C.-H. Hung, R. W. Wagner, D. F. O'Shea, P. D. Boyle, J. S. Lindsey, *J. Org. Chem.* **1999**, *64*, 1391.

[171] N. Fujita, Y. Sakamoto, M. Shirakawa, M. Ojima, A. Fujii, M. Ozaki, S. Shinkai, *J. Am. Chem. Soc.* **2007**, *129*, 4134.
[172] W. W. Porter, T. P. Vaid, A. L. Rheingold, *J. Am. Chem. Soc.* **2005**, *127*, 16559.
[173] M. Fujita, M. Tominaga, A. Hori, B. Therrien, *Acc. Chem. Res.* **2005**, *38*, 369.
[174] M. Fujita, O. Sasaki, T. Mitsuhashi, T. Fujita, J. Yazaki, K. Yamaguchi, K. Ogura, *Chem. Commun.* **1996**, 1535.
[175] M. Fujita, J. Yazaki, K. Ogura, *J. Am. Chem. Soc.* **1990**, *112*, 5645.
[176] Y.-F. Han, Y.-J. Lin, W.-G. Jia, G.-X. Jin, *Organometallics* **2008**, *27*, 4088.
[177] J. Z. Deng, D. V. Paone, A. T. Ginnetti, H. Kurihara, S. D. Dreher, S. A. Weissman, S. R. Stauffer, C. S. Burgey, *Org. Lett.* **2009**, *11*, 345.
[178] A. Zapf, R. Jackstell, F. Rataboul, T. Riermeier, A. Monsees, C. Fuhrmann, N. Shaikh, U. Dingerdissen, M. Beller, *Chem. Commun.* **2004**, 38.
[179] T. Le Diguarher, A.-M. Chollet, M. Bertrand, P. Hennig, E. Raimbaud, M. Sabatini, N. Guilbaud, A. Pierre, G. C. Tucker, P. Casara, *J. Med. Chem.* **2003**, *46*, 3840.
[180] M. Yoshizawa, M. Nagao, K. Kumazawa, M. Fujita, *J. Organomet. Chem.* **2005**, *690*, 5383.
[181] P. M. Antoni, S. Gupta, B. Spingler, unpublished results.
[182] J. F. Mao, Y. M. Zhang, J. H. Zhu, C. L. Zhang, Z. J. Guo, *Chem. Commun.* **2009**, 908.
[183] L. Wu, L. Yang, J. Huang, L. X. Zhang, X. C. Weng, X. L. Zhang, C. Shen, X. Zhou, C. Y. Zheng, *Chem. Biodivers.* **2009**, *6*, 1066.
[184] Q. B. Lu, *J. Med. Chem.* **2007**, *50*, 2601.
[185] E. Crescenzi, A. Chiaviello, G. Canti, E. Reddi, B. M. Veneziani, G. Palumbo, *Mol. Cancer Ther.* **2006**, *5*, 776.
[186] N. J. Farrer, J. A. Woods, V. P. Munk, F. S. Mackay, P. J. Sadler, *Chem. Res. Toxicol.* **2010**, *23*, 413.
[187] B. Michalke, *J. Trace Elem. Med. Biol.* **2010**, *24*, 69.
[188] J. C. Zhang, D. D. Liu, Y. P. Li, J. Sun, L. W. Wang, A. M. Zang, *Mini-Rev. Med. Chem.* **2009**, *9*, 1357.
[189] Sanofi-Aventis, Annual Review
[190] Sanofi-Aventis, Annual Review
[191] M. Y. Nahabedian, R. A. Cohen, M. F. Contino, T. M. Terem, W. H. Wright, M. W. Berns, A. G. Wile, *J. Natl. Cancer Inst.* **1988**, *80*, 739.
[192] R. A. Moorehead, S. G. Armstrong, B. C. Wilson, G. Singh, *Cancer Res.* **1994**, *54*, 2556.
[193] V. V. Vasil'ev, S. M. Borisov, I. V. Golovina, *Opt. Spectrosc.* **2003**, *95*, 29.
[194] R. Luguya, T. J. Jensen, K. M. Smith, M. G. H. Vicente, *Bioorg. Med. Chem.* **2006**, *14*, 5890.
[195] M. F. Zuluaga, N. Lange, *Curr. Med. Chem.* **2008**, *15*, 1655.
[196] G. Guillaume, V. Sarrazy, V. Sol, C. Le Morvan, R. Granet, S. Alves, P. Krausz, *Bioorg. Med. Chem.* **2009**, *17*, 767.
[197] B. Ortel, C. R. Shea, P. Calzavara-Pinton, *Front. Biosci.* **2009**, *14*, 4157.
[198] J. D. Hoeschele, *Dalton Trans.* **2009**, 10648.
[199] F. Arnesano, G. Natile, *Coord. Chem. Rev.* **2009**, *253*, 2070.
[200] S. E. Sherman, D. Gibson, A. H.-J. Wang, S. J. Lippard, *Science* **1985**, *230*, 412.
[201] R. M. Wing, P. Pjura, H. R. Drew, R. E. Dickerson, *EMBO J.* **1984**, *3*, 1201.
[202] S. E. Sherman, S. J. Lippard, *Chem. Rev.* **1987**, *87*, 1153.
[203] J. Reedijk, *Chem. Commun.* **1996**, 801.
[204] Y. Kidani, K. Inagaki, R. Saito, S. Tsukagoshi, *J. Clin. Hematol. Oncol.* **1977**, *7*, 197.
[205] V. Boudny, O. Vrana, F. Gaucheron, V. Kleinwachter, M. Leng, V. Brabec, *Nucleic Acids Res.* **1992**, *20*, 267.
[206] M. A. Graham, G. F. Lockwood, D. Greenslade, S. Brienza, M. Bayssas, E. Gamelin, *Clin. Cancer Res.* **2000**, *6*, 1205.
[207] A. Ibrahim, S. Hirschfeld, M. H. Cohen, D. J. Griebel, G. A. Williams, R. Pazdur, *Oncologist* **2004**, *9*, 8.
[208] S. F. Bellon, S. J. Lippard, *Biophys. Chem.* **1990**, *35*, 179.
[209] L. S. Hollis, A. R. Amundsen, E. W. Stern, *J. Med. Chem.* **1989**, *32*, 128.
[210] A. Eastman, *Pharmacol. Ther.* **1987**, *34*, 155.
[211] J. W. Lee, J. K. Park, S. H. Lee, S. Y. Kim, Y. B. Cho, H. J. Kuh, *Anti-Cancer Drugs* **2006**, *17*, 377.
[212] J. B. Vermorken, *Int. J. Gynecol. Cancer* **2001**, *11*, 21.
[213] J. Welink, B. Pechstein, W. J. F. vanderVijgh, *J. Chromatogr. B* **1996**, *675*, 107.
[214] M. Galanski, M. A. Jakupec, B. K. Keppler, *Curr. Med. Chem.* **2005**, *12*, 2075.
[215] P. Perego, L. Gatti, C. Caserini, R. Supino, D. Colangelo, R. Leone, S. Spinelli, N. Farrell, F. Zunino, *J. Inorg. Biochem.* **1999**, *77*, 59.

[216] I. M. El-Mehasseb, M. Kodaka, T. Okada, T. Tomohiro, K. Okamoto, H. Okuno, *J. Inorg. Biochem.* **2001**, *84*, 157.
[217] Y. Najajreh, J. M. Perez, C. Navarro-Ranninger, D. Gibson, *J. Med. Chem.* **2002**, *45*, 5189.
[218] F. Zak, J. Turanek, A. Kroutil, P. Sova, A. Mistr, A. Poulova, P. Mikolin, Z. Zak, A. Kasna, D. Zaluska, J. Neca, L. Sindlerova, A. Kozubik, *J. Med. Chem.* **2004**, *47*, 761.
[219] B. A. J. Jansen, P. Wielaard, G. V. Kalayda, M. Ferrari, C. Molenaar, H. J. Tanke, J. Brouwer, J. Reedijk, *J. Biol. Inorg. Chem.* **2004**, *9*, 403.
[220] G. V. Kalayda, B. A. J. Jansen, C. Molenaar, P. Wielaard, H. J. Tanke, J. Reedijk, *J. Biol. Inorg. Chem.* **2004**, *9*, 414.
[221] N. Farrell, in *Metal Complexes in Tumor Diagnosis and as Anticancer Agents, Vol. 42* (Eds.: H. Sigel, A. Sigel), Marcel Dekker, **2004**, pp. 251.
[222] M. Gay, A. M. Montana, V. Moreno, M. J. Prieto, J. M. Perez, C. Alonso, *Bioorg. Med. Chem.* **2006**, *14*, 1565.
[223] F. J. Ramos-Lima, A. G. Quiroga, B. Garcia-Serrelde, F. Blanco, A. Carnero, C. Navarro-Ranninger, *J. Med. Chem.* **2007**, *50*, 2194.
[224] G. Marverti, M. Cusumano, A. Ligabue, M. L. Di Pietro, P. A. Vainiglia, A. Ferrari, M. Bergomi, M. S. Moruzzi, C. Frassineti, *J. Inorg. Biochem.* **2008**, *102*, 699.
[225] P. J. He, J. C. Ahn, J. I. Shin, H. J. Hwang, J. W. Kang, S. J. Lee, P. S. Chung, *Oncol. Rep.* **2009**, *21*, 329.
[226] P. J. Bednarski, R. Grunert, M. Zielzki, A. Wellner, F. S. Mackay, P. J. Sadler, *Chem. Biol.* **2006**, *13*, 61.
[227] D. S. Alberts, J. K. Noel, *Anti-Cancer Drugs* **1995**, *6*, 369.
[228] S. Quasthoff, H. P. Hartung, *J. Neurol.* **2002**, *249*, 9.
[229] A. A. Fauser, M. Fellhauer, M. Hoffmann, H. Link, G. Schlimok, R. J. Gralla, *Eur. J. Cancer* **1999**, *35*, 361.
[230] N. Kurihara, T. Kubota, Y. Hoshiya, Y. Otani, N. Ando, K. Kumai, M. Kitajima, *J. Surg. Oncol.* **1996**, *62*, 135.
[231] S. A. Fausti, J. A. Henry, W. J. Helt, D. S. Phillips, R. H. Frey, D. Noffsinger, V. D. Larson, C. G. Fowler, *Ear & Hearing* **1999**, *20*, 497.
[232] H. Lajer, H. Bundgaard, N. H. Secher, H. H. Hansen, K. Kjeldsen, G. Daugaard, *Brit. J. Cancer* **2003**, *89*, 1633.
[233] L. P. Rybak, V. Ramkumar, *Kidney Int.* **2007**, *72*, 931.
[234] S. Budavari, *The Merck index, an encyclopedia of chemicals, drugs, and biologicals*, 11th ed., Merck and Co., Rahway, New Jersey, **1989**.
[235] E. Jerremalm, M. Hedeland, I. Wallin, U. Bondesson, H. Ehrsson, *Pharm. Res.* **2004**, *21*, 891.
[236] E. L. Mamenta, E. E. Poma, W. K. Kaufmann, D. A. Delmastro, H. L. Grady, S. G. Chaney, *Cancer Res.* **1994**, *54*, 3500.
[237] D. Gibson, G. M. Arvanitis, H. M. Berman, *Inorg. Chim. Acta* **1994**, *218*, 11.
[238] H. Brunner, H. Obermeier, *Angew. Chem. Int. Edit.* **1994**, *33*, 2214.
[239] G. Esposito, S. Cauci, F. Fogolari, E. Alessio, M. Scocchi, F. Quadrifoglio, P. Viglino, *Biochemistry* **1992**, *31*, 7094.
[240] R. K. O. Sigel, B. Lippert, *Chem. Commun.* **1999**, 2167.
[241] F. Zobi, B. Spingler, T. Fox, R. Alberto, *Inorg. Chem.* **2003**, *42*, 2818.
[242] M. Trani, F. Cannito, G. Natile, P. A. Marzilli, L. G. Marzilli, *Eur. J. Inorg. Chem.* **2005**, 2826.
[243] E. R. Jamieson, S. J. Lippard, *Chem. Rev.* **1999**, *99*, 2467.
[244] B. Lippert, *Cisplatin: Chemistry and Biochemistry of a Leading Anticancer Drug*, John Wiley & Son Ltd., **1999**.
[245] M. Hagerlof, P. Papsai, C. S. Chow, S. K. C. Elmroth, *J. Biol. Inorg. Chem.* **2006**, *11*, 974.
[246] M. Hagerlof, H. Hedman, S. K. C. Elmroth, *Biochem. Biophys. Res. Commun.* **2007**, *361*, 14.
[247] P. Papsai, A. S. Snygg, J. Aldag, S. K. C. Elmroth, *Dalton Trans.* **2008**, 5225.
[248] M. Hagerlof, P. Papsai, H. K. Hedman, U. Jungwirth, V. Jenei, S. K. C. Elmroth, *J. Biol. Inorg. Chem.* **2008**, *13*, 385.
[249] N. Poklar, D. S. Pilch, S. J. Lippard, E. A. Redding, S. U. Dunham, K. J. Breslauer, *Proc. Natl. Acad. Sci. USA* **1996**, *93*, 7606.
[250] H. Kostrhunova, V. Brabec, *Biochemistry* **2000**, *39*, 12639.
[251] M.-A. Elizondo-Riojas, J. Kozelka, *J. Mol. Biol.* **2001**, *314*, 1227.
[252] J. Malina, J. Kasparkova, G. Natile, V. Brabec, *Chem. Biol.* **2002**, *9*, 629.
[253] V. M. González, M. A. Fuertes, A. Jiménez-Ruíz, C. Alonso, J. M. Pérez, *Mol. Pharmacol.* **1999**, *55*, 770.
[254] Y. Mantri, S. J. Lippard, M. H. Baik, *J. Am. Chem. Soc.* **2007**, *129*, 5023.
[255] B. Wu, P. Dröge, C. A. Davey, *Nat. Chem. Biol.* **2008**, *4*, 110.

[256] P. B. Hopkins, J. T. Millard, J. Woo, M. F. Weidner, J. J. Kirchner, S. T. Sigurdsson, S. Raucher, *Tetrahedron* **1991**, *47*, 2475.
[257] S. F. Bellon, J. H. Coleman, S. J. Lippard, *Biochemistry* **1991**, *30*, 8026.
[258] M. Coll, S. E. Sherman, D. Gibson, S. J. Lippard, A. H. J. Wang, *J. Biomol. Struct. Dyn.* **1990**, *8*, 315.
[259] Y. B. Wu, D. Bhattacharyya, C. L. King, I. Baskerville-Abraham, S. H. Huh, G. Boysen, J. A. Swenberg, B. Temple, S. L. Campbell, S. G. Chaney, *Biochemistry* **2007**, *46*, 6477.
[260] S. Sharma, P. Gong, B. Temple, D. Bhattacharyya, N. V. Dokholyan, S. G. Chaney, *J. Mol. Biol.* **2007**, *373*, 1123.
[261] J. Malina, C. Hofr, L. Maresca, G. Natile, V. Brabec, *Biophys. J.* **2000**, *78*, 2008.
[262] L. G. Marzilli, S. O. Ano, F. P. Intini, G. Natile, *J. Am. Chem. Soc.* **1999**, *121*, 9133.
[263] M. Carlone, F. P. Fanizzi, F. P. Intini, N. Margiotta, L. G. Marzilli, G. Natile, *Inorg. Chem.* **2000**, *39*, 634.
[264] M. Benedetti, J. Malina, J. Kasparkova, V. Brabec, G. Natile, *Environ. Health Persp.* **2002**, *110*, 779.
[265] H. C. Wong, K. Shinozuka, G. Natile, L. G. Marzilli, *Inorg. Chim. Acta* **2000**, *297*, 36.
[266] L. Cerasino, F. P. Intini, J. Kobe, E. de Clercq, G. Natile, *Inorg. Chim. Acta* **2003**, *344*, 174.
[267] M. T. Schütte, P. Schumacher, C. Unger, R. Mülhaupt, F. Kratz, *Inorg. Chim. Acta* **1998**, *267*, 133.
[268] W. H. Ang, E. Daldini, L. Juillerat-Jeanneret, P. J. Dyson, *Inorg. Chem.* **2007**, *46*, 9048.
[269] J. Zlatanova, J. Yaneva, S. H. Leuba, *FASEB J.* **1998**, *12*, 791.
[270] U.-M. Ohndorf, M. A. Rould, Q. He, C. O. Pabo, S. J. Lippard, *Nature* **1999**, *399*, 708.
[271] G. E. Damsma, A. Alt, F. Brueckner, T. Carell, P. Cramer, *Nat. Struct. Mol. Biol.* **2007**, *14*, 1127.
[272] L. D. Mayer, A. S. Janoff, *Mol. Interv.* **2007**, *7*, 216.
[273] J. F. Arambula, J. L. Sessler, M. E. Fountain, W. H. Wei, D. Magda, Z. H. Siddik, *Dalton Trans.* **2009**, 10834.
[274] O. Aronov, A. T. Horowitz, A. Gabizon, D. Gibson, *Bioconjugate Chem.* **2003**, *14*, 563.
[275] O. Aronov, A. T. Horowitz, A. Gabizon, M. A. Fuertes, J. M. Perez, D. Gibson, *Bioconjugate Chem.* **2004**, *15*, 814.
[276] R. R. Allison, C. H. Sibata, *Photodiagn. Photodyn. Ther.* **2010**, *7*, 61.
[277] A. P. Castano, P. Mroz, M. R. Hamblin, *Nat. Rev. Cancer* **2006**, *6*, 535.
[278] D. E. J. G. J. Dolmans, D. Fukumura, R. K. Jain, *Nat. Rev. Cancer* **2003**, *3*, 380.
[279] I. J. MacDonald, T. J. Dougherty, *J. Porphyrins Phthalocyanines* **2001**, *5*, 105.
[280] R. Bonnett, *Chemical Aspects of Photodynamic Therapy, Vol. 1*, Gordon and Breach Science Publishers, Amsterdam, **2000**.
[281] E. Biron, N. Voyer, *Chem. Commun.* **2005**, 4652.
[282] R. Hilf, *J. Bioenerg. Biomembr.* **2007**, *39*, 85.
[283] E. Craver, A. McCrate, M. Nielsen, S. Swavey, *Inorg. Chim. Acta* **2010**, *363*, 453.
[284] J. P. Celli, B. Q. Spring, I. Rizvi, C. L. Evans, K. S. Samkoe, S. Verma, B. W. Pogue, T. Hasan, *Chem. Rev.* **2010**, *110*, 2795.
[285] A. E. O'Connor, W. M. Gallagher, A. T. Byrne, *Photochem. Photobiol.* **2009**, *85*, 1053.
[286] F. S. Mackay, J. A. Woods, P. Heringova, J. Kasparkova, A. M. Pizarro, S. A. Moggach, S. Parsons, V. Brabec, P. J. Sadler, *Proc. Natl. Acad. Sci. USA* **2007**, *104*, 20743.
[287] D. Nowis, M. Makowski, T. Stoklosa, M. Legat, T. Issat, J. Golab, *Acta Biochim. Pol.* **2005**, *52*, 339.
[288] M. Tsutsui, C. P. Hrung, D. Ostfeld, T. S. Srivastava, D. L. Cullen, E. F. Meyer, *J. Am. Chem. Soc.* **1975**, *97*, 3952.
[289] U. Hofstra, R. B. M. Koehorst, T. J. Schaafsma, *Chem. Phys. Lett.* **1986**, *130*, 555.
[290] Y. A. Lee, S. Lee, T. S. Cho, C. Kim, S. W. Han, S. K. Kim, *J. Phys. Chem. B* **2002**, *106*, 11351.
[291] M. Makarska, S. Radzki, J. Legendziewicz, *J. Alloy. Compd.* **2002**, *341*, 233.
[292] O. Raab, *Z. Biol.* **1900**, *39*, 524.
[293] H. von Tappeiner, A. Jesionek, *Münch. Med. Wochenschr.* **1903**, *50*, 2042.
[294] H. Auler, G. Banzer, *Z. Krebsforsch.* **1942**, *53*, 65.
[295] D. S. Rassmussen-Taxdal, G. E. Ward, F. H. J. Figge, *Cancer* **1955**, *8*, 78.
[296] M. Uehara, I. Inokuchi, H. Ikeda, *J. Oral Maxil. Surg.* **2006**, *64*, 390.
[297] Y. Matsumoto, Y. Muro, S. Banno, M. Ohashi, Y. Tamada, *Arch. Dermatol. Res.* **1996**, *289*, 52.
[298] M. Vogeser, M. Schaffer, E. Egeler, U. Spohrer, *Clin. Biochem.* **2005**, *38*, 73.
[299] L. M. Moreira, F. V. dos Santos, J. P. Lyon, M. Maftoum-Costa, C. Pacheco-Soares, N. S. da Silva, *Aust. J. Chem.* **2008**, *61*, 741.
[300] M. Nonaka, H. Ikeda, T. Inokuchi, *Cancer Lett.* **2002**, *184*, 171.
[301] Y. N. Konan, R. Gurny, E. Allemann, *J. Photochem. Photobiol. B* **2002**, *66*, 89.
[302] B. Jin, J. E. Ahn, J. H. Ko, W. Wang, S. W. Han, S. K. Kim, *J. Phys. Chem. B* **2008**, *112*, 15875.

[303] M. Balaz, B. C. Li, J. D. Steinkruger, G. A. Ellestad, K. Nakanishi, N. Berova, *Org. Biomol. Chem.* **2006**, *4*, 1865.
[304] M. J. Lee, G. J. Lee, D. J. Lee, S. K. Kim, J. M. Kim, *Bull. Korean Chem. Soc.* **2005**, *26*, 1728.
[305] N. E. Mukundan, G. Petho, D. W. Dixon, L. G. Marzilli, *Inorg. Chem.* **1995**, *34*, 3677.
[306] S. Gaspard, P. Margaron, C. Tempête, H. T. T. Thu, *J. Photochem. Photobiol. B* **1990**, *4*, 419.
[307] L. O. Klotz, C. Pellieux, K. Briviba, C. Pierlot, J. M. Aubry, H. Sies, *Eur. J. Biochem.* **1999**, *260*, 917.
[308] S. M. Sondhi, N. Singhal, R. P. Verma, S. K. Arora, S. G. Dastidar, *Indian J. Chem.* **2001**, *40B*, 113.
[309] S. Gupta, B. S. Dwarakanath, K. Muralidhar, V. Jain, *Indian J. Exp. Biol.* **2003**, *41*, 33.
[310] N. Aratani, D. Kim, A. Osuka, *Acc. Chem. Res.* **2009**, *42*, 1922.
[311] I. W. Hwang, T. Kamada, T. K. Ahn, D. M. Ko, T. Nakamura, A. Tsuda, A. Osuka, D. Kim, *J. Am. Chem. Soc.* **2004**, *126*, 16187.
[312] A. Bartczak, Y. Namiki, D. J. Qian, J. Miyake, A. Boguta, J. Goc, J. Lukasiewicz, D. Frackowiak, *J. Photochem. Photobiol. A* **2003**, *159*, 259.
[313] Y. Fujii, Y. Tsukahara, Y. Wada, *Bull. Chem. Soc. Jpn.* **2006**, *79*, 561.
[314] S. A. Bejune, A. H. Shelton, D. R. McMillin, *Inorg. Chem.* **2003**, *42*, 8465.
[315] C. Pavani, A. F. Uchoa, C. S. Oliveira, Y. Iamamoto, M. S. Baptista, *Photochem. Photobiol. Sci.* **2009**, *8*, 233.
[316] T. J. Jensen, M. G. H. Vicente, R. Luguya, J. Norton, F. R. Fronczek, K. M. Smith, *J. Photochem. Photobiol. B* **2010**, *100*, 100.
[317] S. Tada-Oikawa, S. Oikawa, J. Hirayama, K. Hirakawa, S. Kawanishi, *Photochem. Photobiol.* **2009**, *85*, 1391.
[318] M. Sibrian-Vazquez, I. V. Nesterova, T. J. Jensen, M. G. H. Vicente, *Bioconjugate Chem.* **2008**, *19*, 705.
[319] G. Canti, A. Nicolin, R. Cubeddu, P. Taroni, G. Bandieramonte, G. Valentini, *Cancer Lett.* **1998**, *125*, 39.
[320] P. Müller, B. Schroder, J. A. Parkinson, N. A. Kratochwil, R. A. Coxall, A. Parkin, S. Parsons, P. J. Sadler, *Angew. Chem. Int. Edit.* **2003**, *42*, 335.
[321] N. J. Farrer, L. Salassa, P. J. Sadler, *Dalton Trans.* **2009**, 10690.
[322] D. Crespy, K. Landfester, U. S. Schubert, A. Schiller, *Chem. Commun.* **2010**, *46*, 6651.
[323] H. Brunner, K. M. Scheller, B. Treittinger, *Inorg. Chim. Acta* **1997**, *264*, 67.
[324] C. Lottner, K. C. Bart, G. Bernhardt, H. Brunner, *J. Med. Chem.* **2002**, *45*, 2064.
[325] K.-C. Bart, G. Bernhardt, H. Brunner, C. Lottner, Zentaris A.-G., Germany; Zentaris GmbH, *WO2003064424*, **2003**, pp. 25.
[326] H. Brunner, K. M. Schellerer, *Inorg. Chim. Acta* **2003**, *350*, 39.
[327] C. Lottner, R. Knuechel, G. Bernhardt, H. Brunner, *Cancer Lett.* **2004**, *203*, 171.
[328] H. Brunner, M. R. Arndt, B. Treittinger, *Inorg. Chim. Acta* **2004**, *357*, 1649.
[329] H. Munakata, H. Imai, S. Nakagawa, A. Osada, Y. Uemori, *Chem. Pharm. Bull.* **2003**, *51*, 614.
[330] R. Song, Y. S. Kim, Y. S. Sohn, *J. Inorg. Biochem.* **2002**, *89*, 83.
[331] R. Song, Y. S. Kim, C. O. Lee, Y. S. Sohn, *Tetrahedron Lett.* **2003**, *44*, 1537.
[332] Y. S. Kim, R. Song, D. H. Kim, M. J. Jun, Y. S. Sohn, *Bioorg. Med. Chem.* **2003**, *11*, 1753.
[333] Y. S. Kim, R. Song, C. O. Lee, Y. S. Sohn, *Bioorg. Med. Chem. Lett.* **2004**, *14*, 2889.
[334] E. Rodriguez-Fernandez, J. L. Manzano, A. Alonso, M. J. Almendral, M. Perez-Andres, A. Orfao, J. J. Criado, *Curr. Med. Chem.* **2009**, *16*, 4314.
[335] B. Steiger, F. C. Anson, *Inorg. Chem.* **1994**, *33*, 5767.
[336] C. Ruzie, M. Krayer, T. Balasubramanian, J. S. Lindsey, *J. Org. Chem.* **2008**, *73*, 5806.
[337] P. Thamyongkit, M. Speckbacher, J. R. Diers, H. L. Kee, C. Kirmaier, D. Holten, D. F. Bocian, J. S. Lindsey, *J. Org. Chem.* **2004**, *69*, 3700.
[338] O. M. Adamov, A. I. Stetsenko, I. B. Pushko, V. G. Pogareva, *Koordinats Khim.* **1990**, *16*, 857.
[339] M. S. Ali, E. Longoria, T. O. Ely, K. H. Whitmire, A. R. Khokhar, *Polyhedron* **2006**, *25*, 2065.
[340] R. K. O. Sigel, B. Lippert, *Chem. Commun.* **1999**, 2167.
[341] H. Okada, H. Imai, Y. Uemori, *Bioorg. Med. Chem.* **2001**, *9*, 3301.
[342] P. Ruiz-Sanchez, S. Mundwiler, B. Spingler, N. R. Buan, J. C. Escalante-Semerena, R. Alberto, *J. Biol. Inorg. Chem.* **2008**, *13*, 335.
[343] HPLC gradients see Chapter 7.8.3.
[344] M. Asanosomeda, S. I. Sato, K. Aoyagi, T. Kitagawa, *J. Phys. Chem.* **1995**, *99*, 13800.
[345] D. Gibson, K. F. Gean, R. Benshoshan, A. Ramu, I. Ringel, J. Katzhendler, *J. Med. Chem.* **1991**, *34*, 414.
[346] J. M. Pérez-Martin, J. M. Requena, D. Craciunescu, M. C. López, C. Alonso, *J. Biol. Chem.* **1993**, *268*, 24774.
[347] T. Mosmann, *J. Immunol. Methods* **1983**, *65*, 55.

[348] T. Gianferrara, A. Bergamo, I. Bratsos, B. Milani, C. Spagnul, G. Sava, E. Alessio, *J. Med. Chem.* **2010**, *53*, 4678.
[349] N. Agorastos, L. Borsig, A. Renard, P. Antoni, G. Viola, B. Spingler, P. Kurz, R. Alberto, *Chem. Eur. J.* **2007**, *13*, 3842.
[350] K. Fujimoto, S. Aizawa, I. Oota, J. Chiba, M. Inouye, *Chem. Eur. J.* **2010**, *16*, 2401.
[351] M. Tabata, A. K. Sarker, E. Nyarko, *J. Inorg. Biochem.* **2003**, *94*, 50.
[352] J. M. Kelly, M. J. Murphy, D. J. McConnell, C. OhUigin, *Nucleic Acids Res.* **1985**, *13*, 167.
[353] J. K. Laha, S. Dhanalekshmi, M. Taniguchi, A. Ambroise, J. S. Lindsey, *Org. Process Res. Dev.* **2003**, *7*, 799.
[354] C.-H. Lee, J. S. Lindsey, *Tetrahedron* **1994**, *50*, 11427.
[355] F. R. Longo, M. G. Finarelli, J. B. Kim, *J. Heterocyclic Chem.* **1969**, *6*, 927.
[356] E. Schlittler, J. Hohl, *Helv. Chim. Acta* **1952**, *35*, 29.
[357] *CrysAlis^{Pro} Software system*; Oxford Diffraction Ltd., vers. 171.32 Oxford, UK, 2007.
[358] A. Altomare, M. C. Burla, M. Camalli, G. L. Cascarano, C. Giacovazzo, A. Guagliardi, A. G. G. Moliterni, G. Polidori, R. Spagna, *J. Appl. Cryst.* **1999**, *32*, 115.
[359] G. M. Sheldrick, *Acta Cryst.* **2008**, *A64*, 112.
[360] A. L. Spek, *J. Appl. Cryst.* **2003**, *36*, 7.
[361] G. M. Sheldrick, *Acta Cryst.* **1990**, *A46*, 467.
[362] S. Sugata, S. Yamanouchi, Y. Matsushima, *Chem. Pharm. Bull.* **1977**, *25*, 884.
[363] D. T. Gryko, M. Tasior, *Tetrahedron Lett.* **2003**, *44*, 3317.
[364] V. Malinovski, L. Tumir, I. Piantanida, M. Zinic, H. J. Schneider, *Eur. J. Org. Chem.* **2002**, 3785.
[365] N. Srinivasan, C. A. Haney, J. S. Lindsey, W. Z. Zhang, B. T. Chait, *J. Porphyrins Phthalocyanines* **1999**, *3*, 283.
[366] B. J. Littler, Y. Ciringh, J. S. Lindsey, *J. Org. Chem.* **1999**, *64*, 2864.
[367] S. Tamaru, L. H. Yu, W. J. Youngblood, K. Muthukumaran, M. Taniguchi, J. S. Lindsey, *J. Org. Chem.* **2004**, *69*, 765.
[368] P. Thamyongkit, J. S. Lindsey, *J. Org. Chem.* **2004**, *69*, 5796.
[369] J. S. Lindsey, S. Tamaru, L. Yu, North Carolina State University, USA, *US2005054858*, **2005**, pp. 23.
[370] R. F. Pasternack, N. Sutin, D. H. Turner, *J. Am. Chem. Soc.* **1976**, *98*, 1908.
[371] E. B. Fleischer, E. I. Choi, P. Hambright, A. Stone, *Inorg. Chem.* **1964**, *3*, 1284.
[372] E. B. Fleischer, *Inorg. Chem.* **1962**, *1*, 493.
[373] D. Li, G. Etemad-Moghadam, S. Cros, C. Auclair, B. Meunier, *J. Med. Chem.* **1991**, *34*, 900.
[374] I. R. Baxendale, C. M. Griffiths-Jones, S. V. Ley, G. K. Tranmer, *Chem. Eur. J.* **2006**, *12*, 4407.
[375] Y. S. Park, E. J. Lee, Y. S. Chun, Y. D. Yoon, K. B. Yoon, *J. Am. Chem. Soc.* **2002**, *124*, 7123.
[376] D. P. Bancroft, C. A. Lepre, S. J. Lippard, *J. Am. Chem. Soc.* **1990**, *112*, 6860.
[377] C. X. Zhang, S. J. Lippard, *Curr. Opin. Chem. Biol.* **2003**, *7*, 481.
[378] T. A. K. Al-Allaf, L. J. Rashan, D. Steinborn, K. Merzweiler, C. Wagner, *Transit. Metal Chem.* **2003**, *28*, 717.
[379] T. Lundbäck, H. Hansson, S. Knapp, R. Ladenstein, T. Härd, *J. Mol. Biol.* **1998**, *276*, 775.
[380] Y. Mikata, M. Yokoyama, K. Mogami, M. Kato, I. Okura, M. Chikira, S. Yano, *Inorg. Chim. Acta* **1998**, *279*, 51.
[381] P. K. Sasmal, S. Saha, R. Majumdar, R. R. Dighe, A. R. Chakravarty, *Inorg. Chem.* **2010**, *49*, 849.
[382] Y. H. He, S. Groleau, R. C. Gaudreault, M. Caron, H. M. Therien, G. Berube, *Bioorg. Med. Chem. Lett.* **1995**, *5*, 2217.
[383] K. R. Barnes, A. Kutikov, S. J. Lippard, *Chem. Biol.* **2004**, *11*, 557.

Curriculum vitae

Philipp Marcel Antoni	Rieterstrasse 79 CH-8002 Zürich Schweiz	antoni@biognosys.ch +41 78 615 8007

born:	10th May 1982, Göttingen, Germany
Family status:	single
Nationality:	deutsch

Academic and Education

University

2006 – 2011 PhD Theses
Inorganic Chemistry Institute, Universität Zürich,
Supervisor: Prof. Dr. R. Alberto, Dr. Bernhard Spingler:
"Metallo – Porphyrins as Anti-Cancer Agents and their Interaction with Different Conformations of DNA"

2003 - 2007 Chemistry (Diploma, Major, Master of Science, Grade 5.2)
Economics (2nd Major)
Inorganic Chemistry Institut, University of Zürich, Switzerland.
Supervisor: Prof. Dr. R. Alberto and Dr. Bernhard Spingler:
"Dinuclear Polypyrazoyl Metal Complexes: Studies on the B – to Z – DNA Transition and the Polymerisation of Ethylene."

2001 - 2003 Chemistry (Diplom)
Economics (Diplom)
Philipps – Universität, Marburg
Vordiplom (4 Semesters)

Extra Curricula

2001 - 2002 Fachverein Chemie, University of Marburg (Student committee)
2003 - 2005 Fachverein Chemie, University of Zürich (Student committee)
2006 - 2007 PhD Representative, Chemistry Institute, University of Zürich.
2007 - 2010 PhD Representative, Chemistry Department and Science Faculty (MNF), University of Zürich. Committee Graduate School for CMSZH, Prof. Roland Sigel.
PhD Representative at the Erweiterte Universitätsleitung (EU, University Board, University of Zürich).

School

1999 - 2001 Werner-Heisenberg-Gymnasium, Weinheim
Abitur (2001, grade 1.4)

1998 - 1999	Star Valley Senior High School in Afton, Wyoming, USA Graduation (1999, Honors)
1997 - 1998	Werner-Heisenberg-Gymnasium, Weinheim
1992 - 1997	Geschwister-Scholl-Gymnasium, Stuttgart
1988 - 1992	Grund- und Hauptschule Heumaden, Stuttgart

Languages

german	fluent (mother language)
english	fluent, negotiating level
french	6 years in school, good in speech, average in written.
latin (Latinum)	

Employment

2008 – now	Biognosys AG General Manager, COO Co-Founder, Member of Board
1999 – 2002	Dörsam Consulting Co-Founder, Consultant

Internships

1999	Naturin, Weinheim: 2 months, Sales and Distribution
2000	Wiley-VCH, Weinheim: 5 months, Customer Service
2001	2 months, lectorate chemistry
2003	3 months, lectorate biochemistry & marketing
2004	GIT Verlag, Darmstadt: 1 month, Sicherheit/Airport communication
2005	Wiley-VCH, Weinheim: 2 months, marketing

Interests

Sport:

2000 - now	Road Bike and Mountainbike Road Bike (Amateur, Elite from 2002 - 2005) Mountainbike (Elite from 2001 - 2005) ASVZ (University Sport, Zürich: Trainer (2004 - now)
1993 - 2003	Track & Fields, Decathlon Kickers Stuttgart, LG VfB Kickers Stuttgart, TSG Weinheim
1998 - 2001	American Football German National Team, Deutschland 1999 - 2001 Weinheim Longhorns, 1999 - 2001 Star Valley School Football (Varsity), 1998-99, USA